Irreversibilities and Nonidealities in Desalination Systems

by

Karan H. Mistry

S.M., Mechanical Engineering
Massachusetts Institute of Technology, Cambridge, 2010

B.S., Mechanical Engineering
University of California, Los Angeles, 2008

Submitted to the Department of Mechanical Engineering
in partial fulfillment of the requirements for the degree of

Doctor of Philosophy in Mechanical Engineering

at the

MASSACHUSETTS INSTITUTE OF TECHNOLOGY

June 2013

Author .....
Department of Mechanical Engineering
May 20, 2013

Certified by .....
John H. Lienhard V
Collins Professor of Mechanical Engineering
Thesis Supervisor

Accepted by .....
David E. Hardt
Chairman, Committee on Graduate Students

Irreversibilities and Nonidealities in Desalination Systems

by

Karan H. Mistry

Submitted to the Department of Mechanical Engineering
on May 20, 2013, in partial fulfillment of the
requirements for the degree of
Doctor of Philosophy in Mechanical Engineering

Abstract

Energy requirements for desalination systems must be reduced to meet increasing global demand for fresh water. This thesis identifies thermodynamic limits for the energetic performance of desalination systems and establishes the importance of irreversibilities and solution composition to the actual performance obtained.

Least work of separation for a desalination system is derived and generalized to apply to all chemical separation processes driven by some combination of work, heat, and chemical energy (fuel) input. At infinitesimal recovery, least work reduces to the minimum least work of separation: the true exergetic value of the product and a useful benchmark for evaluating energetic efficiency of separation processes. All separation processes are subject to these energy requirements; several cases relevant to established and emerging desalination technologies are considered.

The effect of nonidealities in electrolyte solutions on least work is analyzed through comparing the ideal solution approximation, Debye-Hückel theory, Pitzer's ionic interaction model, and Pitzer-Kim's model for mixed electrolytes. Error introduced by using incorrect property models is quantified. Least work is a strong function of ionic composition; therefore, standard property databases should not be used for solutions of different or unknown composition.

Second Law efficiency for chemical separation processes is defined using the minimum least work and characterizes energetic efficiency. A methodology is shown for evaluating Second Law efficiency based on primary energy inputs. Additionally, entropy generation mechanisms common in desalination processes are analyzed to illustrate the effect of irreversibility. Formulations for these mechanisms are applied to six desalination systems and primary sources of loss are identified.

An economics-based Second Law efficiency is defined by analogy to the energetic parameter. Because real-world systems are constrained by economic factors, a performance parameter based on both energetics and economics is useful. By converting all thermodynamic quantities to economic quantities, the cost of irreversibilities can be compared to other economic factors including capital and operating expenses.

By applying these methodologies and results, one can properly characterize the energetic performance and thermodynamic irreversibilities of chemical separation

processes, make better decisions during technology selection and design of new systems, and critically evaluate claimed performance improvements of novel systems.

Thesis Supervisor: John H. Lienhard V
Title: Collins Professor of Mechanical Engineering

Acknowledgments

The work presented in this thesis could not have been completed without the help and support of many individuals; I am extremely grateful for the guidance, advice, and support that I have received during my time at MIT.

Professor John Lienhard, I owe you my deepest thanks for your continued support and encouragement over the past five years. Through your guidance, I have grown as a scientist, an engineer, and most importantly, as an analytical problem solver.

In addition to my adviser, I am thankful for the feedback and guidance I have received from my doctoral committee: Alexander Mitsos, Evelyn Wang, and Mostafa Sharqawy.

To all the members of our research group and the Rohsenow Kendall Heat Transfer Laboratory, and in particular, Ed, Prakash, Greg, Ronan, Jacob, and Leo, thank you for providing years worth of both intellectual discourse and lighthearted banter. I have truly enjoyed my time with the group and have found our interactions both intellectually stimulating and personally rewarding.

To my family, Shaila and Hemant Mistry and Priyanjali Shah, thank you for always believing in me, and more importantly, for always being there to give me a kick in the right direction whenever I need it.

I have been blessed with having a number of extremely close friends. Nick, working with you, both at UCLA and at MIT, has been an absolute pleasure. You were the first of my friends to truly challenge and push me academically and I eagerly look forward to any future projects we may have together. Ben and Amneet, you both have been invaluable in helping me deal with all of the challenges that life has thrown my way.

I would like to thank the King Fahd University of Petroleum and Minerals for funding the research reported in this thesis through the Center for Clean Water and Clean Energy at MIT and KFUPM under project number R13-CW-10.

Lastly, thank you to everyone that I have had the pleasure of working with while at MIT, including students, faculty, and staff, for making the past five years memorable. While I know I will miss MIT dearly, as this chapter of my life comes to a close, I am excited to see where the next chapter will lead me...

—Karan (Rao) Mistry

The future belongs to those who can manipulate entropy;
those who understand but energy will be only accountants.

—Frederic Keffer

Day after day, day after day,
We stuck, nor breath nor motion;
As idle as a painted ship
Upon a painted ocean.

Water, water, every where,
And all the boards did shrink;
Water, water, every where,
Nor any drop to drink.

—Samuel Taylor Coleridge
The Rime of the Ancient Mariner

Contents

List of Figures

List of Tables

Nomenclature

Roman symbols		**Units**
A	Annualized cost	\$/yr
A	Debye-Hückel constant	$\mathrm{kg}^{\frac{1}{2}}/\mathrm{mol}^{\frac{1}{2}}$
A_ϕ	Pitzer constant	$\mathrm{kg}^{\frac{1}{2}}/\mathrm{mol}^{\frac{1}{2}}$
a	activity	-
B	membrane distillation coefficient	$\mathrm{kg}/(\mathrm{m}^2\,\mathrm{Pa\,s})$
b	Davies constant	kg/mol
C	cost	\$
c	specific heat	$\mathrm{J}/(\mathrm{kg\,K})$
c_i	cost of energy	$\$/i$
c_p	specific heat at constant pressure	$\mathrm{J}/(\mathrm{kg\,K})$
D_i	distillate from effect i	kg/s
$D_{f,i}$	distillate from flashing in effect i	kg/s
$D_{fb,i}$	distillate from flashing in flash box i	kg/s
d_{ch}	flow channel depth	m
E	electromotive force	V
$\dot{E}$	Energy flow rate	J/s
e	electron charge	C
F	Faraday constant	C/mol
G	Gibbs free energy	J
$\dot{G}$	Gibbs free energy flow rate	J/s
g	specific Gibbs free energy	J/kg
$\bar{g}$	molar Gibbs free energy	J/mol
$\dot{H}$	enthalpy flow rate	J/s
h	specific enthalpy	J/kg
$\bar{h}$	molar enthalpy	J/mol
h_{fg}	latent heat of vaporization	J/kg
I	current	A
I_m	molal ionic strength	mol/kg
i	interest rate	%
K_{eq}	equilibrium constant	-
K_{sp}	solubility constant	-
L	length	m
M	molecular weight	kg/mol
m	molality	$\mathrm{mol}_{\mathrm{solute}}/\mathrm{kg}_{\mathrm{solvent}}$

$\dot{m}$	mass flow rate	kg/s
m_i	molality of species i	mol/kg
N	number of moles	mol
$\dot{N}$	mole flow rate	mol/s
N_a	Avogadro's number	1/mol
n	number of moles	mol
n	number of effects or stages	-
n	number of species	-
n	plant lifetime	yr
n_e	number of electrons	-
p	pressure	Pa
Q	reaction quotient	-
$\dot{Q}$	rate of heat transfer	J/s
R	gas constant	J/(mol K)
R_R	replacement rate	%
r	recovery ratio, mass basis	$\mathrm{kg_{product}/kg_{feed}}$
$\bar{r}$	recovery ratio, mole basis	$\mathrm{mol_{H_2O\ product}/mol_{H_2O\ feed}}$
S	entropy	J/K
$\dot{S}$	entropy flow rate	J/(s K)
$\dot{S}_{\mathrm{gen}}$	rate of entropy generation	J/(s K)
$\mathcal{S}_{\mathrm{gen}}$	specific entropy generation per unit water produced	J/(kg K)
s	specific entropy	J/(kg K)
$\bar{s}$	molar entropy	J/(mol K)
s_{gen}	specific entropy generation	J/(kg K)
T	temperature	K
t	time	s
U	internal energy	J
V	volume	$\mathrm{m^3}$
$\dot{V}$	volumetric flow rate	$\mathrm{m^3/s}$
v	specific volume	$\mathrm{m^3/kg}$
$\dot{W}$	rate of work transfer	J/s
w	mass fraction	kg/kg
w	specific work transfer	J/kg
w	width	m
x	mole fraction	mol/mol
x	quality	kg/kg
y	salinity (TDS)	$\mathrm{kg_{solutes}/kg_{solution}}$
Z	generalized compressibility	-
z	valence of ion	-

Greek		**Units**
γ_f	fugacity coefficient	-
γ_i	molal activity coefficient of species i	-
γ_i	cost scaling function	$\$/\mathrm{m^3}$
γ_m	molal activity coefficient	-

γ_x	rational activity coefficient	-
Δ	change in a variable	
ϵ_0	permittivity of free space	F/m
ϵ_r	relative permittivity/dielectric constant	-
ζ	reaction coordinate	-
η	First Law efficiency	-
η_e	isentropic efficiency of expander	-
η_p	isentropic efficiency of pump/compressor	-
η_{pp}	Second Law efficiency of power plant	-
η_{II}	Second Law/exergetic efficiency	-
$\eta_{II,\$}$	Economics-based Second Law efficiency	-
μ_i	chemical potential	J/mol
ν	stoichiometric coefficient	-
Ξ	exergy	J
$\dot{\Xi}$	exergy flow rate	J/s
ξ	specific exergy	J/kg
$\bar{\xi}$	molar exergy	J/mol
ρ	density	kg/m^3
ϕ	molal osmotic coefficient	-
ϕ_i	cost scaling function	-

Subscripts

$+$	cation
$-$	anion
$\pm$	mean ionic property
0	solvent
0	dead state
1, 2	states 1 and 2
A, a	anion
a	assist
atm	atmospheric
C, c	cation
c	concentrate
ch	chemical
d	desalination plant
e	electricity
e	environment
f	feed
f	flashing
H	high temperature reservoir
h	heat
i	species (solvent or solutes)
i	state
in	input
j	stream

least	reversible process in which all process streams cross the system boundary at the RDS
m	molal basis
p	product
pp	power plant
r	reaction
ref	reference
rev	reversible
s	electrolyte salt species
s	steam
sep	separation
sw	seawater
w	water
x	rational (mole fraction) basis

Superscripts

$'$	stream before exiting CV
$\circ$	reference/standard state
HX	heat exchanger
IF	incompressible fluid
IG	ideal gas
min	minimum value at infinitesimal recovery
rev	reversible
s	isentropic

Acronyms		**Units**
AF	availability factor	%
BH	brine heater	
CAOW	closed air open water	
CAPEX	capital expenses	$
CD	chemical disequilibrium	
DCMD	direct contact membrane distillation	
DHLL	Debye-Hückel Limiting Law	
ED	electrodialysis	
ERD	energy recovery device	
ERI	Energy Recovery Inc.	
FF	forward feed	
GOR	gained output ratio	-
HDH	humidification-dehumidification	
HP	high pressure	
LHS	left hand side	
MD	membrane distillation	
MED	multiple effect distillation	
MSF	multistage flash	
MVC	mechanical vapor compression	

OPEX	operating expenses	\$
OT	once through	
ppm	parts per million	$\mathrm{mg_{solute}/kg_{solution}}$
ppt	parts per thousand	$\mathrm{g_{solute}/kg_{solution}}$
PR	performance ratio	
PRO	pressure retarded osmosis	
PV	photovoltaic	
PX	pressure exchanger	
RDS	restricted dead state	
RED	reverse electrodialysis	
RHS	right hand side	
RO	reverse osmosis	
SEC	specific electricity consumption	$\mathrm{kWh_e/m^3}$
SGE	salinity gradient engine	
SWRO	seawater reverse osmosis	
TD	temperature disequilibrium	
TDS	total dead state	
TDS	total dissolved solids	$\mathrm{kg_{solute}/kg_{solution}}$
TOTEX	total expenses	\$
TTD	terminal temperature difference	K
WH	water heated	

Chapter 1

Introduction

1.1 The growing water problem

Growing water demand due to rising population, increasing standards of living, industrialization, changing climate, and, in some instances, wasteful water use and management policies is resulting in substantial water shortage and scarcity. While developing countries are often hardest hit by lack of water supply, developed countries have had to face these issues as well [1, 2]. The United Nations World Water Development Report states that as of 2003, over one billion people lack access to adequate drinking water [3]. According to UNICEF, nearly 5,000 children die every day as a result of unsafe water as of 2006 [4]. Unfortunately, as the world population continues to increase and as water supplies continue to be contaminated, it is clear that the current water situation is only going to get much worse. In order to address the worsening water situation, one of the Millennium Development Goals from a UN Summit in 2000 was to halve the population of people without access to safe drinking water [3].

Traditionally, fresh water has been obtained from various fresh water sources including lakes, rivers, and aquifers. In water-scarce locations, water is often transported great distances at great costs (examples include Southern California [5] and

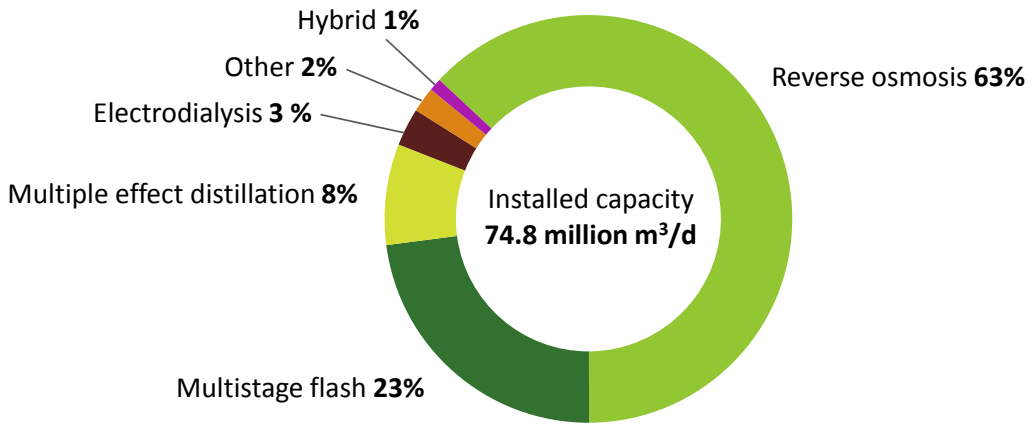

Figure 1-1: Installed desalination capacity by technology, as of 2013 [11].

Northern China [6]). As the demand for freshwater increases, these water sources are increasingly being taxed, often to the point of near-exhaustion. Unquestionably, new water sources must be found in order to alleviate demand. Fortunately, desalination (and in particular, seawater desalination) opens up the oceans—a new and essentially unlimited and renewable source of freshwater.

Desalination has been practiced for over a century as sailors used to evaporate seawater into pieces of cloth and then squeeze the freshwater out to consume [7]. Basic solar stills were also used (and still are for niche applications) to produce limited amounts of water [8]. However, substantial research in desalination technologies has occurred in recent decades in order to develop more efficient and economical methods, both to meet growing needs for potable water and to remediate industrial process waters [9, 10]. In the last 50–60 years, modern engineering has resulted in the development of substantially improved desalination techniques that can produce water efficiently and economically. As of 2013, there is nearly 75 million m^3/d of installed desalination capacity [11]. These plants treat a broad range of waters including seawater, river water, ground water, and others.

In general, the various desalination technologies can be divided into two basic categories based on the method of separation: thermal (distillation) processes and mechanical (typically membrane) processes [12]. Thermal-based processes include multistage flash (MSF), multiple effect distillation (MED), humidification-dehumidification (HDH), vapor compression (VC), and membrane distillation (MD). Mechanical processes include reverse osmosis (RO), forward osmosis (FO), and electrodialysis (ED). Figure 1-1 shows the installed capacity of each of the major desalination technologies.

1.2 Current state of desalination research

Two major limiting phenomenological factors affect the design and operation of desalination plants: energy consumption and scale formation [7]. Techniques have been developed to address both these issues.

Energy consumption is typically minimized by trying to maximize energy recovery. In thermal desalination plants, energy is carried in feed, product, and concentrate (brine) streams in the form of thermal energy. Energy can be recovered through the use of multiple effects (or stages), preheaters, and regenerators. In each effect of an MED plant, the heat of vaporization released during condensation of the vapor stream is used to evaporate more water from the brine stream. Regenerators are used to exchange thermal energy from the warm brine and vapor streams to the cold feed water stream. In each stage of an MSF plant, the heat of vaporization is used to preheat the feed seawater stream through the process of condensation. In both types of plants, increased number of effects (or stages) results in increased energy reuse, resulting in lower energy consumption per unit water produced [13].

Reverse osmosis implements energy recovery in a very different way. Since most of the energy in RO is stored in the mechanical form of a compressed liquid, advanced pressure exchangers are used to transfer energy from the high pressure brine stream to the lower pressure feed stream [14, 15]. Recent developments of pressure exchangers by companies such as Energy Recovery, Inc. (ERI) have greatly increased the efficiency of energy recovery in RO systems and have substantially reduced the net energy cost.

While energy recovery can greatly reduce the energy consumption of a desalination plant, substantial savings can come through the use of water and power cogeneration. It is especially advantageous to run thermal power plants in a cogeneration configuration since they are readily powered using waste heat or steam bled from the last stages of a turbine. Cogeneration can reduce the required energy input by approximately a third [12, 16]. Because of this energy savings, cogeneration is already common practice for large-scale seawater desalination plants, especially MSF and MED which are most common in the Gulf region (approximately 94% of production) where fuel is inexpensive and the additional cost of running the cogeneration plants is minimal [17]. Reverse osmosis is typically powered using electricity from the grid or from a dedicated power plant.

In addition to minimizing energy consumption, reducing the potential for scale formation is also essential when trying to design efficient desalination systems. In thermal plants, scaling greatly reduces heat transfer performance, requiring larger heat transfer surface area; and it limits the maximum brine temperature, which lowers the maximum possible thermodynamic efficiency. In membrane plants, scaling and fouling can block or damage the membranes, requiring down time and even expensive repair or replacement costs [7, 18].

Scale formation, fouling, and deposit build up can be controlled and prevented in three different ways. First, pretreatment can be used to remove dissolved and suspended solids through processes such as softening, ion exchange, filtration, flocculation, coagulation, and dispersion. Next, various chemical treatments, such as scale inhibitors and antifoulants, can be used to try to prevent deposition build up. Finally, if scaling and fouling has occurred, the deposits can be periodically removed through chemical and/or mechanical processes [19]. Through proper pretreatment, the concentration of the major scaling components (divalent ions such as calcium, magnesium, carbonate, and sulfate) can be reduced. By removing the major scaling and fouling agents, the top brine temperature can be raised by as much as 10 K, thus increasing the

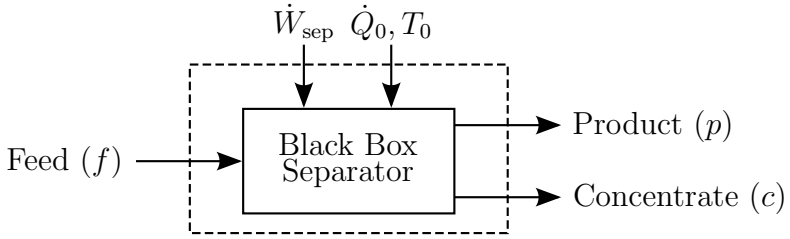

Figure 1-2: A control volume representation of a desalination system is used to derive the least work of separation.

thermodynamic efficiency. Nanofiltration has proven to be particularly successful in this application [20]. In order to assess the potential for scale formation, it is essential to understand the water chemistry of the feed water.

1.3 Energy requirements for desalination systems

As discussed previously, minimizing energy consumption is one of the primary goals when designing a chemical separation process. While any sort of energy improvements must be balanced with the additional cost required to achieve said improvement, it is still useful to analyze the energy requirements at a fundamental level and independently of the economic issues. In Chapter 2, a control volume approach is used to derive an expression for the work of separation requirements for an arbitrary black box chemical separator, as illustrated in Fig. 1-2.

By applying the First and Second Laws of Thermodynamics to the control volume and combining them subject to several requirements discussed in Chapter 2, the power required to drive the separation process is found to be:

$$\dot{W}_{\text{sep}} = \dot{G}_p + \dot{G}_c - \dot{G}_f + T_0 \dot{S}_{\text{gen}} \tag{1.1}$$

where $\dot{G}_i$ is the flow rate of Gibbs free energy of stream i, T_0 is the environment temperature at which heat transfer occurs, and $\dot{S}_{\text{gen}}$ is the entropy generated during the chemical separation process. When Eq. (1.1) is evaluated per unit flow rate of product, it represents the work of separation.

Equation (1.1) can be divided into two parts that are quite distinct and can be studied independently of one another. The first part is a function of the Gibbs free energy of each of the process and streams and is typically referred to as the least work of separation when it is evaluated for unit product mass flow rate:

$$\dot{W}_{\text{least}} = \dot{G}_p + \dot{G}_c - \dot{G}_f \tag{1.2}$$

The least work of separation is purely a function of the composition of each of the process streams (in this case, feed, product, and concentrate) and the recovery ratio with which the separation process is performed. Therefore, in order to fully understand all of the nuances of $\dot{W}_{\text{least}}$, it is important to study the chemistry of the various solutions being treated.

The second part is a function of the irreversibilities that occur during the separation process and is often referred to as the exergy destroyed:

$$\dot{\Xi}_{\text{destroyed}} = T_0 \dot{S}_{\text{gen}} \tag{1.3}$$

Exergy destruction in chemical separation processes is largely not a function of chemistry. While there is some entropy generated during mixing (which is a function of chemistry), the largest sources of entropy generation tend to be heat transfer across finite temperature differences for thermal systems and viscous losses for membrane systems. Therefore, the exergy destruction part of the work of separation can be best understood by analyzing the various sources of irreversibility within a system.

1.4 Research objectives and thesis overview

Given the importance of reducing energy consumption for any process, the primary goal of this thesis is to develop a deeper understanding of the fundamental sources of energy requirements involved in chemical separation processes, and in particular, desalination technologies. As a result, there are four primary areas that are investigated:

1. Work of separation requirements, generalized to any type of energy input.
2. Effect of solution composition and chemistry on the least work of separation.
3. Effect of irreversible processes on the increase in work requirements.
4. Cost of thermodynamic irreversibilities as compared to other economic factors.

In addition to these four areas, a detailed analysis of MED models as well as the development of a novel model is included in Appendix A.

While this thesis is written in such a way that each chapter builds off of the previous chapters, care has been taken to ensure that each chapter can be read largely independently of the others. Therefore, major derivations are briefly summarized in relevant chapters as appropriate.

1.4.1 Generalized least energy of separation

Equation (1.1) is a useful expression for evaluating the work requirements for a desalination process that is powered purely using work. However, many modern systems require some combination of work, heat, and chemical fuel as energy input. Chapter 2 focuses on the development of a generalized equation for calculating the energy of separation requirements for an arbitrary chemical separator that is powered by any type of energy input. Additionally, special cases of the generalized equation, including the least work of separation, least heat of separation, and least fuel of separation are analyzed and compared [21, 22].

1.4.2 Nonidealities in electrolyte solutions

Chemical composition plays a large role in the magnitude of the least work of separation. As a result, standard seawater properties and pure water properties cannot be used for arbitrary source waters that may be composed of very different species. Since

standard datasets do not exist for all solutions that might be considered, physical properties must be evaluated using thermodynamic models. The thermodynamic models are typically composed of two parts, an ideal part that is a function of mole fractions, and a nonideal part that is a function of activity coefficients that represent nonideal solution behavior. Incorrectly using the various models to calculate the nonidealities can result in substantial error in the evaluation of the least work of separation. Chapter 3 focuses on the evaluation of activity coefficients for both single and mixed electrolyte solutions and highlights the importance of considering chemical composition as well as correct usage of existing models [23–25].

1.4.3 Second Law efficiency for separation processes

For most real-world desalination systems, exergy destruction will be several times larger than the least work of separation. Therefore, understanding the irreversibilities within a given system is essential for reducing the overall energy requirements. In Chapter 4, all of the major entropy generation mechanisms present in desalination systems are investigated. The resulting expressions are applied to six different desalination technologies in order to show the primary source of losses in each type of system.

In addition to looking at the sources of entropy generation, Second Law efficiency for chemical separation processes is formally defined. This requires identifying the exergetic value of the product water and all sources of losses. The definition of Second Law efficiency is then applied to the same six technologies. Additionally, it is used for desalination systems that are operating in a cogeneration scheme with a power plant [21, 22].

1.4.4 Economic Second Law efficiency

Real-world systems are ultimately constrained primarily by economic factors; therefore, it is useful to have a performance parameter that can adequately capture both energetic and economic effects. An economics-based Second Law efficiency is defined by analogy to the energetic parameter in order to characterize energetics and economics. By converting all thermodynamic quantities to economic terms, it is found that the cost of irreversibilities can be compared to other important economic factors including capital and operating expenses [26].

Chapter 2

Generalized least energy of separation

Chapter abstract

Increasing global demand for fresh water is driving the development and implementation of a wide variety of seawater desalination technologies driven by different combinations of work, heat, and chemical energy. A consistent basis for comparing the energy consumption of such technologies through the minimum least energy of separation, a parameter that is analogous to Carnot efficiency for power plants, is developed in this chapter. A generalized expression for the least energy of separation is derived for generic chemical separators. The generalized equation is then evaluated through a parametric study considering work input, heat inputs at various temperatures, and various chemical fuel inputs.

This chapter consists of work that is published in [21, 22].

2.1 Introduction

Currently, several different technologies for desalinating water are in wide use, including reverse osmosis (RO), multistage flash (MSF), multiple effect distillation (MED), among others. These systems are typically powered by electricity (work), heat, fuel, or some combination thereof. The description of energy requirements becomes more complicated when one considers that many larger scale water plants are operated in conjunction with power plants in a cogeneration scheme [16]. While advances over the last several decades have resulted in dramatically reduced energy utilization, desalination is still energy intensive, and it is important to be able to fully characterize the performance of these systems and to compare the relative energy costs from system to system. Understanding the fundamental thermodynamic limits on energy requirements is essential in this characterization.

The least work of separation ($\dot{W}_{\text{least}}$) represents the least amount of work required to reversibly separate a single stream into multiple streams of different composition [16, 21, 22, 27–29]. Similarly, the least heat of separation ($\dot{Q}_{\text{least}}$) can be used to represent the least amount of heat required for a separation process. Both are benchmarks to which desalination systems are compared, much as Carnot efficiency is the ideal benchmark to which power plants are compared.

While the least work and least heat of separation are useful parameters for work and heat driven systems respectively, it is difficult to directly compare the energies represented by least work and least heat. Additionally, these parameters are only useful for systems that have a single energy source (work or heat only). Many modern separation processes, including most thermal desalination systems (*e.g.*, MSF and MED), require both thermal and mechanical energy input. Still other systems may be powered by chemical energy. Therefore, a more useful least energy metric would capture simultaneous mechanical, thermal, and chemical energy inputs.

This chapter is based on the work of Mistry et al. [21, 25]. First, the least work and least heat equations are derived from simplified control volumes. Then, the calculation is generalized to consider the least energy of separation for a generic chemical separator. A "least" separation process is defined here as a completely reversible process in which the minimum amount of energy, as required by the Second Law of Thermodynamics, is needed to drive a chemical separation process. This concept is clarified and further developed through several examples.

In Chapter 4, the generalized least energy of separation concept is developed further and is used to define the Second Law efficiency of a generic chemical separator.

2.2 Least work and least heat of separation

Consider a simple black-box separator model for a desalination system, with a separate control volume surrounding it at some distance, as shown in Fig. 2-1. The work of separation entering the system is denoted by $\dot{W}_{\text{sep}}$ and the heat transfer into the system is $\dot{Q}$. Stream f is the incoming feed, stream p is pure water (product), and stream c is the concentrate (brine). By selecting the control volume sufficiently far from the

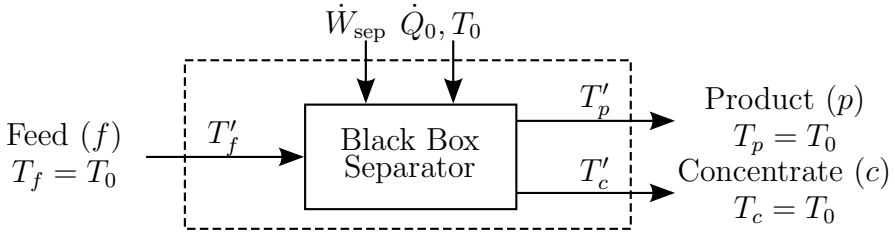

Figure 2-1: When the control volume is selected suitably far away from the physical system, all inlet and outlet streams are at ambient temperature and pressure. The temperature of the streams inside the control volume (T'_i) might not be at T_0.

physical plant, all the inlet and outlet streams enter and leave the control volume at ambient temperature (T_0) and pressure (p_0) but at different chemical composition. Additionally, the heat transfer occurs at ambient temperature.

The logic underlying this latter formulation is that the exergy of the outlet streams attributable to thermal disequilibrium with the environment is not deemed useful. In other words, the purpose of a desalination plant is to produce pure water, not pure *hot* water. Consider separately the thermal conditions at the desalination system boundary (solid box) and the distant control volume boundary (dashed box). Product and reject streams may exit the desalination system at temperatures T'_p and T'_c, different than ambient temperature, T_0. The exergy associated with these streams could be used to produce work that would offset the required work of separation. However, if the exergy associated with thermal disequilibrium is not harnessed in this way, but simply discarded, entropy is generated as the streams are brought to thermal equilibrium with the environment. This entropy generation is analyzed in Section 4.6.5. Similarly, pressure disequilibrium would result in additional entropy generation [30]. In general, differences in concentration between the various streams represent a chemical disequilibrium which could also be used to produce additional work; however, since the purpose of the desalination plant is to split a single stream into two streams of different concentrations (*i.e.*, product water is not in chemical equilibrium with the feed or environment), the outlet streams are not brought to chemical equilibrium with the environment.

The least work and least heat of separation are calculated by evaluating the First and Second Laws of Thermodynamics for the distant control volume. The convention that work and heat input to the system are positive is used.

$$\dot{W}_{\text{sep}} + \dot{Q}_0 + \dot{m}_f h_f = \dot{m}_p h_p + \dot{m}_c h_c \tag{2.1}$$

$$\frac{\dot{Q}_0}{T_0} + \dot{m}_f s_f + \dot{S}_{\text{gen}} = \dot{m}_p s_p + \dot{m}_c s_c \tag{2.2}$$

In Eqs. (2.1) and (2.2), $\dot{m}_i$, h_i, and s_i are the mass flow rate, specific enthalpy and specific entropies of the feed (f), product (p), and concentrate (c) streams. The First and Second Laws are combined by multiplying Eq. (2.2) by ambient temperature, T_0, and subtracting from Eq. (2.1) while noting that the specific Gibbs free energy is,

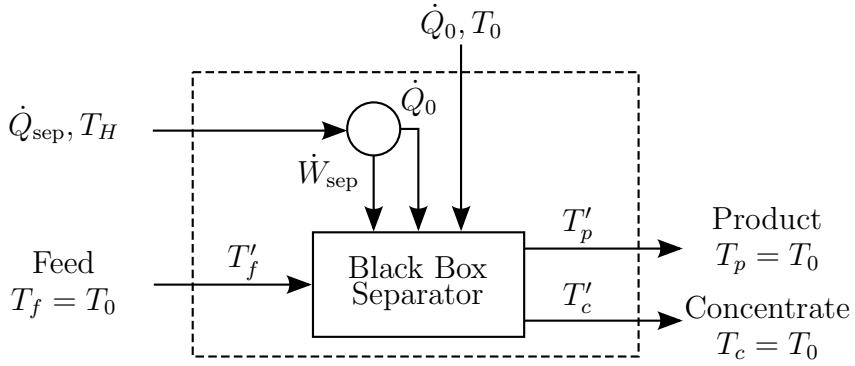

Figure 2-2: Addition of a high temperature reservoir and a Carnot engine to the control volume model shown in Fig. 2-1.

$g = h - Ts$ (all evaluated at $T = T_0$).

$$\dot{W}_{\text{sep}} = \dot{m}_p g_p + \dot{m}_c g_c - \dot{m}_f g_f + T_0 \dot{S}_{\text{gen}} \tag{2.3}$$

In the limit of reversible operation, entropy generation is zero and the work of separation becomes the reversible work of separation, which is also known as the least work of separation:

$$\dot{W}_{\text{least}} \equiv \dot{W}_{\text{sep}}^{\text{rev}} = \dot{m}_p g_p + \dot{m}_c g_c - \dot{m}_f g_f \tag{2.4}$$

Equation (2.3) represents the amount of work required to reversibly produce pure water at a rate of $\dot{m}_p$. If heat is used to power a desalination system instead of work, the heat of separation is a more relevant parameter. Recalling that heat engines produce work and reject heat, the calculation of the heat of separation is straightforward. Figure 2-2 shows the control volume from Fig. 2-1 but with a reversible heat engine providing work of separation. If the heat is provided from a high temperature reservoir, then the First Law for the heat engine is

$$\dot{Q}_{\text{sep}} = \dot{W}_{\text{sep}} + \dot{Q}_0 \tag{2.5}$$

Assuming a reversible heat engine operating between the high temperature reservoir at T_H and ambient temperature T_0 and considering work per unit mass produced,

$$\frac{\dot{W}_{\text{sep}}}{\dot{m}_p} = \frac{\dot{Q}_{\text{sep}}}{\dot{m}_p} - \frac{\dot{Q}_0}{\dot{m}_p} = \frac{\dot{Q}_{\text{sep}}}{\dot{m}_p}\left(1 - \frac{T_0}{T_H}\right) \tag{2.6}$$

where the second equality holds as a result of the entropy transfer that occurs in a reversible heat engine operating between two heat reservoirs. Therefore, the heat of separation is:

$$\frac{\dot{Q}_{\text{sep}}}{\dot{m}_p} = \frac{\dot{W}_{\text{sep}}}{\left(1 - \frac{T_0}{T_H}\right)\dot{m}_p} = \frac{\dot{W}_{\text{least}} + T_0 \dot{S}_{\text{gen}}}{\left(1 - \frac{T_0}{T_H}\right)\dot{m}_p} \tag{2.7}$$

where the second equality holds by combining Eqs. (2.3) and (2.4). Note that Eq. (2.7)

can also be derived from Eqs. (2.1) and (2.2) if $\dot{W}_{\text{sep}}$ is set to zero and the temperature in the Second Law is set to T_H [27]. Equations for the least heat of separation, $\dot{Q}_{\text{least}}$ and the minimum least heat of separation, $\dot{Q}^{\text{min}}_{\text{least}}$ can be obtained from Eq. (2.7) in the same manner as the corresponding work equations.

In practice, the entropy generation term in Eqs. (2.3) and (2.7) dominates over the least work or least heat. Therefore, the parameter, $\dot{S}_{\text{gen}}/\dot{m}_p$ is of critical importance to the performance of desalination systems [27]. This term is referred to as the specific entropy generation, $\mathcal{S}_{\text{gen}}$, and is a measure of entropy generated per unit of water produced:

$$\mathcal{S}_{\text{gen}} = \frac{\dot{S}_{\text{gen}}}{\dot{m}_p} \tag{2.8}$$

In the formulation described above, all streams enter and exit the system at ambient temperature. Therefore, the specific exergy destroyed, ξ_d, in the system is equal to the product of $\mathcal{S}_{\text{gen}}$ and the ambient temperature. This term is physically reflective of the same phenomenon that produces Eq. (2.8):

$$\xi_{\text{destroyed}} = \frac{T_0 \dot{S}_{\text{gen}}}{\dot{m}_p} \tag{2.9}$$

While the present chapter focuses on reversible processes, entropy generation in chemical separation processes will be considered in detail in Chapter 4.

Now that the least work and least heat of separation have been derived for simplified control volumes, a generalized expression is derived that is applicable to all chemical separation systems.

2.3 Generalized least energy of separation

The equation for the generalized least energy of separation is derived using the generalized exergy equation for an arbitrary system control volume shown in Fig. 2-3 [31]. This control volume has q inlet streams and r outlet streams, each potentially at different temperature, pressure, and chemical composition of 0 to n species. For simplicity, kinetic and potential energy is neglected. The system is in thermal contact with p heat reservoirs and is free to transfer work ($p_0\,\mathrm{d}V/\mathrm{d}t$), heat ($\dot{Q}_0$), and mass ($\dot{N}_{0,i}$) with the environment. In Fig. 2-3 and the subsequent equations, the subscript 0 is used to denote environmental conditions and the subscript i is used to denote a specific species (*e.g.*, $\dot{N}_{0,i}$ is the mole flow rate of species i into the system, from the environment at T_0, p_0 with a chemical potential of $\mu_{0,i}$). The sign convention of positive work input is used herein. As a result, the outlet streams can leave the system at thermal, mechanical, and chemical equilibrium with the environment. That is, they can leave the system at the total dead state (TDS). The First and Second

Laws of Thermodynamics are written for the control volume as follows:

$$\frac{\mathrm{d}U}{\mathrm{d}t} = \dot{W} + \sum_{l=0}^{p} \dot{Q}_l + \sum_{j=1}^{q} \dot{N}_j \bar{h}_j - \sum_{k=1}^{r} \dot{N}_k \bar{h}_k + \sum_{i=1}^{n} \dot{N}_{0,i} \bar{h}_{0,i} - p_0 \frac{\mathrm{d}V}{\mathrm{d}t} \tag{2.10}$$

$$\frac{\mathrm{d}S}{\mathrm{d}t} = \sum_{l=0}^{p} \frac{\dot{Q}_l}{T_l} + \sum_{j=1}^{q} \dot{N}_j \bar{s}_j - \sum_{k=1}^{r} \dot{N}_k \bar{s}_k + \sum_{i=1}^{n} \dot{N}_{0,i} \bar{s}_{0,i} + \dot{S}_{\mathrm{gen}} \tag{2.11}$$

Equations (2.10) and (2.11) are combined by eliminating $\dot{Q}_0$, conserving mass, and accounting for volume change of the control volume resulting in the generalized exergy equation for an open system [31]:

$$\frac{\mathrm{d}\Xi_t}{\mathrm{d}t} = \dot{\Xi}_{\dot{W}} + \sum_{l=1}^{p} \dot{\Xi}_{\dot{Q},l} + \sum_{j=1}^{q} \dot{N}_j \bar{\xi}_j - \sum_{k=1}^{r} \dot{N}_k \bar{\xi}_k - T_0 \dot{S}_{\mathrm{gen}} \tag{2.12}$$

where

$$\Xi_t = U - T_0 S + p_0 V - \sum_{i=1}^{n} \mu_{0,i} N_i \tag{2.13}$$

$$\dot{\Xi}_{\dot{W}} = \dot{W} \tag{2.14}$$

$$\dot{\Xi}_{\dot{Q}} = \left(1 - \frac{T_0}{T}\right) \dot{Q} \tag{2.15}$$

$$\bar{\xi}(T, p, N_i) = \bar{h}(T, p, N_i) - T_0 \bar{s}(T, p, N_i) - \sum_{i}^{n} \mu_{0,i}(T_0, p_0) x_i \tag{2.16}$$

While Eq. (2.12) is completely general and applicable to any open system, it can be simplified to be more useful when applied specifically to chemical separation processes. An arbitrary chemical separation process can be powered by mechanical, thermal, or chemical energy. While mechanical and thermal energy inputs are represented by work and heat transfer respectively, chemical energy is input to the system through the inflow and outflow of fuel and exhaust streams. In a chemical separation process, it is important to differentiate between process streams and fuel/exhaust streams. Process streams are any streams directly involved in the chemical separation process and include feed, product, and any waste streams. For a desalination system, this would typically include seawater (feed), pure water (product), and concentrated brine (waste). For an oil separation process, this would include crude oil (feed), various grades of refined hydrocarbons (products), and solid waste. The terms fuel and exhaust are used loosely to represent all streams that are used to provide energy to the system such as fuel, solvents, air, and combustion products. The mole flow rate summation terms in Eq. (2.12) are rearranged into sums over the inlets minus the outlets of the process streams and the fuel/exhaust streams. All of the energy inputs are moved to the left hand side (LHS) of the equation and all the process streams, stored energy,

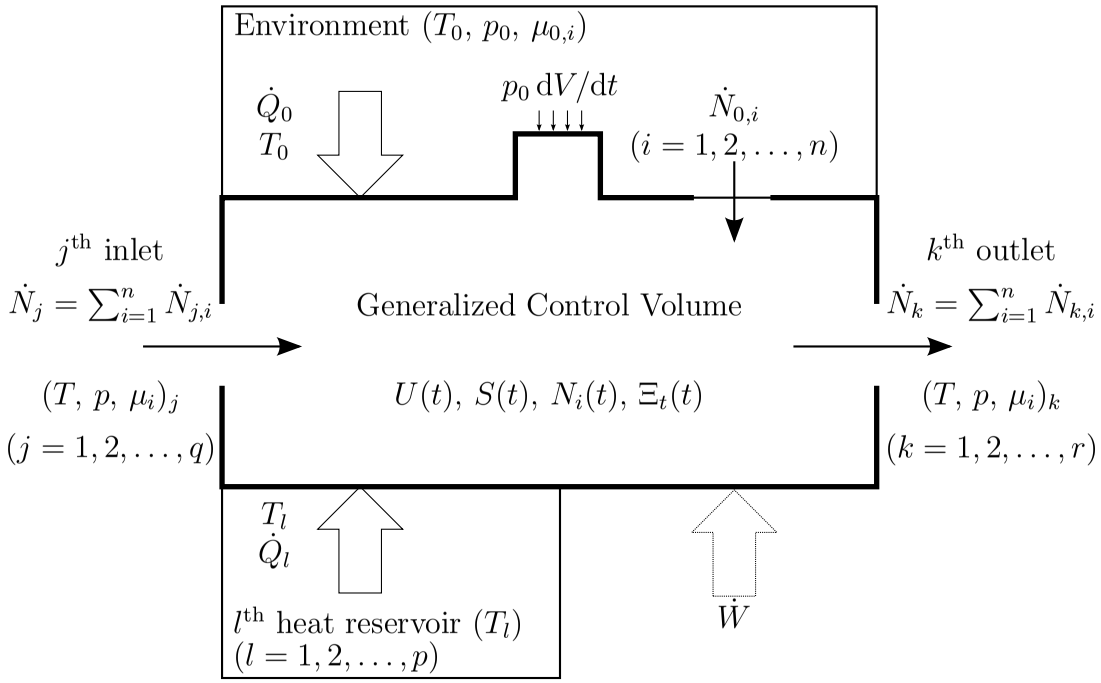

Figure 2-3: A generalized control volume with q inlets, r outlets, p heat transfer inputs, and work input. The control volume can exchange work ($p_0\,\mathrm{d}V/\mathrm{d}t$), heat ($\dot{Q}_0$), and mass ($\dot{N}_{0,i}$) with the environment through the system boundary.

and irreversibilities are moved to the right hand side (RHS).

$$\dot{\Xi}_{\dot{W}} + \sum_{l=1}^{p} \dot{\Xi}_{\dot{Q}_l} + \underbrace{\sum_{\text{in-out}} \dot{N}\bar{\xi}}_{\text{fuel and exhaust streams}} = \frac{\mathrm{d}\Xi_t}{\mathrm{d}t} + \underbrace{\sum_{\text{out-in}} \dot{N}\bar{\xi}}_{\text{process streams}} + T_0 \dot{S}_{\text{gen}} \tag{2.17}$$

The LHS of Eq. (2.17) represents all exergy inputs to the system while the RHS represents the changes associated with the control volume and process streams. Using this equation, the generalized least energy of separation is derived. Consider the RHS first. In order to minimize the required exergetic input, the process must be reversible. Additionally, any thermal and mechanical energy in the exit process streams is considered wasted since the desired product in a separation process is the mass of product. This concept is discussed in detail by Mistry et al. [21]. Therefore, the process streams must exit at the restricted dead state (RDS). Note that the process streams cannot leave at the TDS since the purpose of a chemical separation process is to convert an inlet stream into streams with different composition and allowing chemical equilibrium to occur would have the net effect of undoing the separation process. Under these conditions, the exergy of the process streams reduces to the Gibbs free energy at atmospheric temperature and pressure.

$$\bar{\xi}(T_0, p_0, N_i) = \bar{h}(T_0, p_0, N_i) - T_0 \bar{s}(T_0, p_0, N_i) \equiv \bar{g}(T_0, p_0) \tag{2.18}$$

Equation (2.17) is simplified by substituting Eq. (2.18) into the process stream summation, substituting in Eqs. (2.14) and (2.15), assuming steady state, and assuming reversible behavior. This leaves the generalized least energy of separation equation:

$$\underbrace{\dot{W} + \sum_{l=1}^{p} \left(1 - \frac{T_0}{T}\right)_l \dot{Q}_l}_{\text{energy inputs/outputs}} + \underbrace{\sum_{\text{in-out}} \dot{N}\bar{\xi}(T, p, N_i)}_{\text{fuel and exhaust streams}} = \underbrace{\sum_{\text{out-in}} \dot{N}\bar{g}(T_0, p_0, N_i)}_{\text{process streams}} \tag{2.19}$$

The RHS of the equation represents the least amount of exergy required to separate the input process streams into output streams of different chemical compositions. For a desalination process, a feed stream is separated into a low salinity product stream and a high salinity concentrate stream.

$$\dot{\Xi}_{\text{least}} \equiv \sum_{\text{out-in}} \dot{N}\bar{g}(T_0, p_0, N_i) \tag{2.20}$$

This exergy must be provided to the system by a combination of work, heat, and chemical energy as indicated by the LHS of the equation. Equations (2.19) and (2.20) are derived from a control volume that surrounds the system and only considers the inputs and outputs to the system. They represent the true limit for the least exergy required for separation, regardless of what process occurs within the control volume. Therefore, all technologies, including those which utilize a carrier fluid that does not leave the system boundary, are subject to the energy conservation requirement given

by Eq. (2.19). Such technologies include forward osmosis (FO) [32–35], humidification-dehumidification (HDH) [27, 36–40], and directional solvent extraction [41, 42].

Since it is conventional to discuss desalination systems on a mass basis, rather than a mole basis, it is more convenient to write Eq. (2.20) in terms of mass flow rates. For a system with one inlet stream (feed) and two outlet streams (product and concentrate), this is written as:

$$\dot{\Xi}_{\text{least}} = \sum_{\text{out}-\text{in}} \dot{m} g(T_0, p_0, N_i) = \dot{m}_p g_p + \dot{m}_c g_c - \dot{m}_f g_f \tag{2.21}$$

where g_j is the specific Gibbs free energy per kilogram of solution and is a function of the temperature, pressure, and salinity of each of the dissolved species.

In order to gain better physical insight into the separation process, it is instructive to consider how the least work varies with recovery ratio. The recovery ratio is defined as the ratio of the mass flow rate of product water to the mass flow rate of feed water:

$$r \equiv \frac{\dot{m}_p}{\dot{m}_f} = \frac{\text{mass flow rate of product}}{\text{mass flow rate of feed}} \tag{2.22}$$

Equation (2.21) can be rewritten in terms of the recovery ratio by combining Eq. (2.22) with conservation of mass:

$$\dot{m}_f = \dot{m}_p + \dot{m}_c \tag{2.23}$$

Normalizing by the product flow rate gives:

$$\frac{\dot{\Xi}_{\text{least}}}{\dot{m}_p} = (g_p - g_c) - \frac{1}{r}(g_f - g_c) \tag{2.24}$$

Evaluation of Eq. (2.24) requires physical properties of the feed, product, and concentrate streams. While the Gibbs free energy can be evaluated by summing chemical potentials of each of the species [23–25], seawater property packages based upon a single salinity parameter are available [43–46]. The package by Sharqawy *et al.* [45, 46] is used in this study. Correlations for properties such as specific Gibbs free energy, osmotic coefficients, and chemical potential of water and salts in seawater are given as a function of temperature and salinity. The range of validity of the correlations varies slightly for each property, but in general, they are available for temperatures between 0–120 °C and salinities between 0–120 g/kg. By assuming that the relative concentration of each of the dissolved species is the same in each stream, conservation of mass for the salts is written as:

$$\dot{m}_f y_f = \dot{m}_p y_p + \dot{m}_c y_c \tag{2.25}$$

For seawater desalination, the Gibbs free energy of each of the streams in Eq. (2.24) is evaluated using seawater properties, as a function of temperature and salinity, $g_j = g_j(T, y_j)$ [45]. With the feed and product salinities (y_f, y_p) given, the concentrate

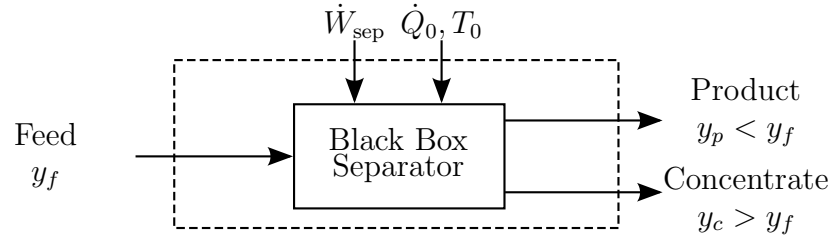

Figure 2-4: A control volume for an arbitrary black box chemical separator powered by work only.

salinity (y_c) is evaluated using Eqs. (2.22), (2.23), and (2.25):

$$y_c = \frac{y_f - r y_p}{1 - r} \tag{2.26}$$

Finally, as discussed by Mistry et al. [21] and illustrated in the subsequent sections, the minimum least exergy of separation occurs in the limit of infinitesimal recovery:

$$\dot{\Xi}^{\min}_{\text{least}} = \lim_{r \to 0} \dot{\Xi}_{\text{least}} \tag{2.27}$$

While $\dot{\Xi}^{\min}_{\text{least}}$ represents the least amount of exergy required to drive a separation process, it does not necessarily give design guidance as infinitesimal recovery would result in infinite cost.

In the following sections, three special cases of Eq. (2.19) are considered: least work of separation, least heat of separation, and least chemical energy of separation. These special cases occur when only one form of energy is input is used.

2.4 Least work of separation

For chemical separation processes that are powered by work only, the schematic diagram shown in Fig. 2-3 can be simplified. Examples of work-driven desalination systems include RO, mechanical vapor compression (MVC), and electrodialysis (ED). In the case of an arbitrary desalination system, the generalized control volume reduces to the schematic diagram illustrated in Fig. 2-4. Note that while work is the only energy input, in order to fulfill the First and Second Laws of Thermodynamics and to allow all streams to enter and exit the control volume at ambient temperature, heat transfer must be allowed with the environment ($\dot{Q}_0$).

Simplifying Eq. (2.19) to the arbitrary desalination system shown in Fig. 2-4, with only work input and heat transfer from the environment, yields the definition of the least work of separation:

$$\dot{W}_{\text{least}} = \sum_{\text{out}-\text{in}} \dot{N} \bar{g}(T_0, p_0, N_i) = \dot{\Xi}_{\text{least}} \tag{2.28}$$

The least work and least exergy of separation are equivalent and the terms are used

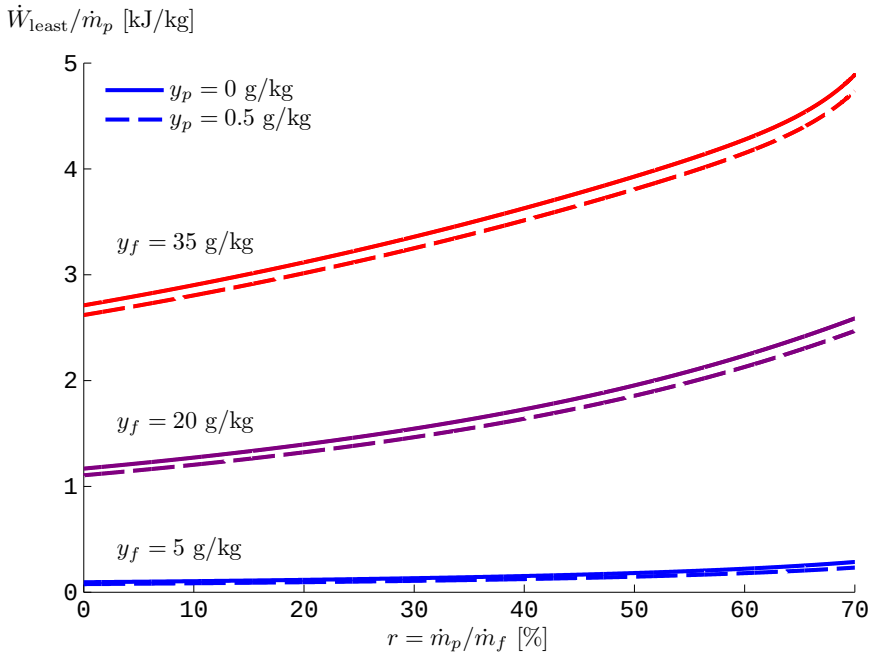

Figure 2-5: Least work of separation as a function of feed salinity and recovery ratio. Feed water is at $T_0 = 25\,^{\circ}\text{C}$.

interchangeably in the remainder of this thesis. Using Eqs. (2.24) and (2.28), the least work of separation is:

$$\frac{\dot{W}_{\text{least}}}{\dot{m}_p} = (g_p - g_c) - \frac{1}{r}(g_f - g_c) \tag{2.29}$$

Equation (2.29) is a function of temperature, feed salinity, product salinity, and recovery ratio and is plotted for various feed salinities and recovery ratios at a constant temperature of 25 °C in Fig. 2-5. The least work of separation is a strong function of feed salinity and recovery ratio, and a weak function of the product salinity (for typically low product salinities).

Holding temperature constant at 25 °C, the least work of separation is plotted as a function of feed salinity and recovery ratio in Fig. 2-5. It is seen that regardless of inlet salinity and product salinity, the least work is minimized as the recovery ratio approaches zero. This is true in general because, in the limit of zero recovery, the only stream that experiences an energy change is the product stream. At finite recovery, work must also be provided to supply the chemical potential energy change of the concentrate stream due to a change in salinity. Since the least work is defined per unit mass of product, the least work represents the amount of energy necessary to create 1 kg of pure water plus the amount of energy necessary to change the chemical potential of the concentrate stream. Therefore, the least work of separation is minimized as the recovery ratio approaches zero (*i.e.*, infinitesimal extraction).

$$\dot{W}_{\text{least}}^{\min} \equiv \lim_{r \to 0} \dot{W}_{\text{least}} \tag{2.30}$$

Using seawater properties [45] and assuming an inlet salinity of 35 g/kg, zero salinity water product, and $T = 25\,^{\circ}\mathrm{C}$, the least work of separation at infinitesimal recovery is 2.71 kJ/kg.

2.5 Least heat of separation

Chemical separation processes can be powered using only heat input. Examples of heat driven desalination systems include MED, MSF, membrane distillation (MD), and HDH. A schematic diagram of an arbitrary desalination plant powered using a high temperature heat source is shown in Fig. 2-6. As with the work-driven case, this control volume allows for atmospheric heat transfer in order to satisfy the First and Second Laws of Thermodynamics. When heat is the only form of energy input, Eq. (2.19) reduces to the least heat of separation:

$$\dot{Q}_{\mathrm{least}} = \left(1 - \frac{T_0}{T_H}\right)^{-1} \sum_{\mathrm{out-in}} \dot{N}_j \bar{g}_j(T_0, p_0, N_i) = \left(1 - \frac{T_0}{T}\right)^{-1} \dot{W}_{\mathrm{least}} \tag{2.31}$$

For the arbitrary desalination system pictured in Fig. 2-6, the least heat of separation can be expressed on a mass basis as follows:

$$\frac{\dot{Q}_{\mathrm{least}}}{\dot{m}_p} = \left(1 - \frac{T_0}{T_H}\right)^{-1} \left[(g_p - g_c) - \frac{1}{r}(g_f - g_c)\right] \tag{2.32}$$

Unlike the least work, $\dot{Q}_{\mathrm{least}}$ is a function of the temperature at which the heat is transfered in addition to the ambient temperature, recovery ratio, and feed and product salinities. As with Carnot efficiency, it is clear that the least heat improves with increasing top temperature (Fig. 2-7). In Fig. 2-7, the least heat is evaluated at four different top temperatures: 50 °C, 75 °C, 100 °C, and 5800 K. The first three represent a range of values typical of common thermal desalination methods. The high temperature represents an upper bound on the temperature at which energy can be transferred from the sun. At such high temperatures, the Carnot efficiency begins to approach one and $\dot{Q}_{\mathrm{least}}$ approaches $\dot{W}_{\mathrm{least}}$.

Gained output ratio (GOR) is a commonly used performance parameter in the thermal desalination industry. GOR is the ratio of the enthalpy required to evaporate the distillate (or equivalently, the energy release in condensation) to the heat input to the system:

$$\mathrm{GOR} \equiv \frac{\dot{m}_p h_{fg}(T_0)}{\dot{Q}_{\mathrm{sep}}} \tag{2.33}$$

In essence, GOR is a measure of how many times the latent heat of vaporization is captured in the condensation of pure water vapor and reused in a subsequent evaporation process to create additional pure water vapor from a saline source. By the First Law of Thermodynamics, a thermal desalination system that has no such heat recovery requires largely the latent heat of vaporization multiplied by the mass of pure water produced as its energy input: its GOR is approximately one. It is important

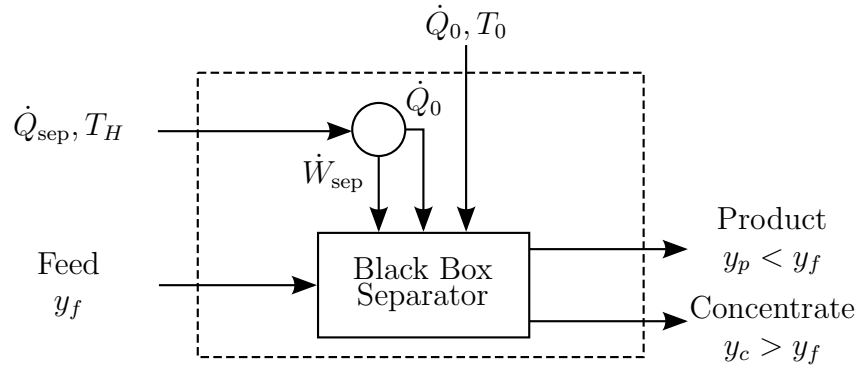

Figure 2-6: A control volume for an arbitrary black box chemical separator when heat is the only form of energy input.

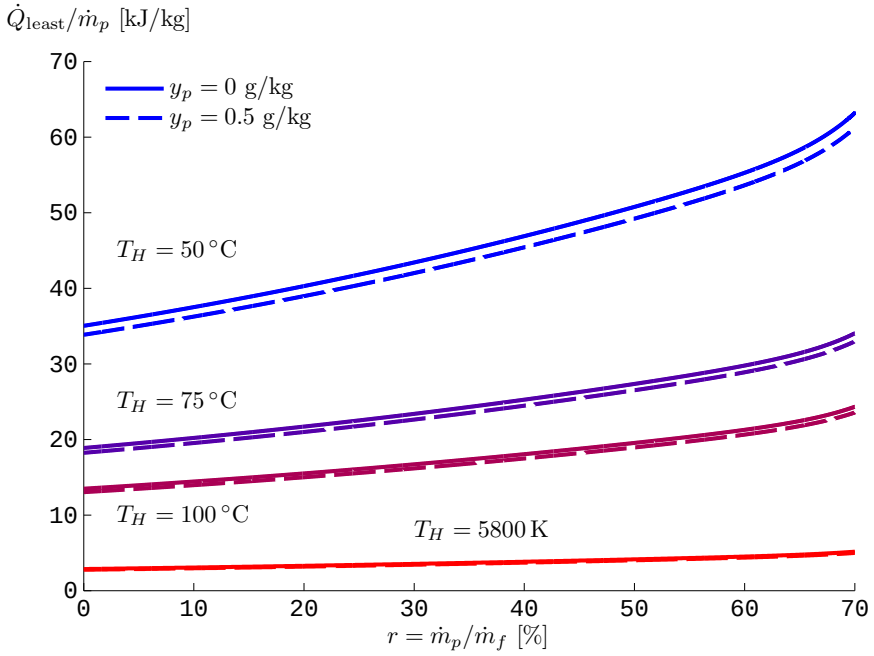

Figure 2-7: Least heat of separation as a function of feed salinity and recovery ratio. Feed water is at $T_0 = 25\,^\circ$C and $y_f = 35\,$g/kg.

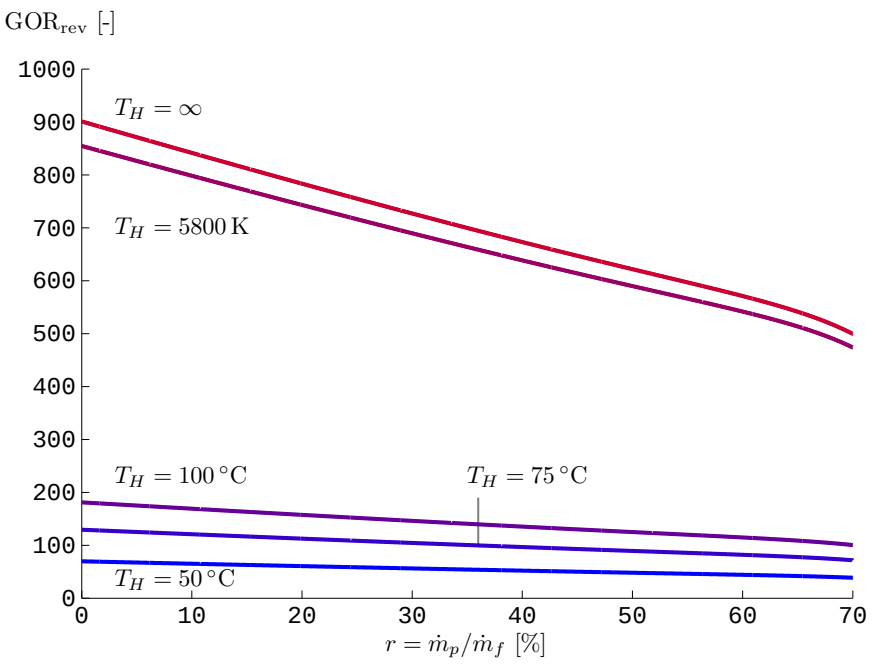

Figure 2-8: Maximum gained output ratio (GOR) for desalination processes with various temperatures of heat input. Feed water is at $T_0 = 25\,^\circ\mathrm{C}$ and $y_f = 35\,\mathrm{g/kg}$.

to note that Eq. (2.33) is valid as written only for a desalination system driven by heat; that is, a thermal desalination system. A work-driven desalination system, in contrast, uses electricity or shaft work to drive the separation process. Normally, this work is produced by a thermal process, such as a heat engine. Thus, to evaluate the heat input required for a work-driven desalination system, a First Law efficiency of the process that produces the work of separation must be known. The highest GOR possible for a given recovery ratio can be calculated by substituting Eq. (2.32) into Eq. (2.33):

$$\mathrm{GOR}_{\mathrm{rev}} \equiv \frac{\dot{m}_p h_{fg}(T_0)}{\dot{Q}_{\mathrm{least}}} \tag{2.34}$$

Reversible GOR is inversely proportional to the least heat; values are plotted in Fig. 2-8. Maximum GOR occurs in the limit of infinitesimal recovery since the least heat is minimized as $r \to 0$. In addition to solar temperature, the limit of GOR as temperature approaches infinity is included in the figure as well.

If the heat addition does not occur at a uniform temperature, then the summation in Eq. (2.19) should be replaced with:

$$\dot{Q} = \int \left(1 - \frac{T_0}{T}\right) \delta\dot{Q} \tag{2.35}$$

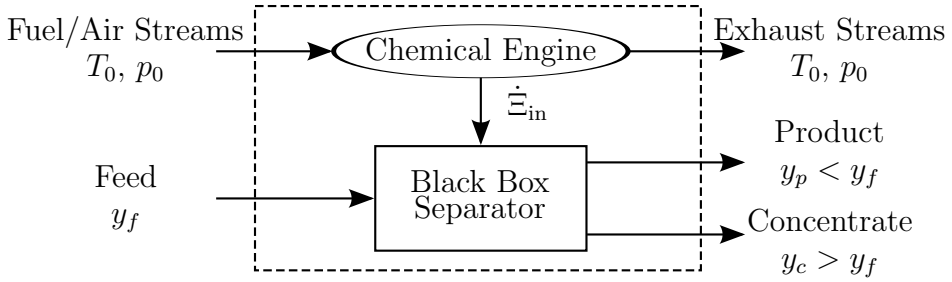

Figure 2-9: A control volume for an arbitrary black box chemical separator when fuel is the only form of energy input.

2.6 Least chemical energy (fuel) of separation

In some chemical separators, chemical energy is the only form of energy input, as shown in Fig. 2-9. In this case, Eq. (2.19) reduces to:

$$\underbrace{\sum_{\text{in}-\text{out}} \dot{N}\bar{\xi}(T,p,N_i)}_{\text{fuel and exhaust streams}} = \dot{\Xi}_{\text{least}} = \underbrace{\sum_{\text{out}-\text{in}} \dot{N}\bar{g}(T_0,p_0,N_i)}_{\text{process streams}} \tag{2.36}$$

Since exergy includes mechanical, thermal, and chemical components, the chemical energy component must be isolated in order to calculate the least chemical energy of separation. Therefore, the fuel is assumed to enter the system at the RDS even though some fuels are inherently not at the RDS (*e.g.*, CNG and LNG). While it is possible to calculate the least amount of fuel needed for fuels not at the RDS, the thermal and mechanical exergy should be accounted for as well. The calculations in this chapter focus purely on chemical exergy. The LHS of Eq. (2.36) may be expanded in terms of the chemical potential of each species within each stream. Further, the LHS of the equation represents the net chemical energy input,

$$\text{Net chemical energy input} = \dot{\Xi}_{\text{in}} = \underbrace{\sum_{\text{in}-\text{out}} \dot{N}\bar{\xi}(T_0,p_0,N_i)}_{\text{fuel and exhaust streams}} \tag{2.37}$$

In order to determine the least amount of fuel required for a chemical separation process, the above equation must be evaluated in the context of specific situations. In the following sections, three different cases are considered.

2.6.1 Combustion

Bejan [31] and Moran [47] analyzed the exergy value of fuels in detail. The maximum amount of energy that can be extracted from a fuel is the amount of work that is extracted through complete combustion when the reactants and products enter and leave the system at the TDS with the fuel entering at the RDS (see Bejan [31, Fig. 7.16

Table 2.1: Chemical exergy of select fuels at $T_0 = 25\,^{\circ}\mathrm{C}$ and $p_0 = 1\,\mathrm{atm}$.

Fuel (Phase)	M_{fuel} [kg/mol]	$\bar{\xi}_{\mathrm{fuel}}$ [kJ/mol]	ξ_{fuel} [MJ/kg]
Hydrogen (g), H_2	0.00201588	235.2	116.6736
Carbon (s), C	0.01201070	410.5	34.1779
Methane (g), CH_4	0.01604246	830.2	51.7502
Propane (g), C_3H_8	0.04409562	2149.0	48.7350
Octane (l), C_8H_{18}	0.11422852	5408.7	47.3498

and Eq. (7.133)]). As an example, for the following reaction

$$\mathrm{C}_\alpha\mathrm{H}_\beta + \left(\alpha + \frac{\beta}{4}\right)\mathrm{O}_2 \longrightarrow \alpha\mathrm{CO}_2 + \frac{\beta}{2}\mathrm{H}_2\mathrm{O}_{\mathrm{vapor}} \tag{2.38}$$

the maximum amount of energy extractable (*i.e.*, exergy) is equal to the change in the chemical potential from the reactants at the restricted dead state to the products at the total dead state:

$$\bar{\xi}_{\mathrm{C}_\alpha\mathrm{H}_\beta} = \mu_{\mathrm{C}_\alpha\mathrm{H}_\beta} + \left(\alpha + \frac{\beta}{4}\right)\mu_{\mathrm{O}_2} - \alpha\mu_{\mathrm{CO}_2} - \frac{\beta}{2}\mu_{\mathrm{H}_2\mathrm{O,vapor}} \tag{2.39}$$

$$= -\Delta G_r^{\circ}(T_0, p_0) + RT_0 \ln \frac{x_{\mathrm{O}_2}^{\alpha+\beta/4}}{x_{\mathrm{CO}_2}^{\alpha} x_{\mathrm{H}_2\mathrm{O}}^{\beta/2}} \tag{2.40}$$

where the standard state Gibbs energy of reaction for the fuel is given as

$$\Delta G_r^{\circ} = \alpha\mu_{\mathrm{CO}_2}^{\circ}(T_0, p_0) + \frac{\beta}{2}\mu_{\mathrm{H}_2\mathrm{O}}^{\circ}(T_0, p_0) - \left[\mu_{\mathrm{C}_\alpha\mathrm{H}_\beta}^{\circ}(T_0, p_0) + \left(\alpha + \frac{\beta}{4}\right)\mu_{\mathrm{O}_2}^{\circ}(T_0, p_0)\right] \tag{2.41}$$

Exergy values for select fuels, evaluated using Eq. (2.40), are provided in Table 2.1 [31].

The total exergy provided by a given mass of fuel is therefore:

$$\Delta\dot{\Xi}_{\mathrm{in}} = \frac{\dot{m}_{\mathrm{fuel}}}{M_{\mathrm{fuel}}}\Delta\bar{\xi}_{\mathrm{C}_\alpha\mathrm{H}_\beta} \tag{2.42}$$

Therefore, the least fuel required to separate water is:

$$\frac{\dot{m}_{\mathrm{fuel,least}}}{\dot{m}_p} = \frac{(g_p - g_c) - \frac{1}{r}(g_f - g_c)}{\bar{\xi}_{\mathrm{fuel}}} M_{\mathrm{fuel}} \tag{2.43}$$

The least amount of fuel required for hydrogen gas, carbon, methane gas, propane gas, and octane liquid is shown in Fig. 2-10. As expected, those fuels with the highest energy density result in the lowest fuel requirements.

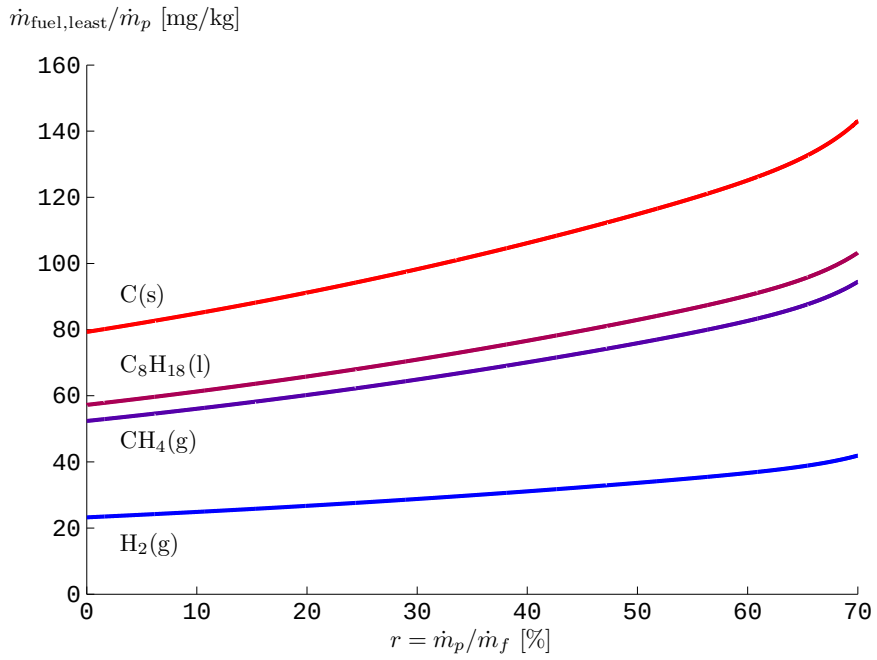

Figure 2-10: Least amount of fuel needed when using combustion as a function of fuel type and recovery ratio. Feed water is at $T_0 = 25\,°\text{C}$ and $y_f = 35\,\text{g/kg}$.

2.6.2 Chemical disequilibrium

While combustion of fuel is the most common way to extract chemical energy, other means are possible. For example, a given solution could be internally at disequilibrium with respect to all possible internal chemical reactions. As the solution runs down to equilibrium, energy may be released to the surroundings if the reactions are exothermic. This energy could be captured and used to power a chemical separation process. Consider a system that is powered using this energy release as the solution comes to chemical equilibrium with respect to all possible internal reactions. For this case, the initial stream at disequilibrium is referred to as the "fuel" and the stream once it has come to internal chemical equilibrium is referred to as the "exhaust." No mass exchange occurs between the fuel and the environment or any of the process streams. Since this system does not allow for mass transfer with the environment (the exhaust leaves at the RDS), the exergy of the fuel and exhaust streams reduces to the Gibbs Free energy:

$$\dot{\Xi}_{\text{in}} = \underbrace{\sum_{\text{in}-\text{out}} \dot{N}\bar{g}(T_0, p_0, N_i)}_{\text{fuel and exhaust streams}} \tag{2.44}$$

For a given stream, the flow Gibbs free energy is written as:

$$\dot{G} = \dot{N}\bar{g} = \dot{N}\sum_{i=1}^{n} x_i\mu_i = \sum_{i=1}^{n} \dot{N}_i\mu_i \tag{2.45}$$

where

$$\mu_i = \mu_i^\circ + RT \ln a_i \tag{2.46}$$

Therefore, the net chemical energy input to the system is:

$$\dot{\Xi}_{\text{in}} = \sum_{\text{in}-\text{out}} \left(\sum_{i=1}^{n} (\dot{N}_i \mu_i) \right) \tag{2.47}$$

Finally, if it is assumed that there is a single fuel stream (includes fuel and air) and a single exhaust stream (reaction products and remaining reactants), then

$$\dot{\Xi}_{\text{in}} = \sum_{\text{fuel}} \dot{N}_i \mu_i - \sum_{\text{exhaust}} \dot{N}_i \mu_i \tag{2.48}$$

Now that the net chemical energy input has been rewritten in a more useful form, the amount of energy input to the system from several chemical processes are considered. For a single chemical reaction of the form:

$$a\text{A} + b\text{B} \rightleftharpoons c\text{C} + d\text{D} \tag{2.49}$$

the Gibbs free energy of reaction, ΔG_r is given by

$$\Delta G_r = c\mu_\text{C} + d\mu_\text{D} - a\mu_\text{A} - b\mu_\text{B} \tag{2.50}$$

ΔG_r represents the change in Gibbs free energy of the system as a result of a differential advancement of the chemical reaction. That is,

$$\Delta G_r = \frac{\text{d}G}{\text{d}\zeta} \qquad \text{where } \text{d}\zeta = \frac{\text{d}n_i}{\nu_i} \tag{2.51}$$

where ζ is the reaction coordinate, n_i is the moles of species i, and ν_i is the stoichiometric coefficient of species i. The reaction coordinate is positive for products and negative for reactants. Substituting Eq. (2.46) into Eq. (2.50),

$$\begin{aligned} \Delta G_r &= (c\mu_\text{C}^\circ + d\mu_\text{D}^\circ - a\mu_\text{A}^\circ - b\mu_\text{B}^\circ) + RT \ln \frac{a_\text{C}^c a_\text{D}^d}{a_\text{A}^a a_\text{B}^b} \\ &= \Delta G_r^\circ + RT \ln Q \end{aligned} \tag{2.52}$$

where Q is the reaction quotient. These equations may be generalized to account for more complex reactions than those of the form indicated by Eq. (2.49):

$$\Delta G_r = \sum_{i=1}^{n} \nu_i \mu_i \qquad \Delta G_r^\circ = \sum_{i=1}^{n} \nu_i \mu_i^\circ \qquad Q = \prod_{i=1}^{n} a_i^{\nu_i} \tag{2.53}$$

At equilibrium, the change in Gibbs free energy is zero and the reaction quotient,

Q, is equal to the equilibrium coefficient:

$$\Delta G_r^\circ = -RT \ln K_{\text{eq}} \tag{2.54}$$

Therefore,

$$\Delta G_r = -RT \ln K_{\text{eq}} + RT \ln Q = RT \ln \frac{Q}{K_{\text{eq}}} \tag{2.55}$$

Equation (2.51) is separated and integrated from zero reaction progress to equilibrium ($\zeta = 0 \to \zeta^*$):

$$\dot{\Xi}_{\text{in}} = -\frac{\dot{m}_{\text{fuel}}}{M_{\text{fuel}}} \int_0^{\zeta^*} \Delta G_r \mathrm{d}\zeta = -\frac{\dot{m}_{\text{fuel}}}{M_{\text{fuel}}} \int_0^{\zeta^*} RT \ln \frac{\prod_{i=1}^n a_i^{\nu_i}(\zeta)}{K_{\text{eq}}} \mathrm{d}\zeta \tag{2.56}$$

Note that the activity of each component, and therefore the reaction quotient and the Gibbs free energy of reaction, are all functions of the reaction progress making the previous equation non-trivial to evaluate for complex reactions. While the theory is the same for multiple-reaction systems, the coupling and nonlinearity of the reactions greatly complicates the calculation.

By convention, ΔG_r is written per mole of the primary reactant. Therefore, the above equation is multiplied by the number of moles of fuel to determine the total energy released in the chemical reaction. Combining Eqs. (2.24), (2.36), and (2.56) gives the least mass of primary reactant needed to drive a separation process using the energy released in the equilibration of chemical species:

$$\frac{\dot{m}_{\text{fuel,least}}}{\dot{m}_p} = -\frac{(g_p - g_c) - \frac{1}{r}(g_f - g_c)}{RT \int_0^{\zeta^*} \ln \frac{\prod_{i=1}^n a_i^{\nu_i}(\zeta)}{K_{\text{eq}}} \mathrm{d}\zeta} M_{\text{fuel}} \tag{2.57}$$

Equation (2.57) is now evaluated for a simplified case in which the energy of solvation released when a salt of the form CA is dissolved in water is used as the driver for the chemical separation process. Equation (2.49) reduces to a simplified form for dissolution reactions:

$$\mathrm{CA} \rightleftharpoons \nu_+ \mathrm{C}^{z+} + \nu_- \mathrm{A}^{z-} \tag{2.58}$$

Activity for each of the dissolved species is written as the product of the molal activity coefficient and the molality: $a_i = \gamma_i m_i$ [23–25]. Activity of the pure salt, CA, is equal to one by definition. Using the definition for reaction progress given in Eq. (2.51), the molality of each of the ions is found to be the product of the stoichiometric coefficient for that ion and the reaction coordinate: $\nu_i \zeta$. Therefore, the activities of CA, C^{z+}, and A^{z-}, expressed in terms of ζ, are:

$$a_{\mathrm{CA}} = 1, \qquad a_{\mathrm{C}^{z+}} = \gamma_+ \nu_+ \zeta, \qquad a_{\mathrm{A}^{z-}} = \gamma_- \nu_- \zeta \tag{2.59}$$

Substituting Eq. (2.59) into Eq. (2.50), the Gibbs free energy of this reaction

reaction is:

$$\Delta G_r = RT \ln \frac{Q(\zeta)}{K_{\text{sp}}} = RT \ln \frac{(\gamma_+^{\nu_+}\gamma_-^{\nu_-})(\nu_+^{\nu_+}\nu_-^{\nu_-})\zeta^{\nu_+ + \nu_-}}{K_{\text{sp}}} \tag{2.60}$$

Substitution into Eq. (2.56) and assuming ideal solution behavior to simplify the calculation (γ is a complex function of ζ) gives:

$$\dot{\Xi}_{\text{in}} = -\frac{\dot{m}_{\text{salt}}}{M_{\text{salt}}} RT\zeta^* \left[\ln \left(\frac{\nu_+^{\nu_+}\nu_-^{\nu_-}}{K_{\text{sp}}} \zeta^{*\nu_+ + \nu_-} \right) - (\nu_+ + \nu_-) \right] \tag{2.61}$$

The equilibrium condition is found by setting $\Delta G_r = 0$ and solving for Eq. (2.60) for ζ:

$$\zeta^* = \left[\frac{K_{\text{sp}}}{\nu_+^{\nu_+}\nu_-^{\nu_-}} \right]^{\frac{1}{\nu_+ + \nu_-}} \tag{2.62}$$

Substituting into $\dot{\Xi}_{\text{in}}$ gives

$$\dot{\Xi}_{\text{in}} = \frac{\dot{m}_{\text{salt}}}{M_{\text{salt}}} RT \left(\nu_+ + \nu_-\right) \left[\frac{K_{\text{sp}}}{\nu_+^{\nu_+}\nu_-^{\nu_-}} \right]^{\frac{1}{\nu_+ + \nu_-}} \tag{2.63}$$

Finally, the least amount of salt dissolution required is:

$$\frac{\dot{m}_{\text{salt,least}}}{\dot{m}_p} = \frac{(g_p - g_c) - \frac{1}{r}(g_f - g_c)}{RT(\nu_+ + \nu_-) \left[\frac{K_{\text{sp}}}{\nu_+^{\nu_+}\nu_-^{\nu_-}} \right]^{1/(\nu_+ + \nu_-)}} M_{\text{salt}} \tag{2.64}$$

Figure 2-11 shows the amount of salt needed to drive a separation process when $CaSO_4$ and Ag_2SO_4 are used. From the results of Fig. 2-11, it is clear that using the energy of solvation for a salt to chemically separate another electrolyte solution is not a practical process since it would require very large quantities of both salt and water and would be unrealistically expensive. In the case of Ag_2SO_4, at the minimum, it requires approximately 7 kg for every kilogram of water produced while nearly 15 kg of $CaSO_4$ is required to produce a kilogram of water. This methodology is given not to suggest that dissolution reactions are a practical way to extract energy, but rather to illustrate a method for evaluating the energy release in an arbitrary chemical reaction.

2.6.3 Electrochemical reactions

Consider a system that is powered by an oxidation-reduction (REDOX) reaction in a fuel cell [48, 49]. As with chemical equilibration reactions, the Gibbs free energy of reaction is:

$$\Delta G_r = \sum_i \nu_i \mu_i = \Delta G_r^\circ + RT \ln Q \tag{2.65}$$

The electromotive force (voltage) generated by a REDOX reaction is found by noting that $\Delta G_r = -n_e F E$ where n_e is the number of electrons transferred per mole of

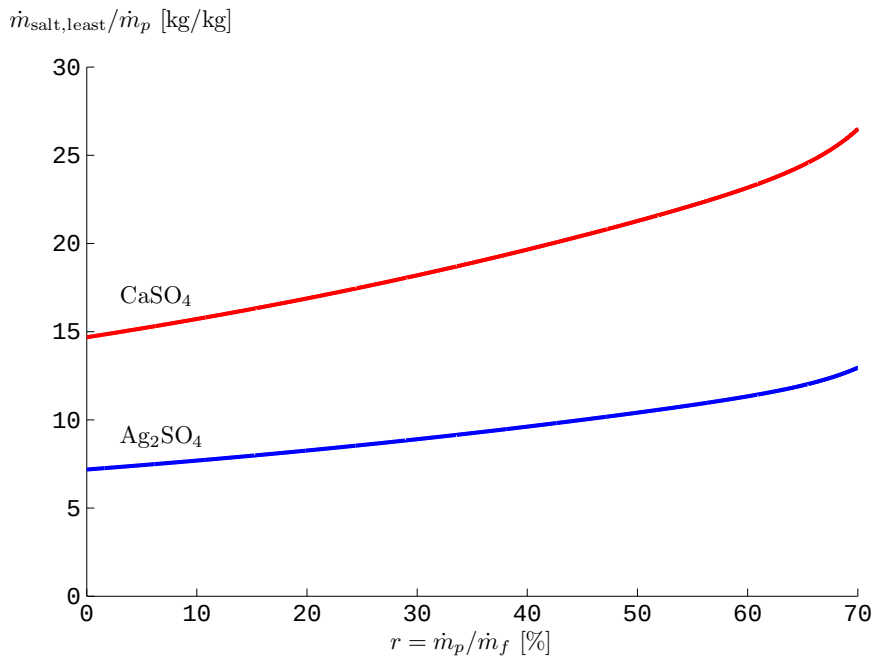

Figure 2-11: Least amount of salt needed when letting a salt dissociate to equilibrium as a function of recovery ratio for $CaSO_4$ and $AgSO_4$. Feed water is at $T_0 = 25\,°C$ and $y_f = 35\,g/kg$.

reactant and F is Faraday's constant. Therefore,

$$-\frac{\Delta G_r}{n_e F} = -\frac{\Delta G_r^\circ}{n_e F} - \frac{RT}{n_e F}\ln Q \tag{2.66}$$

$$E = E^\circ - \frac{RT}{n_e F}\ln Q \tag{2.67}$$

Equation (2.67) is known as the Nernst equation. At 25 °C, it is equal to:

$$E = E^\circ - \frac{0.059}{n_e}\log Q \tag{2.68}$$

The power drawn from an electrochemical cell is found by multiplying the current drawn by the voltage. The current is the charge drawn per time,

$$I = \frac{\text{charge}}{\text{time}} = \frac{n_e e N_a N}{t} = \frac{n_e F N}{t} \tag{2.69}$$

where n_e is the number of electrons per mole of reactant, e is the electron charge, $F = eN_a$, and N is the number of moles of reactant.

$$\dot{\Xi}_{\text{in}} = \sum_{\text{reactants}} \dot{N}_i\mu_i - \sum_{\text{products}} \dot{N}_i\mu_i = -\dot{N}\sum_i \nu_i\mu_i = -\dot{N}\Delta G_r = -\frac{N}{t}n_e F\frac{\Delta G_r}{-n_e F} = IE \tag{2.70}$$

Therefore,

$$\dot{\Xi}_{\text{in}} = IE = \dot{N} n_e F \left(E^\circ - \frac{RT}{n_e F} \ln Q \right) \tag{2.71}$$

Note that for an electrochemical reaction, the change in Gibbs free energy of the reactants minus the products is equal to current times voltage difference (power) which is exactly equal to the power associated with electrical work.

If the products of the fuel cell reaction are allowed to come to chemical equilibrium with the environment, then the reaction quotient will be a function of the activities of the products and reactants at ambient conditions. Under such conditions, Eq. (2.71) reduces to the exergetic value of fuels as seen in the combustion case and Eq. (2.43) can be used to evaluate the least mass of fuel required when driving a separation process using a fuel cell. Therefore, Fig. 2-10 also represents the least amount of fuel needed to drive a separation process when the fuel is used in a fuel cell. This result is expected since the exergetic value of a fuel is independent of the manner in which the chemical energy is extracted.

2.6.4 Limitations

In order to use this methodology as described in the preceding sections, it is essential that the process streams do not exchange mass with the fuel and exhaust streams. If mass exchange were allowed between the process streams and the fuel and exhaust streams, then it would be impossible to clearly define the change in Gibbs free energy of the process streams and the change in exergy of the fuel/exhaust streams as shown in Eq. (2.19) since conservation of mass over these summations would not be maintained. For systems in which there is mass exchange between the process streams and the fuel/exhaust streams, some care is needed in how each of the streams are classified. In order to illustrate how to apply this methodology to such systems, a work-driven system with a chemical energy assist stream is considered in the following section.

2.7 Least work of separation with an assist stream

Some chemical separation processes use an additional process stream in order to assist the overall separation process and reduce the amount of energy input required. One such process is RO coupled with an FO-based energy recovery device (ERD), as shown in Fig. 2-12 [50–52]. In this system, high salinity brine from the RO module is passed through an FO module in which H_2O from a chemical energy assist stream (denoted a) of a different chemical composition is transfered through the FO membrane from the assist stream to the concentrated brine. The additional H_2O transferred to the brine stream allows for a higher volumetric flow rate through the pressure exchanger, thus reducing the amount of feed that must be pressurized through the high pressure pump prior to entering the RO module and reducing the amount of electrical work that must be provided to the system [21].

This RO-FO system, and any other type of chemical separation process that relies on an additional process stream, can be abstracted to a variation of the simple black

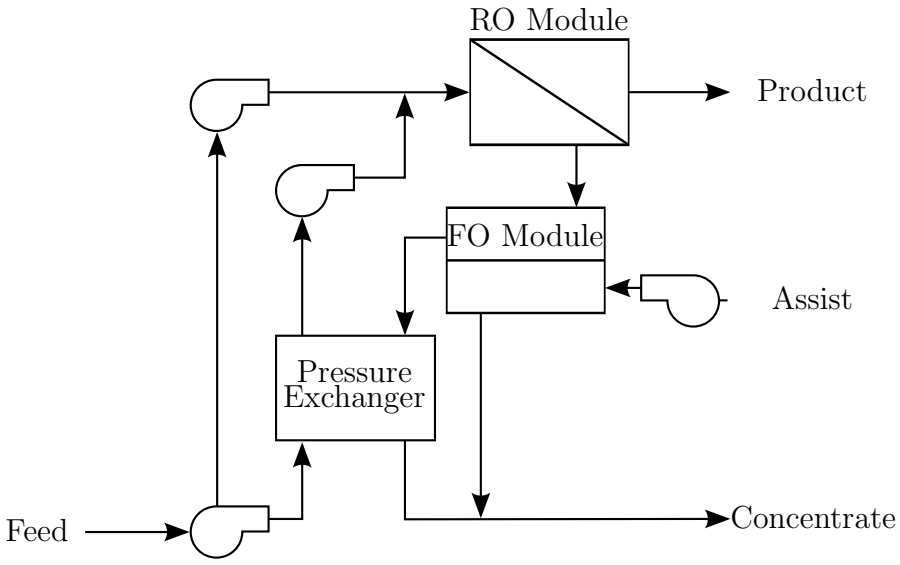

Figure 2-12: Schematic diagram of a typical single stage reverse osmosis system with a forward osmosis and pressure exchanger energy recovery devices.

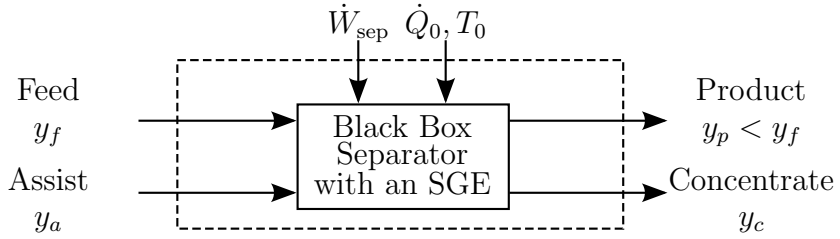

Figure 2-13: A control volume for an arbitrary black box chemical separator powered by work and a salinity gradient engine.

box separator model that has been used in Section 2.4. In this abstraction, the ERD is called a salinity gradient engine (SGE) to account for the fact that the net chemical energy difference between the feed and the assist might be greater than the energy required for the separation process, resulting in positive work output from the system. Note that the FO module and pressure exchanger shown in Fig. 2-12 are only capable of energy recovery, not power production. However, there are SGEs [*e.g.*, pressure retarded osmosis (PRO) and reverse electrodialysis (RED)] that are capable of net power production [53]. A control volume drawn around such a system reduces to a separator with an SGE, four process streams (feed, product, concentrate, and assist), a work input, and heat transfer with the environment (Fig. 2-13). Even though the assist stream is used for providing additional energy into the system, the assist stream cannot be considered a "fuel" stream since part of it is blended into the product stream. Therefore, it is counted as an additional process stream.

Equation (2.20) is expanded in terms of all four process streams:

$$\dot{\Xi}_{\text{least}} = \sum_{\text{out}-\text{in}} \dot{m} g(T_0, p_0, N_i) = \dot{m}_p g_p + \dot{m}_c g_c - \dot{m}_f g_f - \dot{m}_a g_a \tag{2.72}$$

Because there are two material input streams, two parameters are required to fully define the mass flow rates of each of the stream. The first parameter is the recovery ratio, as defined in Eq. (2.22). The second is the ratio of the mass flow rate of the energy recovery stream to the mass flow rate of the feed stream:

$$r_a \equiv \frac{\dot{m}_a}{\dot{m}_f} = \frac{\text{mass flow rate of energy recovery stream}}{\text{mass flow rate of feed}} \tag{2.73}$$

Conservation of mass for both the solution and the salts is written:

$$\dot{m}_f + \dot{m}_a = \dot{m}_p + \dot{m}_c \tag{2.74}$$

$$\dot{m}_f y_f + \dot{m}_a y_a = \dot{m}_p y_p + \dot{m}_c y_c \tag{2.75}$$

Equation (2.72) can be rewritten in terms of the two mass flow rate ratios by combining Eqs. (2.22), (2.73), and (2.74). Normalizing by the product flow rate gives:

$$\frac{\dot{W}_{\text{least}}}{\dot{m}_p} = (g_p - g_c) - \frac{1}{r}(g_f - g_c) - \frac{r_a}{r}(g_a - g_c) \tag{2.76}$$

Provided the salinities of the product, feed, and energy recovery stream are known, the salinity of the concentrate may be evaluated by combining Eqs. (2.22) and (2.73) to (2.75):

$$y_c = \frac{y_f + r_a y_a - r y_p}{1 + r_a - r} \tag{2.77}$$

Note that when $r_a = 0$, Eqs. (2.72), (2.76), and (2.77) reduce to Eqs. (2.21), (2.24), and (2.26). Equation (2.76) can be equated to Eq. (2.19) to express the generalized least energy of separation for a black box separator that includes an SGE and an assist stream. Additionally, all of the conclusions found from the previous sections can be applied to systems of this nature. For brevity, only work input will be considered for the example in this section.

Equation (2.76) is a function of the salinity of each of the four streams, the recovery ratio, the ratio of the mass flow rates of the assist to the feed, temperature, and pressure. For standard seawater at ambient conditions and pure product water, the equation is still a function of r, r_a, and y_a.

First, consider the effect of varying the mass flow rate of the assist stream while holding the salinity of the assist fixed and equal to that of the feed (*i.e.*, $y_a = y_f = 35\,\text{g/kg}$). Additionally, for the sake of simplicity, it is assumed that the assist stream has the same ionic composition as the feed water and that seawater properties may be used [25, 45]. Since the assist has the same salinity (and composition) as the feed water, the total feed to the system can be considered the sum of $\dot{m}_f$ and $\dot{m}_a$ while the product flow rate is fixed. Therefore, as r_a increases, the least work of separation will decrease, as is observed in Fig. 2-14. In the limit as $r_a \to \infty$, the least work of separation approaches the minimum least work of separation, regardless of recovery ratio, since this situation corresponds to the case of infinitesimal recovery [*cf.*, Eq. (2.27)].

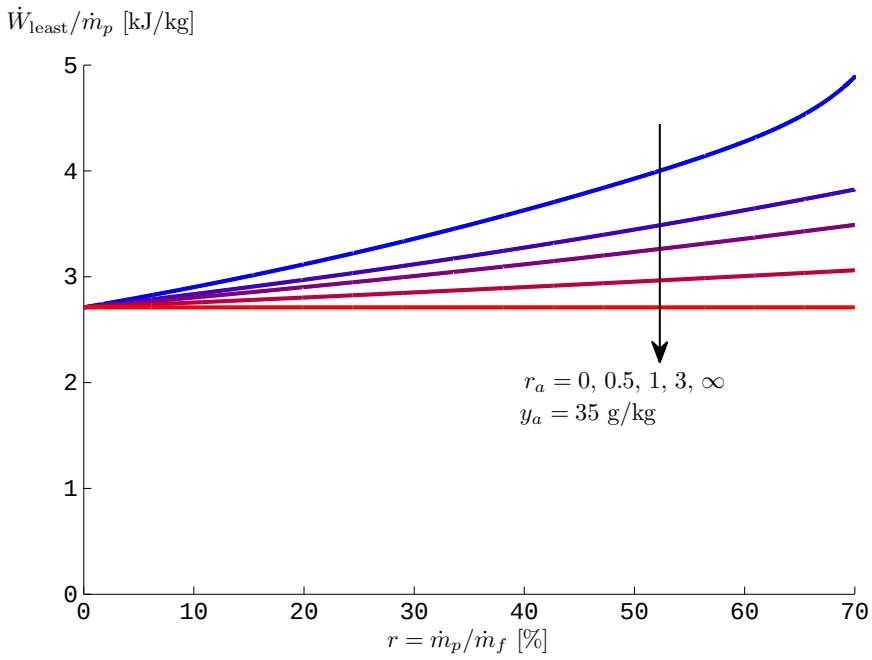

Figure 2-14: Least work of separation for a black box separator with a salinity gradient engine as a function of feed salinity, recovery ratio, and ratio of the energy recovery stream to the feed. Feed water is at $T_0 = 25\,^{\circ}\text{C}$ and $y_f = 35\,\text{g/kg}$.

The case of varying the salinity of the assist while holding r_a fixed results in more interesting (and useful) observations. To examine the effect of varying assist salinity, the flow rate of the assist is held fixed and equal to the flow rate of the feed (*i.e.*, $\dot{m}_a = \dot{m}_f$, or $r_a = 1$). The least work of separation under these conditions with the salinity of the assist varying from 25 to 45 g/kg is shown in Fig. 2-15. Additionally, the least work without the SGE (*i.e.*, $r_a = 0$) is also shown in black for reference. Several important observations can be made from Fig. 2-15. First, at higher recovery ratios, the least work of separation for the system with an SGE decreases with decreasing assist salinity. In all cases, the least work is less than the base case without an SGE since the process is effectively treating a greater amount of feed at a lower recovery ratio than the base system. Second, for all assist streams that are at a salinity that is different than the feed salinity (both greater and less than), as recovery ratio approaches zero, the least work approaches negative infinity. This occurs because the difference in salinity between the assist and the feed represents a chemical energy potential that can be used to drive the separation process.

As the recovery ratio approaches zero, however, the chemical energy potential exceeds the work requirements, and therefore, the system becomes a net work producing system with negative values of work of separation. The tendency toward infinite work production is an artifact caused by plotting least work divided by product flow rate when product flow rate approaches zero. This apparent singularity is not observed in the base case of no assist ($r_a = 0\,\text{kg/kg}$) since the rate at which the least work approaches zero is faster than the rate at which $\dot{m}_p$ approaches zero. However, in the

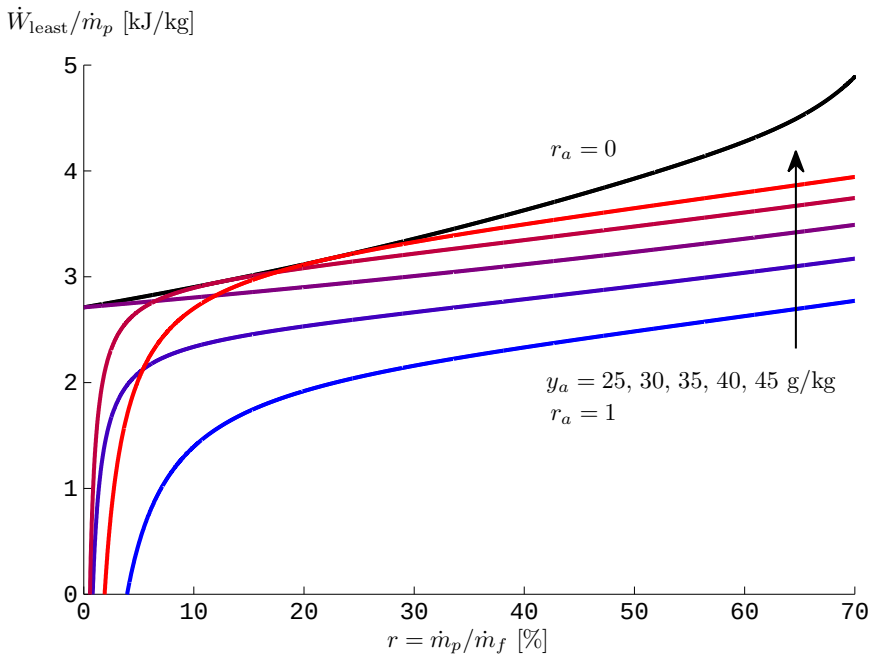

Figure 2-15: Least work of separation for a black box separator with a salinity gradient engine as a function of feed salinity, recovery ratio, and salinity of the energy recovery stream. Feed water is at $T_0 = 25\,^{\circ}\text{C}$ and $y_f = 35\,\text{g/kg}$.

present case of a system with an assist, the least work is a function of both the amount of energy required to produce $\dot{m}_p$ and the amount of energy that can be produced as a result of the chemical energy difference between the feed stream and the assist. While the work required to produce $\dot{m}_p$ approaches zero in the limit of infinitesimal recovery, the chemical energy difference between the feed and assist remains finite and therefore, the ratio of $\dot{W}_{\text{least}}/\dot{m}_p$ tends toward negative infinity. Finally, for assists that are at a greater salinity than the feed, there is a recovery ratio at which the least work requirement is exactly equal to the least work of the system without an SGE which corresponds to the point at which the least work curves are tangent to the base case least work. For recovery ratios near this critical point, the use of an SGE does not lead to significant energy savings.

Introduction of an additional material stream that mixes with the process streams changes the overall system performance characteristics. As shown in this example, under certain conditions, it is possible for the least exergy of separation to be negative when there is an additional energy carrying stream provided to the system. When the least exergy is negative, the system is work producing and the magnitude of $\dot{W}_{\text{least}}$ represents the maximum amount of work that can be produced from the four streams under reversible operation (*e.g.*, the reversible work produced by an osmotic power plant). It is not possible for least work to ever be negative if the only process streams are the feed, product, and concentrate, as was discussed in Sections 2.4 to 2.6.

2.8 Conclusions

In this chapter, the following conclusions have been reached:

1. The least exergy of separation is equal to the change in Gibbs free energy of all of the process streams involved in the separation (typically, feed, product, and concentrate). The exergy inputs can be in the form of work, heat, chemical energy (fuel), or some combination thereof.

2. The least exergy of separation is strictly a function of the composition of the feed and product as well as the recovery ratio and environmental temperature and pressure. If there is an assist stream, it is a function of the assist composition as well. It is not a function of the specific separation process used.

3. Least work of separation is equivalent to least exergy of separation. Least heat of separation is a strong function of the source temperature related through Carnot efficiency. Similarly, least mass of separation is inversely proportional to the chemical exergy of the fuel.

4. When separation systems have material input streams in addition to the feed stream, it is possible for the least exergy to be negative. Under such conditions, the separator becomes a work producing system and magnitude of the least exergy represents the maximum amount of work that can be produced through reversible operation. RO with an FO-based energy recovery device is one such system that relies on an additional material input stream.

Chapter 3

Nonidealities in electrolyte solutions

Chapter abstract

Proper evaluation of physical properties of aqueous solutions is essential in the analysis of desalination systems. While standard seawater property data are readily accessible, they are generally not accurate for aqueous solutions requiring desalination that have significantly different composition than seawater. Since experimental data for a given solution may be unavailable under the conditions of interest, thermodynamic models are needed for relevant physical properties, particularly, activity and fugacity coefficients. Effects of composition and nonidealities in electrolyte solutions are considered through a parametric study of the least work of separation.

First, the effect of nonidealities in a single electrolyte solution (*e.g.*, aqueous NaCl) is investigated and the conditions under which the ideal solution approximation and Debye-Hückel models are valid are determined. It is found that the ideal solution approximation is reasonable within ranges of salinities and recovery ratios typical of those found in the seawater desalination industry because many of the nonidealities cancel out, but not because the solution behaves ideally.

Second, conditions under which existing single electrolyte solution models, including ideal solution approximation, Debye-Hückel theory (Davies equation), and Pitzer's ionic interaction model, are valid when analyzing mixed electrolyte solutions are examined by comparing them to the Pitzer-Kim mixed electrolyte model. It is found that single electrolyte models often result in greater error than the ideal solution approximation when studying all but the most dilute mixed electrolyte solutions. Additionally, an effective molality can be used with the Pitzer model to increase the accuracy of the single electrolyte model as applied to mixed electrolytes. Finally, composition is a significant variable in the overall work of separation requirements.

This chapter consists of work that is published in [23–25].

3.1 Introduction

Accurate evaluation of physical properties of various water sources is essential to the reliable calculation of the energy requirements and performance characteristics of desalination systems. Despite the fact that seawater has been studied in depth and physical properties are well documented [43–45, 54], these properties are only appropriate for water sources that have an ionic composition similar to standard seawater [55]. Unfortunately, many natural and produced waters, including river water, ground water, flowback from hydraulic fracturing, and industrial waste waters, have ionic compositions that are substantially different from that of seawater [56]. Additionally, when studying nanofiltration systems, which may have different permeabilities for different solutes, the concentrate and product streams can have substantially different compositions from the feed stream. Further, scale formation in desalination systems is a direct function of the solution composition. Therefore, it is essential to evaluate physical properties for individual ionic compositions for many desalination-related calculations.

Accurate evaluation of solution properties requires treatment of the activity and

fugacity coefficients in order to properly address nonidealities. There are numerous ways to evaluate the activity coefficients, including Debye-Hückel theory and empirical data. For simplicity, it is common to use the ideal solution approximation, thus entirely avoiding the problem of setting the activity coefficients [30, 57–60]. Unfortunately, it is unclear when this approximation is justifiable.

In this chapter, the validity of the ideal solution approximation is analyzed through calculation of the least work of separation. Gibbs free energy for a sodium chloride (NaCl) solution is evaluated using various property models and the least work is evaluated as a function of feed salinity and recovery ratio. The NaCl solution results are also compared to the least work calculation evaluated using seawater properties because the use of aqueous NaCl solutions is common in laboratory studies of desalination systems [32, 61–64] as well as in industry [65].

Additionally, the validity of the ideal solution approximation as applied to mixed electrolytes of complex composition is also considered. Gibbs free energy for electrolyte solutions is evaluated using several common property models including the ideal solution approximation, Debye-Hückel theory (specifically, Davies equation), Pitzer's ion interaction model, and the Pitzer-Kim model for mixed electrolytes. A parametric study is conducted in which the least work of separation is evaluated as a function of feed salinity and recovery ratio using each of these models. The Pitzer-Kim model for mixed electrolytes is used as a reference to which calculations using the other models are compared. This model is taken as standard because it is based on theory and experimental data and is able to accurately predict activity coefficients across a broad range of compositions and concentrations [29, 66].

It is found that for salinities and recovery ratios typically found in desalination systems, the ideal solution approximation has lower-than-expected error due to fortuitous cancellation of terms, rather than near-ideal solution behavior. The parametric study also shows that use of single electrolyte models for the evaluation of activity and fugacity coefficients of mixed electrolyte solutions often results in substantially greater error than the error resulting from use of the ideal solution approximation. However, the Pitzer ion interaction model can be modified in order to achieve better agreement with the more complicated Pitzer-Kim model for mixed electrolytes. Finally, it is shown that the composition of an electrolyte solution is a significant variable in determining the least work of separation, and therefore, standard seawater properties are not appropriate to use for arbitrary electrolyte solutions.

3.2 Essential chemical thermodynamics

The Gibbs free energy of a mixture is

$$G \equiv \sum_i n_i \mu_i \tag{3.1}$$

Table 3.1: Constants and chemical data

Constant	Value	Units
e	$1.602176565 \times 10^{-19}$	C
F	96.4853365×10^{3}	C/mol
$M_{\mathrm{H_2O}}$	18.00988×10^{-3}	kg/mol
N_a	$6.02214129 \times 10^{23}$	1/mol
R	8.3144621	J/(mol K)
ϵ_0	$8.854187817620 \times 10^{-12}$	F/m

where n_i and μ_i are the number of moles and chemical potential of species i, respectively. Chemical potential is defined as

$$\mu_i \equiv \mu_i^\circ + RT \ln a_i \tag{3.2}$$

Proper evaluation of Gibbs free energy requires careful treatment of the activity (a_i) of each species [29, 66–70].

Values of constants used in the following analysis are summarized in Table 3.1.

3.2.1 Solvent

The standard state for the solvent is that of the pure liquid at the same temperature and pressure. Since the pure solvent coexists with its vapor when at equilibrium, the activity of the solvent is referenced to the pure vapor at the system temperature and 1 bar. Using a modified form of Raoult's Law in which all nonidealities are assumed to occur within the liquid mixture phase [29], the ratio of the partial pressure of the vapor over the solution and the partial pressure of the vapor over pure solvent is written in terms of the mole fraction [29, 67, 68]:

$$\mu_0 = \mu_0^\circ + RT \ln (\gamma_{f,0} x_0) \tag{3.3}$$

Therefore, the activity of the solvent is defined as

$$a_0 = \gamma_{f,0} x_0 \tag{3.4}$$

where $\gamma_{f,0}$ is the fugacity coefficient of the solvent.

3.2.2 Solutes

The chemical potential of a solute can be written in multiple ways, depending on the concentration scale used. For molality and mole fraction, the chemical potential is

written as

$$\mu_i = \mu^\circ_{m,i} + RT \ln a_{m,i} \tag{3.5}$$
$$= \mu^\circ_{x,i} + RT \ln a_{x,i} \tag{3.6}$$

Regardless of which concentration scale is used, the chemical potential is fixed for a given state since the free energy in the standard state (μ°_i, discussed later) depends on the chosen scale [68]. Here, the solute activity is written as

$$a_{m,i} = \gamma_{m,i} m_i \tag{3.7}$$
$$a_{x,i} = \gamma_{x,i} x_i \tag{3.8}$$

Mean concentration and mean activity coefficients are often more convenient and practical to use when considering electrolyte salts. For a strong electrolyte salt, $\mathrm{C}_{\nu_+}\mathrm{A}_{\nu_-}$, which fully dissociates,

$$\mathrm{C}_{\nu_+}\mathrm{A}_{\nu_-} \longrightarrow \nu_+ \mathrm{C}^{z_+} + \nu_- \mathrm{A}^{z_-} \tag{3.9}$$

the mean activity of the dissociated salt molecule is derived from the activities of the individual ions. From Eqs. (3.1) and (3.2):

$$RT \ln a_{\mathrm{C}_{\nu_+}\mathrm{A}_{\nu_-}} = \nu_+ RT \ln a_+ + \nu_- RT \ln a_- \tag{3.10}$$
$$a_{\mathrm{C}_{\nu_+}\mathrm{A}_{\nu_-}} = a_+^{\nu_+} a_-^{\nu_-} \tag{3.11}$$

Using Eq. (3.7), the mean ionic activity of the ion pair is written as:

$$a_{\mathrm{C}_{\nu_+}\mathrm{A}_{\nu_-}} = (\gamma_{m,+} m_+)^{\nu_+} (\gamma_{m,-} m_-)^{\nu_-} = \gamma^\nu_{m,\pm} m^\nu_\pm \tag{3.12}$$

where the stoichiometric coefficient (ν), the mean molal activity coefficient ($\gamma_{m,\pm}$), and the mean molal concentration ($m_\pm$) are defined as:

$$\nu \equiv \nu_+ + \nu_- \tag{3.13}$$
$$\gamma^\nu_{m,\pm} \equiv \gamma^{\nu_+}_{m,+} \gamma^{\nu_-}_{m,-} \tag{3.14}$$
$$m^\nu_\pm \equiv m^{\nu_+}_+ m^{\nu_-}_- \tag{3.15}$$

The mean rational activity coefficient ($\gamma_{x,\pm}$) and the mean mole fraction ($x_\pm$) are similarly defined. For neutral electrolytes in which $\nu_+ = \nu_- = 1$, the mean molality of the salt is equal to the molality of the individual ions. That is, $m_{\mathrm{C}_{\nu_+}\mathrm{A}_{\nu_-}} = m_\pm = m_+ = m_-$.

The standard state of a solute is now defined as a hypothetical solution at a mean concentration of unity referenced to infinite dilution such that the mean activity coefficient is unity when mean concentration is zero, regardless of temperature and pressure [29, 67, 68]. Therefore, $\mu_i = \mu^\circ_i$ at standard state and $\mu^\circ_{m,i} \neq \mu^\circ_{x,i}$ [*cf.*, Eqs. (3.5) and (3.6)]. Activity coefficients corresponding to different concentration scales are not equal, even when evaluated at equivalent concentrations on the respective

scales. An equation to convert from molal to rational activity coefficient is derived by equating Eqs. (3.5) and (3.6) [29, 68]:

$$\gamma_{x,\pm} = \gamma_{m,\pm}\left(1 + M_0 \sum_s \nu_s m_s\right) \tag{3.16}$$

The summation in Eq. (3.16) is over all electrolyte salts (not solute species), m_s is the molality of each salt, and ν_s is the number of moles of ions formed per mole of salt.

For notational simplicity, the $\pm$ subscript is dropped going forward. Instead, it is understood that $\gamma_{x,s}$ and $\gamma_{m,s}$ are the rational and molal activity coefficients of salt species s while $\gamma_{x,i}$ and $\gamma_{m,i}$ are the corresponding activity coefficients of solute species i (*e.g.*, $\gamma_{x,\mathrm{NaCl}}$ is the rational activity coefficient of NaCl and is equal to $\gamma^2_{x,\mathrm{NaCl}} = \gamma^1_{x,\mathrm{Na^+}}\gamma^1_{x,\mathrm{Cl^-}}$).

3.3 Evaluation of activity coefficients

Fluid properties are evaluated in one of two ways in this study. Gibbs free energy of mixed electrolyte solutions is evaluated using Eqs. (3.1) and (3.2), which requires evaluation of the activity and fugacity coefficients. Standard seawater properties are evaluated using a freely-available software package that is based on correlations of experimental data [45, 71].

Activity coefficients for various solution species can be evaluated in many ways. In order of increasing complexity, the following methods are considered: ideal solution approximation, Debye-Hückel theory and the Davies equation, the Pitzer ion interaction model, and the Pitzer-Kim model for mixed electrolytes. While there are additional mixed electrolyte models including those by Guggenheim, Bromley, Meissner, and Chen [66], only the four models listed above are considered here since they represent the most commonly used methods for evaluating the activity coefficients and also span from very simple to complex and accurate [29, 66–68]. These models are based on a combination of statistical mechanical theory as well as curve fitting of empirical data.

Note that while it is common to evaluate single ion activity coefficients and mean molal activity constants for specific salts, single ion activity coefficients are only a useful analytical construct and not physically measurable [66, 69]. It can be shown that the use of single ion activity coefficients, at least in the instance of a single salt, gives algebraically equivalent results to the use of the mean molal activity constant.

3.3.1 Ideal solution

The ideal solution approximation is the simplest method for evaluating activity and fugacity coefficients. An ideal solution is defined as a solution in which the solutes do not interact with each other. Practically speaking, this means the solution is dilute and that solute long range (*e.g.*, electrostatic) forces are negligibly weak. An ideal solution has rational activity coefficients (for solutes) and fugacity coefficients (for

solvent) equal to one [29, 67, 68]:

$$\gamma_{x,s}^{\text{ideal}} = 1 \qquad \gamma_{f,0}^{\text{ideal}} = 1 \qquad \text{for all species} \tag{3.17}$$

Therefore, the activity (based on mole fraction) is equal to the mole fraction. Even though the rational activity coefficient is equal to one for an ideal system, the molal activity coefficient is *not* equal to one as evident from Eq. (3.16). Technically, the rational activity coefficient of each solute ($\gamma_{x,i}$) should be equal to one in the ideal limit; however, Eq. (3.14) shows that this is equivalent to setting the activity coefficient of the salt equal to one.

Due to its simplicity, the ideal solution approximation is widely used to analyze solutions. Unfortunately, it is easy to inadvertently use the model beyond its range of applicability and doing so can result in substantial error for even simple calculations [23, 24]. Additionally, it is incorrect to equate the molal activity coefficient, rather than the rational activity coefficient, to one.

3.3.2 Debye-Hückel theory and the Davies equation

Debye-Hückel theory for electrolytes gives the extended Debye-Hückel equation for activity coefficients [29, 66–68, 72–75]:

$$\log \gamma_{x,\pm} = -\frac{A|z_+ z_-|\sqrt{I_m}}{1 + Ba\sqrt{I_m}} \qquad I_m < 0.1 \tag{3.18}$$

where molal ionic strength (I_m) is defined in terms of molality and charge of each of the solute species.

$$I_m = \frac{1}{2}\sum_i m_i z_i^2 \tag{3.19}$$

where m_i is the molality (moles of solute per kilogram of solvent) of each solute, i. The summation is over all solute species. The constant, A, is defined as [29, 75]:

$$A_\phi = \frac{F^3}{24\pi N_a}\left[\frac{2000\rho_0}{(\epsilon_0\epsilon_r RT)^3}\right]^{1/2} \qquad A = 3A_\phi \log e = 1.8248\times 10^6\left[\frac{\rho_0}{(\epsilon_r T)^3}\right]^{1/2}\left[\frac{\text{kg}^{1/2}}{\text{mol}^{1/2}}\right]$$

At 25 °C, the static dielectric constant (or relative permittivity) of H_2O is $\epsilon_r = 78.54$ and the density of water is $\rho_{H_2O} = 0.997\,05\,\text{kg/L}$. Therefore, $A_\phi = 0.3903\,\text{kg}^{\frac{1}{2}}/\text{mol}^{\frac{1}{2}}$ and $A = 0.5085\,\text{kg}^{\frac{1}{2}}/\text{mol}^{\frac{1}{2}}$. B and a are additional parameters that are not used in this study.

In the limit of very low ionic strength, Eq. (3.18) reduces to the Debye-Hückel Limiting Law (DHLL):

$$\log \gamma_{x,\pm} = -A|z_+ z_-|\sqrt{I_m} \qquad I_m < 10^{-2.3} \tag{3.20}$$

Güntelberg proposed a simplification of Eq. (3.18) since for most common solutes,

$Ba \approx 1$.

$$\log \gamma_{x,\pm} = -\frac{A|z_+ z_-|\sqrt{I_m}}{1+\sqrt{I_m}} \qquad I_m < 0.1 \tag{3.21}$$

Davies proposed a modification of Eq. (3.18) which extends the range of ionic strength in which the equation can be used and gives accurate results for low ionic strength electrolyte solutions.

$$\log \gamma_{x,\pm} = -A|z_+ z_-| \left(\frac{\sqrt{I_m}}{1+\sqrt{I_m}} - bI_m \right) \qquad I_m < 0.5 \tag{3.22}$$

The constant b ranges from 0.2–0.3 depending on the solute. A value of $b = 0.2$ is used herein.

3.3.3 Pitzer ion interaction model for single electrolytes

The Pitzer ion interaction model for single electrolytes (referred to as the Pitzer equation or model) is developed based on the osmotic virial expansion from McMillan-Mayer theory [29]. The expansion is truncated and empirical fitting is used to specify the salt-specific coefficients in order to produce an acceptable model. The activity coefficient and osmotic coefficient for a single salt are evaluated using Eqs. (3.23) and (3.24), respectively [29, 66, 69, 76–80]:

$$\ln \gamma_{m,\mathrm{CA}} = |z_\mathrm{C} z_\mathrm{A}| f^\gamma + m \frac{2\nu_\mathrm{C}\nu_\mathrm{A}}{\nu} B^\gamma_\mathrm{CA} + m^2 \frac{2(\nu_\mathrm{C}\nu_\mathrm{A})^{3/2}}{\nu} C^\gamma_\mathrm{CA} \tag{3.23}$$

$$\phi - 1 = |z_\mathrm{C} z_\mathrm{A}| f^\phi + m \frac{2\nu_\mathrm{C}\nu_\mathrm{A}}{\nu} B^\phi_\mathrm{CA} + m^2 \frac{2(\nu_\mathrm{C}\nu_\mathrm{A})^{3/2}}{\nu} C^\phi_\mathrm{CA} \tag{3.24}$$

where

$$f^\phi = -A_\phi \frac{\sqrt{I_m}}{1+b\sqrt{I_m}}$$

$$f^\gamma = -A_\phi \left[\frac{\sqrt{I_m}}{1+b\sqrt{I_m}} + \frac{2}{b} \ln\left(1+b\sqrt{I_m}\right) \right]$$

$$B^\phi_\mathrm{CA} = \beta_0 + \sum_{k=1}^{2} \beta_k \exp\left(-\alpha_k \sqrt{I_m}\right)$$

$$B^\gamma_\mathrm{CA} = 2\beta_0 + \sum_{k=1}^{2} \frac{2\beta_k}{\alpha_k^2 I_m} \left[1 - \exp\left(-\alpha_k\sqrt{I_m}\right)\left(1+\alpha_k\sqrt{I_m} - 0.5\alpha_k^2 I_m\right) \right]$$

$$C^\gamma_\mathrm{CA} = \frac{3}{2} C^\phi_\mathrm{CA}$$

and $b = 1.2$. Tabulated data for β_i, α_i, and C^ϕ_CA for numerous salt species is available in the literature [29, 77, 78]. The constants α_2 and β_2 are only defined for 2:2 electrolytes. For non-2:2 electrolytes, $\beta_2 = 0$ is set to zero, reducing the second term of the sums in B^ϕ_CA and B^γ_CA to zero.

Equation (3.23) gives the molal activity coefficient. The rational activity coefficient is obtained using Eq. (3.16). The molal activity of water is written in terms of the molal osmotic coefficient [29, 68, 81]:

$$\ln a_{\mathrm{H_2O}} = -\nu m M_{\mathrm{H_2O}} \phi \tag{3.25}$$

The fugacity coefficient of the water is evaluated using Eqs. (3.3) and (3.25):

$$\ln \gamma_{f,\mathrm{H_2O}} = -\nu m M_{\mathrm{H_2O}} \phi - \ln x_{\mathrm{H_2O}} \tag{3.26}$$

3.3.4 Pitzer-Kim model for mixed electrolytes

As with the single electrolyte model, the Pitzer-Kim model for mixed electrolytes (referred to as Pitzer-Kim equation or model) is based on the osmotic virial expansion from McMillian-Mayer theory. Using a similar method of combining the virial coefficients, the mean activity coefficients for electrolyte $\mathrm{C}_{\nu_+}\mathrm{A}_{\nu_-}$ in a mixed solution can be calculated. This model considers binary and ternary interactions between all possible salt pairs in the solution. Higher order interactions are neglected [29, 66, 69, 76–80]:

$$\begin{aligned}
\ln \gamma_{\mathrm{CA}} = {} & |z_{\mathrm{C}} z_{\mathrm{A}}| f^{\gamma} + \frac{2\nu_{\mathrm{C}}}{\nu} \sum_a m_a \left[B_{\mathrm{C}a} + \left(\sum mz \right) C_{\mathrm{C}a} + \frac{\nu_{\mathrm{A}}}{\nu_{\mathrm{C}}} \theta_{\mathrm{A}a} \right] \\
& + \frac{2\nu_{\mathrm{A}}}{\nu} \sum_c m_c \left[B_{c\mathrm{A}} + \left(\sum mz \right) C_{c\mathrm{A}} + \frac{\nu_{\mathrm{C}}}{\nu_{\mathrm{A}}} \theta_{\mathrm{C}c} \right] \\
& + \sum_c \sum_a m_c m_a \left[|z_{\mathrm{C}} z_{\mathrm{A}}| B'_{ca} + \frac{1}{\nu} \left(2\nu_{\mathrm{C}} z_{\mathrm{C}} C_{ca} + \nu_{\mathrm{C}} \psi_{\mathrm{C}ca} + \nu_{\mathrm{A}} \psi_{ca\mathrm{A}} \right) \right] \\
& + \frac{1}{2} \sum_c \sum_{c'} m_c m_{c'} \left[\frac{\nu_{\mathrm{A}}}{\nu} \psi_{cc'\mathrm{A}} + |z_{\mathrm{C}} z_{\mathrm{A}}| \theta'_{cc'} \right] \\
& + \frac{1}{2} \sum_a \sum_{a'} m_a m_{a'} \left[\frac{\nu_{\mathrm{C}}}{\nu} \psi_{\mathrm{C}aa'} + |z_{\mathrm{C}} z_{\mathrm{A}}| \theta'_{aa'} \right]
\end{aligned} \tag{3.27}$$

In the last two terms, the summations over c' and a' are summations over all cations (or anions) other than the cation (or anion) from the outer sum.

$$\begin{aligned}
\phi - 1 = {} & \left(\sum_i m_i \right)^{-1} \left\{ 2 I_m f^{\phi} + 2 \sum_c \sum_a m_c m_a \left[B^{\phi}_{ca} + \frac{\sum mz}{\sqrt{z_c z_a}} C^{\phi}_{ca} \right] \right. \\
& + \sum_c \sum_{c'} m_c m_{c'} \left[\theta_{cc'} + I_m \theta'_{cc'} + \sum_a m_a \psi_{cc'a} \right] \\
& \left. + \sum_a \sum_{a'} m_a m_{a'} \left[\theta_{aa'} + I_m \theta'_{aa'} + \sum_c m_c \psi_{caa'} \right] \right\}
\end{aligned} \tag{3.28}$$

Here, f^{γ}, f^{ϕ} are defined as above for the Pitzer Ion Interaction Model. The

functions B, B', and C are defined as:

$$B_{ij} = B_{ij}^{\gamma} - B_{ij}^{\phi} = \beta_0 + \sum_{k=1}^{2} \frac{2\beta_k}{\alpha_k^2 I_m} \left[1 - \exp\left(-\alpha_k \sqrt{I_m}\right)\left(1 + \alpha_k \sqrt{I_m}\right)\right] \tag{3.29}$$

$$B'_{ij} = \sum_{k=1}^{2} \frac{2\beta_k}{\alpha_k^2 I_m} \left[-1 + \exp\left(-\alpha_k \sqrt{I_m}\right)\left(1 + \alpha_k \sqrt{I_m} + 0.5\alpha_k^2 I\right)\right] \tag{3.30}$$

$$C_{ij} = \frac{C_{ij}^{\phi}}{2\sqrt{z_{\mathrm{C}} z_{\mathrm{A}}}} \tag{3.31}$$

The θ and ψ terms in Eqs. (3.27) and (3.28) represent the binary and ternary interactions respectively and are tabulated [79]. The constants C_{ij}^{ϕ} are tabulated [77, 78]. In accordance with Pitzer's recommendation, the ionic strength dependence of θ is neglected in the present work (*i.e.*, $\theta' = 0$) [79].

Equation (3.27) gives the molal activity coefficient of electrolyte $\mathrm{C}_{\nu_+}\mathrm{A}_{\nu_-}$. The rational activity coefficient is obtained using Eq. (3.16) and the fugacity coefficient of the water is evaluated using a modified version of Eq. (3.26):

$$\ln \gamma_{f,\mathrm{H_2O}} = -\left(\sum_s \nu_s m_s\right) M_{\mathrm{H_2O}} \phi - \ln x_{\mathrm{H_2O}} \tag{3.32}$$

3.3.5 Pitzer model with effective molality for mixed electrolytes

The Pitzer model for single electrolytes is a function of both salt molality and solution ionic strength [*cf.*, Eqs. (3.23) and (3.24)]. For a single electrolyte solution, the molality and molal ionic strength are related by Eq. (3.19):

$$I_m = \frac{1}{2}\left(\nu_+ m z_+^2 + \nu_- m z_-^2\right) \tag{3.33}$$

In mixed electrolyte solutions, there is not a direct relationship between the molality of a single electrolyte and the overall solution ionic strength since the solution ionic strength is a function of the molalities of all electrolytes present. Therefore, the ionic strength can be significantly greater than what the single electrolyte molality would predict. In order to account for this effect, an effective molality is obtained by solving Eq. (3.33) for m:

$$m_{\text{effective}} = \frac{2I_m}{\nu_+ z_+^2 + \nu_- z_-^2} \tag{3.34}$$

This effective molality can be used with Eq. (3.23) in order to more accurately evaluate the activity coefficient of a single salt in a mixed electrolyte solution. Note that an effective molality must be evaluated for each electrolyte in solution and that values of ν_+, ν_-, z_+, and z_- depend on the specific cations and anions formed from the electrolyte being considered.

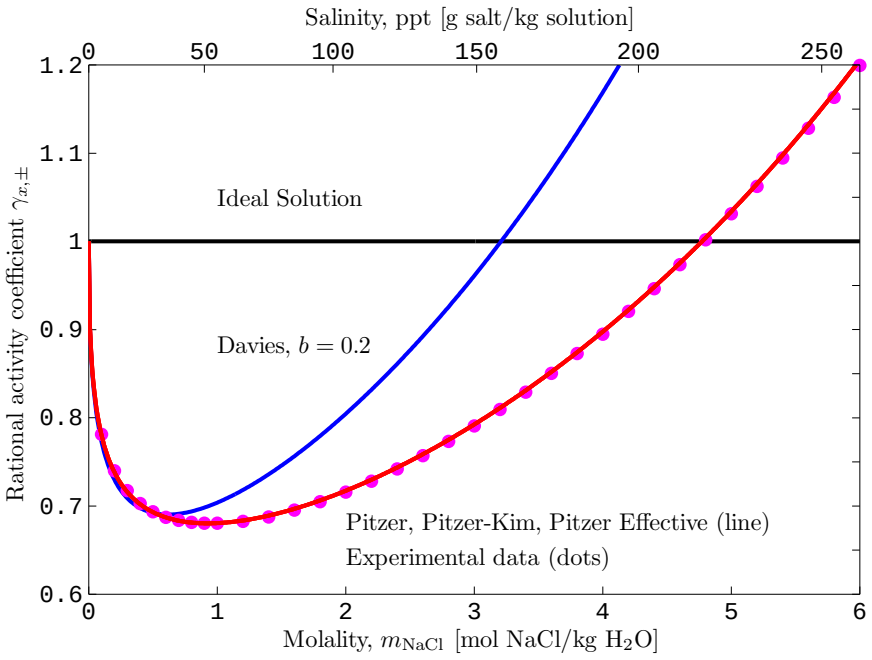

Figure 3-1: Rational activity coefficient for aqueous NaCl evaluated using ideal solution approximation, Davies equation, Pitzer's ion interaction model, and experimental data. Dots are data from [68].

In order to calculate the osmotic coefficient for a mixed electrolyte solution using Eq. (3.24), an effective osmotic coefficient should first be evaluated using Eq. (3.34) for each salt. The osmotic coefficient is the effective molality-weighted average of these effective osmotic coefficients:

$$\phi = \frac{\sum_i m_{\text{effective},i}\phi_{\text{effective},i}}{\sum_i m_{\text{effective},i}} \tag{3.35}$$

Pitzer's equations with an effective molality (referred to as effective Pitzer model) is substantially easier to implement than the Pitzer-Kim model and is a good approximation for the activity and fugacity coefficients as discussed in Section 3.7.

Plots of the rational activity coefficient for NaCl, $MgCl_2$, and Na_2SO_4 are shown in Figs. 3-1 to 3-3 respectively. It is observed that both the Pitzer-Kim model and the effective Pitzer model reduce to the Pitzer model when they are evaluated for a single electrolyte solution in all cases. Additionally, it is observed that for molalities less than approximately 0.5, Davies equation closely approximates available data, but then quickly diverges at higher concentrations.

3.3.6 Experimental data

The most accurate method for evaluating activity coefficients is to use experimental data. Robinson and Stokes [68] and Pitzer *et al.* [82] have tabulated data for the molal activity coefficient of NaCl in H_2O as a function of molality. The data was curve fitted

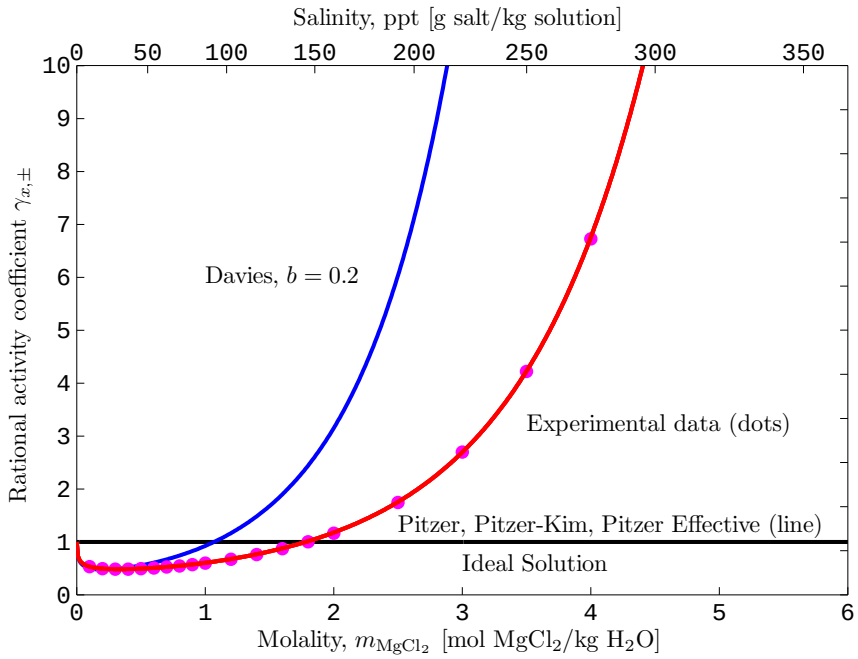

Figure 3-2: Rational activity coefficient for aqueous $MgCl_2$ evaluated using ideal solution approximation, Davies equation, Pitzer's ion interaction model, and experimental data. Dots are data from [68].

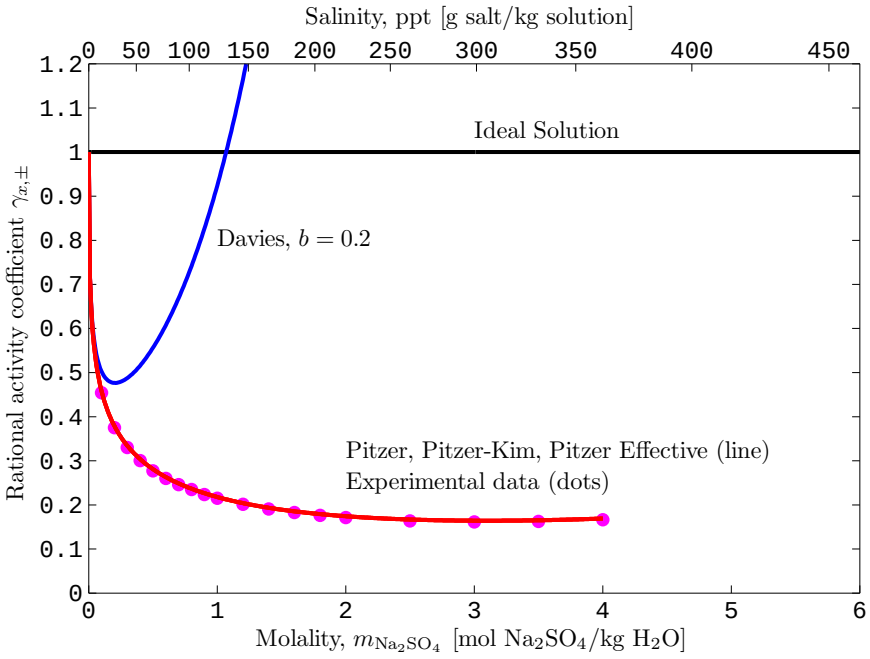

Figure 3-3: Rational activity coefficient for aqueous Na_2SO_4 evaluated using ideal solution approximation, Davies equation, Pitzer's ion interaction model, and experimental data. Dots are data from [68].

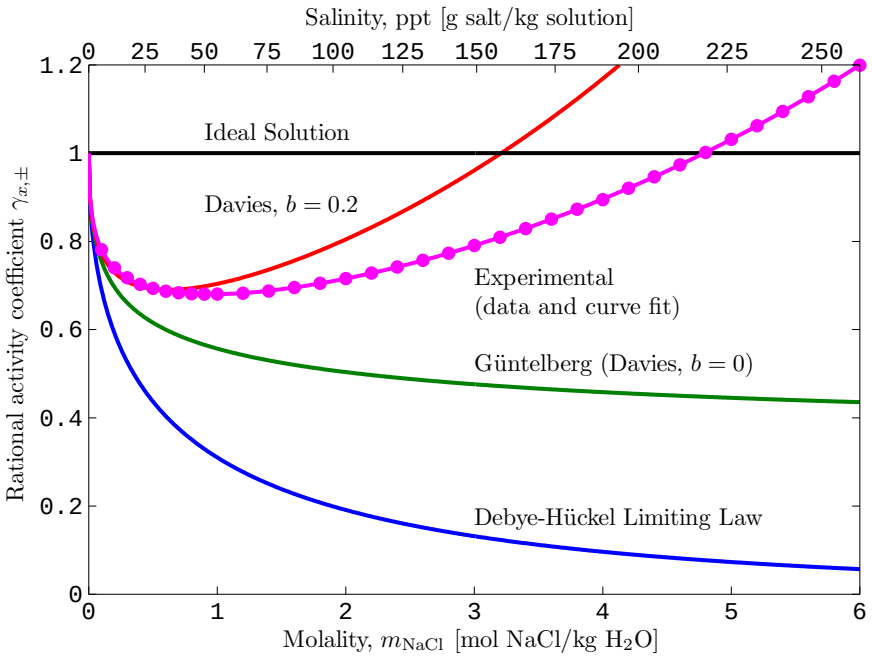

Figure 3-4: Rational activity coefficient for NaCl in H_2O evaluated using Debye-Hückel theory for electrolyte solutions and using experimental data. Dots are data from [68].

in MATLAB [83] using a modified form of the Debye-Hückel equations:

$$\gamma_{m,\pm} = 10^{-a\left(\frac{\sqrt{m}}{1+c\sqrt{m}} - bm\right)} + dm + em^2 + fm^3 \tag{3.36}$$

where $a = 0.5131$, $b = 0.17$, $c = 1.408$, $d = -0.09262$, $e = 0.002$, and $f = -0.001259$. This curve fit has a $1 - R^2$ value of 9×10^{-6}. The rational activity coefficient is then evaluated by substituting Eq. (3.36) into Eq. (3.16).

The mean rational activity coefficient of NaCl in H_2O, evaluated using Eqs. (3.20) to (3.22) is plotted as a function of molality in Fig. 3-4 as solid lines. Additionally, the original data and Eq. (3.36) are converted to rational activity coefficient using Eq. (3.16) and plotted as dots and a solid line, respectively.

The molal activity of water can be written in terms of the molal osmotic coefficient using Eq. (3.25). The osmotic coefficient, ϕ, is curve fit to data provided by Robinson and Stokes [68] and Pitzer *et al.* [82] using the same functional form as Eq. (3.36):

$$\phi = 10^{-a\left(\frac{\sqrt{m}}{1+c\sqrt{m}} - bm\right)} + dm + em^2 + fm^3 \tag{3.37}$$

where $a = 0.1924$, $b = 0.3506$, $c = 2.798$, $d = -0.1019$, $e = -0.001201$, and $f = -0.001324$. This curve fit has a $1 - R^2$ value of 5×10^{-6}.

Using the curve fit, the fugacity coefficient of the water is evaluated using Eq. (3.26).

Osmotic coefficient, fugacity coefficient, mole fraction, and activity of H_2O is plotted versus molality in Fig. 3-5.

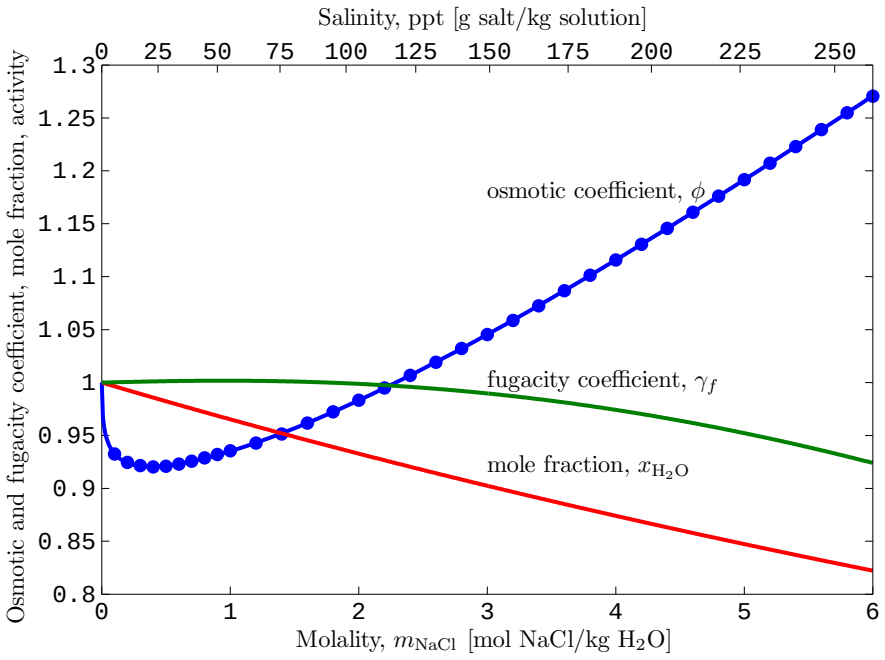

Figure 3-5: H_2O data for NaCl solution. Dots are data [68]. Solid lines are curve fits.

3.3.7 Empirical correlations

There have been multiple attempts to create seawater property packages [43–45]. The work by Sharqawy *et al.* [45, 71] is used in this study. Correlations for properties such as specific Gibbs free energy, osmotic coefficients, and chemical potential of water and salts in seawater are given as a function of temperature and salinity. The range of validity of the correlations varies slightly for each property, but in general, they are applicable for temperatures between 0–120 °C and salinities between 0–120 g/kg. Note that this property package provides properties per kilogram of solution (seawater).

3.4 Least work of separation

The least work of separation ($\dot{W}_{\text{least}}$) is a commonly used metric in desalination which defines the minimum amount of work required to separate a chemical stream into two streams of differing composition in the thermodynamic limit of reversible operation [16, 21, 22, 27–29]. It is a benchmark to which desalination systems are compared, much as Carnot efficiency is an ideal benchmark for power plants. Typically, the least work of separation is evaluated per unit of product produced. In this study, all results are provided for $\dot{m}_p = 1\,\text{kg/s}$ and the least work is written as $\dot{W}_{\text{least}}/\dot{m}_p$ [kJ/kg]. Derivation of the least work of separation for a control volume containing an ideal black-box separator is summarized and then considered on both a mass and mole basis.

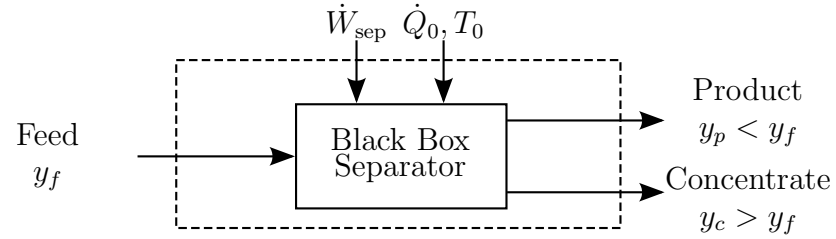

Figure 3-6: A control volume representation of a desalination system is used to derive the least work of separation.

3.4.1 Summary of derivation

Consider a simple black-box separator model for a desalination system as shown in Fig. 2-4. The rate of work applied to the system to drive separation is denoted by $\dot{W}_{\text{sep}}$ and the rate of heat transfer into the system is denoted by $\dot{Q}$. The feed, product, and concentrate streams are denoted by f, p, and c respectively. All the inlet and outlet streams enter and leave the control volume at environmental temperature, T_0, and pressure, p_0, but at different salinities, S. Heat transfer occurs at the environmental temperature. A complete discussion regarding this selection of control volume is provided in Chapter 2 [21, 22].

Combining the First and Second Laws of Thermodynamics yields the rate of work of separation:

$$\dot{W}_{\text{sep}} = \dot{G}_p + \dot{G}_c - \dot{G}_f + T_0 \dot{S}_{\text{gen}} \tag{3.38}$$

where $\dot{G}_i$ is the flow rate of Gibbs free energy of stream i and $\dot{S}_{\text{gen}}$ is the total entropy generation resulting from the separation process. In the limit of reversible operation, entropy generation is zero and Eq. (3.38) reduces to the reversible rate of work of separation, also known as the least work of separation:

$$\dot{W}_{\text{least}} \equiv \dot{W}_{\text{sep}}^{\text{rev}} = \dot{G}_p + \dot{G}_c - \dot{G}_f \tag{3.39}$$

In most real-world desalination systems, the major sources of entropy generation are viscous losses for membrane systems and heat transfer across finite temperature differences for thermal systems [21]. As a result, entropy generation is not strongly related to compositional effects in many systems. Therefore, the least work is a relevant parameter for examining the impact of nonideality on system performance.

3.4.2 Mass basis

For property packages that evaluate properties per unit mass of solution (*e.g.*, [45]), Eq. (3.39) is best written on a mass flow rate basis:

$$\dot{W}_{\text{least}} = \dot{m}_p g_p + \dot{m}_c g_c - \dot{m}_f g_f \tag{3.40}$$

where g_j is the specific Gibbs free energy per kilogram of solution.

The recovery ratio is defined as the ratio of the mass flow rate of product water to

the mass flow rate of feed seawater [see Eq. (2.22)]:

$$r \equiv \frac{\dot{m}_p}{\dot{m}_f} = \frac{\text{mass flow rate of product}}{\text{mass flow rate of feed}} \tag{3.41}$$

Enforcing conservation of mass for the mixture and the salts gives Eq. (2.29):

$$\frac{\dot{W}_{\text{least}}}{\dot{m}_p} = (g_p - g_c) - \frac{1}{r}(g_f - g_c) \tag{3.42}$$

The Gibbs free energy of each of the streams in Eq. (3.42) is evaluated using seawater properties, as a function of temperature and salinity, $g_j = g_j(T, y_j)$ [45]. Provided the feed and product salinities (y_f, y_p) are known, the concentrate salinity (y_c) is evaluated using conservation of mass as shown in Eq. (2.26):

$$y_c = \frac{y_f - r y_p}{1 - r} \tag{3.43}$$

Equation (3.42) is a function of temperature, feed salinity, product salinity, and recovery ratio.

3.4.3 Mole basis

It is more convenient to write Eq. (3.39) on a mole basis when physical properties are evaluated using Eq. (3.1). For aqueous NaCl, Eq. (3.39) becomes:

$$\begin{aligned}\dot{W}_{\text{least}} = &\left[\dot{N}_{\text{H}_2\text{O}}\mu_{\text{H}_2\text{O}} + \dot{N}_{\text{NaCl}}\mu_{\text{NaCl}}\right]_p \\ &+ \left[\dot{N}_{\text{H}_2\text{O}}\mu_{\text{H}_2\text{O}} + \dot{N}_{\text{NaCl}}\mu_{\text{NaCl}}\right]_c \\ &- \left[\dot{N}_{\text{H}_2\text{O}}\mu_{\text{H}_2\text{O}} + \dot{N}_{\text{NaCl}}\mu_{\text{NaCl}}\right]_f\end{aligned} \tag{3.44}$$

Conservation of mass for H_2O and NaCl is written as:

$$\dot{N}_{\text{H}_2\text{O},f} = \dot{N}_{\text{H}_2\text{O},p} + \dot{N}_{\text{H}_2\text{O},c} \tag{3.45}$$

$$\dot{N}_{\text{NaCl},f} = \dot{N}_{\text{NaCl},p} + \dot{N}_{\text{NaCl},c} \tag{3.46}$$

Substituting Eqs. (3.2), (3.45), and (3.46) into Eq. (3.44) gives:

$$\begin{aligned}\dot{W}_{\text{least}} = &\left[\dot{N}_{\text{H}_2\text{O}}RT\ln a_{\text{H}_2\text{O}} + \dot{N}_{\text{NaCl}}RT\ln a_{\text{NaCl}}\right]_p \\ &+ \left[\dot{N}_{\text{H}_2\text{O}}RT\ln a_{\text{H}_2\text{O}} + \dot{N}_{\text{NaCl}}RT\ln a_{\text{NaCl}}\right]_c \\ &- \left[\dot{N}_{\text{H}_2\text{O}}RT\ln a_{\text{H}_2\text{O}} + \dot{N}_{\text{NaCl}}RT\ln a_{\text{NaCl}}\right]_f\end{aligned} \tag{3.47}$$

Note that the standard state terms (μ_i°) cancel out through conservation of H_2O and NaCl [Eqs. (3.45) and (3.46)].

The molar recovery ratio ($\bar{r}$) is defined as:

$$\bar{r} \equiv \frac{\dot{N}_{H_2O,p}}{\dot{N}_{H_2O,f}} = \frac{\text{mole flow rate of water in product}}{\text{mole flow rate of water in feed}} \tag{3.48}$$

Using Eqs. (3.45), (3.46), and (3.48), noting that

$$\frac{\dot{N}_{NaCl,j}}{\dot{N}_{H_2O,j}} = m_{NaCl,j} M_{H_2O}$$

and normalizing the least work by $\dot{N}_{H_2O,p} RT$, Eq. (3.47) becomes:

$$\begin{aligned}\frac{\dot{W}_{least}}{\dot{N}_{H_2O,p} RT} = &\left(\ln \frac{a_{H_2O,p}}{a_{H_2O,c}} + m_{NaCl,p} M_{H_2O} \ln \frac{a_{NaCl,p}}{a_{NaCl,c}} \right) \\ &-\frac{1}{\bar{r}} \left(\ln \frac{a_{H_2O,f}}{a_{H_2O,c}} + m_{NaCl,f} M_{H_2O} \ln \frac{a_{NaCl,f}}{a_{NaCl,c}} \right)\end{aligned} \tag{3.49}$$

Like Eq. (3.42), Eq. (3.49) is a function of temperature, feed molality, product molality, and molar recovery ratio.

Equation (3.49) can be generalized to mixed electrolyte solutions:

$$\begin{aligned}\frac{\dot{W}_{least}}{\dot{N}_{H_2O,p} RT} = &\left(\ln \frac{a_{H_2O,p}}{a_{H_2O,c}} + \sum_s m_{s,p} M_{H_2O} \ln \frac{a_{s,p}}{a_{s,c}} \right) \\ &-\frac{1}{\bar{r}} \left(\ln \frac{a_{H_2O,f}}{a_{H_2O,c}} + \sum_s m_{s,f} M_{H_2O} \ln \frac{a_{s,f}}{a_{s,c}} \right)\end{aligned} \tag{3.50}$$

where s represents all salt species that form the electrolyte mixture recipe and the activities of the solvent and solutes are defined by Eqs. (3.4) and (3.8) respectively. As with Eq. (3.42), Eq. (3.50) is a function of temperature, feed molality, product molality, and molar recovery ratio.

Since activity is written as the product of mole fraction and activity coefficient, Eq. (3.50) can be easily separated into two parts: an ideal term that is a function of mole fraction of each of the species in each of the streams, and a nonideal part that is a function of the activity coefficients of all species in each stream:

$$\dot{W}_{least} = \dot{W}_{least}^{ideal}(x_i) + \dot{W}_{least}^{nonideal}(\gamma_i) \tag{3.51}$$

where

$$\frac{\dot{W}^{\text{ideal}}_{\text{least}}}{\dot{N}_{\text{H}_2\text{O},p}RT} = \left(\ln\frac{x_{\text{H}_2\text{O},p}}{x_{\text{H}_2\text{O},c}} + \sum_s \nu_{s,p} m_{s,p} M_{\text{H}_2\text{O}} \ln\frac{x_{s,p}}{x_{s,c}}\right) - \frac{1}{\bar{r}}\left(\ln\frac{a_{\text{H}_2\text{O},f}}{a_{\text{H}_2\text{O},c}} + \sum_s \nu_{s,f} m_{s,f} M_{\text{H}_2\text{O}} \ln\frac{a_{s,f}}{a_{s,c}}\right) \tag{3.52}$$

$$\frac{\dot{W}^{\text{nonideal}}_{\text{least}}}{\dot{N}_{\text{H}_2\text{O},p}RT} = \left(\ln\frac{\gamma_{\text{H}_2\text{O},p}}{\gamma_{\text{H}_2\text{O},c}} + \sum_s \nu_{s,p} m_{s,p} M_{\text{H}_2\text{O}} \ln\frac{\gamma_{s,p}}{\gamma_{s,c}}\right) - \frac{1}{\bar{r}}\left(\ln\frac{\gamma_{\text{H}_2\text{O},f}}{\gamma_{\text{H}_2\text{O},c}} + \sum_s \nu_{s,f} m_{s,f} M_{\text{H}_2\text{O}} \ln\frac{\gamma_{s,f}}{\gamma_{s,c}}\right) \tag{3.53}$$

The choice of electrolyte system model only affects the nonideal portion of the least work of separation, Eq. (3.53).

Equations (3.49), (3.50), (3.52), and (3.53) can all be written per unit mass flow rate of product through the use of Eq. (B.10).

3.5 Feed water composition

A wide variety of water sources, including brackish water (*e.g.*, ground, river, and lake water), seawater, wastewater, and produced water (such as from hydraulic fracturing) can be treated by desalination systems. Brackish water and seawater are the most common feed sources. While these water classifications are only loosely defined, water with a salinity between 1–10 g/kg is typically considered brackish, seawater typically has salinities of 30–55 g/kg, and water with a salinity less than 0.5 g/kg is typically considered fresh [7, 84]. Even though these natural waters have fairly complex compositions as shown in Table 3.2, sodium and chloride are the typically the dominant species [56]. ASTM International provides guidelines for how to make substitute ocean water for experimental purposes and the primary components are listed in Table 3.3.

The recovery ratio with which a desalination plant can operate is strongly dependent upon the feed water salinity. Scaling, membrane durability, and energy costs all serve to limit the maximum salinity allowable in the system [7, 12]. Brackish water plants can operate at higher recovery ratios than can seawater plants due to the lower feed salinity [7, 84].

3.6 Aqueous sodium chloride

In order to explore the role of nonideality, a parametric study is performed in which Eqs. (3.49), (3.52), and (3.53) are evaluated while varying feed molality ($m_{\text{NaCl},f}$) and molal recovery ratio ($\bar{r}$) at 25 °C and assuming pure product water ($m_{\text{NaCl},p} = 0$). All results, however, are given in kJ/kg product as a function of feed salinity (y_f)

Table 3.2: Representative compositions of brackish ground water and seawater [56]. Unreported data marked with –.

Constituent		Concentration [mg/kg]		
Name	Symbol	Brackish Water	Normal Seawater	Arabian Gulf At Kuwait
Bicarbonate	HCO_3^-	385	140	142
Boric Acid	H_3BO_3	–	26	–
Bromide	Br^-	–	65	80
Calcium	Ca^{2+}	258	400	500
Chloride	Cl^-	870	18,980	23,000
Fluoride	F^-	–	1	–
Iodide	I^-	–	<1	–
Iron	Fe^{2+}	<1	–	–
Magnesium	Mg^{2+}	90	1,262	1,765
Manganese	Mn^{2+}	1	–	–
Nitrate	NO_3^-	1	–	–
Phosphate	PO_4^{3-}	<1	–	–
Potassium	K^+	9	380	460
Silica	SiO_2	25	–	–
Silicate	SiO_3^{2-}	–	1	1.5
Sodium	Na^+	739	10,556	15,850
Strontium	Sr^{2+}	3	13	–
Sulfate	SO_4^{2-}	1,011	2,649	3,200
Total Dissolved Solids		3,394	34,483	45,000

Table 3.3: Primary chemical composition of substitute ocean water [55].

Compound	Concentration [g/L]
NaCl	24.53
$MgCl_2$	5.20
Na_2SO_4	4.09
$CaCl_2$	1.16
KCl	0.695
$NaHCO_3$	0.201
KBr	0.101
H_3BO_3	0.027
$SrCl_2$	0.025
NaF	0.003

and recovery ratio (r) since these units are more typical for the desalination industry. Relevant unit conversions are provided in the Appendix B [Eqs. (B.1), (B.8), and (B.10)]. In order to avoid extrapolating beyond the available data ranges, calculations are only considered in which all streams are 6 molal or less ($y_j < 260\,\mathrm{g/kg}$).

For aqueous NaCl, Eqs. (3.52) and (3.55) reduce to

$$\frac{\dot{W}^{\text{ideal}}_{\text{least}}}{\dot{N}_{\mathrm{H_2O},p}RT} = \left(\ln\frac{x_{\mathrm{H_2O},p}}{x_{\mathrm{H_2O},c}} + \nu_{\mathrm{NaCl}} m_{\mathrm{NaCl},p} M_{\mathrm{H_2O}} \ln\frac{x_{\mathrm{NaCl},p}}{x_{\mathrm{NaCl},c}}\right) - \frac{1}{\bar{r}}\left(\ln\frac{x_{\mathrm{H_2O},f}}{x_{\mathrm{H_2O},c}} + \nu_{\mathrm{NaCl}} m_{\mathrm{NaCl},f} M_{\mathrm{H_2O}} \ln\frac{x_{\mathrm{NaCl},f}}{x_{\mathrm{NaCl},c}}\right) \tag{3.54}$$

$$\frac{\dot{W}^{\text{nonideal}}_{\text{least}}}{\dot{N}_{\mathrm{H_2O},p}RT} = \left(\ln\frac{\gamma_{f,\mathrm{H_2O},p}}{\gamma_{f,\mathrm{H_2O},c}} + \nu_{\mathrm{NaCl}} m_{\mathrm{NaCl},p} M_{\mathrm{H_2O}} \ln\frac{\gamma_{x,\mathrm{NaCl},p}}{\gamma_{x,\mathrm{NaCl},c}}\right) - \frac{1}{\bar{r}}\left(\ln\frac{\gamma_{\mathrm{H_2O},f}}{\gamma_{\mathrm{H_2O},c}} + \nu_{\mathrm{NaCl}} m_{\mathrm{NaCl},f} M_{\mathrm{H_2O}} \ln\frac{\gamma_{x,\mathrm{NaCl},f}}{\gamma_{x,\mathrm{NaCl},c}}\right) \tag{3.55}$$

As part of the parametric study, the least work of separation is evaluated for two different systems: System A has brackish feed with a salinity of 5 g/kg and a recovery ratio of 75%; System B has seawater feed at 35 g/kg and a recovery ratio of 50%. Both the brackish water and seawater systems are evaluated using various NaCl solutions models and the seawater package.

3.6.1 Least work for an NaCl solution

The least work of separation for an NaCl solution, evaluated using Eq. (3.49), is a strong function of feed salinity, regardless of recovery ratio. As the feed salinity increases, it becomes a strong function of recovery ratio as well (Fig. 3-7). For the brackish plant, System A, the least work of separation is 0.73 kJ/kg product at a recovery ratio of 75%. For the seawater plant, System B, the least work of separation is 4.04 kJ/kg product at a recovery ratio of 50%. Values of least work of separation for both Systems A and B evaluated using various activity coefficient models are summarized in Table 3.4.

The ideal part of the least work of separation is shown in Fig. 3-8. By comparing Figs. 3-7 and 3-8, it is clear that the ideal part of the least work is the dominant part. The ideal part is a slightly weaker function of recovery ratio. The ideal part of the least work of separation is 0.79 kJ/kg for System A and 4.27 kJ/kg for System B. These values are 7.7% and 5.5% greater than the actual values.

Unlike the ideal part, the nonidealities are only significant in the least work calculation when the feed salinity and recovery ratio are large (Fig. 3-9). The results of Eq. (3.55), as shown in Fig. 3-9, appear to imply that the NaCl solution behaves approximately ideally for most feed salinities and recovery ratios that are found within the desalination industry and that the nonidealities may reasonably be neglected. However, while it is true that for this particular calculation, the net effect of nonideality is small, it is not because the system is behaving ideally, but rather, because the nonidealities tend to cancel one another, as is shown below.

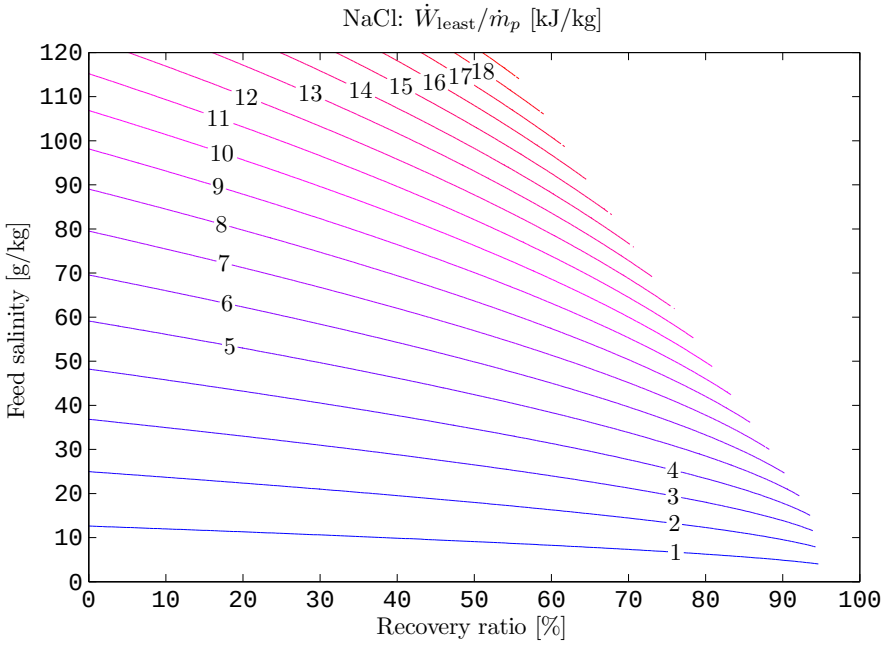

Figure 3-7: Least work of separation for an NaCl solution [Eq. (3.49)] in which activity and fugacity coefficients are evaluated using data from [68].

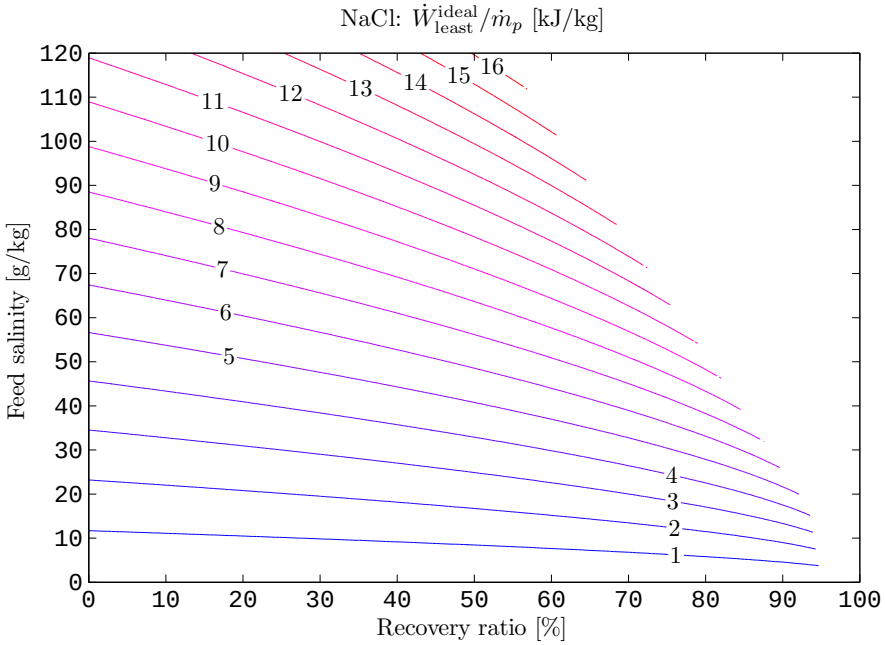

Figure 3-8: Ideal part of the least work of separation for an NaCl solution [EQ. (3.54)].

Table 3.4: Values for the ideal part, nonideal part, and total least work of separation for two desalination systems separating aqueous nAcL solutions evaluated using various property models. Note that the Debye-Hückel models are more accurate for lower salinities and that NaCl solution is a better approximation for seawater at high salinities. Least work values are in kJ/kg product.

Property Model		Brackish Feed, $y_f = 5\,\mathrm{g/kg}$, $r = 0.75$				Seawater Feed, $y_f = 35\,\mathrm{g/kg}$, $r = 0.5$			
NaCl	H_2O	$\dot{W}_{\mathrm{least}}^{\mathrm{ideal}}$	$\dot{W}_{\mathrm{least}}^{\mathrm{nonideal}}$	$\dot{W}_{\mathrm{least}}$	Error [%]	$\dot{W}_{\mathrm{least}}^{\mathrm{ideal}}$	$\dot{W}_{\mathrm{least}}^{\mathrm{nonideal}}$	$\dot{W}_{\mathrm{least}}$	Error [%]
data	data	0.79	-0.06	0.73	0	4.27	-0.22	4.04	0
ideal	ideal	0.79	0	0.79	7.66	4.27	0	4.27	5.47
ideal	data	0.79	0.01	0.80	8.38	4.27	-0.21	4.06	0.36
data	ideal	0.79	-0.06	0.73	-0.74	4.27	-0.01	4.25	5.11
DHLL	data	0.79	-0.19	0.60	-18.52	4.27	-2.62	1.64	-59.39
Güntelberg	data	0.79	-0.09	0.70	-4.70	4.27	-0.84	3.43	-15.29
Davies	data	0.79	-0.06	0.73	0.05	4.27	0.09	4.36	7.68
Seawater [45]		-	-	0.33	-	-	-	3.93	-

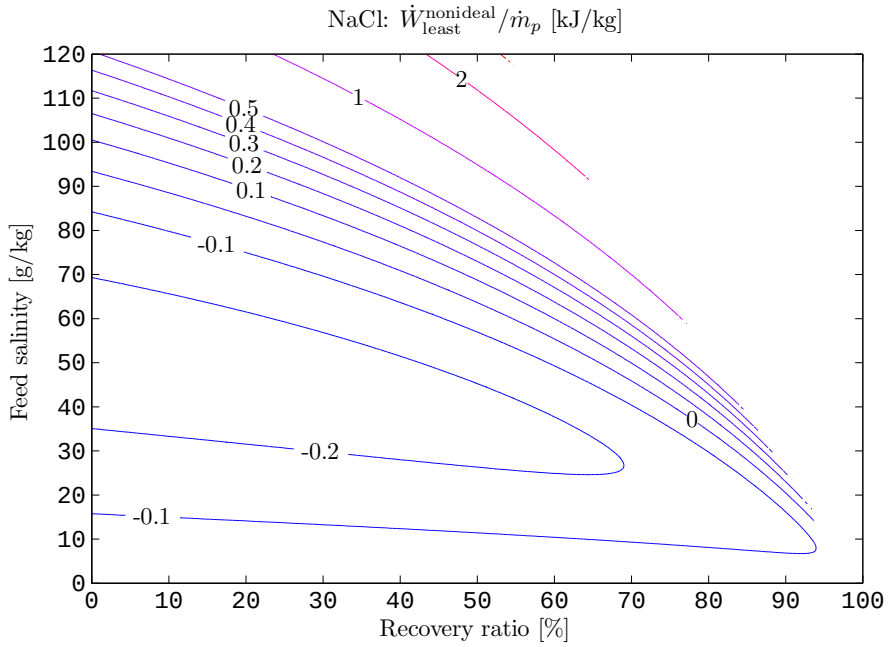

Figure 3-9: The nonideal part of the least work of separation for an NaCl solution [EQ. (3.55)] only becomes significant at high feed salinities and high recovery ratios. Activity and fugacity coefficients are evaluated using data from [68].

3.6.2 Error associated with ideal behavior approximation

The effect of the nonidealities can be visualized by considering the relative error between an ideal NaCl solution (least work values shown in Fig. 3-8) and an actual NaCl solution (least work values shown in Fig. 3-7). Relative error, defined as

$$\text{Relative Error } [\%] = \left(\frac{\dot{W}_{\text{least}}^{\text{ideal}}}{\dot{W}_{\text{least}}(\text{actual})} - 1 \right) \times 100 \tag{3.56}$$

between the ideal and actual cases is shown in Fig. 3-10a. As the feed salinity increases at fixed recovery ratio, the magnitude of the relative error first decreases and then begins to increase once a critical feed salinity is reached. This behavior is not intuitive and in order to properly understand the behavior of the nonidealities in the given system, the nonideality associated with the dissolved species and those associated with the solvent are isolated and considered independently.

First, the nonidealities associated with NaCl are considered by looking at the least work evaluated while approximating NaCl as ideal and treating H_2O as nonideal. The relative error under these approximations is shown in Fig. 3-10b. Even when it is assumed that NaCl is ideal, it is clear that there are certain conditions when this assumption has no effect on the overall calculation—these conditions are illustrated by the zero relative error contour line in Fig. 3-10b.

Since the nonidealities for saline solutions are non-zero, the only way for the

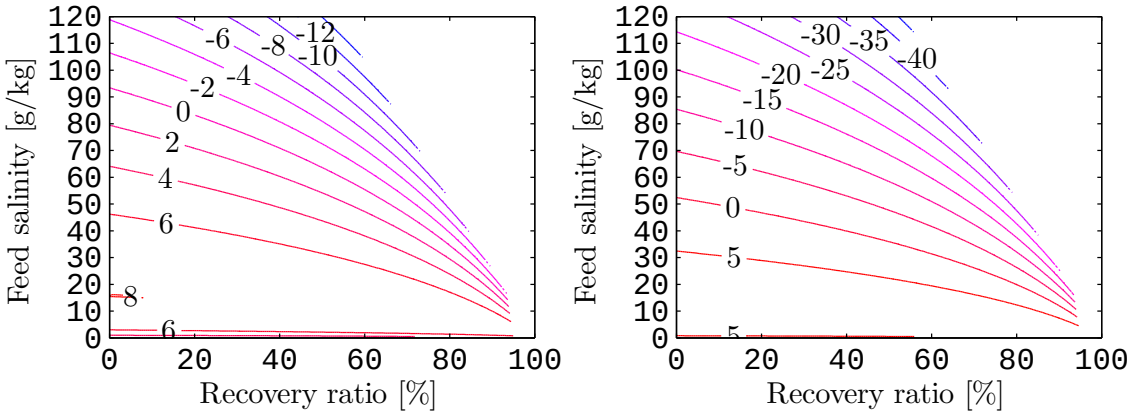

(a) Ideal solution approximation

(b) Ideal for salt, data for water

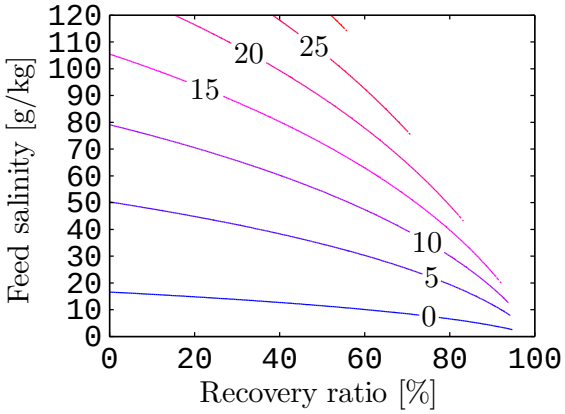

(c) Data for salt, ideal water

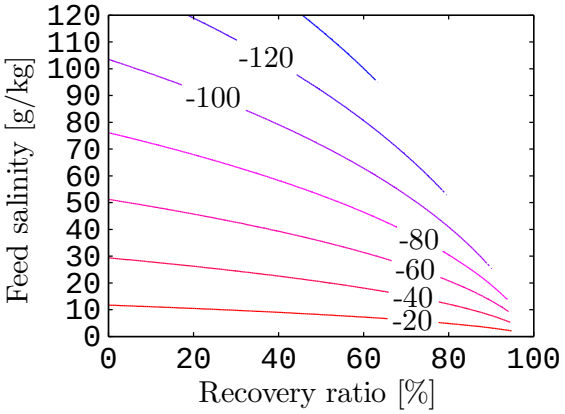

(d) DHLL for salt, data for water

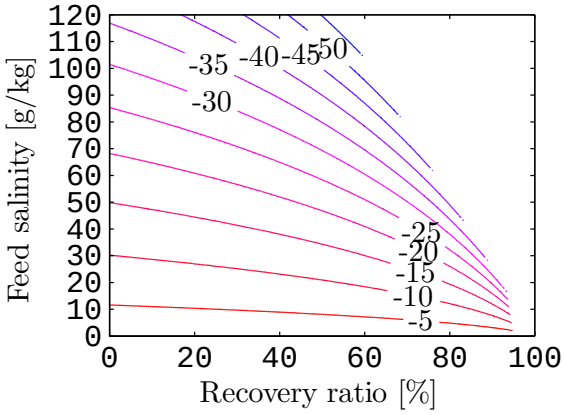

(e) Güntelberg for salt, data for water

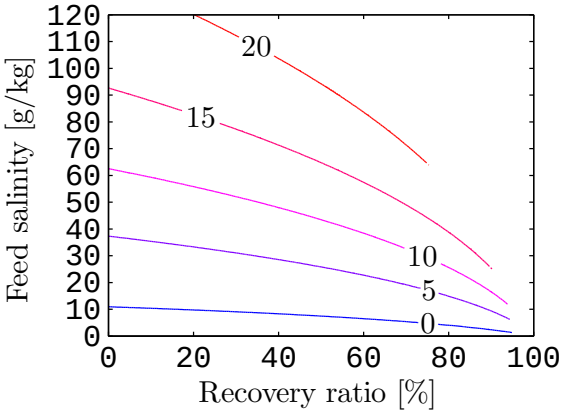

(f) Davies for salt, data for water

Figure 3-10: Percent relative error in least work of separation, as a function of feed salinity and recovery ratio, resulting from various activity coefficient modeling methods for aqueous NaCl.

nonidealities to be zero is if they cancel out. Since it is assumed that the product stream is pure H_2O, the nonidealities due to salt appear as the final term of Eq. (3.55):

$$\frac{\nu_{\mathrm{NaCl}} m_{\mathrm{NaCl},f} M_{\mathrm{H_2O}}}{\bar{r}} \ln \frac{\gamma_{x,\mathrm{NaCl},c}}{\gamma_{x,\mathrm{NaCl},f}}$$

When the activity coefficient of salt in the concentrate stream equals the activity coefficient of salt in the feed stream, the ln term equals zero and the salt nonidealities exactly cancel out. Figure 3-4 shows that except when $\gamma > 1$, there are two molalities that will give the same value of the activity coefficient. As long as the feed and brine concentrations are such that the resulting activity coefficients are equal, the nonidealities cancel and the relative error goes to zero as seen in Fig. 3-10b. Any deviation in molality from either stream from this condition will result in error. The least work of separation, when only salt is approximated as ideal, is 0.80 kJ/kg for System A and 4.06 kJ/kg for System B (8.4% and 0.36% error, respectively).

Nonidealities associated with H_2O are considered by looking at the least work evaluated while approximating H_2O as ideal and treating NaCl as nonideal. From Eq. (3.55), it is seen that when

$$\ln \frac{\gamma_{f,\mathrm{H_2O},p}}{\gamma_{f,\mathrm{H_2O},c}} + \frac{1}{\bar{r}} \ln \frac{\gamma_{\mathrm{H_2O},c}}{\gamma_{\mathrm{H_2O},f}} = 0$$

the nonidealities associated with H_2O in all three streams cancel out. Figure 3-5 shows that as long as the molality of the NaCl solution is less than 3 ($y_j < 150$ g/kg), the fugacity coefficient is within 1% of unity. Therefore, it is expected that except for combinations of feed salinity and recovery ratio that result in concentrate streams with greater than 3 molal (149 g/kg) concentrations, the error introduced by assuming the water is ideal should be negligible. This is clearly seen to be the case in Fig. 3-10c. The least work of separation, when only water is approximated as ideal, is 0.73 kJ/kg for System A and 4.25 kJ/kg for System B (-0.74% and 5.1% error, respectively).

Figures 3-10b and 3-10c both show that there is significant error introduced when it is assumed that either water or salt is ideal. However, the error associated with assuming salt is ideal decreases with increasing feed salinity while the error associated with assuming water is ideal increases with increasing feed salinity. As a result of these reverse trends, the net effect of assuming both the solutes and the solvent are ideal is less than the individual errors. For this reason, it appears that the effect of nonidealities on the least work of separation is small (Fig. 3-10a).

The error introduced by using each of the analytical models for the NaCl activity coefficient is now considered. Unsurprisingly, the error introduced by using the Debye-Hückel Limiting Law [Eq. (3.20)] is substantial except at the lowest salinities (Fig. 3-10d). This is because the limiting law is only applicable at very low molalities, typically less than $10^{-2.3}$. The least work of separation, when the salt activity coefficient is evaluated using the limiting law, is 0.60 kJ/kg for System A and 1.64 kJ/kg for System B (-19% and -59% error, respectively).

The Güntelberg equation [Eq. (3.21)] is substantially more accurate than the

limiting law. However, even at seawater feed salinities, the relative error is at least 10% (Fig. 3-10e). The least work of separation, when the salt activity coefficient is evaluated using Güntelberg equation, is 0.70 kJ/kg for System A and 3.43 kJ/kg for System B (-4.7% and -15% error, respectively).

Finally, the Davies equation [Eq. (3.22)] is quite accurate for all but the highest salinities. For seawater salinities, the error does not exceed 10% except at extremely high recovery ratios (Fig. 3-10f). The least work of separation, when the salt activity coefficient is evaluated using the Davies equation, is 0.73 kJ/kg for System A and 4.36 kJ/kg for System B (-0.05% and -7.7% error, respectively).

3.7 Mock seawater

The effects of various electrolyte solution approximations are illustrated through a parametric study of the least work of separation. Recovery ratio and feed salinity are varied and the least work of separation is calculated while evaluating the activity coefficients using various models discussed in the preceding sections. These calculations are performed for two different types of feed waters. The first is a mock seawater based on the seawater recipe shown in Table 3.2. The second feed water is a two salt electrolyte solution in which both salts are composed of divalent ions. Mock seawater is analyzed in the present section.

For computational convenience, the mock seawater solution consists of only the five most predominant salts listed in Table 3.2 (accounting for over 99% of the dissolved salts in seawater). When the feed salinity is varied, the relative concentration of each of the five salts is held constant. That is the mass ratio of NaCl : $MgCl_2$: Na_2SO_4 : $CaCl_2$: KCl is 24.53 : 5.20 : 4.09 : 1.16 : 0.695, regardless of feed salinity.

Before quantifying the error introduced by making various approximations, the absolute value of the least work of separation for the mock seawater solution is calculated using the Pitzer-Kim model (shown as a contour plot in Fig. 3-11). As expected, the required separation work increases with both increasing recovery ratio and feed salinity. Note that increasing the feed salinity has a greater effect on the required work of separation than increasing the recovery ratio. That is, producing one kilogram of product water from a higher salinity feed at lower recovery ratio will take substantially more energy than producing the same amount of product from lower salinity feed at a higher recovery ratio. Additionally, at low feed salinities, the marginal increase in the least work for increasing the recovery ratio is low. That is, $\left(\frac{\mathrm{d}(\dot{W}_{\mathrm{least}}/\dot{m}_p)}{\mathrm{d}r}\right)_{y_f}$ is small. This has important implications for those industries that require processing high salinity water and also partially explains why brackish water treatment plants operate at high recovery ratios.

The contours in Fig. 3-11 and all subsequent contour plots end in the upper right hand corner since those combinations of high feed salinity and recovery ratio result in a concentrate stream salinity that exceeds the pure salt solubility limit of any of the individual salts present in solution. While the common-ion effect does change the solubility of the salts in mixture, this effect is neglected in this analysis.

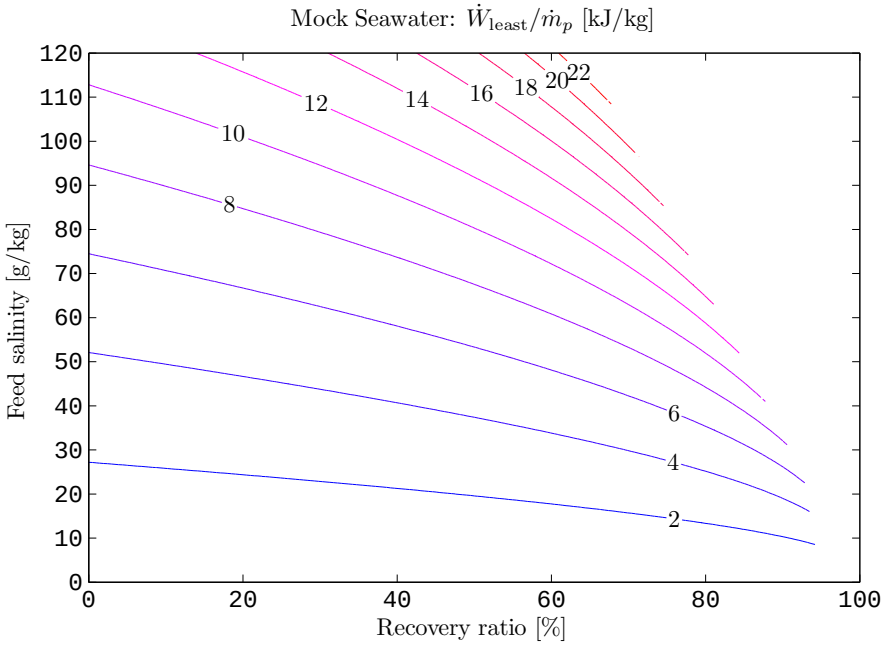

Figure 3-11: The least work of separation for mock seawater solution consisting of NaCl, $MgCl_2$, Na_2SO_4, $CaCl_2$, and KCl according to the proportions listed in Table 3.2. Required separation work increases with increasing recovery ratio and feed salinity.

Since the ideal solution approximation is so simple to use, it is commonly taken as a first step in desalination studies. However, improper use of it has the potential to introduce significant error into calculations. Again, relative error is defined by Eq. (3.56).

The least work of separation is evaluated for mock seawater while assuming ideal solution behavior, and the relative error is shown in Fig. 3-12a. Even at low salinities and low recovery ratios, significant error (approximately 10%) is introduced by assuming that the solutions behave ideally. While there is a contour at which the error is identically equal to zero, this should not be mistaken for ideal solution behavior. Rather, under those combinations of feed salinity and recovery ratio, the nonidealities in all of the streams have the net effect of canceling out. That is, Eq. (3.53) is equal to zero despite activity coefficients that are not equal to unity. This effect is discussed by Mistry and Lienhard [23, 24] in regard to single electrolyte solutions.

A very common approach to electrolyte solution modeling, especially in the study of natural waters, is to approximate the solvent (water) as ideal since it is assumed to be present in high concentration and to approximate the solutes (electrolytes) as nonideal using Debye-Hückel theory since they are assumed to be relatively dilute. Figure 3-12b shows the percent relative error in least work of separation when the Davies equation is used for the electrolytes and ideality is assumed for water. For many naturally occurring brackish waters, this is not an unreasonable assumption, but for seawater and higher salinity waters, the approximation breaks down. Specifically, it is seen that for feed salinities approaching 30 g/kg, the error introduced by these

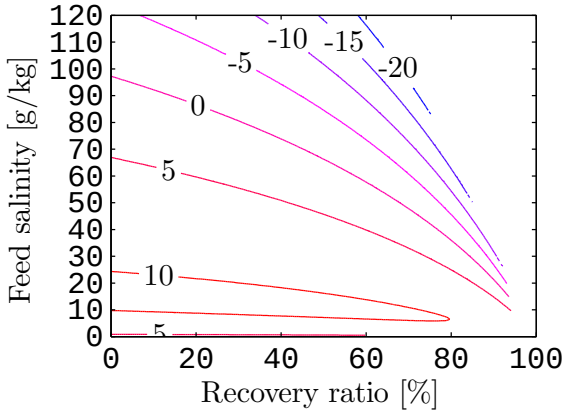

(a) Ideal solution approximation

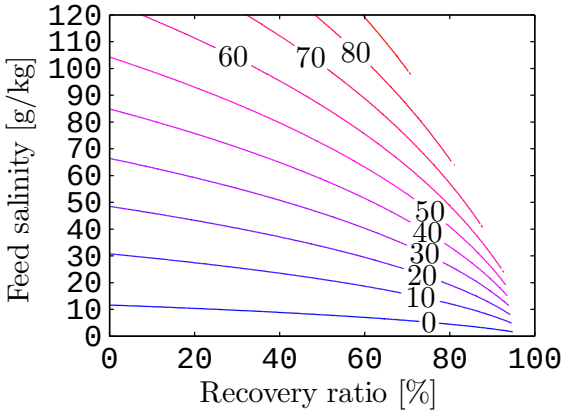

(b) Davies equation for salts, ideal water

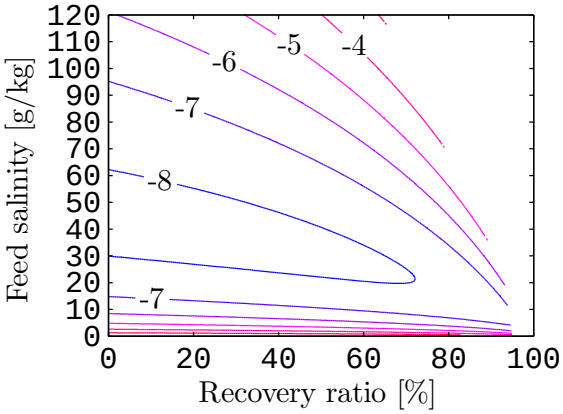

(c) Pitzer equation for salts, ideal water

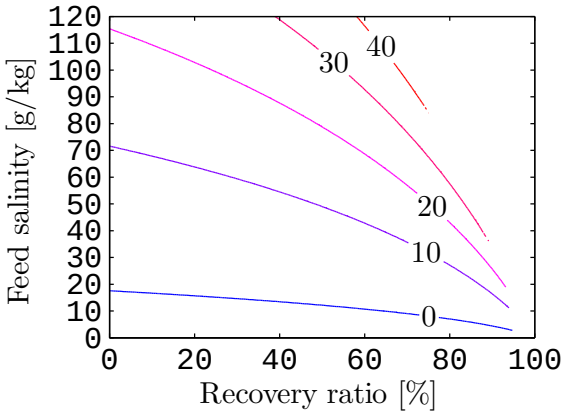

(d) Pitzer effective for salts, ideal water

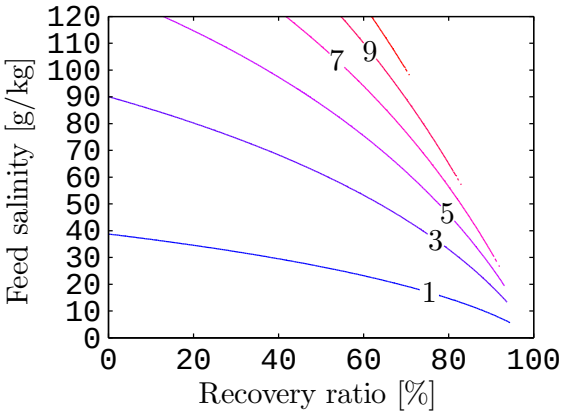

(e) Pitzer effective for salts and water

Figure 3-12: Percent relative error in least work of separation, as a function of feed salinity and recovery ratio, resulting from various activity coefficient modeling methods for a five salt mock seawater solution.

approximations is typically less than 10%. However, as the feed salinity increases, the error dramatically increases. The error introduced for a typical seawater desalination plant operating at 50% recovery ratio on feed at 35 g/kg is nearly 20% and the error increases from there. This approximation method should only be used if all streams in the system are at low salinity (feed stream should be roughly less than 20 g/kg). Note that this increase in error expected since Davies equation was derived under the dilute solution assumption.

When more accuracy is required than what is provided by use of Debye-Hückel theory, Pitzer's ion activity model is particularly useful. However, the standard Pitzer model is designed for use with single electrolyte solutions only. Given that Debye-Hückel theory is used to evaluate single ion activity coefficients which are non-physical values, some might use Pitzer's single electrolyte model for mixed electrolytes hoping to gain improved accuracy. Figure 3-12c shows the error introduced by assuming water is ideal and evaluating the salt activity coefficients using Pitzer's equation. Comparing Figs. 3-12b and 3-12c, it is seen that using Pitzer's equation gives better results overall, but, at lower feed salinities, the error is actually worse. This happens since the molality and ionic strength in Eqs. (3.23) and (3.24) have a one to one relationship for single electrolytes, but not for mixed electrolytes as discussed in Section 3.3.5.

In order to correct for the differences between molality and ionic strength, the effective Pitzer equation can be used to determine the activity coefficients of the salts using an effective molality. The relative error in the least work of separation when using this approximation while assuming that water behaves ideally results in reduced error at lower feed salinities as compared to the Davies equation as expected (*cf.*, Figs. 3-12b and 3-12d).

Finally, if the effective Pitzer equation for osmotic coefficient is also used, the relative error is reduced substantially (Fig. 3-12e). The error under the effective Pitzer model is an order of magnitude less than the error observed when using Davies equation (*cf.*, Figs. 3-12b and 3-12e). The effective Pitzer model works well because it better predicts the activity coefficients of the individual salts than the standard Pitzer model itself. To illustrate this, the activity and fugacity coefficients for the mock seawater solution, evaluated using the Pitzer-Kim (solid lines), Pitzer (dotted lines), and effective Pitzer (dashed lines), are shown in Fig. 3-13. In all cases, the effective Pitzer model is in closer agreement to the Pitzer-Kim values.

3.8 High valence electrolyte solution

Some industrial waste waters may be dominated by higher valence salts than what is typically found in natural waters. In particular, water produced from hydraulic fracturing sometimes has a high concentration of divalent ions [85, 86]. Therefore, the same parametric study that was performed on mock seawater is performed on a 50-50 mixture (by mass) of $MgSO_4$ and $ZnSO_4$ and the effects of the various solution models are discussed. These two salts were selected since they both have high enough solubilities to allow the parametric study to be conducted over the same range of salinities and recovery ratios that was used for the mock seawater solution. The least

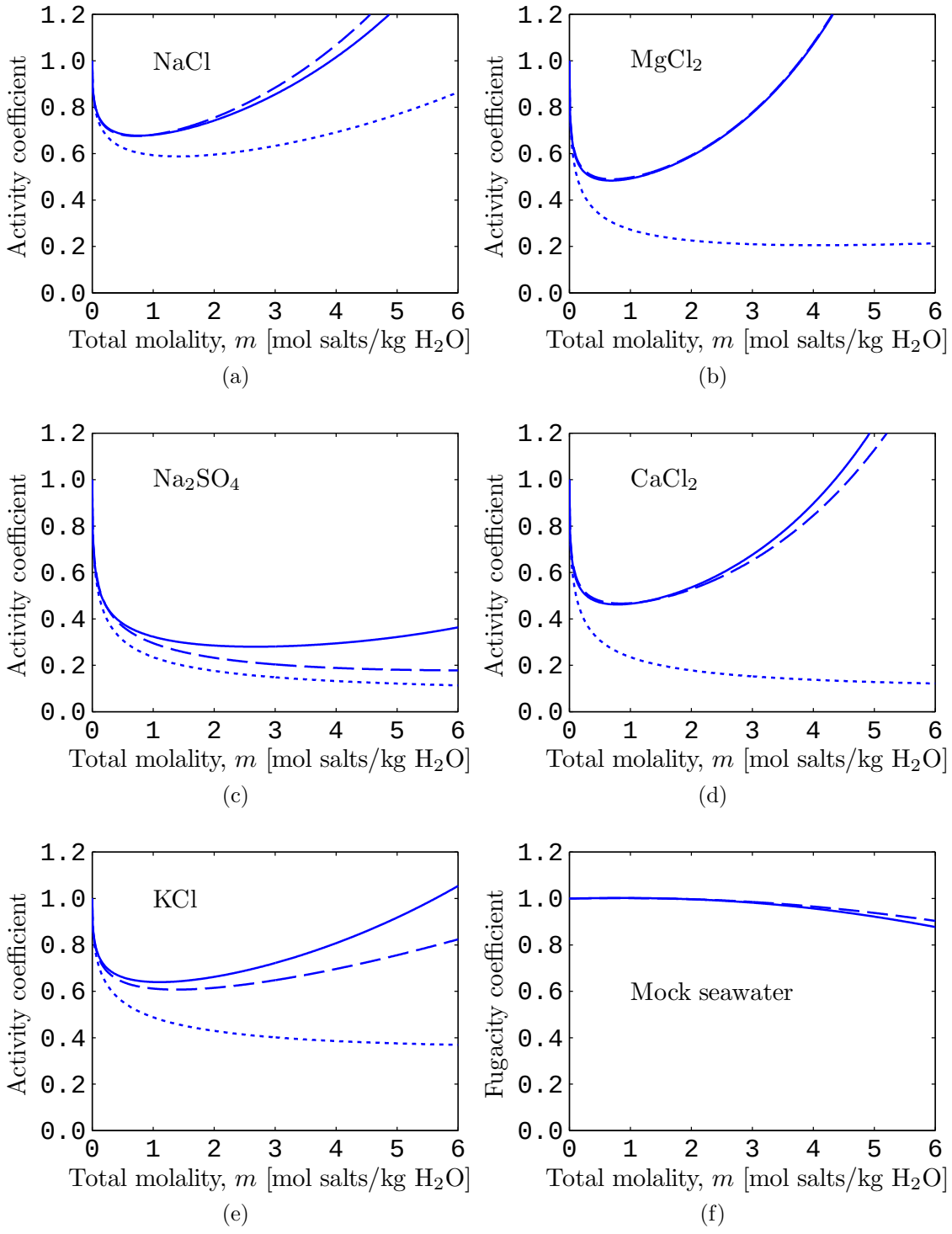

Figure 3-13: Rational activity coefficient for each salt and fugacity coefficient for water in the mock seawater solution. Solid lines (—) are evaluated using Pitzer-Kim, dashed lines (- - -) using effective Pitzer, and dotted lines ($\cdots$) using Pitzer.

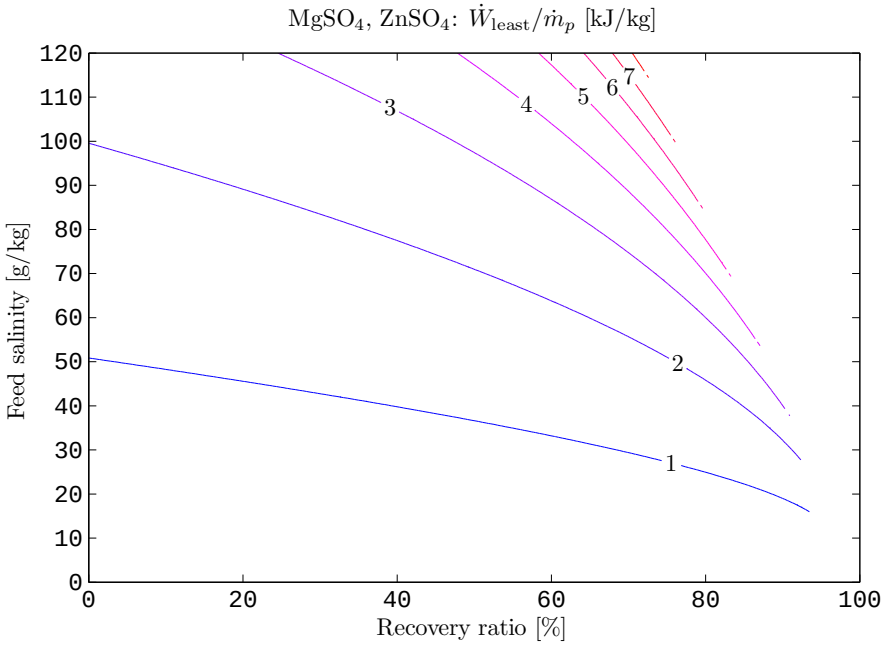

Figure 3-14: The least work of separation for a 50-50 mixture (by mass) of $MgSO_4$ and $ZnSO_4$. Required separation work increases with increasing recovery ratio and feed salinity.

work of separation for this mixture is evaluated and shown in Fig. 3-14. Comparing to Fig. 3-11, it is clear that the required separation work is substantially lower for this high valence electrolyte mixture. The lower separation work requirements are due to several factors: the salts considered here have a lower activity resulting in lower separation requirements, sulphate tends to participate in ion pairing (aqueous complexation), and heavier ions have a lower molality for a given salinity (weight fraction). Clearly, the specific composition, rather than simply salinity, is essential to the separation work requirements.

The relative error in least work of separation introduced by each of the various solution models is shown in Fig. 3-15. Under the ideal solution approximation, the relative error reaches values in excess of 90% (Fig. 3-15a). Even at relatively low salinities and recovery ratios, the relative error is in excess of 50%. Therefore, for this divalent electrolyte solution, the ideal solution approximation is not valid for any solutions of reasonable salinity.

Use of Debye-Hückel theory through the Davies equation gives better results than the ideal solution model at the lowest concentrations (below approximately 5 g/kg) but yields substantially worse results at higher salinities. For seawater salinities of about 35 g/kg, the relative error is in excess of 200% and at the higher salinities, the error can exceed 1000% (Fig. 3-15b). As a result, it is not advisable to use Davies equation for high valence salts except for extremely dilute solutions. When Pitzer's single electrolyte model is used for evaluation of the salt activity coefficients while assuming that water behaves ideally, the relative error introduced drops substantially (Fig. 3-

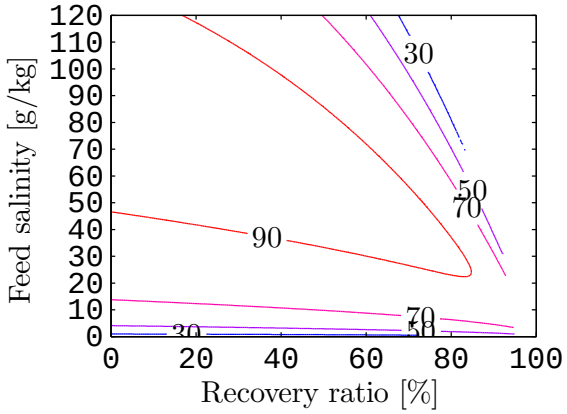

(a) Ideal solution approximation

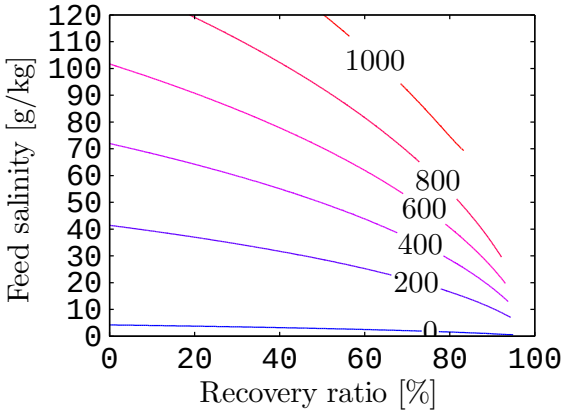

(b) Davies equation for salts, ideal water

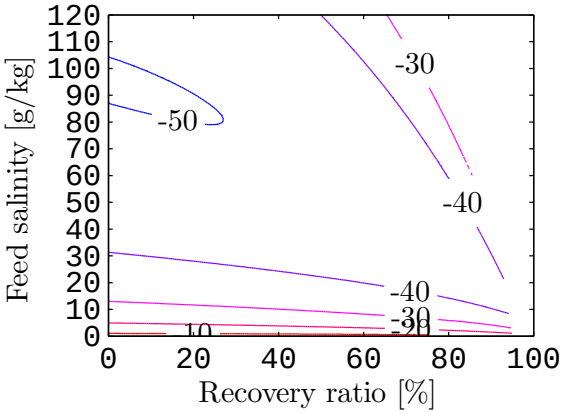

(c) Pitzer equation for salts, ideal water

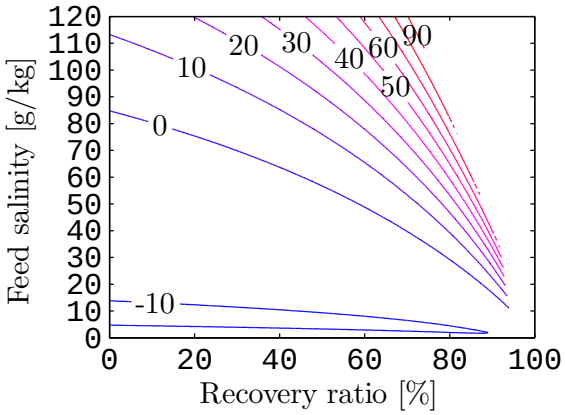

(d) Pitzer effective for salts, ideal water

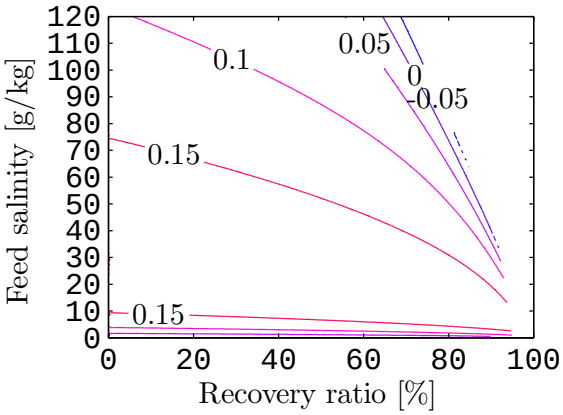

(e) Pitzer effective for salts and water

Figure 3-15: Percent relative error in least work of separation, as a function of feed salinity and recovery ratio, resulting from various activity coefficient modeling methods for a 50-50 mixture of $MgSO_4$ and $ZnSO_4$

15c). The maximum relative error under the conditions considered is approximately 50%. While this is better than assuming ideality or using Debye-Hückel theory, the error is still unacceptably high for most engineering calculations.

Pitzer's model based on effective molalities for the salt activity coefficient gives reasonable accuracy for a large range of feed salinities and recovery ratios (relative error is less than 10% for most of the range of salinities and recovery ratios considered, Fig. 3-15d). At higher recovery ratios and very high feed salinities, the error begins to approach greater than 80% so care should be used when using this method. Finally, using the effective Pitzer model for both salts and water results in near perfect agreement with the Pitzer-Kim model (Fig. 3-15e). The effective Pitzer model works better on this solution than the mock seawater solution because both salts are of the same general form and are of equal proportions. That is, they are both 2:2 electrolytes and the effective molality is equal to the total molality for both salts. As a result, the approximated values obtained from the effective molality calculations closely predict the actual values from the Pitzer-Kim model.

3.9 Comparison to seawater

As stated in the introduction, standard seawater properties are only appropriate for solutions that have an ionic composition similar to that of the standard seawater solution. As illustrated in Figs. 3-11 and 3-14, it is clear that the least work of separation, and therefore, the Gibbs free energy, is a strong function of the composition of the solution being considered. In order to further illustrate this point, the least work of separation for the five-salt mock seawater solution and the two-salt high valence electrolyte solution are compared to the least work of separation for standard seawater [30], an NaCl solution, and an NaCl$-$$MgSO_4$ solution (Fig. 3-16).

First, all five solutions are compared when the feed salinity is 35 g/kg (Fig. 3-16a). The NaCl solution has the highest work of separation requirements, followed by standard seawater, mock seawater, NaCl$-$$MgSO_4$, and $MgSO_4$$-$$ZnSO_4$. It is clear that the mock seawater very closely approximates the standard seawater solution. The NaCl solution has the highest work requirements and the $MgSO_4$$-$$ZnSO_4$ solution has the lowest work requirements for many of the reasons discussed previously: lighter salts result in higher molality for fixed salinity, differences in charge of the ions, and the role of aqueous complexation. Similarly, the mock seawater and NaCl$-$$MgSO_4$ solutions have intermediate work requirements between the two extreme cases.

Since the molality of the solutes in each of the streams considered in Fig. 3-16a is different, it is unclear whether the difference in work requirements is purely due to the molal concentration. Therefore, the least work of separation is calculated for the different solutions while holding the ionic molality of all of the feed solutions fixed at 1.24 mol/kg. Note that a 0.62 molal NaCl solution has a salinity of 35 g/kg and an ionic molality of 1.24 mol/kg (Fig. 3-16b). Standard seawater is not shown since the ionic composition of the properties provided by [30] is unknown. Figure 3-16b shows the same trend observed in Fig. 3-16a.

Finally, the calculations are repeated again while holding the feed solution ionic

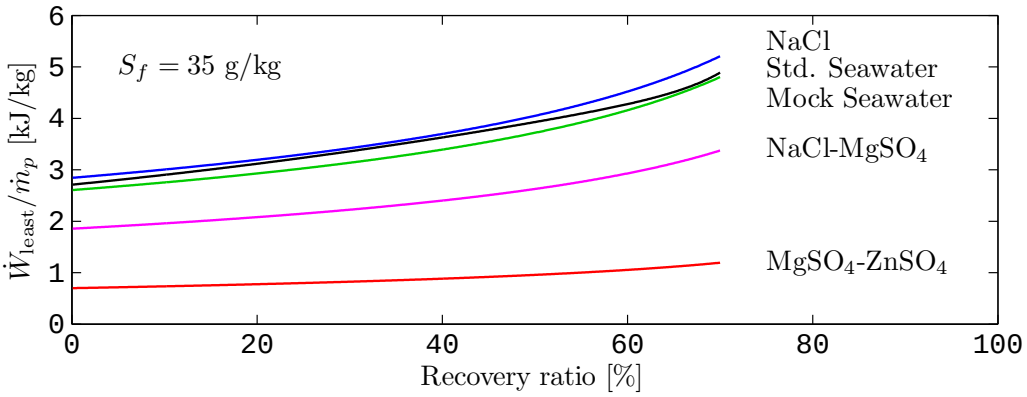

(a) Salinity of all feed streams is 35 g/kg.

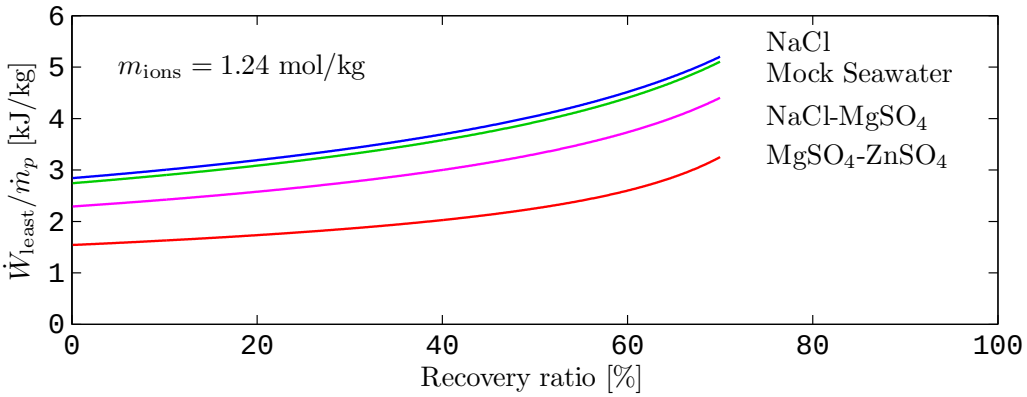

(b) Molality of all ions in all feed streams is 1.24 mol/kg, equivalent to a 35 g/kg NaCl solution.

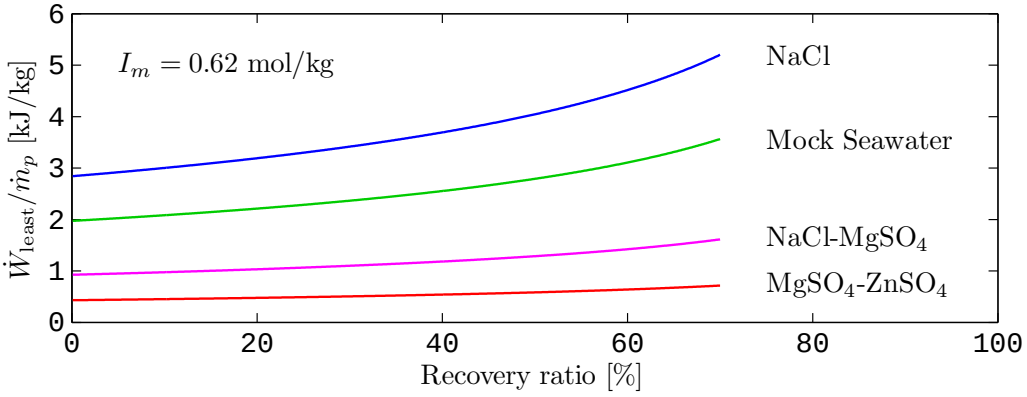

(c) Molal ionic strength of all feed streams is 0.62 mol/kg, equivalent to a 35 g/kg NaCl solution.

Figure 3-16: The least work of separation for various mixed electrolyte solutions at equal salinity, ionic molality, and ionic strength.

strength fixed at 0.62 mol/kg which is the ionic strength of a 35 g/kg NaCl solution (Fig. 3-16c). Again, the same trend is observed. Given that increasing concentration results in higher work requirements while increasing valence tends to reduce work requirements, it is clear that ionic strength, which is a function of both concentration and valence, cannot be used by itself to estimate the work requirements. This can be seen by noting that increasing the concentration of the NaCl solution would serve to both increase the ionic strength and the work of separation requirements.

The fact that the least work of separation is dependent on the specific ions present at a given concentration is also apparent when considering single electrolyte solutions. In order to illustrate this, Fig. 3-16 is recreated for the following single electrolyte solutions in Fig. 3-17: NaCl, KCl, $CaCl_2$, $MgCl_2$, Na_2SO_4, $MgSO_4$, and $ZnSO_4$. Again, all of the single electrolyte solutions are compared under three different conditions: equal salinity (Fig. 3-17a), equal ionic molality (Fig. 3-17b), and equal ionic strength (Fig. 3-17c).

In all comparisons, it is seen that there is a wide range in the work of separation requirements, indicating that the specific ions present are an important variable in this calculation. As with the comparison of mixed electrolyte solutions, it is seen that at fixed salinity, the heavier salts tend to have lower separation requirements, due in part to lower molality, higher ionic charge, and increased ion pairing (Fig. 3-17a). At fixed ionic molality, the solutions are grouped roughly based on ion composition. The chloride salts all have higher requirements than the sulphate salts (Fig. 3-17b). Finally, at fixed ionic strength, the results group strongly based on ν_s as well as charge, which is to be expected given that ionic strength is a function of molal concentration and ionic charge. As the charge of the ions increases for fixed ionic strength, the molality of the ions necessarily decreases. Therefore, it is not surprising to see three groups: NaCl and KCl as 1:1 salts; $MgCl_2$, $CaCl_2$, and Na_2SO_4 as 2:1 salts; and $MgSO_4$ and $ZnSO_4$ as 2:2 salts (Fig. 3-17c).

Based on Figs. 3-16 and 3-17, it is clear that the least work of separation is a very strong function of the composition of the electrolyte solution. In all cases, the molality, molecular weight, valence of the electrolytes, and aqueous complexation serve to alter the work of separation requirements. Therefore, it is concluded that composition plays a substantial role in the overall energy requirements for desalination processes. This has important implications for both desalination and forward osmosis processes. Naturally, desalination systems' energy requirements will be a strong function of the given feed solution. Similarly, if the draw solution in a forward osmosis process is composed of heavy and high valence electrolytes, the required separation energy for the subsequent removal of H_2O from the draw solution will be substantially lower than what is required for the separation of H_2O from seawater, or any other solution composed mostly of lighter, single charged ions that are not prone to complexation.

3.10 Conclusions

Based on the parametric study of aqueous sodium chloride, mock seawater, and a high-valence electrolyte solution, the following conclusions are made:

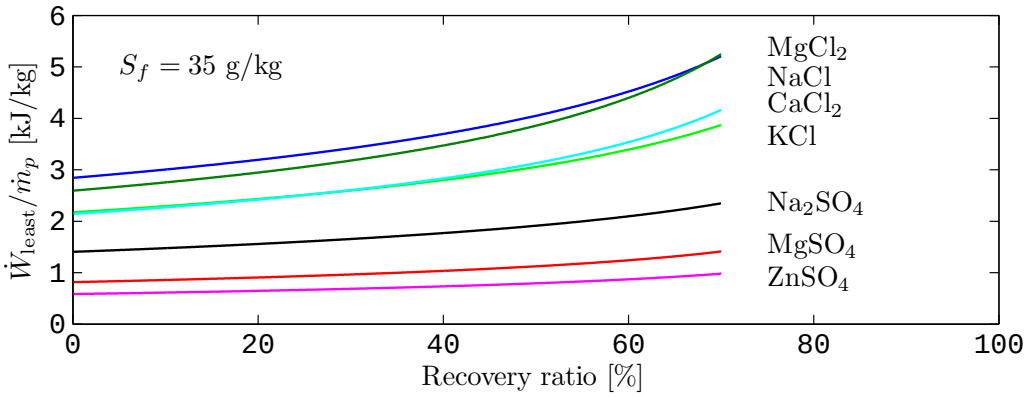

(a) Salinity of all feed streams is 35 g/kg.

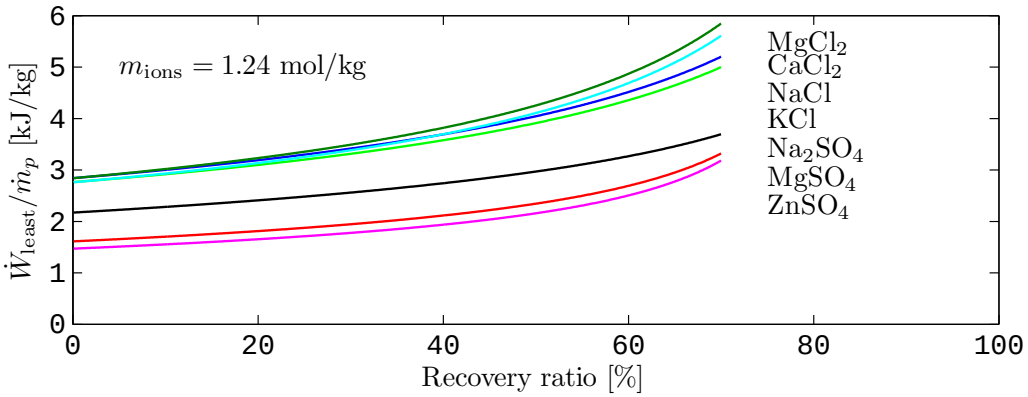

(b) Molality of all ions in all feed streams is 1.24 mol/kg, equivalent to a 35 g/kg NaCl solution.

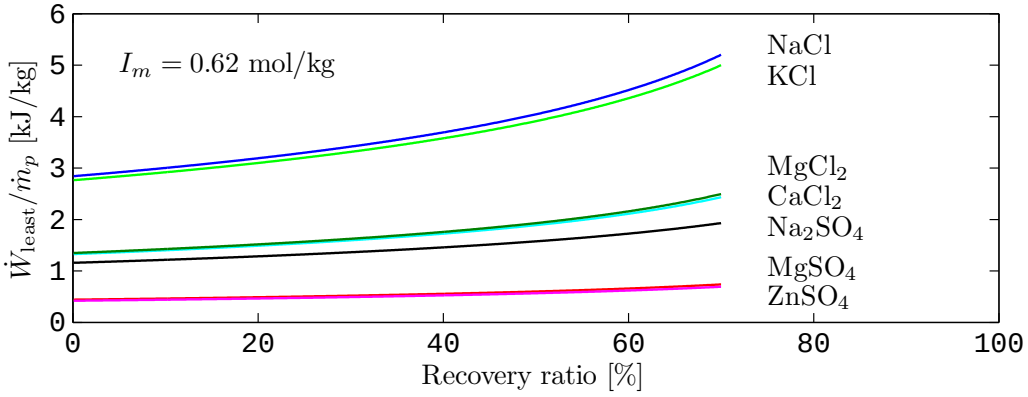

(c) Molal ionic strength of all feed streams is 0.62 mol/kg, equivalent to a 35 g/kg NaCl solution.

Figure 3-17: The least work of separation for various single electrolyte solutions at equal salinity, ionic molality, and ionic strength.

1. The least work of separation can be divided into ideal and nonideal parts. The ideal part is a function of composition (specifically, mole fraction). The nonideal part is a function of the fugacity coefficients of the solvent and the rational activity coefficients of the solutes in the feed, product, and concentrate streams. Both are functions of temperature, feed and product molality, and molar recovery ratio.

2. Approximating a sodium chloride solution as ideal introduces small error in calculating the least work of separation for salinities and recovery ratios representative of seawater and brackish water desalination systems since the effects of the nonidealities of water and salt tend to have opposite signs, thus partially canceling out. The relatively low error is *not* attributable to near-ideal behavior of the solution itself.

3. Nonidealities associated with the salts become negligible in evaluating least work under certain operating conditions because they cancel out, not because they are insignificant. The nonidealities associated with water are negligible except for highly concentrated solutions.

4. The ideal solution approximation for both single and mixed electrolyte solutions sometimes yields accurate results due to happenstance cancellation, not due to nearly ideal solution behavior.

5. Sodium chloride solutions tend to approximate seawater more accurately at higher salinities.

6. Single salt models for the evaluation of salt specific activity coefficients in mixed electrolyte solutions should only be used for very dilute solutions. Using them for non-dilute solutions can result in error greater than what is caused by assuming ideal solution behavior. This is especially true for Debye-Hückel equations such as Davies equation.

7. Using an effective molality for each salt, defined based on the solution ionic strength, in conjunction with the Pitzer ion interaction model (single electrolyte model) gives good agreement with the more complicated Pitzer-Kim mixed electrolyte model. This method can be used as an approximation for determining both salt and water activity coefficients.

8. Error introduced through the use of single-electrolyte models and the ideal solution approximation is greatly increased when the valence of electrolytes increases.

9. The specific set of ions composing a solution has a significant impact on the least work of separation that cannot be accounted for simply by looking at overall salinity or using single variables such as ionic strength or total dissolved solids (TDS). In particular, improper application of seawater properties to other kinds of saline water can result in substantial error.

10. Electrolyte solutions that are more prone to aqueous complexation, have higher valence, and heavier molecular weights tend to have lower work of separation requirements. Ionic strength is not strongly correlated with the least work of separation.

Chapter 4

Second Law efficiency for separation processes

Chapter abstract

Entropy generation analysis, and specifically, Second Law efficiency, is an important tool for illustrating the influence of irreversibilities within a system on the required energy input. When defining Second Law efficiency, the useful exergy output of the system must be properly defined. For chemical separation systems, this is the minimum least work of separation required to extract a unit of product from a feed stream of a given chemical composition. For a desalination process, this is the minimum least work of separation for producing one kilogram of product water from feed of a given salinity. The generalized least energy of separation equation is used to derive an expression for Second Law efficiency that can be applied to any chemical separation process, including those driven by a combination of work, heat, and fuel inputs.

Further, since most modern, large-scale desalination plants operate in cogeneration schemes, a methodology for correctly evaluating Second Law efficiency for the desalination plant based on primary energy inputs is demonstrated. It is shown that, from a strictly energetic point of view and based on currently available technology, cogeneration using electricity to power a reverse osmosis system is energetically superior to thermal systems such as multiple effect distillation and multistage flash distillation, despite the very low grade heat input normally applied in those systems.

Finally, in order to evaluate the Second Law efficiency while considering specific sources of irreversibility, entropy generation mechanisms present in a wide range of desalination processes are analyzed. In particular, entropy generated in the run down to equilibrium of discharge streams must be considered. Physical models are applied to estimate the magnitude of entropy generation by component and individual processes. These formulations are applied to calculate the total entropy generation in several desalination systems including multiple effect distillation, multistage flash, membrane distillation, mechanical vapor compression, reverse osmosis, and humidification-dehumidification. Within each technology, the relative importance of each source of entropy generation is discussed in order to determine which should be the target of entropy generation minimization. As given here, the correct application of Second Law efficiency shows which systems operate closest to the reversible limit and helps to indicate which systems have the greatest potential for improvement.

This chapter consists of work that is published in [21, 22]. Sections on multistage flash, membrane distillation, and mechanical vapor compression were co-authored with Gregory P. Thiel, Edward K. Summers, and Ronan K. McGovern, respectively. Additionally, they provided valuable input during the development of the derivation of work-based definition of Second Law efficiency.

4.1 Introduction

Advances over the last several decades have dramatically reduced the energy costs associated with seawater desalination. However, seawater desalination is still an energy intensive process that is made more so as a result of irreversibilities within the various system components. Therefore, there is a need to understand and reduce the sources

of irreversibility within the systems in order to improve their performance and reduce energy consumption. In order to gain a deeper understanding of the irreversibilities, a Second Law analysis is used to determine the components with maximum entropy generation in six different systems: multiple effect distillation (MED), multistage flash (MSF), direct contact membrane distillation (DCMD), mechanical vapor compression (MVC), reverse osmosis (RO), and humidification-dehumidification (HDH).

Second Law analysis of desalination systems is not new [27, 52, 87–91]. However, there have been many conflicting definitions for Second Law efficiency; and, to the authors' knowledge, comprehensive studies identifying all sources of entropy generation have not been conducted. In this chapter, a consistent definition of Second Law efficiency for generic chemical separators is presented since it is a parameter that can be used to compare the thermodynamic performance of systems, much like Carnot efficiency is used to benchmark power generating systems. First, the exergetic value of the product is defined in terms of the generalized least energy of separation (as defined in Chapter 2). By using the generalized least energy of separation, the definition of Second Law efficiency is generalized such that it may be applied to systems that utilize any combination of mechanical, thermal, or chemical energy inputs. Additionally, the required energy of separation is decomposed into the least work of separation plus the contribution from all significant sources of irreversibilities within the system, and methods of evaluating the entropy generation due to specific physical processes are derived. Then, these methods are applied ot the six desalination systems mentioned above in order to evaluate the Second Law efficiency. Finally, Second Law efficiency is evaluated for separation systems that are part of a larger cogeneration plant through a parametric analysis.

4.2 Energetic performance parameters

Second Law (or exergetic) efficiency (η_{II}) is employed as a measure of the thermodynamic reversibility of a desalination system [21]. Unlike First Law efficiency, which measures the amount of an energy source that is put to use, Second Law efficiency measures the extent of irreversible losses within a system. As a result, a completely reversible system will have a Second Law efficiency of 1 even though the First Law efficiency is likely to be lower. Bejan [31] and others [47, 89] define the exergetic efficiency as the ratio of the exergy of the process products to the process fuel. In other words, the exergetic efficiency is the ratio of the useful exergy of the outputs of the process ($\dot{\Xi}_{\text{out,useful}}$) to the exergy of the process inputs ($\dot{\Xi}_{\text{in}}$):

$$\eta_{II} \equiv \frac{\dot{\Xi}_{\text{out,useful}}}{\dot{\Xi}_{\text{in}}} = 1 - \frac{\dot{\Xi}_{\text{destroyed}} + \dot{\Xi}_{\text{lost}}}{\dot{\Xi}_{\text{in}}} \tag{4.1}$$

The second equality in Eq. (4.1) is valid since the useful exergy out is equal to the exergy in minus the sum of the exergy destroyed ($\dot{\Xi}_{\text{destroyed}}$) and the exergy lost ($\dot{\Xi}_{\text{lost}}$). Exergy destroyed represents lost available work due to irreversibilities within the system. Exergy lost represents lost available work due to discarding exergy carrying

streams to the environment. Note that when the material inputs to the system are taken to be at equilibrium with the environment, Ξ_{in} equals $\Xi_{\dot{W}_{\text{sep}}}$, $\Xi_{\dot{Q}_{\text{sep}}}$, or Ξ_{fuel}, depending on the energy input.

In addition to η_{II}, there are three often used parameters for describing the energetic performance of desalination systems. The first, called gained output ratio (GOR), is the ratio of the enthalpy required to evaporate the distillate (or equivalently, the energy release in condensation) and the heat input to the system, or

$$\text{GOR} \equiv \frac{\dot{m}_p h_{fg}(T_0)}{\dot{Q}_{\text{sep}}} \tag{4.2}$$

As described in Chapter 2, GOR is a direct measure of how many times the latent heat of vaporization is captured in the condensation of purified water vapor and reused in a subsequent evaporation process to create additional water vapor.

The second parameter, known as the performance ratio (PR), is defined as the ratio of the mass flow rate of product water to that of the heating steam:

$$\text{PR} \equiv \frac{\dot{m}_p}{\dot{m}_s} \tag{4.3}$$

For a thermal desalination system in which the heat input is provided by condensing steam, as is typical of large-scale thermal processes such as MED and MSF, the values of PR and GOR are quite similar. In that case, the two parameters differ only by the ratio of the latent heat of vaporization at the distillate and heating steam temperatures. That is, GOR = PR$\times\frac{h_{fg}(T_0)}{h_{fg}(T_{\text{steam}})}$.

The third parameter, specific electricity consumption (SEC) is best suited to work-driven desalination systems. It is defined as the ratio of the work of separation (or work input) to the mass flow rate of product water, or

$$\text{SEC} \equiv \frac{\dot{W}_{\text{sep}}}{\dot{m}_p} \tag{4.4}$$

As was the case with GOR, because thermal and electrical energy are not directly comparable, numerical values of SEC cannot be compared between thermal- and work-driven systems without appropriate conversion factors for the work of separation.

4.3 Exergetic value of product

Prior to applying Eq. (4.1) to desalination systems, it is important to understand the differences between the three definitions of work that are presented. The work of separation ($\dot{W}_{\text{sep}}$) is the actual amount of work necessary to produce a given amount of water from a fixed feed stream using a real separation process. The least work of separation ($\dot{W}_{\text{least}}$) represents the amount of work necessary to produce the same amount of product water from the feed stream while operating under reversible conditions. Finally, the minimum least work ($\dot{W}^{\text{min}}_{\text{least}}$) is the minimum required work

of separation in the limit of reversible operation and infinitesimal extraction. As a result, the following relation will always hold:

$$\dot{W}_{\text{sep}} > \dot{W}_{\text{least}}(r > 0) > \dot{W}^{\text{min}}_{\text{least}}(r = 0) \tag{4.5}$$

In a desalination process, purified water is considered to be the useful product. The useful exergy associated with pure water is the minimum least work (or heat) of separation that is required to obtain purified water from feed water of a given salinity (*i.e.*, infinitesimal extraction of pure water with inlet and outlet streams at ambient temperature). The minimum least work (at zero recovery), rather than the least work (at finite recovery), is used since it represents the actual exergetic value of pure water. To further illustrate, when analyzing a unit of pure water, it is impossible to know the process that was used to produce it. Therefore, the minimum energy required to produce it must be the exergetic value and $\dot{\Xi}_{\text{out,useful}} = \dot{W}^{\text{min}}_{\text{least}}(r = 0)$.

Since the control volume is defined so that the inlet stream is at the dead state, the only exergy input to the system comes in the form of either a work ($\dot{W}_{\text{sep}}$) or heat ($\dot{Q}_{\text{sep}}$) input (exergy of the feed stream is zero). The work of separation is equivalent to the useful work done within the system plus the exergy destroyed within that system which can be evaluated in one of two ways.

In order to calculate the work of separation, two processes may be considered. The first involves a separation process where the products are brought to thermal and mechanical equilibrium with the environment, whereas the concentrate is also brought into chemical equilibrium (total dead state, TDS). The reversible work required to achieve this process corresponds to the least work at zero recovery. The total work of separation is given by the sum of the reversible work required plus the exergy destruction associated with entropy generated in the separation and run down to equilibrium processes:

$$\dot{W}_{\text{sep}} = \dot{W}^{\text{min}}_{\text{least}}(r = 0) + T_0 \dot{S}^{\text{TDS}}_{\text{gen}} \tag{4.6}$$

The second involves a separation process where the products are only brought to thermal and mechanical equilibrium with the environment (restricted dead state, RDS). The reversible work required to achieve this process corresponds to the least work at finite recovery. The total work of separation again is given by the sum of the reversible work required plus the exergy destruction associated with entropy generated in this process:

$$\dot{W}_{\text{sep}} = \dot{W}_{\text{least}}(r > 0) + T_0 \dot{S}^{\text{RDS}}_{\text{gen}} \tag{4.7}$$

It can be shown that Eqs. (4.6) and (4.7) are equivalent [*cf.*, Section 4.6.6. Substitution of $\dot{W}^{\text{min}}_{\text{least}}$ from Eq. (4.66) into Eq. (4.7) while noting that $\dot{S}^{\text{TDS}}_{\text{gen}} = \dot{S}^{\text{RDS}}_{\text{gen}} + \dot{S}^{\text{concentrate RDS}\to\text{TDS}}_{\text{gen}}$ exactly gives Eq. (4.6)]. Note that the work of separation for a system can also be directly evaluated using a First Law analysis.

4.4 Second Law efficiency for a chemical separator

As discussed in the previous section, the useful output from a desalination system is the amount (mass) of purified product water that is created. Exergetically, the mass of the product water is represented by the minimum least work of separation, which is the least work of separation at infinitesimal recovery:

$$\dot{W}_{\text{least}}^{\text{min}} \equiv \lim_{r \to 0} \dot{W}_{\text{least}} = \lim_{r \to 0} \dot{\Xi}_{\text{least}} \tag{4.8}$$

Similarly, the minimum least heat of separation is at infinitesimal recovery:

$$\dot{Q}_{\text{least}}^{\text{min}} \equiv \lim_{r \to 0} \dot{Q}_{\text{least}} = \lim_{r \to 0} \left(1 - \frac{T_0}{T}\right)^{-1} \dot{\Xi}_{\text{least}} \tag{4.9}$$

A new parameter called the minimum least fuel of separation may also be introduced:

$$\dot{m}_{\text{least}}^{\text{min}} \equiv \lim_{r \to 0} \dot{m}_{\text{least}} = \lim_{r \to 0} \xi_{\text{fuel}}^{-1} \dot{\Xi}_{\text{least}} \tag{4.10}$$

Using the minimum least work, heat, and fuel of separation, the Second Law efficiency can be defined in three different ways:

$$\eta_{II} = \frac{\dot{W}_{\text{least}}^{\text{min}}}{\dot{W}_{\text{sep}}}, \qquad \eta_{II} = \frac{\dot{Q}_{\text{least}}^{\text{min}}}{\dot{Q}_{\text{sep}}}, \qquad \eta_{II} = \frac{\dot{m}_{\text{least}}^{\text{min}}}{\dot{m}_{\text{sep}}} \tag{4.11}$$

A more general way to define Second Law efficiency is simply to use exergy:

$$\eta_{II} = \frac{\dot{\Xi}_{\text{least}}^{\text{min}}}{\dot{\Xi}_{\text{sep}}} \tag{4.12}$$

Note that Eq. (4.12) reduces to the three special cases given in Eq. (4.11) depending on which energy inputs are used.

Clearly, the three definitions of Second Law efficiency presented in Eq. (4.11) are bounded by 0 and 1 because $\dot{W}_{\text{sep}} > \dot{W}_{\text{least}}$, $\dot{Q}_{\text{sep}} > \dot{Q}_{\text{least}}$, and $\dot{m}_{\text{sep}} > \dot{m}_{\text{least}}$. Observe that $\dot{W}_{\text{least}}$, $\dot{Q}_{\text{least}}$, and $\dot{m}_{\text{least}}$ are functions of feed salinity, product salinity, recovery ratio, and T_0. Additionally, η_{II} will only equal 1 in the limit of completely reversible operation, as expected. Note that the selection of the control volume suitably far away such that all streams are at thermal and mechanical equilibrium allows for this bounding.

It is important to ensure that control volume selection is consistent for all systems being considered in order to fairly compare the Second Law performance. While Eq. (4.12) is straight forward to evaluate for systems with only one source of energy input, some care is required when using it to evaluate systems with multiple energy inputs. First, consider the numerator, which is defined by Eq. (2.27). The minimum least exergy of separation is fixed and is a function of the environmental temperature and pressure as well as the salinities of the feed, concentrate, and product streams only, regardless of the energy input.

The denominator is a little less straightforward to evaluate and is highly dependent on how the control volume is drawn. For a stand-alone desalination system in which some combination of work, heat, and fuel is used to power the separation process, the denominator is simply the left hand side of Eq. (2.17):

$$\dot{\Xi}_{\text{sep}} = \dot{W}_{\text{sep}} + \left(1 - \frac{T_0}{T}\right)\dot{Q}_{\text{sep}} + \xi_{\text{fuel}}\dot{m}_{\text{sep}} \tag{4.13}$$

since this represents the sum of the exergy of each of the various energy inputs provided to the desalination system. To illustrate the evaluation of Eq. (4.12) using Eq. (4.13), η_{II} is calculated for various stand-alone desalination systems that are driven using a combination of electrical and thermal energy input. Relevant values of $\dot{W}_{\text{sep}}$, $\dot{Q}_{\text{sep}}$, and other parameters for HDH [40] and FO [35] are taken from literature and the results are provided in Table 4.1.

Equation (4.13) should not be used for desalination systems in which those energy inputs (*i.e.*, $\dot{W}_{\text{sep}}$, $\dot{Q}_{\text{sep}}$, and $\dot{m}_{\text{sep}}$) are not of the same form and quality as the energy inputs to the larger cogeneration system. It is essential that η_{II} be evaluated in terms of primary energy sources (*i.e.*, in terms of the energy inputs to the larger system control volume, not just to the desalination plant control volume) in order to properly account for all thermodynamic losses that occur, including those in energy conversion processes such as the generation of electricity from heat. Given that many large-scale desalination processes are done in a cogeneration scheme in which some form of primary energy (typically fuel) is used to generate both electricity and desalinated water, η_{II} for those systems should be evaluated in terms of the primary energy input for the cogeneration system as is discussed in Section 4.5.

In addition to Eqs. (4.11) and (4.12), the Second Law efficiency may be expanded in terms of the irreversibilities that occur within the system using Eqs. (4.6) and (4.7):

$$\eta_{II} = \frac{\dot{W}^{\min}_{\text{least}}}{\dot{W}_{\text{sep}}} = \frac{\dot{W}^{\min}_{\text{least}}}{\dot{W}^{\min}_{\text{least}} + T_0\dot{S}^{\text{TDS}}_{\text{gen}}} = \frac{\dot{W}^{\min}_{\text{least}}}{\dot{W}_{\text{least}} + T_0\dot{S}^{\text{RDS}}_{\text{gen}}} \tag{4.14}$$

$$\eta_{II} = \frac{\dot{Q}^{\min}_{\text{least}}}{\dot{Q}_{\text{sep}}} = \frac{\dot{Q}^{\min}_{\text{least}}}{\dot{Q}^{\min}_{\text{least}} + \left(1 - \frac{T_0}{T_H}\right)^{-1} T_0\dot{S}^{\text{TDS}}_{\text{gen}}} = \frac{\dot{Q}^{\min}_{\text{least}}}{\dot{Q}_{\text{least}} + \left(1 - \frac{T_0}{T_H}\right)^{-1} T_0\dot{S}^{\text{RDS}}_{\text{gen}}} \tag{4.15}$$

Both of these equations are used in detail in Section 4.6.

While it was shown in Chapter 2 that there are three relevant Second Law based performance parameters for desalination systems: specific entropy generation, Eq. (2.8); specific exergy destruction, Eq. (2.9); and Second Law efficiency, Eq. (4.11). This chapter focuses on specific entropy generation and Second Law efficiency.

Table 4.1: Second Law efficiency for various stand-alone experimental desalination systems. Values marked with * are estimated. Values marked with † are evaluated using estimated figures. Note that Ξ_{sep} is a strong function of T_H and η_{II} is a strong function of T_H and y_f.

System	y_f [g/kg]	$\dot{W}_{\text{sep}}$ [kJ/kg (kWh_e)]	$\dot{Q}_{\text{sep}}$ [kJ/kg]	T_H [°C]	$\dot{\Xi}_{\text{sep}}$ [kJ/kg]	η_{II} [%]
HDH [40]	35*	1.44 (0.40)	848 (GOR = 2.6)	90	153	1.8†
HDH (extraction) [40]	35*	1.62 (0.45)	551 (GOR = 4.0)	90	100	2.7†
FO [35]	73	30.6 (8.50)	990 (275 kWh_t)	100 [92]	230	2.5

4.5 Second Law efficiency for a desalination system operating as part of a cogeneration plant

Since many large-scale desalination processes are done in a cogeneration scheme, it is useful to consider the amount of additional energy that must be provided to the power plant in order to generate the required amount of heat and work to power the desalination plant. In order to do so, consider a cogeneration system in which a power plant is connected to a desalination plant as shown in Fig. 4-1. In this system, a heat input ($\dot{Q}_H$) is provided to a power plant. This heat input is equal to the amount of heat necessary to drive the power plant ($\dot{Q}_{pp}$) plus the additional amount necessary to generate steam and electricity for the desalination plant ($\dot{Q}_d$ to produce $\dot{Q}_{\text{sep}}$ and $\dot{W}_{\text{sep}}$). The power plant produces a net amount of work equal to the desired plant work production ($\dot{W}_{pp}$) plus the amount of work necessary to drive the desalination plant ($\dot{W}_{\text{sep}}$). Note that typically, fuel, rather than heat, is the primary energy input to cogeneration systems and therefore, the analysis should be done in terms of the amount of fuel required to drive the power plant plus the additional amount of fuel required to produce the heat and work necessary to drive the desalination plant ($\dot{m}_{\text{fuel}} = \dot{m}_{pp} + \dot{m}_d$). However, for simplicity and with the goal of highlighting the difference between work and heat driven systems, the control volume for this analysis is drawn under the assumption that heat, and not fuel, is transferred into the system. The effect of including the combustor is discussed briefly below.

The following derivation is based on the work of El-Sayed and Silver [16]. The First and Second Laws of Thermodynamics are written about the power plant control volume:

$$\dot{Q}_{pp} + \dot{Q}_d = \dot{Q}_{\text{sep}} + \dot{Q}_0 + \dot{W}_{pp} + \dot{W}_{\text{sep}} \tag{4.16}$$

$$\dot{S}_{\text{gen}} + \frac{\dot{Q}_{pp}}{T_H} + \frac{\dot{Q}_d}{T_H} = \frac{\dot{Q}_{\text{sep}}}{T_s} + \frac{\dot{Q}_0}{T_0} \tag{4.17}$$

Multiplying the Second Law by T_0 and substituting into the First Law to eliminate ambient heat transfer ($\dot{Q}_0$) gives:

$$\dot{W}_{pp} + \dot{W}_{\text{sep}} = \left(\dot{Q}_{pp} + \dot{Q}_d\right)\left(1 - \frac{T_0}{T_H}\right) - \dot{Q}_{\text{sep}}\left(1 - \frac{T_0}{T_s}\right) - T_0\dot{S}_{\text{gen}} \tag{4.18}$$

In order to deal with the irreversibilities within the system, it is assumed that the rate of entropy generation is proportional to the amount of work produced by a reversible power plant operating within the same heat transfer loads. That is,

$$T_0\dot{S}_{\text{gen}} \propto \left(\dot{W}_{pp} + \dot{W}_{\text{sep}}\right) = \left(\dot{Q}_{pp} + \dot{Q}_d\right)\left(1 - \frac{T_0}{T_H}\right) - \dot{Q}_{\text{sep}}\left(1 - \frac{T_0}{T_s}\right) \tag{4.19}$$

Letting the constant of proportionality be $(1 - \eta_{pp})$, where $\eta_{pp} = \eta/\eta_{\text{Carnot}}$ is the

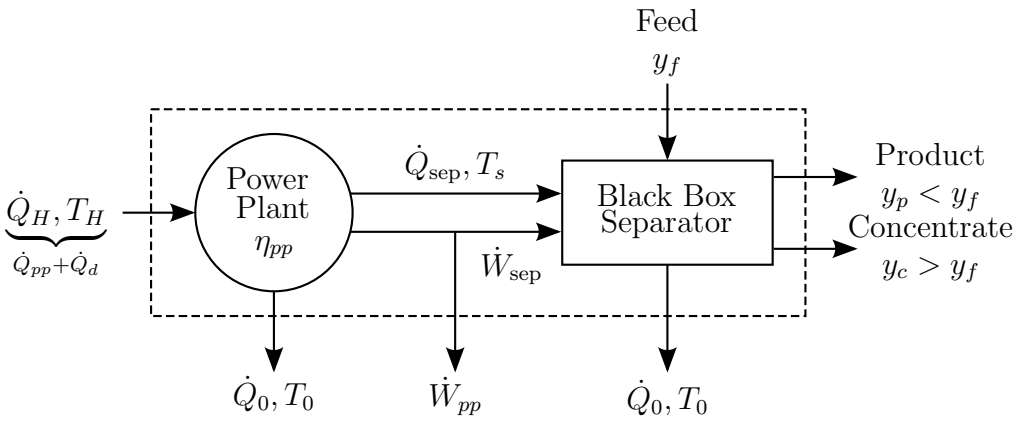

Figure 4-1: In a combined water and power cogeneration plant, the power plant converts heat input into work output, work for the desalination plant, and heat for the desalination plant. It is assumed that the power plant operates at a Second Law efficiency of η_{pp}.

Second Law efficiency of the power plant,

$$T_0\dot{S}_{\text{gen}} = \left[\left(\dot{Q}_{pp}+\dot{Q}_d\right)\left(1-\frac{T_0}{T_H}\right)-\dot{Q}_{\text{sep}}\left(1-\frac{T_0}{T_s}\right)\right](1-\eta_{pp}) \tag{4.20}$$

Substituting $T_0\dot{S}_{\text{gen}}$ into Eq. (4.18) gives:

$$\dot{W}_{pp}+\dot{W}_{\text{sep}} = \left(\dot{Q}_{pp}+\dot{Q}_d\right)\left(1-\frac{T_0}{T_H}\right)\eta_{pp}-\dot{Q}_{\text{sep}}\left(1-\frac{T_0}{T_s}\right)\eta_{pp} \tag{4.21}$$

Since the goal is to determine how much additional heat is necessary to drive the desalination system, $\dot{Q}_d$ must be independent of the amount of work produced by the power plant. To do so, first consider the same power plant in which the desalination system is not operating and the power plant is producing a net output of $\dot{W}_{pp}$. Then, setting $\dot{Q}_d$, $\dot{Q}_{\text{sep}}$, and $\dot{W}_{\text{sep}}$ to zero, $\dot{Q}_{pp}$ is found to be:

$$\dot{Q}_{pp} = \frac{\dot{W}_{pp}}{\left(1-\frac{T_0}{T_H}\right)\eta_{pp}} \tag{4.22}$$

Substituting this back into the above equation results in $\dot{Q}_{pp}$ and $\dot{W}_{pp}$ canceling out. Solving for $\dot{Q}_d$,

$$\dot{Q}_d = \frac{\dot{W}_{\text{sep}}}{\left(1-\frac{T_0}{T_H}\right)\eta_{pp}}+\dot{Q}_{\text{sep}}\frac{\left(1-\frac{T_0}{T_s}\right)}{\left(1-\frac{T_0}{T_H}\right)} \tag{4.23}$$

In order to evaluate the Second Law efficiency of the desalination plant, one might think to use Eq. (4.13) for the denominator in Eq. (4.12) since it represents the energy inputs to the desalination system. While this would be correct for a stand alone system, $\dot{W}_{\text{sep}}$ and $\dot{Q}_{\text{sep}}$ do not represent the true energy inputs for separation system

shown in Fig. 4-1. Instead, the energy input for the desalination system is the extra heat transfer provided to the power plant, $\dot{Q}_d$. Therefore, the Second Law efficiency should be evaluated based on this quantity. Substituting Eq. (4.23) into Eq. (4.12) gives:

$$\eta_{II} = \frac{\dot{\Xi}^{\min}_{\text{least}}}{\dot{\Xi}_{\text{sep}}} = \frac{\dot{W}^{\min}_{\text{least}}}{\frac{\dot{W}_{\text{sep}}}{\eta_{pp}} + \dot{Q}_{\text{sep}}\left(1 - \frac{T_0}{T_s}\right)} \tag{4.24}$$

The important difference between using Eq. (4.13) and Eq. (4.23) is the fact that the work input ($\dot{W}_{\text{sep}}$) is divided by the Second Law efficiency of the power plant. This effectively accounts for the fact that the work is not produced reversibly from the heat source, and therefore, cannot be directly compared to the thermal exergy value. If there is no work input, then $\dot{W}_{\text{sep}} = 0$ and Eq. (4.24) correctly reduces to Eq. (4.12). Similarly, if there is no heat input, then $\dot{Q}_{\text{sep}} = 0$ and Eq. (4.24) reduces to:

$$\eta_{II} = \eta_{pp} \frac{\dot{W}^{\min}_{\text{least}}}{\dot{W}_{\text{sep}}} \tag{4.25}$$

In the limit of reversible operation for the power plant (*i.e.*, $\eta_{pp} = 1$), Eq. (4.25) reduces to Eq. (4.12). The Second Law efficiency of the power plant is present in Eq. (4.25) since the work used to power the desalination plant is produced irreversibly. Had the losses in the combustor been included in this analysis, both $\dot{W}_{\text{sep}}$ and $\dot{Q}_{\text{sep}}$ in Eq. (4.24) would be divided by the Second Law efficiency of the combustor, $\eta_{II,\text{combustor}}$. This would have the effect of reducing the Second Law efficiency of the desalination process in proportion to the Second Law efficiency of the combustor. Both the heat and work terms are effected equally since the losses occur prior to the power generation process.

In order to better understand the energetic behavior of both membrane and thermal systems, a parametric study of Eq. (4.24) is conducted in the following three sections for systems using standard seawater as the feed source (35 g/kg, 25 °C). Under these conditions, the minimum least work of separation of seawater per kilogram of product is 2.71 kJ/kg [21]. The Second Law efficiency is evaluated under three different conditions: (1) work is the only input, (2) heat is the only input at varying temperatures, (3) heat at 100 °C is the primary input and the amount of pumping work is varied.

4.5.1 Desalination powered by work

For desalination systems that are powered entirely using work, $\dot{Q}_{\text{sep}} = 0$ and Eq. (4.24) reduces to Eq. (4.25). As a result, it is clear that unless the power plant operates reversibly, a work powered desalination system can never achieve 100% Second Law efficiency, even if the desalination process is conducted reversibly. This is a direct result of the fact that the primary energy source in the cogeneration scheme is heat to the power plant, not electricity to the desalination plant. For the following study, it is assumed that the power plant is a representative combined cycle plant operating

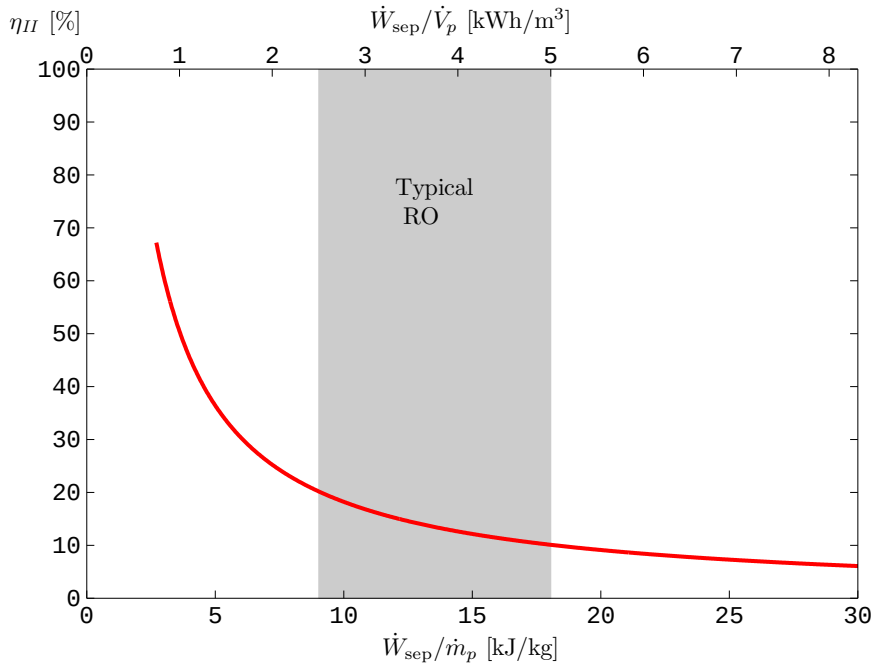

Figure 4-2: The Second Law efficiency of a work-driven desalination system operating in a cogeneration scheme can never reach 100% unless the power plant operates reversibly. Typical values for current reverse osmosis systems are highlighted. Feed water is at $T_0 = 25\,°\text{C}$ and $y_f = 35\,\text{g/kg}$.

between 1400 and 298.15 K with a First Law efficiency of 52.8% and a Second Law efficiency of 67.2% [93]. The Second Law efficiency of a work-driven desalination plant is shown in Fig. 4-2 as a function of $\dot{W}_{\text{sep}}$ starting at a minimum value of $\dot{W}_{\text{sep}} = \dot{W}_{\text{least}}$.

All work-driven systems in this cogeneration scheme pay an energetic penalty on efficiency since the initial energy source (heat) must go through a conversion process (power plant) that operates irreversibly, and therefore, the limiting Second Law efficiency as $\dot{W}_{\text{sep}} \to \dot{W}_{\text{least}}$ is η_{pp}, not 1. If the primary source of energy was considered to be mass of fuel, then the limiting Second Law efficiency would be equal to the product of the Second Law efficiencies of the combustor and the power plant. That is, $\eta_{II}^{\text{combustor}}\eta_{pp}$. The typical range of operation for current RO technologies is between 2.5–5 kWh and is highlighted in Fig. 4-2. RO systems with energy recovery tend to be on the lower end of this range while systems without energy recovery tend to be on the higher end of this range. Exact values are a function of system design and feed water characteristics [15, 94–98]. This represents Second Law efficiency values ranging from approximately 10–20%.

4.5.2 Desalination powered by heat

Nearly all large-scale thermal desalination systems are connected to a power plant since large quantities of steam are required to provide heating to the feed. For a thermal desalination plant powered purely using steam at T_s, Eq. (4.24) reduces to

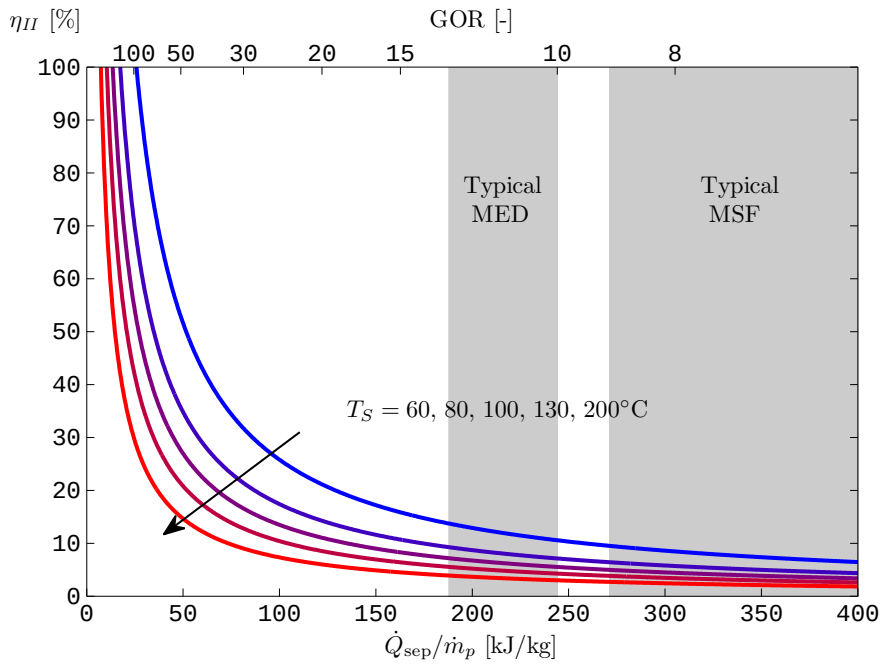

Figure 4-3: The power plant converts heat input into work output, work for the desalination plant, and heat for the desalination plant. Feed water is at $T_0 = 25\,°C$ and $y_f = 35\,g/kg$.

the heat based definition of the Second Law efficiency as given in Eq. (4.11):

$$\eta_{II} = \frac{\dot{Q}^{\min}_{\text{least}}}{\dot{Q}_{\text{sep}}} \tag{4.26}$$

Note that this expression is not a function of the high temperature heat source, T_H. This is a result of the assumption made that the entropy generated in the power plant is proportional to the reversible work produced by the power plant operating between two set temperatures. Additionally, the effect of the entropy generation is reflected by η_{pp} in the work portion of the energy input which is equal to zero in this case.

Unlike the work powered case, the thermal desalination plants do not experience the same energetic penalty that is attributed to the irreversibilities within the power production process. Therefore, it is theoretically possible for a reversible thermal desalination plant operating within a cogeneration scheme to achieve 100% Second Law efficiency. This is shown in Fig. 4-3 in which the Second Law efficiency approaches 100% as $\dot{Q}_{\text{sep}} \to \dot{Q}_{\text{least}}$, regardless of steam temperature (T_S). Note that infinitely large heat exchangers and infinitely many stages would be required for a thermal plant to achieve such efficiencies.

Several observations are made from Fig. 4-3. First, at fixed heat of separation, the Second Law efficiency increases with decreasing steam temperature. This is expected since the exergetic value of heat increases with increasing temperature and if the same amount of higher temperature heat (fixed $\dot{Q}_{\text{sep}}$ with rising T_s) is required for

a separation process, then the process is utilizing higher exergy heat less efficiently. Second, the minimum heat of separation is a function of steam temperature as is indicated by the fact that it is a function of Carnot efficiency. Third, the rate of increase of Second Law efficiency with respect to a decrease in the heat of separation ($-\mathrm{d}\eta_{II}/\mathrm{d}\dot{Q}_{\mathrm{sep}}$) is most significant at lower values for the heat of separation.

Typical heat requirements for modern MED and MSF plants are shown as grey bands in Fig. 4-3. MED and MED-TVC systems typically have performance ratios between about 10–13 and operate with steam around 80 °C [94, 95, 99, 100]. MSF systems typically have performance ratios between about 6–9 and operate with steam around 100 °C [94, 95]. This translates to Second Law efficiencies between 7–9% for MED and less than 5% for MSF. Based on the second observation above, it might seem that operating at a lower steam temperature would enable higher energy efficiency. However, for both MED and MSF plants, the number of effects (or stages) that can practically be built is related to the trade off between capital and operating expenses [100]. While increasing the number of effects results in increased energy recovery, and therefore increased efficiency and reduced operating costs, it also results in increased capital costs as a result of the increased heat transfer area. As the steam temperature decreases with fixed environment temperature, the temperature pinches in each effect decrease, requiring additional heat transfer area and increased capital cost. At lower steam temperatures, the number of effects that can economically be built is reduced, resulting in higher overall energy requirements and lower overall Second Law efficiency.

Comparing Figs. 4-2 and 4-3, it is clear that from a purely energetic point of view, work-driven systems are able to operate more efficiently than thermally driven systems. This point is made even more convincing when it is considered that nearly all thermal systems require substantial work input for running pumps and other equipment. This case is considered subsequently. The comparison between the two figures can only be made because the Second Law efficiency of both the work-driven and thermal driven plants is evaluated using the common energy input, $\dot{Q}_d$. If η_{II} for the two plants were not evaluated using the same primary energy input, the comparison between the two figures would not be meaningful.

4.5.3 Desalination powered by cogenerated heat and work

The Second Law efficiency of a thermal desalination plant operating using steam at 100 °C with pump work requirements ranging from 0–4 kWh is shown in Fig. 4-4. In the case of zero pump work, 100% Second Law efficiency is theoretically possible. However, once pump work is required, the possible Second Law efficiency drops substantially (*e.g.*, approximately 50% for 0.5 kWh of electrical work to drive pumps). Clearly, regardless of what the required heat of separation is, the additional requirement of pump work results in a decrease in the Second Law efficiency.

The results shown in Fig. 4-4 are generated based on the assumption that all energy provided to the desalination system originally comes from a common energy source, $\dot{Q}_d$. This value of heat input is then substituted into Eqs. (4.12) and (4.13) to get Eq. (4.24). Should a desalination plant have energy inputs from multiple primary

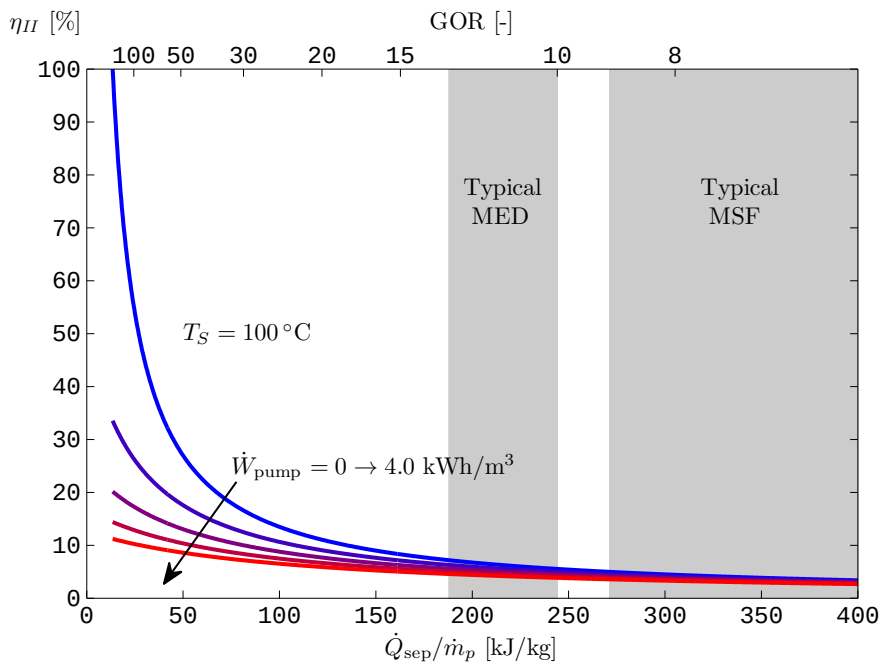

Figure 4-4: Second Law efficiency for a thermal desalination plant requiring work for pumping. Lines for pump work are in increments of 0.5 kWh. As the pump work increases, the Second Law efficiency decreases. Feed water is at $T_0 = 25\,°C$ and $y_f = 35\,g/kg$.

energy sources, then the analysis to derive the correct form of η_{II} will change slightly. All energy inputs should be traced to their primary sources (as was done for $\dot{W}_{\text{sep}}$ and $\dot{Q}_{\text{sep}}$ from $\dot{Q}_d$) and then each primary input should be combined based on the exergetic value as done in Eq. (4.13).

Based on Figs. 4-2 to 4-4, it is clear that for a desalination plant operating as part of a cogeneration scheme, the work-driven systems (based on currently available technology) always behave in an exergetically more favorably manner than the thermal driven systems (*i.e.*, higher η_{II}). This is true even when accounting for the energy penalty that comes from converting the source heat to work: and it is even further exemplified when considering that thermal systems typically require large amounts of electrical work for pumping (these are sometimes as high as the work requirements for an RO system).

While it can be concluded that current membrane systems are more efficient from a Second Law point of view, it should not be concluded that there is no role for thermal systems. It should, however, be concluded that exergetically, current work-driven systems are better performing than current thermal systems. Ultimately, several factors are considered when selecting a desalination technology including capital and operating costs, quality of feed water, and existing expertise and infrastructure. While the work systems are favored energetically, these other factors can lead to thermal systems being more desirable for a given location or application.

Table 4.2: Representative values of reference state constants for Eqs. (4.29), (4.30), (4.33), and (4.34).

Pure water and vapor constants, $T_{sat} = 50\,°C$, $p_{sat} = 12.3\,kPa$			
c	$4.18\,kJ/(kg\,K)$	h_{ref}^{IG}	$2590\,kJ/kg$
c_p	$1.95\,kJ/(kg\,K)$	h_{ref}^{IF}	$209\,kJ/kg$
R	$0.462\,kJ/(kg\,K)$	s_{ref}^{IG}	$8.07\,kJ/(kg\,K)$
v	$1.01 \times 10^{-3}\ m^3/kg$	s_{ref}^{IF}	$0.704\,kJ/(kg\,K)$
Seawater constants, $50\,°C$, $35\,g/kg$			
c	$4.01\,kJ/(kg\,K)$	h_{ref}^{IF}	$200\,kJ/kg$
v	$0.986 \times 10^{-3}\ m^3/kg$	s_{ref}^{IF}	$0.672\,kJ/(kg\,K)$

4.6 Analysis of entropy generation mechanisms

Several common processes in desalination systems result in entropy generation, including heat transfer, pressure differentials, and non-equilibrium conditions. By utilizing the ideal gas and incompressible fluid models, simple expressions are derived to show the important factors in entropy generation for various physical processes. Physical properties, evaluated at a representative reference state of 50 °C, are provided in Table 4.2 for pure water [101] and seawater [45]. Proper selection of the reference state is discussed below. In all equations in this section, states 1 and 2 are the inlet and outlet states, respectively, for each process.

Before analyzing the entropy generation mechanisms, the ideal gas and incompressible fluid models are discussed. By definition, the density of an incompressible fluid does not vary. As a result, an incompressible fluid is one which satisfies the following equations:

$$\mathrm{d}h^{IF} = c\mathrm{d}T + v\mathrm{d}p \tag{4.27}$$

$$\mathrm{d}s^{IF} = c\frac{\mathrm{d}T}{T} \tag{4.28}$$

Integrating Eqs. (4.27) and (4.28) from an arbitrary reference state to the state of interest while assuming constant specific heat (c) yields the following expressions:

$$h^{IF} = c(T - T_{ref}) + v(p - p_{ref}) + h_{ref}^{IF} \tag{4.29}$$

$$s^{IF} = c\ln\frac{T}{T_{ref}} + s_{ref}^{IF} \tag{4.30}$$

Similarly, an ideal gas follows the equation of state, $pv = RT$, and is governed by

the following equations:

$$\mathrm{d}h^{\mathrm{IG}} = c_p \mathrm{d}T \tag{4.31}$$

$$\mathrm{d}s^{\mathrm{IG}} = c_p \frac{\mathrm{d}T}{T} - R\frac{\mathrm{d}p}{p} \tag{4.32}$$

Integrating Eqs. (4.31) and (4.32) from an arbitrary reference state to the state of interest while assuming constant specific heat at constant pressure, c_p, yields the following expressions:

$$h^{\mathrm{IG}} = c_p(T - T_{\mathrm{ref}}) + h^{\mathrm{IG}}_{\mathrm{ref}} \tag{4.33}$$

$$s^{\mathrm{IG}} = c_p \ln\frac{T}{T_{\mathrm{ref}}} - R\ln\frac{p}{p_{\mathrm{ref}}} + s^{\mathrm{IG}}_{\mathrm{ref}} \tag{4.34}$$

For increased accuracy, the generalized compressibility model, $pv = ZRT$ can be used instead if R is replaced with ZR in Eqs. (4.31) to (4.34) and all future equations.

When evaluating Eqs. (4.29), (4.30), (4.33), and (4.34), the physical properties (specific heat, volume, compressibility factor, *etc.*) and reference values of enthalpy and entropy should be evaluated at a suitable reference state. The reference state should be selected as the saturated state corresponding to the average temperature between the inlet and outlet streams. Representative values of these constants, evaluated for pure water [101] at 50 °C, are provided in Table 4.2. For seawater, the average salinity should be used. Representative values of these constants, evaluated for seawater [45] at 50 °C and 35 g/kg, are also provided in Table 4.2. It should be noted that the specific heat of seawater is significantly lowered with increasing salinity. Therefore, these approximations should not be used for processes in which composition substantially changes. Instead, Gibbs free energy should be used (see Section 4.6.6).

4.6.1 Flashing

When liquid water near saturation conditions passes through a throttle, a portion will vaporize as a result of the pressure drop through the device. The exiting fluid, a mixture of vapor and liquid, can be modeled as an ideal gas and incompressible fluid, respectively. Application of the First and Second Laws to the flash box (throttle) control volume reduces to:

$$h^{\mathrm{IF}}_1 = h_2 = (1-x)h^{\mathrm{IF}}_2 + xh^{\mathrm{IG}}_2 \tag{4.35}$$

$$s^{\mathrm{flashing}}_{\mathrm{gen}} = s_2 - s_1 = \left[(1-x)s^{\mathrm{IF}}_2 + xs^{\mathrm{IG}}_2\right] - s^{\mathrm{IF}}_1 \tag{4.36}$$

Substitution of Eqs. (4.29), (4.30), (4.33), and (4.34) into Eqs. (4.35) and (4.36) with simplification gives the quality and entropy generation due to flashing.

The entropy generated in this process is

$$s_{\text{gen}}^{\text{flashing}} = c \ln \frac{T_2}{T_1} + x \left\{ (c_p - c) \ln T_2 - R \ln p_2 + \left[s_{\text{ref}}^{\text{IG}} - s_{\text{ref}}^{\text{IF}} - (c_p - c) \ln T_{\text{ref}} + R \ln p_{\text{ref}} \right] \right\} \tag{4.37}$$

where the quality, x, is given by:

$$x = \frac{c(T_1 - T_2) + v(p_1 - p_2)}{(c_p - c)T_2 - vp_2 + [h_{\text{ref}}^{\text{IG}} - h_{\text{ref}}^{\text{IF}} - (c_p - c)T_{\text{ref}} + vp_{\text{ref}}]} \tag{4.38}$$

and c_p is the specific heat at constant pressure, c is the specific heat of an incompressible fluid, R is the ideal gas constant for steam, v is the specific volume of the liquid, $h_{\text{ref}}^{\text{IG}}$ and $s_{\text{ref}}^{\text{IG}}$ are the enthalpy and entropy for steam at the reference state, and $h_{\text{ref}}^{\text{IF}}$ and $s_{\text{ref}}^{\text{IF}}$ are the enthalpy and entropy for liquid water at the reference state.

4.6.2 Flow through an expansion device without phase change

Although the physical causes for pressure drops differ when considering flow through expanders, pipes, throttles, membranes, and other flow constrictions, the control volume equations that govern the entropy generated remains constant. As with the analysis of the flashing case, the First and Second Laws for an isenthalpic process simplify to:

$$w = \frac{\dot{W}}{\dot{m}} = h_2 - h_1 \tag{4.39}$$

$$s_{\text{gen}} = s_2 - s_1 \tag{4.40}$$

For an expansion device, the isentropic efficiency, η_e, is defined as:

$$\eta_e \equiv \frac{w}{w^s} = \frac{h_2 - h_1}{h_2^s - h_1} \tag{4.41}$$

where w is the work produced per unit mass through the device and w^s is the work produced assuming isentropic expansion.

For entropy generation in the expansion of an incompressible fluid, Eq. (4.30) shows that for an isentropic expansion from p_1 to p_2, $T_2^s = T_1$. Combining this result with Eqs. (4.29), (4.39), and (4.41) and solving for T_2 gives

$$T_2 = T_1 + \frac{v}{c}(p_1 - p_2)\,(1 - \eta_e) \tag{4.42}$$

Substitution of Eqs. (4.30) and (4.42) into Eq. (4.40) yields the entropy generated due to irreversible expansion of an incompressible fluid:

$$s_{\text{gen}}^{\text{expansion,IF}} = c \ln \left[1 + \frac{v}{cT_1}(p_1 - p_2)\,(1 - \eta_e) \right] \approx \frac{v}{T_1}(p_1 - p_2)\,(1 - \eta_e) \tag{4.43}$$

In the limit of a completely irreversible pressure drop (such as through a throttle) in which no work is generated, $\eta_e = 0$ and (4.43) reduces to:

$$s_{\text{gen}}^{\Delta p,\text{IF}} = c \ln \left[1 + \frac{v}{cT_1}(p_1 - p_2) \right] \approx \frac{v}{T_1}(p_1 - p_2) \tag{4.44}$$

For entropy generation in the expansion of an ideal gas, Eq. (4.34) shows that for an isentropic expansion from p_1 to p_2,

$$T_2^s = T_1 \left(\frac{p_2}{p_1} \right)^{R/c_p}$$

Combining this result with Eqs. (4.33), (4.39), and (4.41) and solving for T_2 gives

$$T_2 = T_1 \left\{ 1 + \eta_e \left[\left(\frac{p_2}{p_1} \right)^{R/c_p} - 1 \right] \right\} \tag{4.45}$$

Substitution of Eqs. (4.34) and (4.45) into Eq. (4.40) yields the entropy generated due to irreversible expansion of an ideal gas:

$$s_{\text{gen}}^{\text{expansion,IG}} = c_p \ln \left\{ 1 + \eta_e \left[\left(\frac{p_2}{p_1} \right)^{R/c_p} - 1 \right] \right\} - R \ln \frac{p_2}{p_1} \tag{4.46}$$

In the limit of a completely irreversible pressure drop (such as through a throttle) in which no work is generated, $\eta_e = 0$ and Eq. (4.46) reduces to:

$$s_{\text{gen}}^{\Delta p,\text{IG}} = -R \ln \frac{p_2}{p_1} \tag{4.47}$$

Based on Eqs. (4.44) and (4.47), for an incompressible fluid, entropy generation is determined by the pressure difference, whereas for an ideal gas, it is determined by the pressure ratio.

4.6.3 Pumping and compressing

Application of the First and Second Laws to a pump (or compressor) control volume yields Eqs. (4.39) and (4.40). For pumping and compressing, the isentropic efficiency, η_p, is defined as:

$$\eta_p \equiv \frac{w^s}{w} = \frac{h_2^s - h_1}{h_2 - h_1} \tag{4.48}$$

For entropy generation in pumping, assume that the liquid can be modeled as an incompressible fluid. Equation (4.30) shows that for an isentropic expansion from p_1 to p_2, $T_2^s = T_1$. Combining this result with Eqs. (4.29), (4.39), and (4.48) and solving for T_2 gives

$$T_2 = T_1 + \frac{v}{c}(p_2 - p_1) \left(\frac{1}{\eta_p} - 1 \right) \tag{4.49}$$

Substitution of Eqs. (4.30) and (4.49) into Eq. (4.40) yields the entropy generated due to irreversible pumping:

$$s_{\text{gen}}^{\text{pumping}} = c \ln \left[1 + \frac{v}{cT_1}(p_2 - p_1) \left(\frac{1}{\eta_p} - 1 \right) \right] \approx \frac{v}{T_1}(p_2 - p_1) \left(\frac{1}{\eta_p} - 1 \right) \tag{4.50}$$

The entropy generated due to irreversible pumping can also be derived by noticing that the difference between the actual work and the reversible work is simply the exergy destruction. Since irreversibilities during the compression process of an incompressible fluid will result in only minor changes in temperature (*i.e.*, $T_2 \approx T_1$), the entropy generation can be determined by dividing the exergy destruction by the inlet temperature in accordance with Gouy-Stodola theorem [31]:

$$\begin{aligned} s_{\text{gen}}^{\text{pumping}} &= \frac{\Xi_d}{T_1} = \frac{w - w^s}{T_1} = \frac{h_2 - h_2^s}{T_1} = \frac{h(T_2, p_2) - h(T_1, p_2)}{T_1} \\ &= \frac{v}{T_1}(p_2 - p_1) \left(\frac{1}{\eta_p} - 1 \right) \end{aligned} \tag{4.51}$$

Note that Eq. (4.51) is simply the Taylor series expansion of Eq. (4.50). This alternate derivation is only appropriate since the pumping process is nearly isothermal.

For entropy generation in compression, assume that both the inlet and outlet vapor can be modeled as an ideal gas that follows the generalized compressibility form. Equation (4.34) shows that for an isentropic expansion from p_1 to p_2,

$$T_2^s = T_1 \left(\frac{p_2}{p_1} \right)^{R/c_p}$$

Combining this result with Eqs. (4.33), (4.39), and (4.48) and solving for T_2 gives

$$T_2 = T_1 \left\{ 1 - \frac{1}{\eta_p} \left[1 - \left(\frac{p_2}{p_1} \right)^{R/c_p} \right] \right\} \tag{4.52}$$

Substitution of Eqs. (4.34) and (4.52) into Eq. (4.40) yields the entropy generated due to irreversible compression:

$$s_{\text{gen}}^{\text{compression}} = c_p \ln \left\{ 1 - \frac{1}{\eta_p} \left[1 - \left(\frac{p_2}{p_1} \right)^{R/c_p} \right] \right\} - R \ln \frac{p_2}{p_1} \tag{4.53}$$

Note that unlike in the incompressible fluid case, Eq. (4.53) cannot be derived through the use of the Gouy-Stodola theorem since the compression of a gas is not an isothermal process.

4.6.4 Approximately isobaric heat transfer process

In actual heat exchangers, there is always a pressure drop associated with viscous forces. However, without knowledge of specific flow geometry or the local temperature and pressure fields, it is impossible to partition entropy generation according to particular transport phenomena. For example, Bejan [102] has shown that for a simple, single-fluid heat exchanger, comparing the trade off between entropy generation due to heat transfer across a finite temperature difference and pressure drop across a finite flow volume yields an optimum heat exchanger geometry.

In heat exchangers within typical desalination processes, however, the effect of pressure drop on physical properties is insignificant. Thus, entropy generation may be calculated as a function of terminal temperatures alone. For the range of temperatures and flow configurations encountered in the present analysis, this approximation holds for fluids that may be modeled as both ideal gases and incompressible fluids.

The entropy generation equation for a heat exchanger is

$$S_{\text{gen}}^{\text{HX}} = [\dot{m}(s_2 - s_1)]_{\text{stream 1}} + [\dot{m}(s_2 - s_1)]_{\text{stream 2}} \tag{4.54}$$

In the case of a device that transfers heat at a relatively constant pressure, an approximate expression may be developed for entropy generation as a function of inlet and outlet temperatures alone. Entropy may be written as:

$$\mathrm{d}s = \frac{1}{T}\mathrm{d}h - \frac{v}{T}\mathrm{d}p \tag{4.55}$$

Integrating Eq. (4.55) at constant pressure gives:

$$s_2 - s_1 = \int_1^2 \frac{1}{T}\mathrm{d}h \tag{4.56}$$

For an ideal gas, Eq. (4.55) is written as Eq. (4.32) which can be integrated at constant pressure to give:

$$s_2 - s_1 = c_p \ln \frac{T_2}{T_1} \tag{4.57}$$

For an incompressible fluid, entropy is not a function of pressure as seen in Eq. (4.28). Therefore, the entropy difference is given by:

$$s_2 - s_1 = c \ln \frac{T_2}{T_1} \tag{4.58}$$

If it is now assumed that the heat exchanger is adiabatic with respect to the environment and that there is no work, then the above equations can be substituted into Eq. (4.54).

For an isobaric phase change from a saturation state (either liquid or vapor), the entropy change is

$$s_2 - s_1 = x s_{fg} = x(s^{\text{IG}} - s^{\text{IF}}) \qquad \text{for evaporation} \tag{4.59}$$

$$= (x-1)s_{fg} = (x-1)(s^{\text{IG}} - s^{\text{IF}}) \qquad \text{for condensation} \tag{4.60}$$

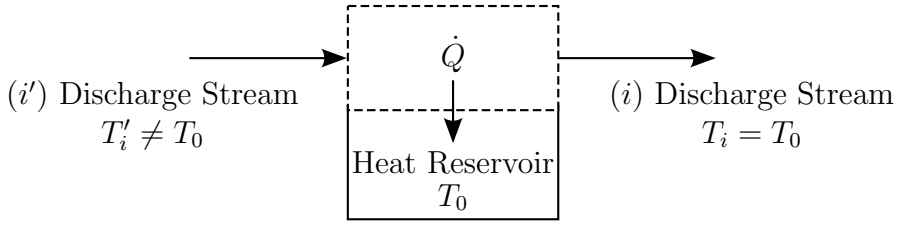

Figure 4-5: Entropy is generated in the process of a stream reaching thermal equilibrium with the environment.

where x is the quality at the exit of the process.

4.6.5 Thermal disequilibrium of discharge streams

Referring again to Fig. 2-1, the entropy generated in bringing outlet streams from the system control volume to the ambient temperature reached at the exit of the distant control volume may be calculated. Consider a stream that is in mechanical, but not thermal equilibrium with the environment (Fig. 4-5). The environment acts as a heat reservoir, and through an irreversible heat transfer process, the stream is brought to thermal equilibrium.

The First and Second Laws for this control volume give:

$$\dot{Q} = \dot{m}_i(h_i - h_i') \tag{4.61}$$

$$\dot{S}_{\text{gen}} = \dot{m}_i \left[(s_i - s_i') - \frac{\dot{Q}}{T_0} \right] = \dot{m}_i \left[(s_i - s_i') - \frac{h_i - h_i'}{T_0} \right] \tag{4.62}$$

For incompressible fluids at mechanical equilibrium with the environment, $s_i - s_i' = c_i \ln \frac{T_0}{T_i}$ and $h_i - h_i' = c_i(T_0 - T_i)$. Substituting into Eq. (4.62) gives the entropy generated in bringing a stream of fluid to thermal equilibrium with the environment:

$$\dot{S}_{\text{gen}}^{T \text{ disequilibrium}} = \dot{m}_i c_i \left[\ln\left(\frac{T_0}{T_i}\right) + \frac{T_i}{T_0} - 1 \right] \tag{4.63}$$

4.6.6 Chemical disequilibrium of concentrate stream

When considering a desalination system, the concentrate is typically considered to be waste and is discharged back to the ocean. Since the concentrate is at higher salinity than the ocean, entropy is generated in the process of restoring the concentrate to chemical equilibrium (also called distributive equilibrium) with the seawater. This entropy generation can be calculated in one of two ways.

First, consider the addition of the concentrated concentrate stream at the restricted dead state to a large reservoir of seawater at the total dead state. An energy balance governing the mixing of the concentrate stream with the seawater reservoir is written

as follows:

$$\dot{\Xi}^{\text{mixing}}_{\text{destroyed}} = -[(\dot{m}_c + \dot{m}^{\text{reservoir}}_{\text{sw}})g_{\text{out}} - \dot{m}_c g_c - \dot{m}^{\text{reservoir}}_{\text{sw}} g_{\text{sw}}] \tag{4.64}$$

where $\dot{\Xi}^{\text{mixing}}_{d}$ is the exergy destroyed as a result of irreversible mixing. In the limit that $\dot{m}_c/\dot{m}^{\text{reservoir}}_{\text{sw}} \to 0$, g_{out} approaches g_{sw} and the concentrate stream is brought to chemical equilibrium with the environment. Using the Gouy-Stodola theorem [31], the exergy destroyed due to irreversible mixing can be used to evaluate the entropy generated as the concentrate stream runs down to chemical equilibrium:

$$\dot{S}^{\text{concentrate RDS}\to\text{TDS}}_{\text{gen}} = \frac{\dot{\Xi}^{\text{mixing}}_{\text{destroyed}}}{T_0} \tag{4.65}$$

The mixing process described by Eq. (4.64) is analogous to the separation process shown in Fig. 2-1 performed in reverse.

A second method to evaluate the entropy generation due to chemical disequilibrium of the concentrate stream is based on the least work of separation. When considering the control volume given by Fig. 2-1 and the minimum least work of separation, there is an infinitesimally small product stream of pure water along with a stream of concentrate of salinity that is infinitesimally above that of seawater. Therefore, the concentrate stream is in thermal, mechanical, and nearly chemical equilibrium with the environment. If, however, there is a finite recovery ratio, the concentrate stream salinity is greater than that of seawater. Additionally, as the recovery ratio increases, the flow rate of the concentrate stream decreases and flow rate of the product water increases (assuming fixed input feed rate). Since the concentrate stream is not at equilibrium with the environment, there is a chemical potential difference that can be used to produce additional work. This additional work is exactly equal to the difference between the least work of separation, Eq. (2.4), and the minimum least work of separation, Eq. (2.30). When the concentrated concentrate is discarded to the ocean, this work potential is lost. Therefore, entropy generation due to chemical disequilibrium of the concentrate stream can also be evaluated through the use of the Gouy-Stodola theorem as follows:

$$T_0 \dot{S}^{\text{concentrate RDS}\to\text{TDS}}_{\text{gen}} = \dot{W}_{\text{least}}(r > 0) - \dot{W}^{\text{min}}_{\text{least}}(r = 0) \tag{4.66}$$

Evaluation of entropy generation using Eqs. (4.65) and (4.66) gives equivalent results.

4.7 Application to desalination technologies

Using the methods developed in preceding sections, the component and system level entropy production and the Second Law efficiency of several common seawater desalination technologies are now evaluated.

4.7.1 Multiple effect distillation

A very simple model based on approximations from El-Sayed and Silver [16], Darwish et al. [103], and El-Dessouky and Ettouney [13] is used to generate all the temperature profiles and mass flow rates within a multiple effect distillation (MED) forward feed (FF) cycle (Fig. 4-6).[1]

Several common approximations and design decisions are made: The temperature drop between effects is assumed to be constant, $\Delta T = (T_{\text{steam}} - T_{\text{last effect}})/n$. Additionally, the driving temperature difference between condensing vapor and evaporating brine and the temperature rise across feed heaters are both taken to be ΔT. The temperature rise in the condenser is set to 10 °C.

The distillate is approximated as pure water, and it is assumed that distillate is produced in each effect (D_i) at a rate of 99% of that produced in the previous effect (*i.e.*, $D_{i+1} = 0.99 D_i$) to approximate the effect of increasing latent heat with decreasing effect temperature. Distillate produced from flashing in each effect is given by $D_{f,i} = \dot{m}_{b,i-1} c_{p,i} \Delta T / h_{fg,i}$ where $m_{b,i-1}$ is the brine from the previous effect which becomes the feed to the current effect. The remainder of the distillate is produced from boiling in the effect. There is no flashing in the first effect. Distillate produced from flashing in the flash boxes is given by $D_{fb,i} = \sum_{j=1}^{i-1} D_j c_{p,i} \Delta T / h_{fg,i}$, for $i \geq 2$. The quality of the distillate leaving the feed heater is calculated using an energy balance on the heater, $\dot{m}_F c_{p,i} \Delta T = (D_i + D_{fb,i})(1 - x_i) h_{fg}$, where $\dot{m}_F$ is the mass flow rate of the feed seawater.

Water and salinity mass balances for the effects are:

$$\dot{m}_{b,i-1} = D_i + \dot{m}_{b,i}$$
$$\dot{m}_{b,i-1} y_{b,i-1} = \dot{m}_{b,i} y_{b,i}$$

where $y_{b,i}$ is the salinity of the i^{th} brine stream.

An energy balance on the first effect gives the required amount of heating steam: $\dot{m}_s h_{fg,s} = D_1 h_{D,1} + \dot{m}_{b,1} h_{b,1} - \dot{m}_F h_F$. Accurate properties for seawater [45] and steam [101], including enthalpies, entropies, specific heats, *etc.*, are used and evaluated at each state.

The inputs to the simplified MED FF model with 6 effects include: 1 kg/s of distillate, seawater salinity of 42 g/kg, maximum salinity of 70 g/kg, steam temperature of 70 °C, last effect temperature of 40 °C, and seawater (and environment) temperature of 25 °C.

Using the above approximations and inputs, all thermodynamic states for the MED FF system are found. Entropy generation in each component is computed by using a control volume for each component. Pumping work and entropy generated due to flashing in effects are evaluated using Eqs. (4.37) and (4.50), respectively.

Figure 4-7 shows the entropy generated in each component, whereas Fig. 4-8 shows the percentage of entropy generated in each type of component. Pumping is not

[1] While a much more detailed MED model has been developed [99, 100], a simple model is used here in order to a highlight the importance of the various entropy generation mechanisms. The detailed model is presented in Appendix A.

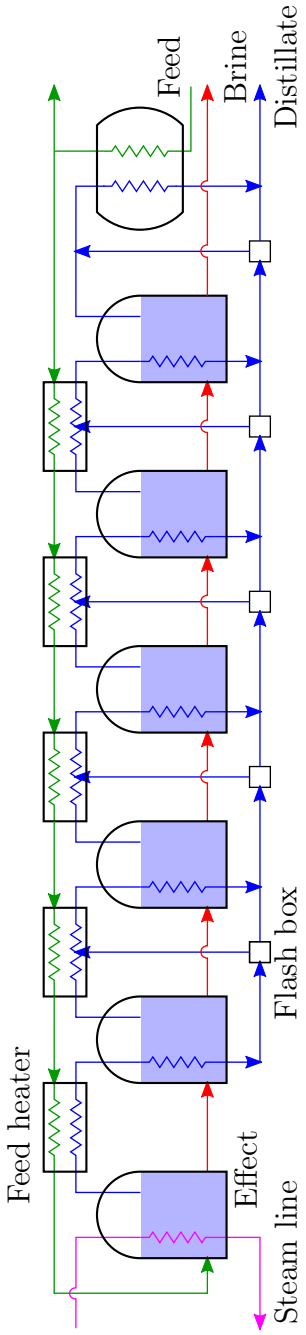

Figure 4-6: A typical flow path for a forward feed multiple effect distillation system.

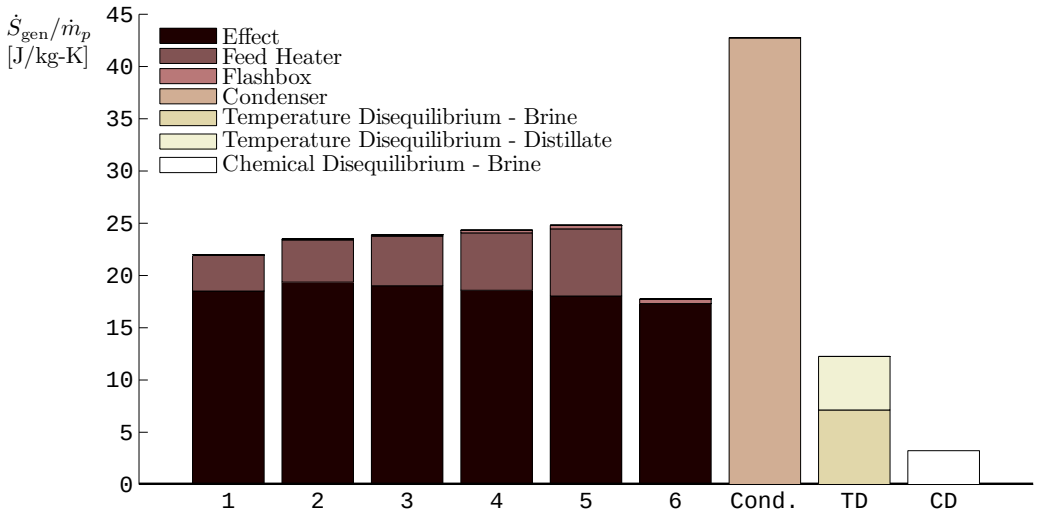

Figure 4-7: Entropy production in the various components of a 6 effect forward feed multiple effect distillation system.

included since the entropy generated due to pumping is much less than 1% of the overall amount. Looking at Fig. 4-8, it is clear that heat transfer is the dominant source of entropy generation in MED systems since most of the generation occurs in the heat exchange devices (effects, feed heaters, and condenser). It was found that entropy generated due to flashing in the effects was very small.

Although the effects result in the greatest portion of the entropy generated, it is important to note that the condenser is the single greatest source of irreversibility, as seen in Fig. 4-7. The condenser is such a large source of entropy generation because very large flow rates of water are needed to condense the vapor from the final effect, and because of the low temperature at which the heat transfer is occurring.

Many modern MED plants operate using a thermal vapor compressor (TVC).

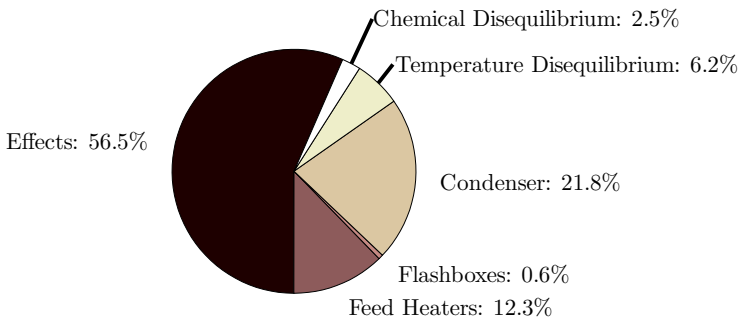

Figure 4-8: Relative contribution of sources of entropy generation in a forward feed multiple effect distillation system. Irreversibilities in the effects dominate. Total specific entropy generation is 196 J/(kg K).

The TVC is used to entrain the vapor from the final effect and re-inject it into the first effect. MED-TVC plants have much higher performance ratios than non-TVC plants and they reduce the size of the final condenser, thus reducing this large source of irreversibilities. It is important to note, however, that the TVC is also a highly irreversible device so that total entropy production may not be as much reduced.

Finally, it is seen that for this MED plant, entropy generated as a result of the non-equilibrium discharge of the brine and distillate corresponds to approximately 8.7% of the plant's overall losses. The Second Law efficiency, accounting for disequilibrium of the discharge, is $\eta_{II} = 5.9\%$. Additionally, PR = 5.2 and GOR = 5.4.

4.7.2 Multistage flash

A simple once-through multistage flash (MSF-OT) process with 24 stages is modeled.[2] A schematic diagram of such a process is shown in Fig. 4-9. As is done in several simple MSF modeling schemes [13, 16], the stage drop, or difference in sequential flashing chamber saturation temperatures, is assumed to be a constant. Mass and energy balances for each component (brine heater, feed heaters, and flash evaporators) are then solved simultaneously to obtain inlet and outlet conditions for each such component. The mass and energy balances on the i^{th} feed heater are:

$$\begin{aligned} \dot{m}_{d,i} &= D_{f,i} + \dot{m}_{d,i-1} \\ \dot{m}_f(h_{h,i} - h_{h,i-1}) &= \dot{m}_{d,i}h_{d,i} - D_{f,i}h_{f,i} - \dot{m}_{d,i-1}h_{d,i-1} \end{aligned}$$

where $D_{f,i}$ is the amount of vapor flashed in the i^{th} stage. An energy balance on the brine heater is written as $\dot{m}_s h_{fg,s} = \dot{m}_f(h_{b,0} - h_{h,0})$. The required conservation equations for the evaporators are mass, salinity, and energy, respectively given as:

$$\begin{aligned} \dot{m}_{b,i-1} &= \dot{m}_{b,i} + D_{f,i} \\ \dot{m}_{b,i-1}y_{i-1} &= \dot{m}_{b,i}y_i \\ \dot{m}_{b,i-1}h_{b,i-1} &= \dot{m}_{b,i}h_{b,i} + D_{f,i}h_{f,i} \end{aligned}$$

The inputs to the model are: feed temperature (25 °C); steam temperature (116 °C); brine reject temperature (40 °C); distillate mass flow rate (378.8 kg/s); feed mass flow rate (3384 kg/s); and seawater salinity (42 g/kg). These values are taken from representative MSF-OT data analyzed by El-Dessouky and Ettouney [13]. Table 4.3 displays key outputs from the model; the values agree with the more complex model presented in [13] within 5%. Values of specific enthalpy, specific entropy, and other properties are obtained from [45] for seawater, and [101] for pure water. Results from the present model are given in Table 4.3.

Applying the definition of Second Law efficiency, Eq. (4.15), to the system yields a value of 2.9%, which is of the same order as the value presented for the similarly large-scale MED system considered in Section 4.7.1. As can be seen in Figs. 4-10 and 4-11, the largest source of entropy generation in this particular configuration

[2]This section was co-authored with Gregory P. Thiel [36].

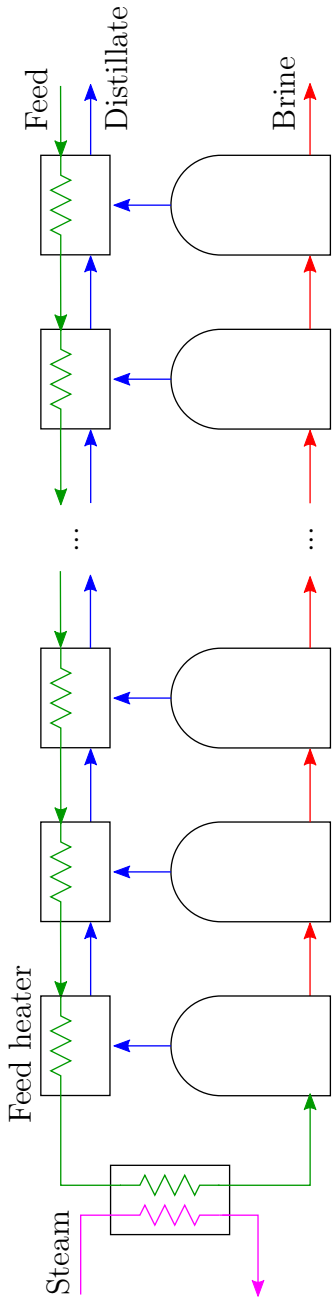

Figure 4-9: A typical flow path for a once-through multistage flash system.

Table 4.3: MSF-OT Plant Outputs.

Output		Model Value
Performance ratio	PR	4.2
Gained output ratio	GOR	4.6
Top brine temperature	T_h [°C]	109
Steam flow rate	$\dot{m}_s$ [kg/s]	91.1
Max salinity	y_n [g/kg]	47.3

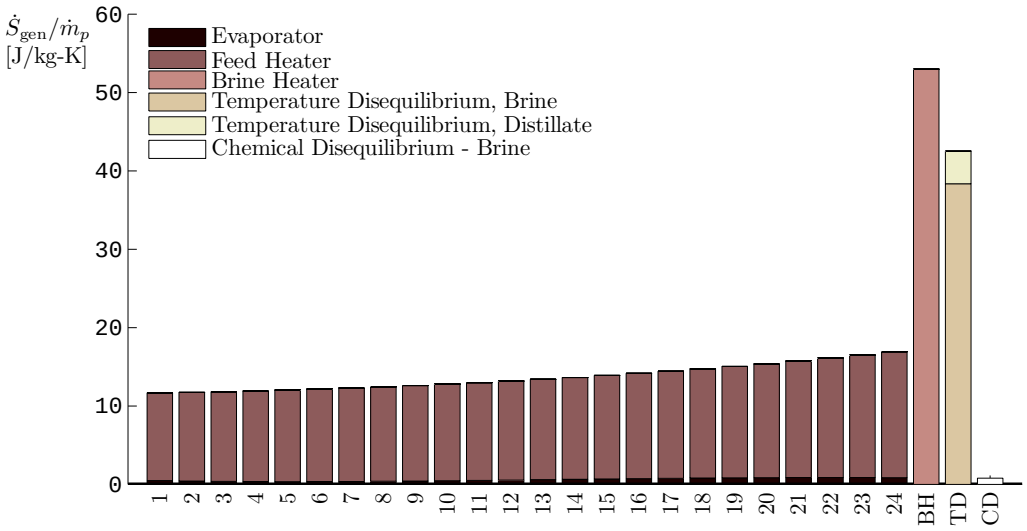

Figure 4-10: Sources of entropy generation in a 24 stage once through multistage flash system.

is the feed heaters, whereas the approximately isothermal evaporators contribute a nearly negligible portion of the plant-wide entropy generation. The relatively small amount of entropy generated in each evaporator is a consequence of the low recovery rate (11%) of the system modeled: the evaporator is approximately isothermal, so the entropy generated is largely the specific entropy of vaporization for a small quantity of flashed vapor. Were the recovery ratio larger and the number of stages similar, more vapor would be flashed in each stage, and entropy generation in the evaporators would increase. Likewise, the dominating portion of entropy generated in the feed heaters can be explained by the low recovery ratio. At low recovery ratios, the circulated brine is the largest thermal mass in the system, and the majority of heat transfer to this stream occurs in the feed heaters.

Including the exergy destruction associated with the temperature disequilibrium between the brine and distillate outputs and the dead state proves to be significant here, accounting for roughly 10% of total entropy production. In particular, the relatively high contribution of the brine disequilibrium to total entropy generation is due to the low recovery ratio inherent in MSF-OT, and the correspondingly high

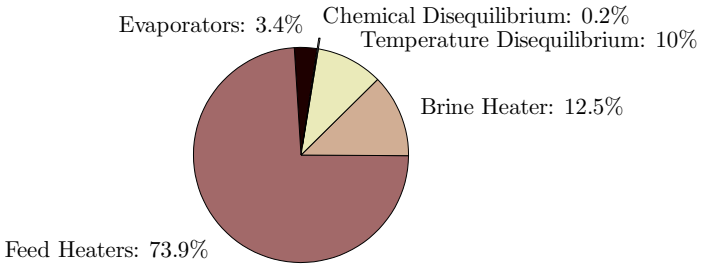

Figure 4-11: Relative contribution of sources of entropy generation in a once-through multistage flash system. Irreversibilities in the feed heaters dominate. Total specific entropy generation is 423 J/(kg K).

brine reject flow rate that occurs at a temperature significantly above the dead state.

4.7.3 Direct contact membrane distillation

Direct contact membrane distillation (DCMD) is a membrane-based thermal distillation process in which heated feed passes over a hydrophobic microporous membrane [104].[3] The membrane holds back a meniscus of water near the pores. On the opposing side, cooled fresh water passes over the membrane. The temperature difference between the water streams induces a vapor pressure difference that drives evaporation through the pores. This can be described in terms of a vapor pressure difference multiplied by a membrane distillation coefficient B, which represents the diffusion resistance through the pores. It is based on material properties, pore geometry, and depends weakly on temperature and is assumed to be constant for this calculation. On the feed side, boundary layers in concentration, temperature, and momentum are present, with corresponding diffusional transport of heat and mass. On the cooler fresh water side, there is condensation of vapor and warming of the fresh water, with boundary layer processes similar to those on the feed side. Direct contact membrane distillation has been successfully used to produce fresh water at small scale (0.1 m^3/d) [106–109].

A transport process model for DCMD based on validated models by Bui et al. [110] and Lee et al. [109] was implemented to obtain the permeate flux, and outlet temperatures of a DCMD module. The calculation of system performance used heat transfer coefficients calculated from correlations based on module geometry [111]. While the Bui et al. [110] model used a hollow-fiber membrane configuration, the present calculations are done for a flat-sheet configuration. Membrane geometry and operating conditions are taken from some pilot-sized plants the literature [112, 113]. Seawater enters into the system at 27 °C and 35 g/kg total dissolved solids at a mass flow rate of 1 kg/s, The feed inlet temperature is held constant at 85 °C, and the required heat is provided by a 90 °C source. The permeate side contains fresh water with an inlet flow rate of 1 kg/s. The resulting recovery ratio for this system is

[3]This section was co-authored with Edward K. Summers [36, 105].

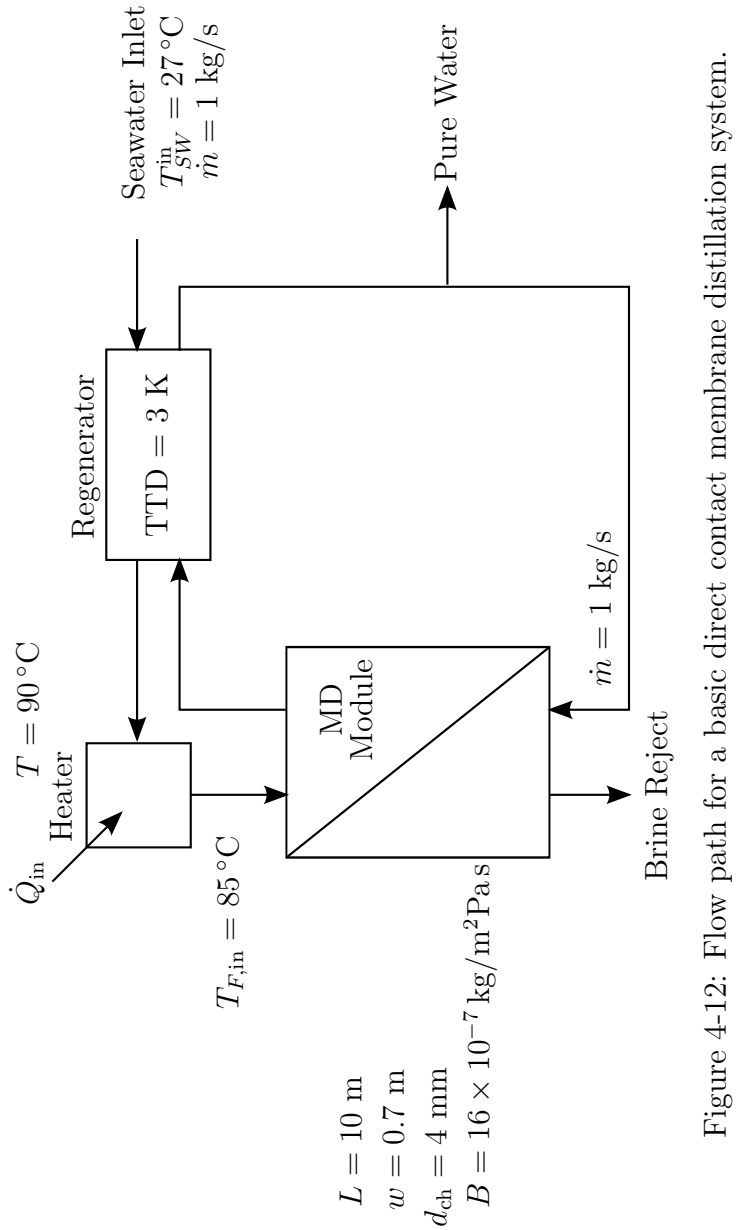

Figure 4-12: Flow path for a basic direct contact membrane distillation system.

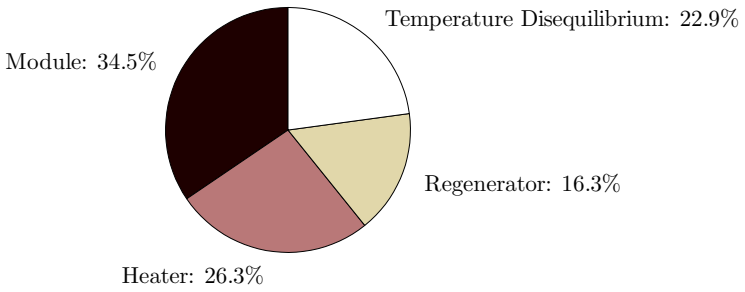

Figure 4-13: Relative contribution of sources of entropy generation in a direct contact membrane distillation system. Total specific entropy generation is 925.4 J/(kg K).

4.4%. The regenerator is a liquid-liquid heat exchanger with a terminal temperature difference of 3 K. The pressure drop through the thin channel in the membrane module was found to be the dominant pressure drop in the system and was the basis for calculating the entropy generation due to pumping power. Properties for seawater [45] were used in the calculation. A schematic diagram of the system is shown in Fig. 4-12, with module geometry and constants shown.

Entropy generation was calculated for each component in the system by using a control volume analysis. Figure 4-13 shows the breakdown of entropy generation in each component.

The greatest source of entropy generation is the module. This is owed mostly to diffusion through the pores and to a lesser extent heat conduction losses, as only a thin membrane separates the cold and hot streams in the module. The small pore size contributes substantially to the diffusion resistance; the pore diameter is usually on the order of 1000 times less than the membrane thickness. The heater contributes substantially due to the large amount of heat transferred, and the large temperature difference between the source temperature (usually a steam saturation temperature) and the heater inlet. The regenerator has lower entropy generation as it transfers energy through a lower temperature difference, which remains constant throughout its length. The discharge temperature disequilibrium entropy generation is low compared to other thermal systems, as the brine reject temperature is lower. Additionally, since the recovery ratio is low, the chemical disequilibrium of the brine is also found to be negligible (entropy generation due to brine disequilibrium is approximately three orders of magnitude smaller than from other sources). Like most other systems discussed here, the pumping entropy generation was found to be negligible.

Reducing the top temperature, $T_{F,\text{in}}$, results in a net increase in specific entropy generation. This is primarily due to the heater, as a lower top temperature gives rise to a higher temperature difference in the heater. Specific entropy generation in the module goes down slightly, as evaporation happens at a lower temperature; however, this is negated by an increase in specific entropy generation in the regenerator, as water production decreases faster than the temperature gradient in the regenerator. Entropy generation to temperature disequilibrium goes up primarily owing to the

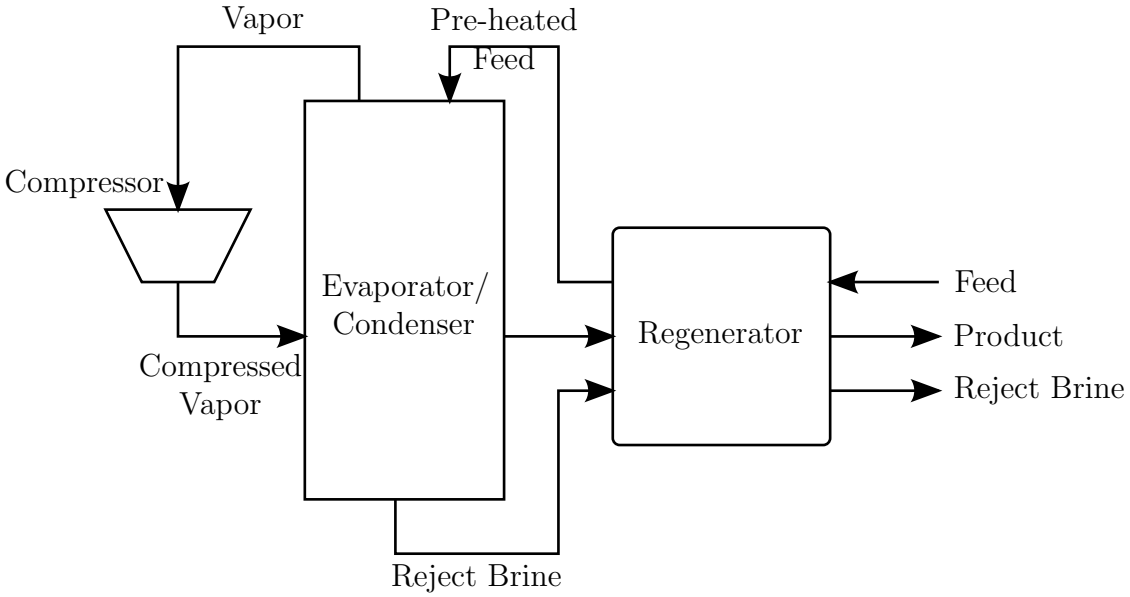

Figure 4-14: Single effect mechanical vapor compression process.

lower recovery ratio and additional brine reject.

Given the MD's low recovery ratio and high discharge temperature, entropy generation is high when compared to other desalination systems, and as a result $\eta_{II} = 1.0\%$, as calculated with Eq. (4.14) and taking account all sources of entropy generation.

4.7.4 Mechanical vapor compression

A simple single effect mechanical vapor compression (MVC) model is considered.[4] A schematic diagram of the process is shown in Fig. 4-14. The design values chosen for the process are guided by those reported for single stage MVC plants analyzed by Veza [90] and Aly [114] and are listed in Table 4.4.

The inlet pressure to the compressor is taken to be the average of the saturation pressure of seawater at a salinity corresponding to the average of the feed and reject salinity. The regenerating heat exchanger is thermally balanced and thus the temperature difference is taken to be constant between the rejected brine and the feed stream and also between the product water and the feed stream. By employing energy conservation equations for each component, the unknown thermodynamic states may be computed. Knowing the thermodynamic states at each point, the entropy generated within each component may be calculated along with the entropy generated when the discharged brine is returned to a body of water with the same composition and temperature as the feed. The key outputs from the model are reported in Table 4.5. The breakdown of entropy generation among components is indicated within Fig. 4-15.

The majority of entropy generation may be attributed to heat transfer across a finite temperature difference from the condensation process to the evaporation process.

[4]This section was co-authored with Ronan K. McGovern [36].

Table 4.4: MVC design inputs.

Input	Value
Seawater inlet temperature	25 °C
Seawater inlet salinity	35 g/kg
Product water salinity	0 g/kg
Discharged brine salinity	58.33 g/kg
Top brine temperature	60 °C
Pinch: evaporator-condenser	2.5 K
Recovery ratio	40%
Isentropic compressor efficiency	70%
Compressor inlet pressure	19.4 kPa

Table 4.5: MVC model outputs.

Output	Value
Specific electricity consumption	8.84 kW h/m^3
Discharged brine temperature	27.2 °C
Product water temperature	29.7 °C
Compression ratio	1.15
Second Law efficiency, η_{II}	8.5%

Entropy generation within the regenerator is less significant, primarily because the sensible heat transferred in the regenerator is substantially smaller than the large amount of latent heat recovered in the evaporator-condenser. Entropy generation due to irreversibility within the compressor is important and depends upon the compression ratio and its isentropic efficiency. Entropy generated in returning concentrated brine to a body of seawater is considerable as the recovery ratio is high (40%). Entropy generated in returning product streams to the temperature of inlet seawater is small as the regenerator is effective in bringing these streams to a temperature close to that of the inlet seawater.

The MVC system modeled above is a simple single effect system, satisfactory for demonstrating the distribution of entropy generation throughout MVC plants. Detailed thermoeconomic models with multiple effects have been analyzed in literature [59]. Research has also been undertaken on improving the heat transfer coefficients within the evaporation and condensation processes of phase change. Lara et al. [115] investigated high temperature and pressure MVC, where dropwise condensation can allow greatly enhanced heat transfer coefficients. Lukic et al. [116] also investigated the impact of dropwise condensation upon the cost of water produced. Such improvements in heat transfer coefficients reduce the driving temperature difference in the evaporator-condenser leading to a lower compression ratio and thus reduced compressor work requirements per unit of water produced. As the present analysis shows, reduction of entropy generation within the evaporator-condenser and

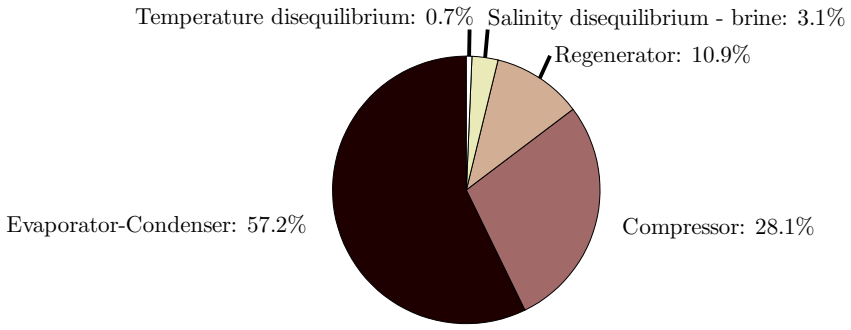

Figure 4-15: Relative contribution of sources of entropy generation in a mechanical vapor compression system. Total specific entropy generation is 98.0 J/(kg K). Contributions of the temperature disequilibrium of the distillate and brine streams are 0.5% and 0.2%, respectively.

the compressor are crucial if exergetic efficiency is to be improved upon.

4.7.5 Reverse osmosis

A typical flow path for a single stage reverse osmosis (RO) plant with energy recovery is shown in Fig. 4-16 [117]. Since RO is a mechanically driven system and thermal effects are of second order to pressure effects, reasonably accurate calculations can be performed while only considering pressure work. The following approximations are made:

Feed seawater is assumed to enter at ambient temperature and pressure (25 °C, 1 bar) and at standard seawater salinity (35 g/kg). Pure water (0 g/kg salinity) is assumed to be produced at a recovery ratio of 40%. Further, it is assumed that 40% of the feed is pumped to 69 bar using a high pressure pump while the remaining 60% is pumped to the same pressure using a combination of a pressure exchanger driven by the rejected brine as well as a booster pump. The high pressure, booster, and feed pump efficiencies are assumed to be 85%. The concentrated brine loses 2 bar of pressure through the RO module while the product leaves the module at 1 bar. Energy Recovery Inc. [118] makes a direct contact pressure exchanger that features a single rotating part. The pressure exchanger pressurizes part of the feed using work produced through the depressurization of the brine in the rotor. Equations (4.29), (4.41), and (4.48) are used to match the work produced in expansion to the work required for compression. Assuming the expansion and compression processes are 98% efficient [118], the recovered pressure is calculated as follows:

$$p_{\text{recovered}} = p_{\text{feed}} + \eta_{\text{expansion}}\eta_{\text{compression}} \left(\frac{\rho_{\text{feed}}}{\rho_{\text{brine}}}\right) (p_{\text{brine}} - p_{\text{atm}}) \tag{4.67}$$

and the pressure exchanger efficiency is evaluated using ERI's definition [117]:

$$\eta_{\mathrm{PX}} = \frac{\sum_{\mathrm{out}} \mathrm{Pressure} \times \mathrm{Flow}}{\sum_{\mathrm{in}} \mathrm{Pressure} \times \mathrm{Flow}} \tag{4.68}$$

Density of seawater is evaluated using seawater properties [45].

Using the above assumptions, approximations, and inputs, the entropy generated in the various components can be directly calculated using equations derived in Section 4.6. The entropy generated in the high pressure pump, booster pump, and the feed in the pressure exchanger is evaluated using Eq. (4.50). The entropy generated through the expansion of the pressurized brine in the pressure exchanger is evaluated using Eq. (4.43).

Additional consideration is necessary for the entropy generation in the RO module because both the mechanical and chemical state of the seawater is changing. Since entropy is a state variable, the process can be decomposed into two sub-processes for the purpose of calculating the overall change of state. First, the high pressure seawater is isobarically and isothermally separated into two streams of different composition. Next, the two streams are depressurized at constant salinity in order to account for the pressure drop associated with diffusion through the membrane (product, $\Delta p = 68\,\mathrm{bar}$) and that associated with hydraulic friction (brine, $\Delta p = 2\,\mathrm{bar}$).

In order to evaluate the entropy change as a result of the separation process, the physical properties of seawater are needed as function of temperature, pressure, and salinity. For the model of separation considered here, the compositional change is taken at constant high pressure and temperature, so that the entropy change due to compositional change is easily evaluated:

$$\Delta\dot{S}_{\mathrm{composition}} = \dot{m}_p s_p(T_0, p_{\mathrm{HP}}, y_p) + \dot{m}_c s_p(T_0, p_{\mathrm{HP}}, y_p) - \dot{m}_F s_F(T_0, p_{\mathrm{HP}}, y_F) \tag{4.69}$$

Since seawater is nearly incompressible, entropy is independent of p, and can be evaluated using the property package developed by Sharqawy et al. [45] (which does not currently include pressure effects). Note that $\Delta\dot{S}_{\mathrm{composition}} \approx -\dot{W}_{\mathrm{least}}(r > 0)/T_0$ since $\dot{W}_{\mathrm{least}}(r > 0) = \Delta\dot{G}_{\mathrm{composition}} = \Delta\dot{H}_{\mathrm{composition}} - T\Delta\dot{S}_{\mathrm{composition}}$ [*cf.*, Eq. (2.4)] and $\Delta\dot{H}_{\mathrm{composition}}$ is small.

Entropy generation due to the irreversible depressurization of both the brine and product streams is evaluated through the use of Eq. (4.44). The total entropy generated in the RO module is the sum of the entropy change due to compositional changes, Eq. (4.69), and the entropy generated in the depressurization of the product and brine streams, Eq. (4.44).

The energy dissipated by pressure loss and pump inefficiency results in very small increases in the system temperature. As a result, the entropy generation associated with the transfer of this energy out of the system as heat (if any) through the very small temperature difference from the environment is negligible relative to the mechanical sources of entropy production [see Eq. (4.63)].

Figure 4-17 is a pie chart showing the relative amounts of entropy generation within the single stage RO system. The greatest irreversibility occurs within the RO module.

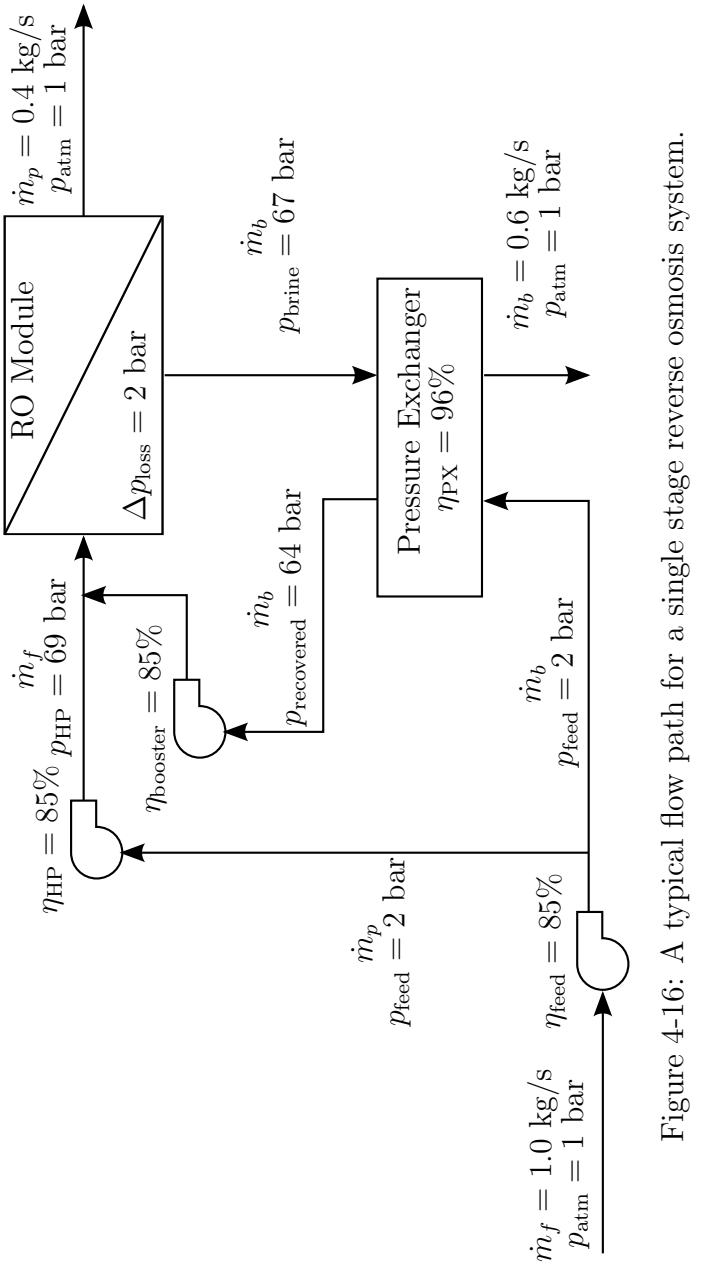

Figure 4-16: A typical flow path for a single stage reverse osmosis system.

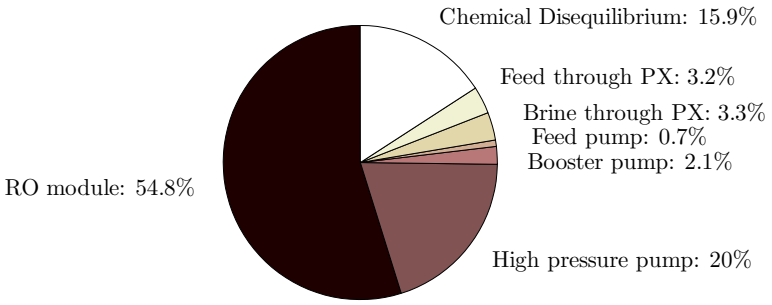

Figure 4-17: Relative contribution of sources to entropy generation in the reverse osmosis system. Irreversibilities associated with product flow through the membrane dominates. Total specific entropy generation is 19.4 J/(kg K).

Further examining the entropy generation in the RO module, it is found that the change in entropy from the depressurization of the product is 22.6 J/($\text{kg}_{\text{product}}$ K), while the change in entropy from the depressurization of the brine is only 1.0 J/($\text{kg}_{\text{product}}$ K); the entropy change from compositional change is -12.9 J/($\text{kg}_{\text{product}}$ K). Therefore, the diffusion of water through the RO membrane is the largest source of irreversibility, owing mainly to the large pressure drop (68 bar). Note that the high pressure pump handles the same flow rate of water through the same pressure difference, but does so at 85% efficiency and therefore generates substantially less entropy than the (zero efficiency) flow through the membrane.

Based on these conditions, the minimum least work is found to be 2.71 kJ/kg and the total entropy generation is 19.4 J/(kg K). Therefore, the required work of separation is 8.50 kJ/kg (2.35 kW h/m^3) and the Second Law efficiency, per Eq. (4.14), is 31.9%.

Since RO systems tend to operate at higher Second Law efficiency than thermal plants, the irreversibility due to discharge disequilibrium of the brine stream has a larger contribution to the total entropy generation. As seen in Fig. 4-17, the high salinity of the brine accounts for almost 16% of the plant's total irreversibility. The only way to reduce this effect is to lower the recovery ratio or to implement an osmotic power recovery device on the reject brine stream.

When trying to improve RO systems, designers target the irreversibilities in the module. The simplest way to improve the performance of the system is to use a two (or more) stage RO system (e.g., as described by Elimelech and Phillip [119]). In a two stage system, water is extracted at a lower recovery ratio from the first stage, resulting in a lower brine concentration. Since the required pressure of the feed is dependent on the osmotic pressure, which itself is a function of the feed concentration, a lower recovery ratio means that lower pressures are needed in the first stage. Next, the brine from the first stage is then further pressurized to the top pressure and additional water is extracted in a second stage. Even though the same top pressure is reached, since the flow rates at the highest pressure are smaller, less total entropy is generated in the

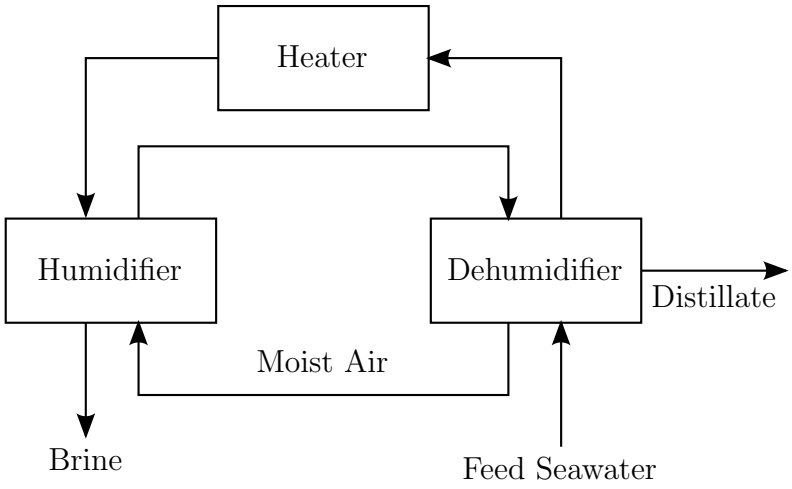

Figure 4-18: A schematic diagram of a closed air open water, water heated humidification-dehumidification desalination cycle.

two stage system. Batch processing of seawater, as done by Desalitech Ltd. [120], also serves to reduce the volume of water that needs to be pressurized to the maximum pressure.

4.7.6 Humidification-dehumidification

A solar driven closed air open water (CAOW) humidification-dehumidification (HDH) desalination cycle with water heating (WH) is modeled [27, 36–39, 121]. A schematic diagram of the CAOW-WH HD cycle is shown in Fig. 4-18. Specifically, the model developed by Mistry et al. [36] is used with additional equations added to calculate entropy generation due to temperature and chemical disequilibrium as well as Second Law efficiency.

In this model, all components are modeled as black boxes. The humidifier and dehumidifier are characterized by an effectiveness parameter designed to capture the effects of simultaneous heat and mass transfer [122]. The solar heater is approximated as a constant heat flux surface. Pumping losses are ignored since all streams are approximated to be at atmospheric pressure. Physical properties are evaluated for seawater [45], moist air [123], and pure water [124].

Operating conditions are selected as: mass flow rate ratio of seawater to dry air is 3; effectiveness of the humidifier and dehumidifier is 90%; seawater temperature and salinity are 30 °C and 35 g/kg respectively; and brine top temperature is 70 °C. A breakdown of the contributions to the entropy generation for the CAOW-WH HDH cycle is shown in Fig. 4-19. For this example, the dehumidifier is the limiting component as it is the greatest source of irreversibility. Further discussion regarding the sources of irreversibility within the components is provided in [36].

Entropy generation due to thermal disequilibrium accounts for approximately 16% of the total irreversibility in the system. As with the MSF-OT and DCMD systems considered earlier, the low recovery ratio (4.5%) results in very low entropy

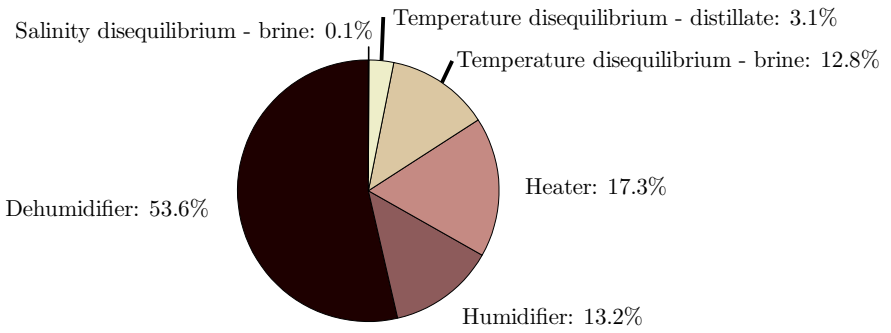

Figure 4-19: Relative contribution of sources to entropy generation in the closed air open water, water heated humidification-dehumidification system. Irreversibilities in the dehumidifier dominate. Total specific entropy generation is 370 J/(kg K).

generation due to chemical disequilibrium of the brine. Based on these conditions, the minimum least work is 2.76 kJ/kg and the total entropy generation is 370 J/(kg K). Therefore, the required heat of separation is 962 kJ/kg (GOR is 2.5) and the Second Law efficiency is 2.4%.

Mistry et al. [27] performed an exergy analysis of a wide range of CAOW HDH cycle configurations (water heated, air heated) at various operating conditions (top temperature, mass flow rate ratio, component effectiveness, *etc.*) and found that there was no consistent correlation between a cycle's exergetic efficiency and GOR (see [27], Table 1 and Fig. 10). In addition to the reasons discussed in [27], the lack of consistent correlation between the two parameters is largely a result of defining η_{II} as $\dot{\Xi}_{\text{out}}/\dot{\Xi}_{\text{in}}$ rather than $\dot{\Xi}_{\text{out,useful}}/\dot{\Xi}_{\text{in}}$. Accounting for the exergy lost in the discarded streams (*i.e.*, exergy destroyed due to thermal and chemical disequilibrium) in the definition of η_{II}, as discussed in Section 4.2, reconciles the inconsistencies that were observed. The original data from ([27], Fig. 10) is provided in Fig. 4-20a. Additionally, the data is plotted against the proper definition of Second Law efficiency, Eq. (4.15), in Fig. 4-20b and it is seen that there is a definite positive correlation between GOR and η_{II}, regardless of the cycle configuration or operating conditions, as expected.

4.8 Conclusions

In this chapter, the following conclusions have been reached:

1. A Second Law efficiency is developed for desalination systems and is defined as the useful work output divided by the total work input to the system. The useful work output of a desalination system is the minimum least work of separation, since the useful output of the system is pure water, not pure *hot* water. Minimum least work of separation is defined such that all input and output streams with exception of the product stream are in thermal, mechanical, and chemical equilibrium with the environment (total dead state). The product

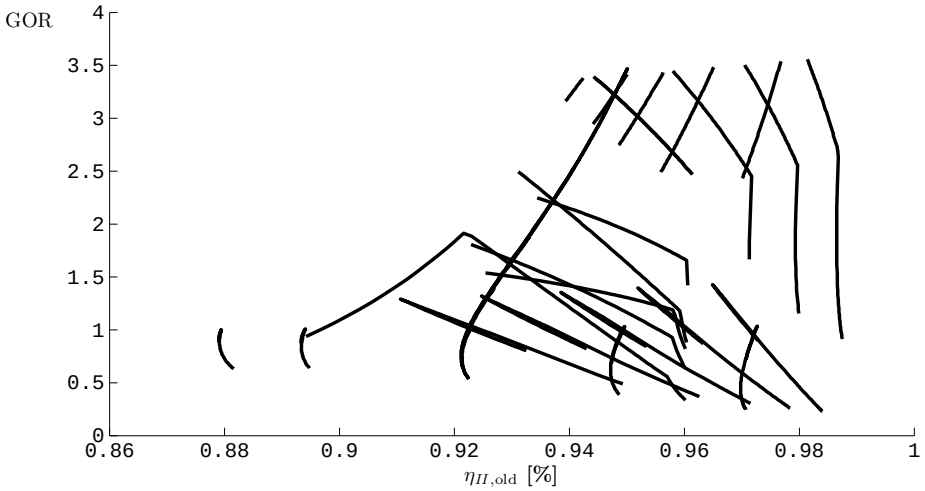

(a) GOR *versus* $\eta_{II,\mathrm{old}} = \dot{\Xi}_{\mathrm{out}}/\dot{\Xi}_{\mathrm{in}}$

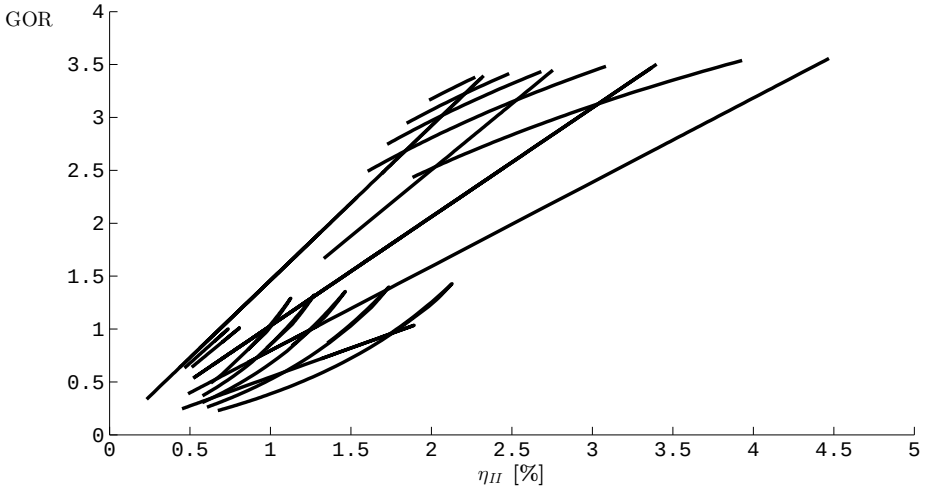

(b) GOR *versus* $\eta_{II} = \dot{\Xi}_{\mathrm{out,useful}}/\dot{\Xi}_{\mathrm{in}}$

Figure 4-20: GOR versus Second Law efficiency for closed air open water humidification-dehumidification cycle configurations analyzed by Mistry et al. [27]. The original data, Fig. 4-20a ([27], Fig. 10), shows no correlation between GOR and the old definition of η_{II}. Figure 4-20b shows that using a minimum least work of separation based definition for Second Law efficiency results in a positive correlation between the energetic performance (GOR) and Second Law performance (η_{II}) of the cycles.

stream is in thermal and mechanical equilibrium with the environment (restricted dead state). The exergy input to the desalination systems analyzed is either in the form of work or heat. See Eq. (4.14).

2. When evaluating the Second Law efficiency, it is essential that the control volume is selected in such a way that only primary energy sources are considered and that all process streams are allowed to come to thermal and mechanical equilibrium (restricted dead state).

3. In a cogeneration scheme where the primary energy input is heat, a work-driven separation process can never achieve 100% Second Law efficiency unless the power plant is also reversible since the work is created through an irreversible process.

4. Based on currently available technology, work-driven desalination systems are able to achieve a much higher Second Law efficiency than thermally driven systems. From a purely exergetic point of view (based on primary energy input), it is always favorable to produce work to drive an RO system rather than to use MED or MSF. Factors such as cost, feed quality, robustness to difficult conditions, and existing infrastructure may still result in thermal systems being preferred.

5. When considering the work input to be the minimum least work of separation plus lost work due to entropy generation, it is essential to consider entropy generated not only due to irreversibilities in the separation process, but also due to temperature disequilibrium of the discharge and the irreversible mixing of the concentrate with the ambient seawater. See Eq. (4.6).

6. The application of entropy generation analysis to various desalination technologies showed that thermal disequilibrium of the discharge streams results in a substantial portion of the entropy generated in thermal systems. Similarly, it was seen that entropy generation due to chemical disequilibrium is important only in systems with high recovery ratios. Depending on whether thermal or chemical disequilibrium is important, modifications to the systems can be implemented in order to capitalize on the potential differences between the discharge streams and the environment and reduce the required energy input.

The entropy generation techniques discussed herein provide a useful set of tools for analyzing desalination systems in order to determine major sources of lost work. However, it is important to note that entropy generation analysis is primarily useful for understanding how to improve a specific system. Comparing Second Law efficiency of various systems (*e.g.*, MED *vs.* RO) only shows which system is operating closer to the reversible limit (Fig. 4-21). While this is useful for understanding which systems have the potential for further improvement, it is often more useful, for system engineering purposes, to compare η_{II} of a single system operating under various conditions since this allows a designer to understand the irreversibilities within a system. One should be careful when comparing η_{II} for systems with electrical energy input to those with

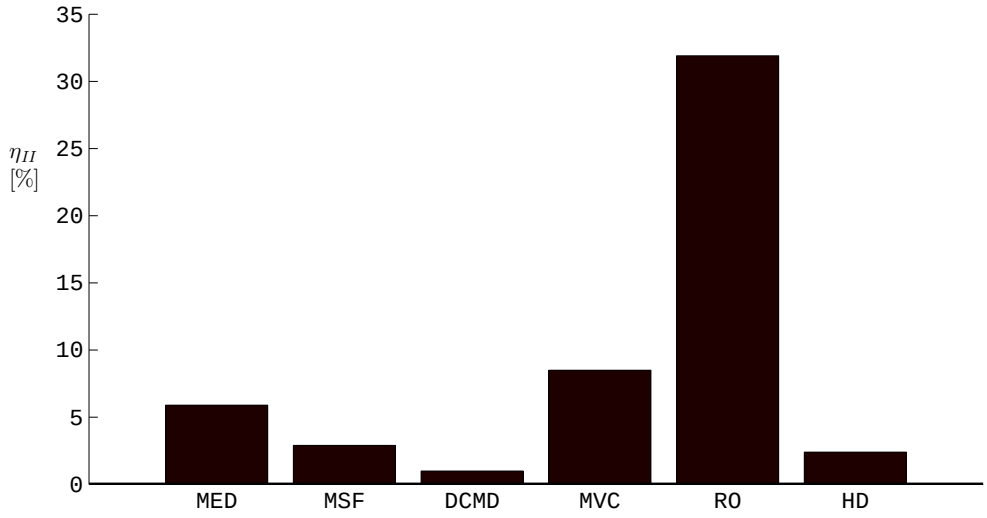

Figure 4-21: Second Law efficiencies calculated for the systems modeled in this chapter. Reverse osmosis has a substantially higher Second Law efficiency than the other desalination processes considered in this chapter.

thermal energy input. Electricity is a higher grade energy source than heat, and additional entropy is generated in the conversion from heat (or fuel) to electricity.

Chapter 5

Economic Second Law efficiency

Chapter abstract

Second Law efficiency is a useful parameter for characterizing the energy requirements of a system in relation to the limits of performance prescribed by the Laws of Thermodynamics. However, since energy costs typically represent less than 50% of the overall cost of product for many large scale plants (and in particular, for desalination plants), it is useful to have a parameter that can characterize both energetic and economic effects. In this paper, an economics-based Second Law efficiency is defined by analogy to the exergetic Second Law efficiency and is applied to several desalination systems. It is defined as the ratio of the minimum cost of producing a product divided by the actual cost of production. The minimum cost of producing the product is equal to the cost of the primary source of energy times the minimum amount of energy required, as governed by the Second Law. The analogy is used to show that thermodynamic irreversibilities can be assigned costs and compared directly to non-energetic costs such as capital expenses, labor, and other operating costs. The

economics-based Second Law efficiency identifies costly sources of irreversibility and places these irreversibilities in context with the overall system costs. These principles are illustrated through three case studies. First, a simple analysis of multistage flash and multiple effect distillation systems is performed using available data. Second, a complete energetic and economic model of a reverse osmosis plant is developed to show how economic costs are influenced by energetics. Third, a complete energetic and economic model of a solar powered direct contact membrane distillation system is developed to illustrate the true costs associated with so-called free energy sources.

This chapter has been submitted for publication in [26].

5.1 Introduction

Substantial research in desalination has been conducted in recent decades in order to develop more efficient and economical technologies, both to provide potable water and to remediate industrial process waters [9, 10].

Several energetics-based performance parameters are regularly used in the desalination industry in order to describe the energy requirements of various technologies and to compare the energy efficiency of systems. These performance parameters include specific electricity consumption (SEC), gained output ratio (GOR), performance ratio (PR), least heat and least work, and Second Law efficiency [21, 22]. While all of these energetic parameters are useful, unfortunately, they all have certain limitations. For example, parameters such as SEC and GOR are based purely on energy consumption and fail to capture thermodynamic limits on system performance. Second Law efficiency references the energy consumed to the theoretical minimum energy requirements (minimum least work of separation), and therefore, is an expression of how close a real-world system is to achieving the reversible limit of energy efficiency. However, this parameter is also limited in that it only captures exergetic effects. Since it is only a reflection of exergetic costs, optimization based on Second Law efficiency alone will result in impractical systems requiring very large, or infinite, transfer areas (heat transfer surfaces, membranes, *etc.*).

All real-world systems are ultimately limited by total cost of the end product. The cost of a system is a function of many parameters, of which energy is just one. For typical large-scale desalination plants, the cost of energy is less than 50% of the overall cost [7, 12]. Therefore, it is useful to have a parameter that can adequately capture both energetic and economic effects.

An economics-based Second Law efficiency that is defined in analogy to the standard exergetic Second Law efficiency is such a parameter that can be used to consider both energetic and economic factors and can be used to compare various systems. Additionally, by subdividing the energy costs based on individual sources of irreversibility, as is typically done in an exergy analysis, the cost of thermodynamic irreversibility can be compared to other non-energetic costs such as capital expenses, labor, and so on. Then, the greatest sources of economic loss can be identified. While thermoeconomics and the costing of exergy destruction are not new ideas, the use of an efficiency parameter to relate actual costs to idealized costs is novel [125–132].

In this study, a method for defining and evaluating an economics-based Second Law efficiency is introduced and demonstrated for multiple desalination technologies. While only desalination technologies are considered herein, these methods are completely general and can be applied to any type of system.

5.2 Second Law efficiency for a chemical separator

Second Law (or exergetic) efficiency is a commonly employed metric that measures the thermodynamic reversibility of a system. While First Law efficiency measures the amount of an energy source that is put to use, Second Law efficiency (η_{II}) measures the extent of irreversible losses within a system. As a result, a completely reversible system will have a Second Law efficiency of one even though the First Law efficiency is likely to be lower. Bejan [31] defines the exergetic efficiency as the ratio of the exergy of the process products to the process fuel. In other words, the exergetic efficiency is the ratio of the useful exergy of the outputs of the process ($\dot{\Xi}_{\text{out,useful}}$) to the exergy of the process inputs ($\dot{\Xi}_{\text{in}}$):

$$\eta_{II} \equiv \frac{\dot{\Xi}_{\text{out,useful}}}{\dot{\Xi}_{\text{in}}} = 1 - \frac{\dot{\Xi}_{\text{destroyed}} + \dot{\Xi}_{\text{lost}}}{\dot{\Xi}_{\text{in}}} \tag{5.1}$$

The second equality in Eq. (5.1) is valid since the useful exergy out is equal to the exergy in minus the sum of the exergy destroyed ($\dot{\Xi}_{\text{destroyed}}$) and the exergy lost ($\dot{\Xi}_{\text{lost}}$). Exergy destroyed represents lost available work due to irreversibilities within the system. Exergy lost represents lost available work due to discarding streams to the environment that carry exergy. Note that when the material inputs to the system are taken to be at equilibrium with the environment, $\dot{\Xi}_{\text{in}}$ equals $\dot{\Xi}_{\dot{W}_{\text{sep}}}$, $\dot{\Xi}_{\dot{Q}_{\text{sep}}}$, or $\dot{\Xi}_{\text{fuel}}$, depending on the energy input.

Mistry et al. [21] discussed many of the subtleties associated with the Second Law efficiency as applied to a desalination system and showed that the useful exergy output of the system is equal to the minimum least work of separation. In order to define the minimum least work of separation, consider a black box desalination system as illustrated in Fig. 5-1. By applying the First and Second Laws of Thermodynamics, conservation of mass, requiring all streams to cross the system boundary at the restricted dead state (RDS, thermal and mechanical equilibrium with the environment), and assuming steady state and reversible behavior, the least work of separation can be shown to be equal to [21–25]:

$$\frac{\dot{W}_{\text{least}}}{\dot{m}_p} = (g_p - g_c) - \frac{1}{r}(g_f - g_c) \tag{5.2}$$

where the mass based recovery ratio is defined as:

$$r \equiv \frac{\dot{m}_p}{\dot{m}_f} = \frac{\text{mass flow rate of product}}{\text{mass flow rate of feed}} \tag{5.3}$$

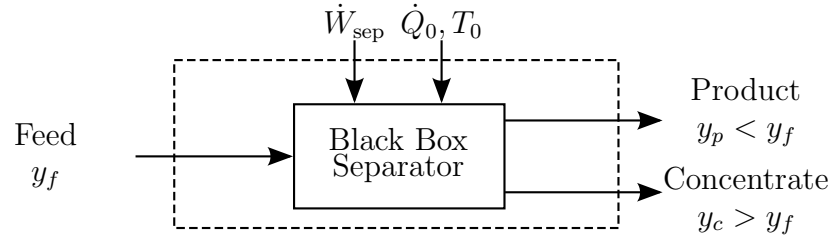

Figure 5-1: A control volume for an arbitrary black box chemical separator powered by work only. Heat transfer with the environment is allowed to ensure all streams leave the control volume at the restricted dead state.

and the Gibbs free energy of each of the streams is evaluated as a function of ambient temperature (T_0) and salinity (y_i). Using mass balance on the dissolved solids, the salinity of the concentrate stream is given as:

$$y_c = \frac{y_f - r y_p}{1 - r} \tag{5.4}$$

Note that while work is the only energy input, in order to fulfill the First and Second Laws of Thermodynamics and to allow all streams to enter and exit the control volume at ambient temperature, heat transfer must be allowed with the environment ($\dot{Q}_0$).

The minimum least work of separation is equal to the least work of separation at infinitesimal recovery and is equal to the true exergetic value of the product of a chemical separation process [21, 22]:

$$\dot{W}^{\min}_{\text{least}} \equiv \lim_{r \to 0} \dot{W}_{\text{least}} = \lim_{r \to 0} \dot{\Xi}_{\text{least}} \equiv \dot{\Xi}^{\min}_{\text{least}} \tag{5.5}$$

Mistry et al. [21] provided definitions for the Second Law efficiency of desalination systems in terms of the minimum least work ($\dot{W}^{\min}_{\text{least}}$) and in terms of the minimum least heat ($\dot{Q}^{\min}_{\text{least}}$). Similarly, Mistry and Lienhard [22] introduced the minimum least fuel and these three definitions for η_{II} are:

$$\eta_{II} = \frac{\dot{W}^{\min}_{\text{least}}}{\dot{W}_{\text{sep}}} \qquad \eta_{II} = \frac{\dot{Q}^{\min}_{\text{least}}}{\dot{Q}_{\text{sep}}} \qquad \eta_{II} = \frac{\dot{m}^{\min}_{\text{least}}}{\dot{m}_{\text{sep}}} \tag{5.6}$$

Mistry and Lienhard V [22] also generalized the expressions for Second Law efficiency given in Eq. (5.6) in order to allow for systems that are powered by any combination of energy inputs. The generalized equation is defined as:

$$\eta_{II} = \frac{\dot{\Xi}^{\min}_{\text{least}}}{\dot{\Xi}_{\text{sep}}} = \frac{\dot{\Xi}^{\min}_{\text{least}}}{\dot{\Xi}_{\dot{W}} + \dot{\Xi}_{\dot{Q}} + \dot{\Xi}_{\text{ch}}} \tag{5.7}$$

where

$$\dot{\Xi}_{\dot{W}} = \dot{W} \qquad \dot{\Xi}_{\dot{Q}} = \eta_{\text{Carnot}} \dot{Q} \qquad \dot{\Xi}_{\text{ch}} = \xi_{\text{fuel}} \dot{m}_{\text{fuel}}$$

Care must be taken when evaluating the denominators in Eq. (5.7). For stand-alone systems, the denominator is simply the sum of the exergetic inputs. For systems that

are part of a cogeneration scheme, it is essential that only primary energy inputs are considered [22]. For the case of a desalination plant operating in conjunction with a power plant, this means that the exergetic input is the additional heat input required by the power plant in order to produce the necessary work and steam to drive the desalination process.

Equation (5.7) is completely general and is written in terms of the various exergy inputs that can be provided to a system. It is particularly useful when trying to evaluate the system in terms of the inputs. An alternative way to express the Second Law efficiency is in terms of the losses that occur within the system. That is, in terms of the exergy destruction. As discussed by Mistry et al. [21], it is essential that all sources of irreversibility are considered, including those that occur outside of the system as a result of discharging streams that are at disequilibrium with the environment:

$$\eta_{II} = \frac{\dot{\Xi}^{\min}_{\text{least}}}{\dot{\Xi}_{\text{sep}}} = \frac{\dot{\Xi}^{\min}_{\text{least}}}{\dot{\Xi}^{\min}_{\text{least}} + T_0 \dot{S}^{\text{TDS}}_{\text{gen}}} = \frac{\dot{\Xi}^{\min}_{\text{least}}}{\dot{\Xi}_{\text{least}} + T_0 \dot{S}^{\text{RDS}}_{\text{gen}}} \tag{5.8}$$

The two forms of Eq. (5.8) are provided to show that the entropy destroyed in taking the concentrate stream to the total dead state (TDS, thermal, mechanical, and chemical equilibrium with the environment) must be considered [21].

While Eqs. (5.7) and (5.8) are useful for understanding and characterizing the exergetic inputs and thermodynamic irreversibilities, respectively, they are both limited in that they only provide information about the energetic requirements of a system. Even though it is important to understand energetic requirements and it is typically desired to minimize the requirements through the reduction of irreversibilities, economic constraints often result in system designs that are not optimized from a purely energetic point of view. Therefore, it is desirable to have a parameter that can account for both energetic factors and economic factors. Such a parameter is proposed in the following section.

5.3 Derivation of an economics-based Second Law efficiency

Before the economics-based Second Law efficiency can be defined, one must consider what Eq. (5.7) means physically. Expressed in words,

$$\eta_{II} \equiv \frac{\text{Useful exergetic value of the product}}{\text{Actual exergetic value of all inputs}} \tag{5.9}$$

As discussed by many authors [21, 22, 31, 47, 131], η_{II} is useful since it expresses how efficiently a process is able to produce output when compared to the limitations imposed by the Second Law of Thermodynamics. However, as explained above, energetics alone are not fully descriptive in characterizing practical, thermodynamic systems. Instead, energetic efficiency needs to be considered while accounting for economic costs. Unfortunately, improved efficiency typically comes at the expense of increased capital costs. Therefore, it is important to maintain a trade-off between the

objectives of maximum energy efficiency and minimum cost.

Now, consider a modification of the existing definition for Second Law efficiency. As shown in Eq. (5.9), η_{II} is the ratio of two exergetic quantities, measured in J or W. By analogy, a new economics-based Second Law efficiency, denoted $\eta_{II,\$}$, is introduced in the form of a ratio of quantities measured in currency (*e.g.*, US dollars):

$$\eta_{II,\$} \equiv \frac{\text{Minimum cost of producing product}}{\text{Actual cost of producing product}} \tag{5.10}$$

In order to properly define $\eta_{II,\$}$, both the numerator and denominator of Eq. (5.10) must be carefully analyzed.

5.3.1 Minimum cost of producing product

Comparing Eqs. (5.9) and (5.10), it is clear that the minimum cost of producing product should be defined by analogy to the useful exergetic value of the product. Therefore, the cost function should be related to the exergetic cost of producing the product, as defined by thermodynamics. Note that since the price of the product is not a function of the system itself, but rather, it is a function of the current economic market, product price is not an appropriate metric to use here.

According to thermodynamics, the only exergetic cost is for the exergy inputs. Thermodynamics cannot place a limit on other costs, such as capital expenses, labor, and interest rates since these costs are a function of economic markets, not of inherent system properties. Additionally, under ideal conditions of infinite plant life and infinitesimal interest rate, the amortization factor goes to zero:

$$\lim_{\substack{i\to 0\\ n\to\infty}} \frac{i(1+i)^n}{(1+i)^n - 1} = 0 \tag{5.11}$$

Therefore, the minimum cost of production is related to the required energy of separation. When exergy is needed, it is purchased in terms of energy, not exergy. That is, electricity (work) is typically sold per kWh and thermal energy is typically sold per BTU or therm. Therefore, the minimum cost should be expressed in terms of the primary energy input (not exergy) and the cost of that energy input. Since cost of each specific form of energy is tied to many factors, it may not be directly related to the exergetic value of the energy. The minimum least work of separation represents the least amount of work required to produce product, and therefore, this quantity should be used. Similarly, the minimum least heat or the minimum least mass of fuel can be used for systems that are driven using heat or fuel. Thus,

$$\text{Minimum cost of producing product with work} = c_e \dot{W}^{\min}_{\text{least}} \tag{5.12}$$

$$\text{Minimum cost of producing product with heat} = c_h \dot{Q}^{\min}_{\text{least}} \tag{5.13}$$

$$\text{Minimum cost of producing product with fuel} = c_{\text{fuel}} \dot{m}^{\min}_{\text{least}} \tag{5.14}$$

where c_e, c_h, and c_{fuel} are the costs of electricity, heat, and fuel respectively. These

cost functions will vary from location to location and should be equal to the actual cost functions that a plant at that location would have to pay for the respective type of energy.

Note that while the least work and least heat are related through the Carnot efficiency ($\dot{W}_{\text{least}} = \eta_{\text{Carnot}}\dot{Q}_{\text{least}}$), the same is not true for the cost functions ($c_e \neq c_h/\eta_{\text{Carnot}}$). As a result, it is clear that the values obtained through evaluation of Eqs. (5.12) to (5.14) will all be different. This is to be expected since the price of various energy inputs can vary substantially as a function of numerous factors, including but not limited to availability, state of the economy, political stability, and regulatory policies. In order to account for the fact that each primary fuel has a different cost associated with it, $\eta_{II,\$}$ cannot be simplified to one generic equation in the same manner that η_{II} is in Eq. (5.7). Instead, there will be three definitions based each on work, heat, or fuel analogously to the expressions in Eq. (5.6):

$$\eta_{II,\$} = \frac{c_e \dot{W}^{\min}_{\text{least}}}{\text{Total Cost}} \qquad \eta_{II,\$} = \frac{c_h \dot{Q}^{\min}_{\text{least}}}{\text{Total Cost}} \qquad \eta_{II,\$} = \frac{c_{\text{fuel}} \dot{m}^{\min}_{\text{least}}}{\text{Total Cost}} \tag{5.15}$$

At this point, it is important to emphasize that even for fixed total costs, the value of $\eta_{II,\$}$ will be different depending on which of the three expressions in Eq. (5.15) is used. This raises a problem as the value of $\eta_{II,\$}$ strongly depends on the selection of the primary energy input and therefore, a way to select which expression to use must be determined. Three possible options include: use the minimum value of the three expressions; always use the work, heat, or fuel-based definition; or use the definition based on the primary fuel source to be used for the given system. Each of these options is considered.

The first option is to always use the minimum value of the cost of energy times the respective energy source. From a purely Second Law and reversibility point of view, this makes sense since it would technically give the lowest cost of desalination (analogous to the lowest energy of separation), regardless of energy input. However, the physical meaning of this selection (or lack thereof) must be considered. As an example, reverse osmosis (RO) plants are powered (exclusively) using electricity. However, at the location of a given RO plant, the cost of low temperature steam might be substantially less than that of electricity such that $c_h\dot{Q}^{\min}_{\text{least}}$ is less than $c_e\dot{W}^{\min}_{\text{least}}$. In this instance, using option one, the numerator for the economic Second Law efficiency should be evaluated in terms of heat. Unfortunately, the problem with evaluating it in this manner is that the cost of heat is completely irrelevant to an RO plant's operational costs. Therefore, $\eta_{II,\$}$ defined based on this energy input is equally irrelevant and this approach should not be used.

The second option is to always use one of the expressions given in Eq. (5.15), regardless of the system being considered. Always using work is relatively simple and straightforward, and it has the benefit that the exergetic value of work is the value of work itself. Additionally, work is a quantity that is simple to think about and does not come with the added complication of defining the temperature at which heat is transferred into the system. Unfortunately, it is not necessarily useful to compare thermal energy costs to the cost of electricity since thermal energy may be available

under conditions very different than those associated with electricity generation; and it is definitely not useful to compare off-grid systems (such as solar driven systems) to a non-existent electricity source. For similar reasons, always using heat or fuel costs is also impractical in various situations. This approach introduces the same problem as discussed previously: if the primary energy considered is not relevant to the actual system's operating costs, then the parameter has no physical meaning.

The third option is to use the cost of energy of the primary energy source times the minimum amount of that energy source required for the separation process. Using this method has several advantages. Principally, evaluating the numerator in this manner will ensure that $\eta_{II,\$}$ is always scaled to the primary energy expense. For example, MED requires both thermal and electrical energy input. As a distillation (thermal) process, steam is the primary energy source used for driving separation. However, since energy recovery can be enhanced by operating at reduced pressure, electrical work in the form of pumping is needed to pump the product and brine streams back to atmospheric pressure. Additionally, pump work is required to overcome various frictional losses internal to the system. From an ideal thermodynamic point of view, distillation processes are driven using heat transfer alone. That is, the minimum energy required for a distillation processes is measured by the minimum least heat. Pump work required to maintain sub-atmospheric conditions and to overcome viscous losses clearly represent excess energy required beyond the reversible limit as a result of system design and irreversibilities. Therefore, the cost of said heat transfer alone should be the numerator for $\eta_{II,\$}$. Thus, $\eta_{II,\$}$ can be generalized to:

$$\eta_{II,\$} = \frac{(c\dot{E}^{\min}_{\text{least}})_{\text{primary energy source}}}{\text{Total Cost}} \tag{5.16}$$

There is a special case that must be considered explicitly at this point. From Eq. (5.16), it is seen that if there is a "free" source of energy, then, $\eta_{II,\$}$ will always equal zero. This implies that that any system operating using the supposedly "free" energy will always have a zero economic Second Law efficiency and be lesser-performing than any other system where energy has a finite cost. However, there is a fundamental problem with the notion of "free energy" that must be addressed.

In defining Eq. (5.16), there is an inherent assumption that the system being considered exists in an energy resource-constrained environment. When resources are constrained, they are given finite prices based on the laws of supply and demand. So-called renewable energies, such as solar and wind power, are available from the environment at some rate, and cannot be depleted by ongoing use. Consequently, they are sometimes regarded as free sources of energy. However, although these energies may exist freely in the environment, harvesting and using them requires (often substantial) capital and operating investment which must be amortized into the unit cost of energy from these sources. More specifically, if a plant uses solar generated electricity, then, a solar collection system, including photovoltaic panels, electronics, storage, and so on is required. The additional expense for the hardware is the actual cost of the "free" solar energy, and the amortized value of this expense should be used as the cost function in the numerator of Eq. (5.16). An example of a

solar powered system is considered in the next section in order to demonstrate this calculation.

Now that the numerator has been defined, the total costs in the denominator are considered.

5.3.2 Actual cost of producing product

In the preceding section, it was shown that the numerator of $\eta_{II,\$}$ should be defined analogously to the numerator of η_{II}. Comparing Eqs. (5.9) and (5.10) it is clear that the denominators are also defined analogously. For η_{II}, it is the total exergetic input, and for $\eta_{II,\$}$, it is the total cost. From Eq. (5.7), the total exergetic input is:

$$\text{Total exergetic input: } \dot{\Xi}_{\text{sep}} = \dot{W} + \eta_{\text{Carnot}}\dot{Q} + \xi_{\text{fuel}}\dot{m}_{\text{fuel}} \tag{5.17}$$

By analogy, the total cost of all of the energy inputs is defined as:

$$\text{Total cost of energy inputs: } = c_e\dot{W} + c_h\dot{Q} + c_{\text{fuel}}\dot{m}_{\text{fuel}} \tag{5.18}$$

where c_e, c_h, and c_{fuel} are the costs of work, heat, and fuel, respectively. The primary difference between Eqs. (5.17) and (5.18) (other than the obvious unit difference) is that each of the three terms ($\dot{W}$, $\dot{Q}$, and $\dot{m}_{\text{fuel}}$) are weighted differently. In Eq. (5.17), the heat and fuel terms are weighted using exergetic parameters (Carnot efficiency and exergy value of fuel, respectively) whereas in Eq. (5.18), all three terms are weighted using their respective cost values (in terms of dollars per kWh or dollars per kg).

At this point, a rudimentary definition for $\eta_{II,\$}$ can be introduced that is strictly analogous to η_{II} as defined by Eq. (5.7):

$$\eta_{II,\$} = \frac{(c\dot{E}^{\min}_{\text{least}})_{\text{primary energy source}}}{c_e\dot{W} + c_h\dot{Q} + c_{\text{fuel}}\dot{m}_{\text{fuel}}}$$

If, for sake of argument, it is assumed that work is the primary energy source, the above equation reduces to:

$$\eta_{II,\$} = \frac{\dot{W}^{\min}_{\text{least}}}{\dot{W} + \frac{c_h}{c_e}\dot{Q} + \frac{c_{\text{fuel}}}{c_e}\dot{m}_{\text{fuel}}}$$

As expected, the only difference between this expression and Eq. (5.7) is the weighting of the heat and fuel terms in the denominator. Depending on the ratio of the cost of heat and fuel to electricity, these terms will have more or less weight. Ultimately, this expression does not provide substantially more information than one can obtain from studying η_{II}. In order to make $\eta_{II,\$}$ useful, the expression needs to be further developed.

One of the limiting factors of any Second Law analysis is that it is only able to provide information about the exergetics of the process since it is a direct application of the First and Second Laws of Thermodynamics. This is made clear by the fact that all of the terms in Eq. (5.7) are in units of energy (or power). For many large scale

desalination systems, the energy cost typically represents only about a third to half of the overall costs [7, 12], so looking at a purely exergetic parameter fails to capture many of the practical considerations that are necessary for selecting a technology and designing a plant. Some of the other costs include, but are not limited to, capital costs and operating costs (consumables, maintenance, labor).

Since the preliminary definition of $\eta_{II,\$}$ is already written in terms of quantities that are expressed in dollars, it is trivial to add additional costs to the denominator in order to get the actual total cost of producing product.

$$\text{Total cost water} = \underbrace{c_e\dot{W} + c_h\dot{Q} + c_{\text{fuel}}\dot{m}_{\text{fuel}}}_{\text{cost of energy inputs}} + C_{\text{CAPEX}} + C_{\text{OPEX}} + \cdots \tag{5.19}$$

Now that the total cost of producing product has been identified, the proper definition of the economics-based Second Law efficiency is obtained:

$$\eta_{II,\$} = \frac{(c\dot{E}^{\min}_{\text{least}})_{\text{primary energy source}}}{c_e\dot{W} + c_h\dot{Q} + c_{\text{fuel}}\dot{m}_{\text{fuel}} + C_{\text{CAPEX}} + C_{\text{OPEX}} + \cdots} \tag{5.20}$$

This expression represents the efficiency, from a thermodynamic and economic point of view, with which a system is able to produce product. Since η_{II} does not include any non-energetic terms, it is clear that $\eta_{II,\$}$ will always be less than η_{II}.

An additional useful analogy can be made. As shown above, there are two useful ways for writing η_{II}, one in terms of the exergetic input [Eq. (5.7)], and another in terms of the exergy destruction [Eq. (5.8)]. Using the exergy destruction approach, $\eta_{II,\$}$ is rewritten:

$$\eta_{II,\$} = \frac{(c\dot{E}^{\min}_{\text{least}})_{\text{primary energy source}}}{(cE^{\min}_{\text{least}}) + \sum_i c_i T_0 \dot{S}_{\text{gen},i} + C_{\text{CAPEX}} + C_{\text{OPEX}} + \cdots} \tag{5.21}$$

When considering $\eta_{II,\$}$ from this point of view, it is clear that all non-energetic costs represent a "loss" to the system from a purely thermodynamic point of view. Therefore, the non-energetic terms can be combined with and compared to the entropy generation terms. In doing so, it becomes easy to compare the relative effects of each of the sources of losses and to understand which parts of a system require the most attention. For example, one could compare the cost of the additional energy needed to account for the losses in a heat transfer process to the operating costs associated with consuming chemicals. Depending on which loss (on a cost basis) is more significant, a designer can decide how to further optimize the process in order to reduce the overall cost of the product.

In the Section 5.4, Eqs. (5.20) and (5.21) are applied to various desalination systems in order to illustrate how they can be used.

5.3.3 Generalized to cogeneration systems

Cogeneration systems, by definition, generate multiple products with economic value. Therefore, multiple terms must be included in the definition of an economics-based Second Law efficiency for cogeneration systems. In the case of water and power cogeneration, $\eta_{II,\$}$ could be written in the form of:

$$\eta_{II,\$} = \frac{\text{Minimum cost of producing electricity + Minimum cost of desalinating water}}{\text{Actual cost of producing both}} \tag{5.22}$$

Some care is needed when considering the numerator in Eq. (5.22), and in particular, the minimum cost of desalination water. Since the desalination plant is powered using energy derived from some primary energy input to the larger cogeneration system, the cost scaling function on the minimum least energy must be based on the cost of the primary energy. This is equivalent to the evaluation of η_{II} for desalination plants in cogeneration systems as discussed by Mistry and Lienhard [22]. A methodology for evaluating the primary energy input to a desalination plant in a larger cogeneration system is presented in [16, 22]. For simplicity, all of the examples considered in this paper are stand-alone desalination systems.

5.4 Application to various desalination systems

In order to illustrate the application of Eqs. (5.20) and (5.21), energetic and economic analysis of several desalination systems are considered. First, a simplified calculation of η_{II} and $\eta_{II,\$}$ is performed for a multistage flash (MSF) plant and a multiple effect distillation plant (MED) using cost data available in the literature coupled with some simple approximations. Second, a much more detailed analysis of an RO system is performed in which the energetics are modeled by evaluating all of the irreversibilities in the system. The energetic model is coupled with a full cost model in order to show how economic costs are influenced by energetics. Third, a complete energetic and economic model of a solar powered direct contact membrane distillation (DCMD) is analyzed in order to demonstrate how systems powered using "free" energy should be studied.

5.4.1 Multistage flash and multiple effect distillation

MSF and MED are the two most common thermal desalination technologies [11]. Both are distillation methods in which the overall energy requirements are reduced through the use of energy recovery in each stage or effect of the system [99, 100]. Cost information for representative 100 000 m^3/d MSF and MED plants is provided by [133–137]. It is shown that the total cost of water production for the MSF and MED plants is \$0.89/m^3 and \$0.72/m^3. A breakdown of the costs is provided in Table 5.1. Additionally, the thermal and electrical energy requirements are provided.

Using the information in Table 5.1, it is possible to calculate both η_{II} and $\eta_{II,\$}$ as well as to compare all of the contributions to the total cost of producing water for the

Table 5.1: Breakdown of costs for a 100 000 m^3/d multistage flash and multiple effect distillation system [133].

	MSF	MED
Costs [\$/m^3]:		
Amortization	0.29	0.22
Maintenance	0.01	0.01
Chemical	0.05	0.08
Labor	0.08	0.08
Thermal energy	0.27	0.27
Electrical energy	0.19	0.06
Total	0.89	0.72
Energy requirements:		
Thermal energy [kWh_t/m^3]	78	69
Electrical energy [kWh_e/m^3]	4.0	1.0

two systems provided some additional assumptions are made. The feed is assumed to be standard seawater at 25 °C and 35 g/kg [45, 46] while the steam temperature is assumed to be 100 °C. Note that the minimum least heat of separation is a function of steam temperature so the exact values found in the following calculation are subject to change based on the actual (but unreported) steam temperature. However, since this example is used to demonstrate a methodology, rather than to draw significant comparisons between the two plants, this broad approximation is deemed acceptable. Finally, it is assumed that thermal energy is the primary energy input to the system. While MSF and MED plants are typically operated in cogeneration schemes, without further information, it is not possible to characterize the actual conversion efficiencies involved in the cogeneration power plant [22].

Using the generalized least energy of separation equation from Mistry and Lienhard [22],

$$\underbrace{\dot{W} + \sum_{l=1}^{p} \left(1 - \frac{T_0}{T}\right)_l \dot{Q}_l}_{\text{energy inputs/outputs}} + \underbrace{\sum_{\text{in}-\text{out}} \dot{N}\bar{\xi}(T, p, N_i)}_{\text{fuel and exhaust streams}} = \underbrace{\sum_{\text{out}-\text{in}} \dot{N}\bar{g}(T_0, p_0, N_i)}_{\text{process streams}} \tag{5.23}$$

the least heat of separation is equal to the least work of separation divided by Carnot efficiency. Using Eq. (5.2) and a standard seawater property package [45, 46], the minimum least heat of separation for seawater using a steam temperature of 100 °C is 13.5 kJ/kg (3.7 kWh_t/m^3) [133].

The price of both the thermal and electrical energy is evaluated by dividing the cost by the energy requirements. For MSF, this corresponds to heat and electricity prices of \$0.0034/kWh_t and \$0.0467/kWh_e, respectively. For MED, this corresponds

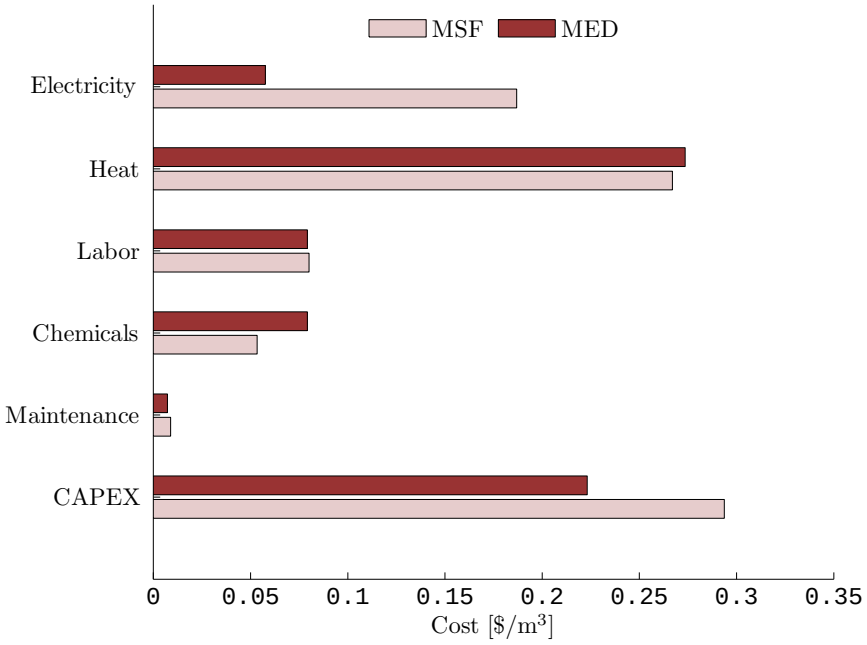

Figure 5-2: Breakdown of costs associated with the production of water using MSF and MED.

to \$0.0040/kWh$_t$ and \$0.0576/kWh$_e$.

Finally, the total energy input for both systems is equal to the sum of the exergies of the heat and work. Expressed in terms of heat (*i.e.*, $Q + W/\eta_{\text{Carnot}}$), the effective thermal input to the MSF and MED systems is 97.9 kWh$_t$/m^3 and 74.0 kWh$_t$/m^3, respectively. Using these values coupled with the minimum least heat of separation, η_{II} for the MSF and MED plants is 3.8% and 5.1%, respectively.

Similarly, $\eta_{II,\$}$ can be evaluated by multiplying the price of the primary energy (heat for thermal systems) and the minimum least heat of separation and dividing the result by the total cost of water production. Using the prices for heat determined above, $\eta_{II,\$}$ for the MSF and MED plants is evaluated to be 1.4% and 2.1% respectively. The specific breakdown of the costs, as shown in Table 5.1, is shown in Fig. 5-2.

The values of $\eta_{II,\$}$ found above are evaluated using Eq. (5.20). If instead, Eq. (5.21) is used, then the cost of the energetic input can be split into the cost of providing the minimum least heat of energy plus the sum of the costs of providing extra energy required to account for all of the thermodynamic irreversibilities. The results are shown in Fig. 5-3.

From Fig. 5-3, it is clear that the cost of excess energy required by the irreversibilities is the single greatest source of the total cost of producing water for these two representative MSF and MED plants. Given more detailed information about the systems in question, the irreversibilities could be further subdivided in order to isolate the specific source of loss. Then, a system designer could identify which components or processes should be addressed in order to try to reduce the overall system cost.

At this point, it should be reiterated that these are just representative numbers

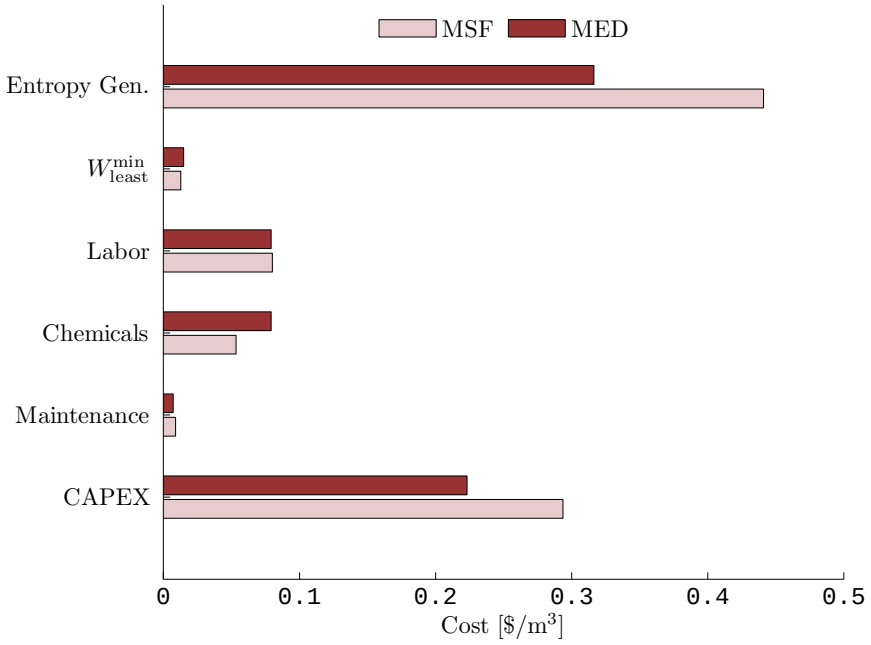

Figure 5-3: Breakdown of costs associated with the production of water using MSF and MED with entropy generation isolated.

and that these two examples (and the following examples) are not meant to be used to draw sweeping conclusions about the superiority of one technology over another.

In the next section, an energetic and economic model for a reverse osmosis system is presented and studied in greater detail than was possible based on the information available for the MSF and MED systems. By using an energetic model, specific sources of irreversibilities for the RO system are isolated.

5.4.2 Reverse osmosis

Reverse osmosis is the most common form of desalination [11]. A representative flow path of a single stage RO plant with energy recovery is shown in Fig. 5-4 [117]. A simple model based on the pressure differences throughout the system is used to evaluate the energetic requirements of this system [21]. In order to simplify the analysis of this system, thermal effects are neglected since they are of second order to pressure effects. Additionally, several approximations and design decisions are made.

Feed seawater enters the system at ambient conditions (25 °C, 1 bar, 35 g/kg salinity). The product is pure H_2O (0 g/kg salinity) produced at a recovery ratio of 40%. In order to match flow rates in the pressure exchanger, 40% of the feed is pumped to 69 bar using a high pressure pump while the remaining 60% is pumped to the same pressure using a combination of a pressure exchanger driven by the rejected brine as well as a booster pump. All pumps are assumed to have isentropic efficiencies of 85%. The concentrated brine loses 2 bar of pressure through the RO module while the product leaves the module at 1 bar. Energy Recovery Inc. [118]

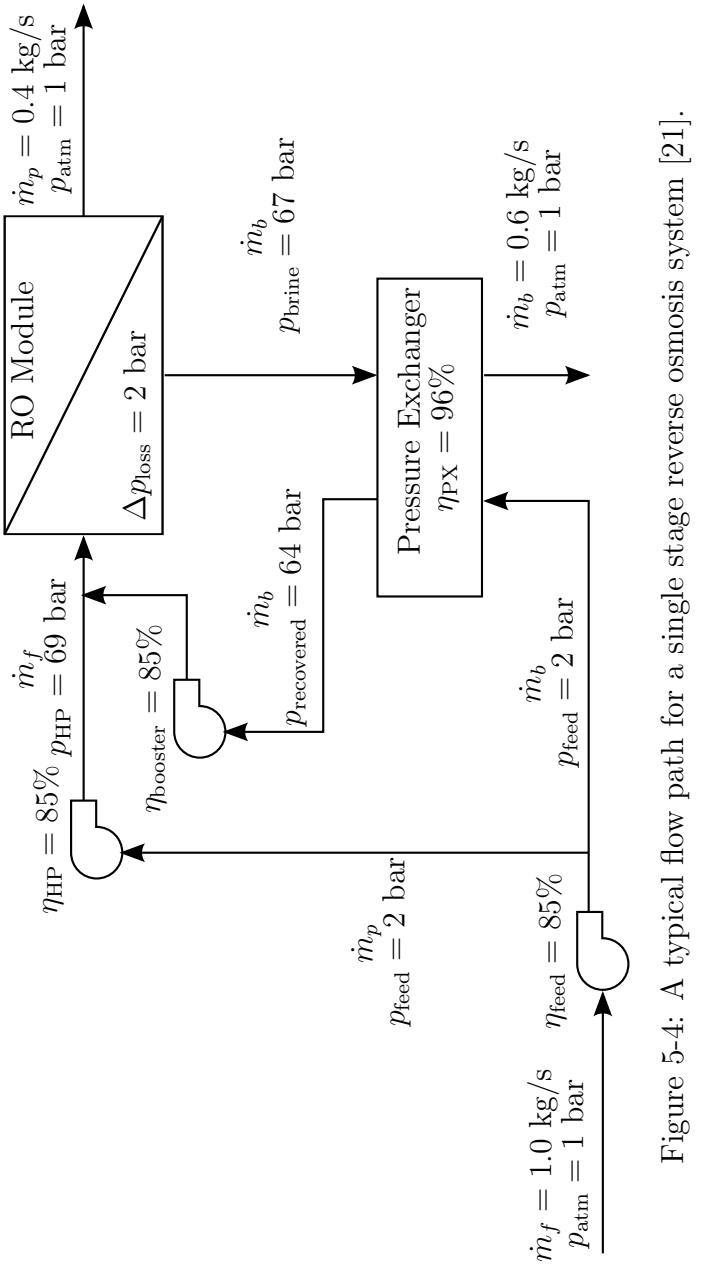

Figure 5-4: A typical flow path for a single stage reverse osmosis system [21].

makes a direct contact pressure exchanger that features a single rotating part. The pressure exchanger pressurizes part of the feed using work produced through the depressurization of the brine in the rotor. Assuming the expansion and compression processes are 98% efficient [21, 118], the recovered pressure is calculated as follows:

$$p_{\text{recovered}} = p_{\text{feed}} + \eta_{\text{expansion}}\eta_{\text{compression}} \left(\frac{\rho_{\text{feed}}}{\rho_{\text{brine}}}\right) (p_{\text{brine}} - p_{\text{atm}}) \tag{5.24}$$

and the pressure exchanger efficiency is evaluated using ERI's definition [117]:

$$\eta_{\text{PX}} = \frac{\sum_{\text{out}} \text{Pressure} \times \text{Flow}}{\sum_{\text{in}} \text{Pressure} \times \text{Flow}} \tag{5.25}$$

Density of seawater is evaluated using standard seawater properties [45, 46].

Mistry et al. [21] derived simple formulas based on the ideal gase and incompressible fluid models for the entropy generation through various mechanisms found in desalination processes. Entropy generated in the high pressure pump, booster pump, and the feed in the pressure exchanger is given by:

$$s_{\text{gen}}^{\text{pumping}} = c \ln \left[1 + \frac{v}{cT_1}(p_2 - p_1)\left(\frac{1}{\eta_p} - 1\right)\right] \approx \frac{v}{T_1}(p_2 - p_1)\left(\frac{1}{\eta_p} - 1\right) \tag{5.26}$$

where c is the specific heat, v is the specific volume, η_p is the isentropic efficiency of the pump, and states 1 and 2 correspond to the inlet and outlet, respectively. Similarly, entropy generated through the expansion of the pressurized brine in the pressure exchanger is given by:

$$s_{\text{gen}}^{\text{expansion,IF}} = c \ln \left[1 + \frac{v}{cT_1}(p_1 - p_2)\,(1 - \eta_e)\right] \approx \frac{v}{T_1}(p_1 - p_2)\,(1 - \eta_e) \tag{5.27}$$

where η_e is the isentropic efficiency of the expansion device.

Entropy generation in the RO module is a function of the change of both the mechanical and chemical states of seawater. In order to evaluate entropy generation, the change in entropy associated with all parts of the process path must be considered. Given that entropy is a state variable, the process can be decomposed into two sub-processes for the purpose of calculating the overall change of state. First, the high pressure seawater is isobarically and isothermally separated into two streams of different composition (note, in a real system, this would require a heat transfer process with the environment; however, thermal effects are neglected in this analysis). Second, the two streams are depressurized at constant salinity in order to account for the pressure drop associated with diffusion through the membrane (product, $\Delta p = 68\,\text{bar}$) and that associated with hydraulic friction (brine, $\Delta p = 2\,\text{bar}$).

Entropy change due to the separation process is evaluated as a function of temperature, pressure, and salinity of each of the process streams. For the model of separation considered here, the compositional change is taken at constant high pressure and

temperature:

$$\Delta\dot{S}_{\text{composition}} = \dot{m}_p s_p(T_0, p_{\text{HP}}, y_p) + \dot{m}_c s_p(T_0, p_{\text{HP}}, y_p) - \dot{m}_f s_f(T_0, p_{\text{HP}}, y_f) \tag{5.28}$$

Standard seawater properties [45, 46] are used for evaluating entropy. Even though this property package is independent of pressure, it may be used because seawater is nearly incompressible resulting in entropy being largely independent of p.

Mistry et al. [21] showed that entropy generation due to the irreversible depressurization of both the brine and product streams is given by:

$$s_{\text{gen}}^{\Delta p,\text{IF}} = c \ln\left[1 + \frac{v}{cT_1}(p_1 - p_2)\right] \approx \frac{v}{T_1}(p_1 - p_2) \tag{5.29}$$

The total entropy generated in the RO module is the sum of the entropy change due to compositional changes, Eq. (5.28), and the entropy generated in the depressurization of the product and brine streams, Eq. (5.29).

Entropy generated as a result of the discard of disequilibrium streams to the environment must also be considered. Thermal and chemical disequilibrium entropy generation can be evaluated using [21]:

$$\dot{S}_{\text{gen}}^{T\ \text{disequilibrium}} = \dot{m}_i c_i \left[\ln\left(\frac{T_0}{T_i}\right) + \frac{T_i}{T_0} - 1\right] \tag{5.30}$$

$$\dot{S}_{\text{gen}}^{\text{concentrate RDS}\rightarrow\text{TDS}} = -\frac{(\dot{m}_c + \dot{m}_{\text{sw}}^{\text{reservoir}})g_{\text{out}} - \dot{m}_c g_c - \dot{m}_{\text{sw}}^{\text{reservoir}} g_{\text{sw}}}{T_0} \tag{5.31}$$

Since thermal effects are neglected in this analysis, Eq. (5.30) reduces to zero. The energy dissipated by pressure loss and pump inefficiency results in very small increases in the system temperature. As a result, the entropy generation associated with the transfer of this energy out of the system as heat (if any) through the very small temperature difference from the environment is negligible relative to the mechanical sources of entropy production.

Using Eqs. (5.24) and (5.26) to (5.29) and the denominator of Eq. (5.8), the required energy input to the RO system as well as the entropy generation within each component can be evaluated. The results of this model are provided in Table 5.2 and a discussion is provided by Mistry et al. [21].

A basic cost model based on the work of Bilton *et al.* [138, 139] is used to generate an estimate of the total cost of producing water. The total annualized cost (TOTEX) is equal to the sum of the capital expenses (CAPEX) and the operating expenses (OPEX) [12, 131, 140]

$$A_{\text{TOTEX}} = A_{\text{CAPEX}} + A_{\text{OPEX}} \tag{5.32}$$

It is typically more convenient to refer to the unit cost of producing water than the annual cost of the system. Cost per unit water can be evaluated by dividing the annualized cost by the yearly water production:

$$C_w = \frac{A_{\text{TOTEX}}}{\dot{V}_w} \tag{5.33}$$

Table 5.2: Contributions to the overall energy requirements of a reverse osmosis system, evaluated in terms of entropy generated within each component.

Sources of Energy Consumption	Entropy Generation [J/(kg K)]	Energy Contribution [kJ/kg]
$W_{\text{least}}^{\text{min}}$	-	2.71
RO Module	10.6	3.16
High pressure pump	3.87	1.15
Pressure exchanger	1.26	0.377
Booster pump	0.407	0.121
Feed pump	0.145	0.043
Chemical disequilibrium	3.08	0.918
Total:	19.4	8.48 (2.35 kWh/m^3)

Yearly water production is equal to the daily capacity times the number of days in a year times the availability factor (AF):

$$\dot{V}_w = 365\text{AF}\dot{V}_{\text{capacity}} \tag{5.34}$$

CAPEX for a standard RO plant is subdivided into the cost of the RO system and the infrastructure:

$$C_{\text{CAPEX}} = C_{\text{infrastructure}} + C_{\text{RO}} \tag{5.35}$$

The RO system is composed of the RO components, pre-treatment, post-treatment, and piping:

$$C_{\text{RO}} = C_{\text{pre}} + C_{\text{RO comp}} + C_{\text{pipe}} + C_{\text{post}} \tag{5.36}$$

The RO components include membranes, pressure vessels, pumps, motors, energy recovery, and connections:

$$C_{\text{RO comp}} = C_{\text{membranes}} + C_{\text{pressure vessels}} + C_{\text{pumps}} + C_{\text{motors}} + C_{\text{ERD}} + C_{\text{connections}} \tag{5.37}$$

Costs for the components are given in Table 5.3. The booster pump and motor are approximated as costing one third the cost of the high pressure pump and motor [141]. Total component costs are based on a system size of $\dot{V}_{\text{capacity}} = 10\,000\,\text{m}^3/\text{d}$.

For typical RO systems, both pre- and post-treatment are needed. Pre-treatment is used to provide basic filtration and treatment to remove large debris, biological contaminants, and other suspended solids that might damage the RO membranes [84]. Similarly, post-treatment is needed to add essential minerals back to the water so that the water can safely be added to municipal pipelines [84]. In order to simplify the analysis in this model, both the pre- and post-treatment costs are assumed to be proportional to the total cost of the RO components. Post-treatment costs can also

Table 5.3: Cost of components required for a reverse osmosis system. Number required is determined for a 10 000 m^3/d system, based on volumetric flow rate capacity of each device. Cost of replacement is considered separately in Table 5.5.

Component	Cost [$]	Capacity [m^3/d]	Number [-]	Total Cost [$]
Membrane [142, 143]	550	25	1000	550,000
Pressure vessel (6 mem.) [144, 145]	1945	-	167	325,000
High Pressure pump [146, 147]	50000	720	14	700,000
Booster pump [141]	17000	1000	15	255,000
High pressure motor [148]	12000	-	14	168,000
Booster motor [141]	4000	-	15	60,000
ERD [141, 143, 149]	24000	1000	15	360,000
Total ($C_{\text{RO comp}}$)				2,420,000

include the cost of storage.

$$C_{\text{pre}} = \phi_{\text{pre}} C_{\text{RO comp}} \tag{5.38}$$

$$C_{\text{post}} = \phi_{\text{post}} C_{\text{RO comp}} + C_{\text{storage}} \tag{5.39}$$

Values for ϕ_{pre} and ϕ_{post} are taken to be 0.35 and 0.03, respectively [150]. For large municipal-scale systems, it is assumed that the water is fed directly to the water grid and that storage costs may be neglected.

In addition to the cost of the RO plant, there are a number of costs associated with infrastructure. These costs include: land, intake and brine dispersion systems, connections to the grid, installation and construction, *etc.* As with the pre- and post-treatments, for simplicity, it is assumed that these costs scale linearly with the cost of the RO plant:

$$C_{\text{infrastructure}} = \phi_{\text{infrastructure}} C_{\text{RO}} \tag{5.40}$$

where $\phi_{\text{infrastructure}}$ is taken to be 1.71 [150].

Now that all of the CAPEX are accounted for, they must be converted to annualized costs. This is done by multiplying the CAPEX by an amortization factor, given by:

$$A_{\text{CAPEX}} = \frac{i(1+i)^n}{(1+i)^n - 1} C_{\text{CAPEX}} \tag{5.41}$$

where i is the annual interest rate and n is the expected plant life in years [151]. For this analysis, a 7.5% interest rate for a plant with a 25 year expected lifetime is assumed [7]. All capital expenses are summarized in Table 5.4. Note that replacement is considered separately in Table 5.5.

Total OPEX is composed of the costs of labor, chemicals, power, and replacements. Labor, chemicals, and power all scale with the yearly water production, $\dot{V}_w$. If it is assumed the system operates 95% of the time (AF = 0.95), then the costs of labor,

Table 5.4: Summary of capital expenses for a representative reverse osmosis system.

Capital Expenses	Scaling Factor		Cost [$]
RO Components ($C_{\text{RO comp}}$)			2,420,000
Piping and connections [131]	$\phi_{\text{pipe}} = 0.66$	$\times C_{\text{RO comp}}$	1,600,000
Pre-treatment [150]	$\phi_{\text{pre}} = 0.35$	$\times C_{\text{RO comp}}$	846,000
Post-treatment [150]	$\phi_{\text{post}} = 0.03$	$\times C_{\text{RO comp}}$	72,500
Total RO (C_{RO})			4,930,000
Infrastructure [150]	$\phi_{\text{infrastructure}} = 1.71$	$\times C_{\text{RO}}$	8,430,000
Total Plant (C_{CAPEX})			13,400,000
Annualized CAPEX	$i = 7.5\%$, $n = 25$ years		1,200,000
Per m^3			0.346

chemicals, and power are:

$$A_{\text{labor}} = \gamma_{\text{labor}} \dot{V}_w \tag{5.42}$$

$$A_{\text{chemicals}} = \gamma_{\text{chemicals}} \dot{V}_w \tag{5.43}$$

$$A_{\text{electricity}} = \gamma_{\text{electricity}} W_{\text{sep}} \dot{V}_w \tag{5.44}$$

where γ_{labor} is the specific operating cost of labor, $\gamma_{\text{chemicals}}$ is the average cost of chemicals, $\gamma_{\text{electricity}}$ is the cost of electricity, and W_{sep} is the electricity requirements for the RO system. The electrical requirements for pre- and post-treatment are neglected in this study. For this analysis, $\gamma_{\text{labor}} = \$0.05/\text{m}^3$ [151, 152] and $\gamma_{\text{chemicals}} = \$0.033/\text{m}^3$ [151]. The cost of electricity varies widely depending on location. While the average price for electricity for industrial use in the US is $\$0.652/(\text{kW h})$, a price more typical of the population-dense areas of the East and West Coasts is closer to $\$0.11/(\text{kW h})$ [153]. Therefore, the cost of electricity is taken to be $\gamma_{\text{electricity}} = \$0.11/\text{kWh}$ while $\dot{W}_{\text{sep}}$ is evaluated using the RO model described above and summarized in Table 5.2 [21].

Part of the operating expenses is the cost of replacing parts as they reach their product lifetime. Given that many components will not last the entire lifetime of the overall plant, it is important to properly account for replacement of expensive components. The annualized cost of replacement is given by:

$$\begin{aligned} A_R = {} & C_{\text{membrane}} R_{R,\text{membrane}} + C_{\text{pump}} R_{R,\text{pump}} \\ & + C_{\text{motor}} R_{R,\text{motor}} + C_{\text{ERD}} R_{R,\text{ERD}} + C_{\text{pre}} R_{R,\text{pre}} + C_{\text{post}} R_{R,\text{post}} \end{aligned} \tag{5.45}$$

where R_R is the annual replacement rate. Values of R_R along with the corresponding component costs are provided in Table 5.5. All OPEX are summarized in Table 5.6.

Combining all of the CAPEX and OPEX, an estimate of the cost of water using the RO system shown in Fig. 5-4 can be evaluated. For a system that produces $10\,000\,\text{m}^3/\text{d}$, the cost of water is estimated to be $\$0.791/\text{m}^3$. A bar chart showing the relative contributions to the cost of water production is given in Fig. 5-5. The

Table 5.5: Replacement rate for various reverse osmosis components.

Component	R_R	C_i [$]	Total [$]
Membrane	0.2	550,000	110,000
Pumps	0.1	955,000	95,500
Motors	0.1	228,000	22,800
ERD	0.1	360,000	36,000
Pre-treatment	0.1	846,235	84,600
Post-treatment	0.1	72,534	7,250
Total Replacement Cost (A_R)			356,000

Table 5.6: Summary of operating expenses for a representative reverse osmosis system.

Operating Expenses	Scaling Factor		Cost [$]
Labor [151, 152]	$\gamma_{\text{labor}} = 0.05$	$\times \dot{V}_w$	173,000
Chemicals [151]	$\gamma_{\text{chemicals}} = 0.033$	$\times \dot{V}_w$	114,000
Electricity [153]	$\gamma_{\text{electricity}} = 0.11$	$\times W_{\text{sep}} \dot{V}_w$	899,000
Replacement			356,000
Total Annual OPEX			1,540,000
Per m^3			0.445

economic Second Law efficiency of this system can now be evaluated using Eq. (5.20). Using Eq. (5.2) and a standard seawater property package [45, 46], the minimum least work of separation for the feed seawater 2.71 kJ/kg (0.75 kWh_e/m^3). Therefore,

$$\eta_{II,\$} = \frac{c_e \dot{W}^{\min}_{\text{least}}}{\text{Total Cost}} = \frac{\gamma_{\text{electricity}} W^{\min}_{\text{least}}}{C_w} = \frac{(\$0.11/\text{kWh})(0.75\,\text{kWh/m}^3)}{\$0.791\,/\text{m}^3} = 10\% \quad (5.46)$$

Compare this to the value of the Second Law efficiency:

$$\eta_{II} = \frac{\dot{W}^{\min}_{\text{least}}}{\dot{W}_{\text{sep}}} = \frac{0.75}{2.35} = 32\% \quad (5.47)$$

As shown in Fig. 5-5, costs associated with capital expenses and replacement of parts are the most significant contributors to the overall cost of this particular RO system. However, the cost of energy is also significant, and represents about 34% of the overall cost. The overall energy cost can be further subdivided into costs associated with the thermodynamic process of separation ($\dot{W}^{\min}_{\text{least}}$) and those associated with irreversibilities ($T_0 \dot{S}_{\text{gen}}$) as shown in Table 5.2. Scaling the various energy components using $\gamma_{\text{electricity}}$, Fig. 5-5 is redrawn in terms of each of the sources of irreversibilities (Fig. 5-6).

Fig. 5-6 shows that the costs associated with thermodynamic irreversibility are on the same order as the costs associated with replacement costs and the minimum

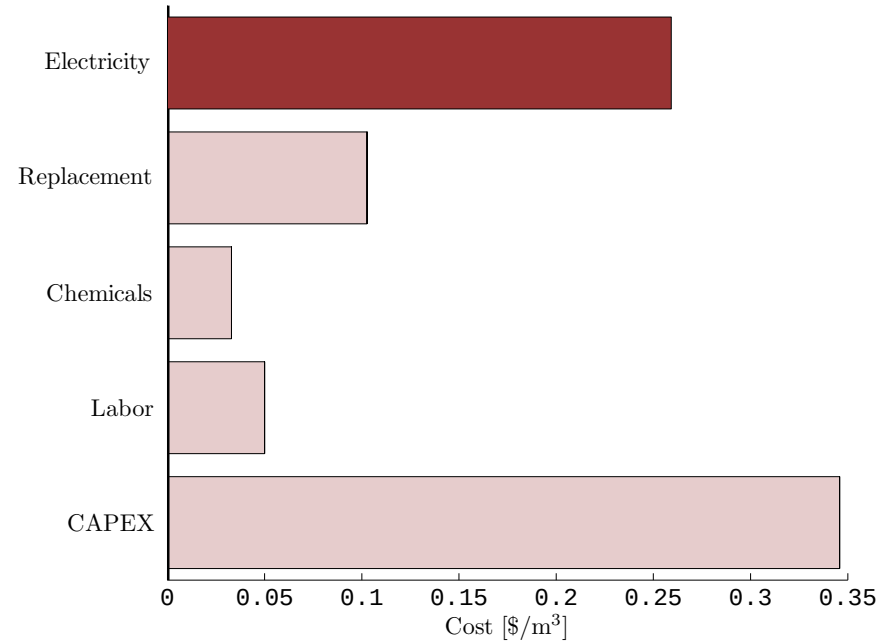

Figure 5-5: Breakdown of costs associated with the production of water using reverse osmosis.

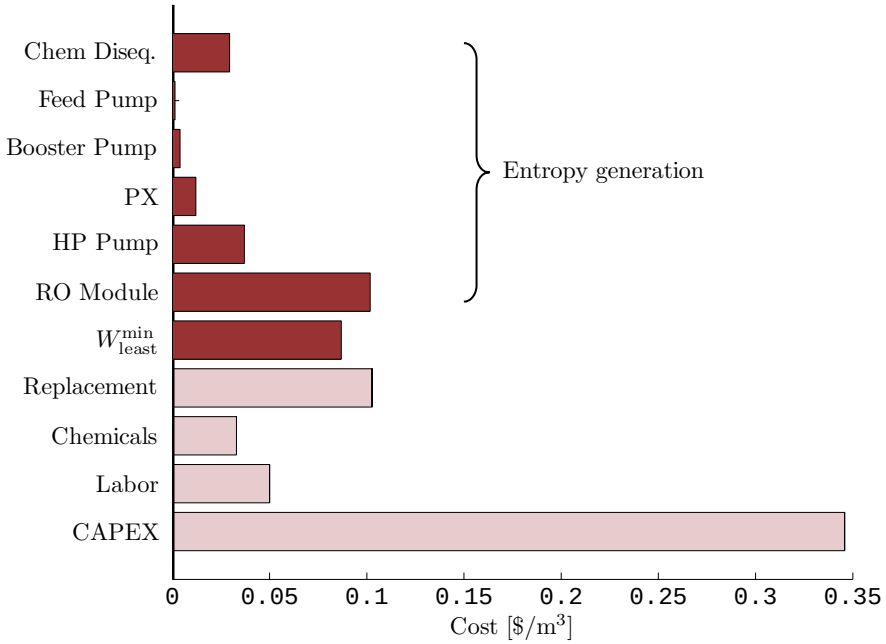

Figure 5-6: Breakdown of costs associated with the production of water using reverse osmosis with the costs of entropy generation isolated by component.

least energy of separation. Since CAPEX is the greatest source of cost by a wide margin, the system and hardware selection is the most crucial part of the design process. Similarly, replacement cost is a significant contributor to the total cost. This can be reduced by selecting parts with longer lifetimes. In terms of irreversibilities, the energy costs associated with losses in the RO module, the high pressure pump, and the chemical energy in the brine are most significant. Losses in the RO module can be reduced through staging and/or batch processing [154]. Losses in the HP pump can be reduced through use of higher performance pumps, or enhanced energy recovery [143, 155]. Unfortunately, the irreversibilities associated with the chemical disequilibrium of the concentrate cannot be reduced unless the recovery ratio of the process is reduced.

Through this analysis, one can clearly see all of the costs associated with the reverse osmosis process and can easily compare the cost of irreversibility in each of the major components. For the particular system seen here, it is clear that CAPEX, and not irreversibility, is the dominant contributor to the total cost of water production.

5.4.3 Membrane distillation

Direct contact membrane distillation (DCMD) is a membrane-based thermal distillation process [104] that can be driven using solar energy. Therefore, it provides a good example for considering the evaluation of $\eta_{II,\$}$ for systems with so-called "free" energy input. In DCMD, a hydrophobic microporous membrane is used to separate the feed and product streams. The temperature difference between a heated feed stream and the cooled fresh water stream induces a vapor pressure difference that drives evaporation through the pores. The vapor diffusion transport process is characterized by the membrane distillation coefficient, B, a parameter that is used to measure the pore's diffusion resistance. Experimental DCMD systems have successfully produced fresh water at small scale ($0.1\,\mathrm{m^3/d}$) [106–109, 156].

A transport process model for DCMD implemented by Saffarini et al. [105], Summers et al. [156] is used in this study. A schematic diagram of the system considered is shown in Fig. 5-7. Key module geometry and constants are shown. The model is based on validated models by Bui et al. [110] and Lee et al. [109] and was also used by Mistry et al. [21] in a previous study. The present calculations are performed for a flat-sheet membrane configuration (Bui et al. [110] relied on a hollow-fiber membrane configuration) using membrane geometry and operating conditions typical of pilot-sized plants found in literature [112, 113]. Feed seawater (27 °C, 35 g/kg total dissolved solids) enters the system at a mass flow rate of 1 kg/s. The feed is heated to 85 °C using a 90 °C source. In order to balance the mass flow rates through the membrane, the permeate side contains fresh water, also at a flow rate of 1 kg/s. Recovery ratio for this system and operating conditions is 4.4%. A liquid-liquid heat exchanger with a 3 K terminal temperature difference is used to regenerate heat. All pressure drops in the system other than that through the membrane are considered negligible. The pressure drop through the thin channel in the membrane module was found to be the dominant pressure drop in the system and was the basis for calculating the entropy generation due to pumping power. As with the RO model, standard seawater

Table 5.7: Contributions to the overall energy requirements of a direct contact membrane distillation system, evaluated in terms of entropy generated within each component.

Sources of energy consumption	Entropy generation [J/(kg K)]	Energy contribution [kJ$_t$/kg]
$Q_{\text{least}}^{\text{min}}$	-	15.7
Module	319	552
Heater	243	421
Regenerator	151	262
Temperature disequilibrium	212	366
Total:	925	1620

properties are used in this calculation [45, 46].

Entropy generation in each component was evaluated using control volume analysis [21] while entropy generation due to the temperature disequilibrium of the product and concentrate is evaluated using Eq. (5.30). Modeling results are tabulated in Table 5.7.

A cost model similar to that for the RO system is used for the DCMD system. Saffarini et al. [105] develop and describe a DCMD cost model in detail and the major cost figures are summarized herein. The total annualized cost of water can be expressed as the sum of the capital and operating expenses as per Eq. (5.32). The capital expenses can be split into several parts: membrane/module costs, solar energy costs (photovoltaic modules and solar thermal collectors), all other miscellaneous costs including piping, installation, and so on.

$$C_{\text{CAPEX}} = C_{\text{membranes}} + C_{\text{PV}} + C_{\text{heat}} + C_{\text{HEX}} + C_{\text{pump}} + C_{\text{fixed}} \tag{5.48}$$

Membranes, including module, cost \$350/m^2 of membrane area [157]. Solar heaters are used to provide the necessary heat input and are estimated at \$160/m^2 of collector area [84, 158]. Photovoltaic (PV) panels are used for supplying electrical energy to the pumps and other electroncis as needed. PV costs are approximately \$4/W [107]. Heat exchangers and pumps cost \$750 and \$700, respectively [158]. The remaining fixed capital costs include piping, batteries, monitoring equipment, and installation and may be estimated as \$5550 [105, 158]. A summary of all of the capital expenses is provided in Table 5.8.

Once all capital costs are evaluated, they are converted to annualized costs using an amortization factor:

$$A_{\text{CAPEX}} = \left(\frac{i(1+i)^n}{(1+i)^n - 1} \right) C_{\text{CAPEX}} \tag{5.49}$$

For this analysis, an 8% interest rate for a plant with a 20 year expected lifetime is assumed [105].

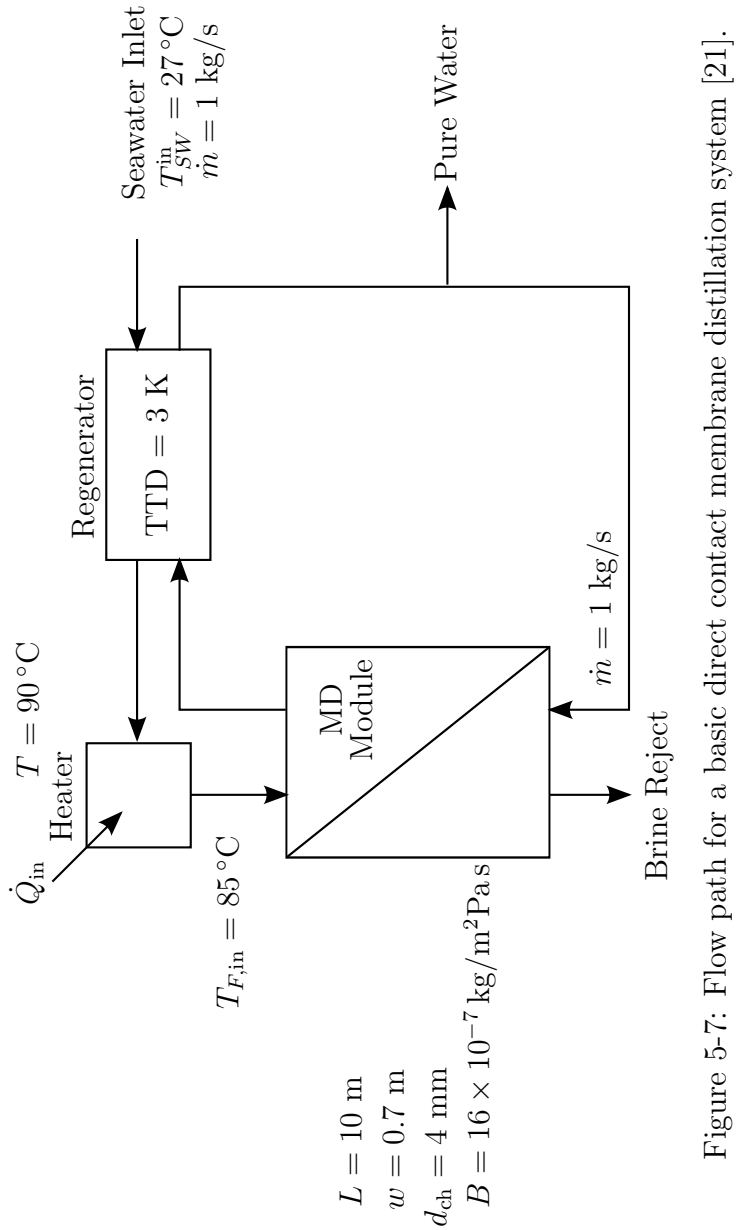

Figure 5-7: Flow path for a basic direct contact membrane distillation system [21].

Table 5.8: Summary of capital expenses for a representative direct contact membrane distillation.

Capital Costs	Specific Cost	Scaling	Total Cost [$]
Membranes [157]	$\$350/m^2$	$7\,m^2$	2450
Heat exchanger [158]	\$750 /unit	1 unit	750
Pump [158]	\$700 /unit	2 unit	1400
Fixed costs [105, 158]	\$5550	-	5550
Solar heaters [84, 158]	$\$160/m^2$	$200\,m^2$	32000
PV [107]	\$4/W	33 W	131
Total			42300
Amortized			4310
Per m^3			9.77

Table 5.9: Summary of operating expenses for a representative direct contact membrane distillation.

Operating Expenses	Scaling Factor	Times	Total Cost [$]
Maintenance	0.005	42300	212
Membrane replacement	0.12	2450	294
Total			506
Per m^3			1.15

Operating costs for the DCDM system are assumed to consist of only maintenance and membrane replacement. No chemical pretreatment is required for most MD systems [105] and it is assumed that the required labor for this small scale system is provided by the owners. Therefore, both can be negelected. Maintenance is approximated as 0.5% of CAPEX [157], and it is estimated that 12% of the membranes are replaced each year [158]. Operating costs are summarized in Table 5.9.

Combining the CAPEX and OPEX as shown in Tables 5.8 and 5.9, the total annualized cost of water is shown to be $\$10.90/m^3$. A breakdown of all of the CAPEX and OPEX for the DCMD system is shown in Fig. 5-8

In order to calculate $\eta_{II,\$}$, the cost of heating the feed in the DCMD system must be determined. Since the CAPEX of the solar heaters is known, this is easily calculated by considering the amortized cost of the solar heater divided by the amount of heating required by the system per kilogram of product produced. That is,

$$c_h = \frac{C_{heat}\left(\frac{i(1+i)^n}{(1+i)^n-1}\right)}{Q_{\text{solar}}} = \frac{\$32\,000 \cdot 0.1119}{85\,\text{kW} \cdot 3600 \cdot 8 \cdot 365 \cdot 0.96} = \$0.015/\text{kWh}_\text{t} \tag{5.50}$$

This value represents the amortized cost of the solar heaters per unit thermal energy provided. The minimum least heat of separation for 35 g/kg seawater at 27 °C is

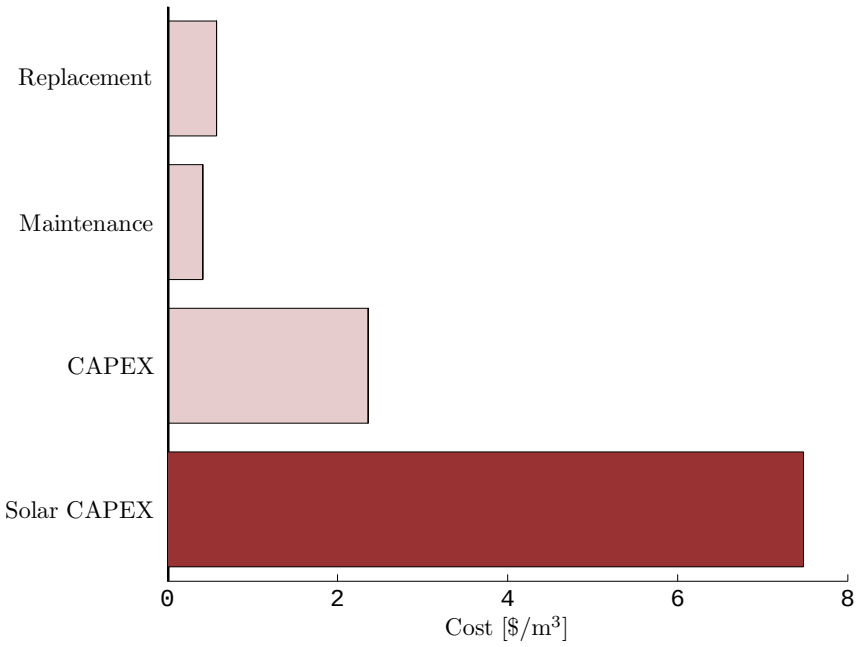

Figure 5-8: Breakdown of costs associated with the production of water using direct contact membrane distillation.

15.7 kJ/kg (4.37 kWh/m^3). Therefore, $\eta_{II,\$}$ is evaluated as:

$$\eta_{II,\$} = \frac{c_h \dot{Q}^{\min}_{\text{least}}}{\text{Total Cost}} = \frac{(\$0.015/\text{kWh})(4.37\,\text{kWh/m}^3)}{\$10.90\,/\text{m}^3} = 0.60\% \tag{5.51}$$

Despite the fact that the cost of solar-thermal energy is very low, this DCMD system has a very poor $\eta_{II,\$}$ value since the system requires substantially more thermal energy than $\dot{Q}^{\min}_{\text{least}}$. Additionally, electrical energy is required to overcome pressure losses within the system. This is characterized by a low η_{II} value as well:

$$\eta_{II} = \frac{\dot{Q}^{\min}_{\text{least}}}{\dot{Q}_{\text{sep}} + \dot{W}_{\text{sep}}/\eta_{\text{Carnot}}} = 1\% \tag{5.52}$$

Since the cost of energy in the solar powered DCMD system is captured by the capital expense associated with building and installing the solar heaters, it is useful to separate that cost into its component parts. Namely, it can be split into the cost of the minimum least heat of separation and all of the entropy generation in the various components in the system and due to chemical and thermal disequilibrium of the discharged streams. The solar heater costs are split and compared to all the other costs in Fig. 5-9. It is clear that the costs associated with entropy generation in each component is of the same order of magnitude as the entire capital expense of the rest of the DCMD system. In particular, losses in the module are the single greatest source of cost for this system.

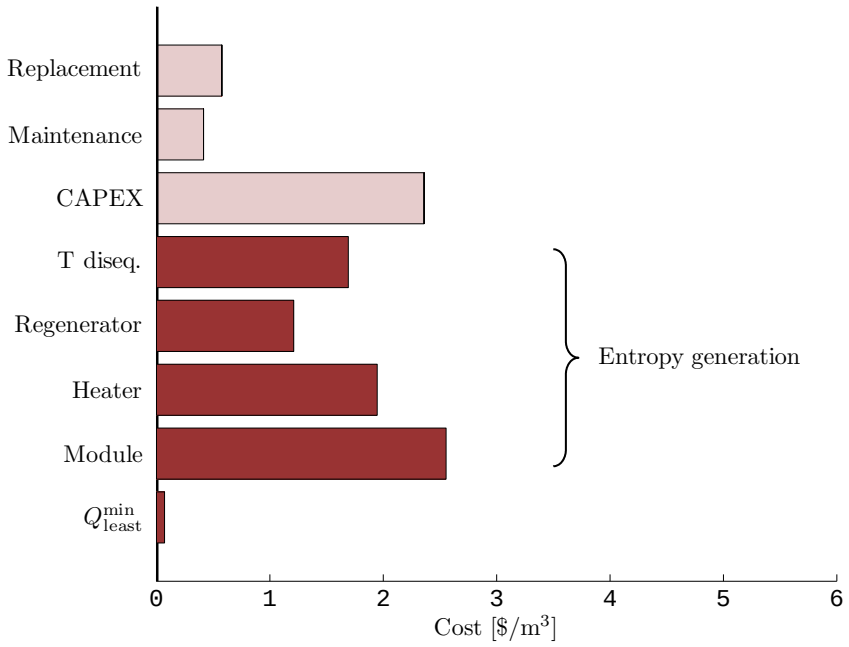

Figure 5-9: Breakdown of costs associated with the production of water using direct contact membrane distillation with the cost of entropy generation expanded.

From this example, it is evident that freely available energy, such as solar power, is not truly free. The capital expense required to harvest the solar thermal energy is significant and in some cases, can be the majority of a system cost.

5.5 Conclusions

In this paper, the following conclusions have been reached:

1. An economics-based Second Law efficiency is defined in analogy to the exergetics-based Second Law efficiency. It is defined as the ratio of the cost of the minimum least (primary) energy of separation to the actual cost of separation. The actual cost should include all factors, including all CAPEX and OPEX.

2. The energy costs can be broken up into the cost of the minimum least work of separation plus the sum of the costs for all of the irreversibilities (exergy destruction). When the energy costs are expressed in terms of the cost of exergy destroyed, all other costs (CAPEX, labor, replacement, *etc.*) can be likened to exergetic irreversibilities and viewed as "losses."

3. For energies typically considered to be free (*e.g.*, solar energy and wind energy), the additional capital expense for the infrastructure required to harvest the energy must be included in the cost function.

4. By comparing the cost of thermodynamic irreversibilities to all other system costs, it is easy to identify what aspects of a system design should be optimized. For cases where energy costs, as a result of irreversibilities, dominate the total cost of production, attention should be paid to improving the system thermodynamics. In cases where energy costs are not the primary contributor to overall cost, the non-thermodynamic parameters should be investigated for possibles sources of cost reduction.

Chapter 6

Conclusions

Increasing global demand for fresh water is driving the development and implementation of a wide variety of seawater desalination technologies. While there have been substantial improvements to desalination technologies over the past few decades, there is still a need to further reduce the energy requirements. Additionally, there is a need for a method for fairly comparing the energetic efficiency of a wide range of desalination technologies. Understanding all sources of energy consumption, including those required by thermodynamic laws and those caused through real-world inefficiencies, is essential for improving energy efficiency. Similarly, in order to fairly compare energetic efficiency between different separation technologies, a thermodynamics-based benchmark for the value of the product must be established. Therefore, the research efforts covered in this thesis focus on energy requirements for separation processes in order to address these issues. Major findings are summarized below while detailed conclusions are provided within each chapter.

6.1 Generalized least energy of separation

The least work of separation is a commonly used parameter for characterizing separation systems much like Carnot efficiency is used to characterize power production systems. Least work of separation, and more generally, the least exergy of separation is equal to the change in Gibbs free energy of all of the process streams involved in the separation. The generalized least energy of separation equation can be used to determine the least amount of work, heat, or chemical fuel that is required to drive a reversible separation

process. This parameter represents the absolute minimum amount of energy required, regardless of system technology, process, internal streams, or types of energy input. It is strictly a function of the composition of the feed and product as well as the recovery ratio and environmental temperature and pressure. If there is an assist stream, it is a function of the assist composition as well. It is not a function of the specific separation process used. For systems that utilize a material input stream in addition to the feed stream, it is possible for the least exergy to be negative and under such conditions, the separator becomes a work producing system. All separation processes are subject to the energy requirements prescribed by the minimum least work of separation, regardless of system design, process, or use of internal streams and several cases relevant to established and emerging desalination technologies are considered.

6.2 Nonidealities in electrolyte solutions

Through parametric studies of single and mixed electrolyte solutions, it is found that chemical composition is a critical variable in the evaluation of the least work of separation. Several single and mixed electrolyte solutions were considered under a range of concentrations and it was found that the least work of separation varied substantially between the various mixtures. As a result it is concluded that standard property packages (such as those for seawater) cannot be reliably used for arbitrary feed waters of different or unknown ionic composition. Use of these packages under such conditions can result in substantial error.

The reason specific ionic composition (as opposed to simply overall molality) plays such an important role in the magnitude of the least work of separation is because the least work can be divided into two parts: an ideal part which is a function of the mole fractions of each of the species (*i.e.*, purely colligative behavior), and a nonideal part which is a function of the activity coefficients of each of the species. Activity coefficients vary widely from species to species and are a function of a large number of parameters. As a result, the nonideal part of the least work of separation differs substantially from solution to solution. Proper evaluation of the activity coefficients is essential for accurately calculating the nonideal part of the least work. While there are many models for activity coefficients in the literature, the ideal solution approximation is commonly used due to its simplicity, despite the fact that very few feed waters of interest to the desalination industry are sufficiently dilute for the ideal solution approximation to be reliable. Under certain circumstances, the approximation may predict accurate results; but this is the result of happenstance cancellation, rather than near-ideal solution behavior. Similarly, Debye-Hückel models are only appropriate for very dilute species and the use of these models at higher salinities may actually introduce greater error than does the ideal solution approximation. This is especially true for mixed electrolyte solutions. Therefore, care must be taken anytime these elementary models are used beyond their range of applicability. A simple modification of the Pitzer ionic interaction model for single electrolytes is proposed that allows it to accurately predict activity coefficients for mixed electrolyte solutions.

6.3 Second Law efficiency for separation processes

Second Law efficiency is a useful parameter for quantifying the degree of reversibility of a thermodynamic system. Unfortunately, there are many conflicting definitions for the Second Law efficiency of separation processes in literature. Therefore, a robust definition, based on the minimum least exergy of separation is developed since the minimum least exergy represents the true useful output of a separation system. A methodology for evaluating Second Law efficiency for desalination plants that are part of larger cogeneration systems is shown. For such systems, it is important that Second Law efficiency is evaluated using primary energy inputs to the overall system, not just the inputs to the desalination plant. Based on currently available technology, producing electricity to power a reverse osmosis system will always result in a higher Second Law efficiency than using low grade heat as an input to power a thermal system.

The definition of Second Law efficiency can be expanded such that the energy input is written in terms of the minimum least energy of separation plus the sum of all of the irreversibilities present in the separation process. In order to evaluate the Second Law efficiency while considering specific sources of irreversibility, the entropy generation mechanisms present in a wide range of desalination processes are analyzed. Formulations for these mechanisms are applied to several desalination systems, including multiple effect distillation, multistage flash, membrane distillation, mechanical vapor compression, reverse osmosis, and humidification-dehumidification, in order to determine the primary sources of loss. When studying the energetic losses, it is essential to consider entropy generated not only due to irreversibilities in the separation process, but also due to temperature disequilibrium of the discharge and the irreversible mixing of the concentrate with the ambient seawater. Entropy generated through thermal and chemical disequilibrium can be substantial, depending on the specific separation process and operating parameters.

6.4 Economic Second Law efficiency

An economics-based Second Law efficiency is defined by analogy to the exergy-based Second Law efficiency as the ratio of the cost of the minimum least (primary) energy of separation to the actual cost of separation, where the actual cost includes all factors, including all CAPEX and OPEX. This parameter captures both energetic and economic factors. Much as the energetic requirements can be subdivided in terms of the system irreversibilities, the energy costs can be broken up into the cost of the minimum least work of separation plus the sum of the costs for all of the irreversibilities (exergy destruction). By expressing energy costs in terms of the cost of exergy destroyed, all other costs (CAPEX, labor, replacement, *etc.*) can be likened to energetic irreversibilities and viewed as "losses." This comparison allows one to identify what aspects of a system design should be optimized. For cases where energy costs, as a result of irreversibilities, dominate the total cost of production, attention should be paid to improving the system thermodynamics. In cases where energy costs

are not the primary contributor to overall cost, the non-thermodynamic parameters should be investigated for possibles sources of cost reduction.

6.5 Implications

Based on the analysis presented in this thesis, it is possible to properly characterize the energetic performance of various chemical separation technologies as well as to identify the relative importance of various sources of thermodynamic irreversibilities that occur within a system. Additionally, it is possible to characterize various feed waters and to understand how the composition of the feed will affect the behavior of the separation systems. Using these findings, one can make better informed decisions during the technology selection and design processes when building new desalination systems, and one may critically evaluate claimed performance improvements of novel systems.

Appendix A

Multiple effect distillation modeling

Chapter abstract

Increasing global demand for fresh water is driving research and development of advanced desalination technologies. As a result, a detailed model of multiple effect distillation (MED) is developed that is flexible, simple to implement, and suitable for use in optimization of water and power cogeneration systems. The MED system is modeled in a modular method in which each of the subcomponents is modeled individually and then instantiated as necessary in order to piece together the complete plant model. Modular development allows for studying various MED configurations (such as forward feed, parallel feed, *etc*) with minimal code duplication. Use of equation oriented solvers, such as Engineering Equation Solver (EES) and JACOBIAN, rather than sequential solvers, simplifies the coding complexity dramatically and also reduces the number of required approximations and assumptions. The developed model is compared to four prominent MED forward feed models from literature: El-Sayed and Silver (1980), El-Dessouky et al. (1998) (Detailed), El-Dessouky et al. (2002) (Basic), and Darwish et al. (2006). Through a parametric analysis, it is found that the present model compares very well with the simple model provided by El-Sayed and Silver while providing substantially more detail in regards to the various temperature profiles within the MED system. Further, the model is easier to implement than the detailed El-Dessouky model while relying on fewer assumptions. The increased detail of the model allows for proper sensitivities to key variables related to input, operating, and design conditions necessary for use in a cogeneration or hybrid system optimization process.

This chapter is published in [99, 100].

Chapter Nomenclature

Greek		**Units**
A_c	heat transfer area in condenser	m^2
A_e	heat transfer area in effect	m^2
A_{fh}	heat transfer area in feed heater	m^2
B	brine flow rate from effect	kg/s
B_e	brine flow rate in effect after flashing, before boiling	kg/s
c	specific heat at constant pressure	kJ/kg-K
D	total distillate from effect	kg/s
D_b	distillate from boiling in effect	kg/s
D_c	distillate that will condense in effect	kg/s
D_f	distillate from flashing in effect	kg/s
D_{fb}	distillate from flash box	kg/s
D_{bd}	distillate blow down from flash box	kg/s
F	feed flow rate into effect	kg/s
h	specific enthalpy	kJ/kg
h_{fg}	specific heat of vaporization	kJ/kg
i	i^{th} effect	-

$\dot{m}_B$	final brine flow rate	kg/s
$\dot{m}_{cw}$	cooling water flow rate	kg/s
$\dot{m}_{\text{cond}}$	mass flow rate of seawater in condenser	kg/s
$\dot{m}_D$	distillate flow rate	kg/s
$\dot{m}_F$	feed water flow rate	kg/s
$\dot{m}_S$	input steam flow rate	kg/s
$\dot{m}_{\text{sw}}$	input seawater flow rate	kg/s
n	number of effects	-
p	pressure	kPa
T	temperature	K
U_c	overall heat transfer coefficient in condenser	kW/m^2-K
U_e	overall heat transfer coefficient in effect	kW/m^2-K
U_{fh}	overall heat transfer coefficient in feed heater	kW/m^2-K
X	salinity	kg/kg
y	quality	kg/kg
ΔT_e	temperature difference between effects	K

Greek		**Units**
ϵ	sum of BPE and temperature change due to pressure loss	K

Subscripts	**Units**
e	effect
fh	feed heater
c	condenser
S	steam
sat	saturated, at saturation temperature
sat, f	saturated liquid
sat, g	saturated vapor
sw	seawater

Superscripts	
in	in flow to CV
out	out flow from CV
prev	previous

Acronyms		**Units**
BPE	boiling point elevation	K
CV	control volume	
FF	forward feed	
GOR	gained output ratio	-
LMTD	log mean temperature difference	K
MED	multiple effect distillation	
MSF	multistage flash	
NEA	non-equilibrium allowance	K
PR	performance ratio	-

RR	recovery ratio	-
SA	specific area	m^2-s/kg
TBT	top brine temperature	K
TTD	terminal temperature difference	K
TVC	thermal vapor compressor	

A.1 Introduction

As global demand for fresh water increases, the need for development and implementation of a wide variety of desalination technologies continues to grow. Despite the vast improvements to reverse osmosis in recent years, there is still a need for thermal methods of desalination, especially when dealing with harsh feed waters of high temperature, salinity, or contamination. While multistage flash (MSF) is the dominant type of large-scale thermal desalination currently in use, multiple-effect distillation (MED) is thermodynamically superior and is currently receiving considerable attention as a strong competitor to MSF, especially in the Middle East-Arabian Gulf area. The MED process is characterized by lower energy consumption (≈ 2 kWh/m^3) compared to the MSF process (≈ 4 kWh/m^3) since recirculating large quantities of brine is not required. Additionally, MED provides higher overall heat transfer coefficients by utilizing primarily latent-heat transfer and avoiding the lower specific heat transfer surface areas associated with sensible heat transfer found in MSF [88]. The ability to operate at low temperature and use low grade heat from power station turbines as the primary heat source for MED yield very low specific energy costs for seawater desalination and allows the use of lower grade materials for heat transfer tubes (*e.g.*, aluminum alloys) and the evaporator body (*e.g.*, carbon steel epoxy coated shells) [159]. As a result, MED systems are established in many locations within the Kingdom of Saudi Arabia with capacities ranging from 1,500–800,000 m^3/day [160].

However, the high energy consumption associated with desalination processes such as MED, especially as compared to the least work of separation [21], suggests that further research on these and other technologies is needed in order to lower the cost and increase the availability of potable water. One way to accomplish this is to combine thermal desalination systems, such as MED, with electricity production plants in a combined water-power cogeneration scheme. Cogeneration has the advantage of being able to produce both water and power at lower costs and increased flexibility than if they were produced independently. In this chapter, a new MED model is developed that is well-suited for studying and optimizing in a cogeneration plant model. The new model is also compared to four MED models from literature and the advantages and limitations of each are discussed.

While there are numerous MED models in the literature, the models by El-Dessouky and Ettouney [13], Darwish et al. [103], El-Dessouky et al. [161] are among the most cited. Additionally, the model by El-Sayed and Silver [16] is very simple, yet based on clear thermodynamic principles. While these models have utility, they do not provide adequate sensitivity to key parameters necessary for a complete cogeneration system optimization. Therefore, a new model that relies on fewer assumptions and is solved

using a simultaneous equation solver, rather than an iterative sequential solver, is developed.

A.2 Overview of multiple effect distillation and review of existing models

Accurate system modeling is essential for developing understanding and for exploring possibilities for improvement. As such, numerous MED models have been developed. El-Sayed and Silver [16] developed one of the earliest forward feed MED models and were able to calculate performance ratio and heat transfer areas through several simplifying thermodynamic assumptions. El-Dessouky et al. [161], El-Dessouky and Ettouney [162], El-Dessouky et al. [163] analyzed different MED configurations including the parallel flow, the parallel/cross flow, and systems combined with a thermal vapor compressor (TVC) or mechanical vapor compressor (MVC). The heat transfer equations used in the model assume that the area calculated is the sum of the area of brine heating and the area for evaporation. They found that the thermal performance ratio of the TVC and specific power consumption of the MVC decrease at higher heating steam temperatures. In addition, increasing heating steam temperature reduces the specific heat transfer area. The conversion ratio is found to depend on the brine flow configuration and to be independent of the vapor compression mode. El-Dessouky and Ettouney [13] also developed a simplified model. Darwish et al. [103], Darwish and Abdulrahim [164] also developed a simple MED model and analyzed various configurations and discussed the trade off between performance ratio and required heat transfer area.

El-Allawy [165] examined how the gained output ratio (GOR) of an MED (with and without TVC) system varied with top brine temperature (TBT) and number of effects. Results revealed that increase of number of effects from 3 to 6 result in the increase of the GOR by nearly two-fold. Aly and El-Figi [166] developed a steady state mathematical model to study the performance of forward feed MED process and found that the performance ratio is significantly dependent on the number of rather than the top brine temperature. Al-Sahali and Ettouney [167] developed simple simulation model for MED-TVC based on a sequential solution method, rather than iterative procedure while assuming constant temperature drop, specific heat, and heat transfer coefficients. Ameri et al. [168] studied the effect of design parameters on MED system specifications and found that optimum performance depends on an optimum number of effects which itself depends on sea water salinity, feed water temperature, and effect temperature differences. Kamali and Mohebinia [169] developed a simulation program to improve the performance of an existing MED unit of 7 effects and nominal production of 1,800 m^3/day. They found that the unit production increased by 15% with the same top brine temperature of 70 °C by increasing the area of condenser tubes by 32%.

Kamali et al. [170] optimized the performance of actual MED producing 1500 ton/day whereas Darwish and Alsairafi [160] compared MSF with MED using a simple

simulation model assuming equal vapor generated by boiling in all effects, equal boiling temperature difference between effects, and equal specific heat. They reported that MED is favored on MSF by less shell volume of order half of that of MSF, lower pumping energy, less treatment of feed, and lower temperature losses. For a constant flux of 12.6 kW/m^2, Minnich et al. [171] reported that the optimum GOR and TBT were found to be 14 and 110 °C, respectively. They added that limiting TBT of MED to 60 °C prevents the system from utilizing higher heat transfer coefficients and constant temperature difference that drives the heat transfer.

Second Law analysis for MED was conducted by [172–174] where the major subsystems for exergy destruction were the TVC and effects which accounted more than 70% of the total amount. Hamed [175], Hamed et al. [176] investigated the thermal performance of the MED desalination system at different variables including number of effects, TBT, and inlet seawater. He concluded that the performance ratio increased with increasing number of effects while TBT and inlet seawater a slight affect on plant performance. Greogorzewski and Genthner [177] reported an analytical study restricted to different configurations of MED systems without TVC.

Four models from literature are considered in more detail.

A.2.1 El-Sayed and Silver

El-Sayed and Silver [16] developed a simple model for a forward feed (FF) MED system with flash evaporation (Fig. A-1). All fluid properties are assumed constant [mean latent heat ($\bar{h}_{fg}$), specific heat (c), and boiling point elevation (BPE)]. The fluids are assumed to be an ideal solution and the pressure drop due to friction is modeled based on a mean saturation temperature drop augmented by the effect of BPE. Based on these assumptions, El-Sayed and Silver explicitly solve for the performance ratio of the system:

$$\mathrm{PR} = \frac{h_{fg,S}}{\dfrac{\bar{h}_{fg}}{n} + \dfrac{\dot{m}_F}{\dot{m}_D} c\,(\mathrm{TTD}_{fh} + \epsilon) + \dfrac{n-1}{2n} c \Delta T_e} \tag{A.1}$$

where $h_{fg,S}$ is the enthalpy of vaporization of steam, n is the number of effects, $\dot{m}_F$ and $\dot{m}_D$ are the mass flow rates of feed and distillate, TTD_{fh} is the terminal temperature difference in the feed heaters, ϵ is the sum of BPE and temperature change due to pressure loss, and ΔT_e is a temperature difference between two effects. Additional equations are provided for calculating the required heat transfer surface area as a function of a known or assumed overall heat transfer coefficient.

Despite its simplicity, Eq. (A.1) is derived using strong thermodynamic arguments and is useful for quickly approximating the performance ratio and required transfer areas for an MED-FF system under known operating conditions. However, it cannot be used to find detailed information regarding various specific streams or to understand system sensitivities to various parameters.

A.2.2 Darwish et al.

Darwish et al. [103] developed a simple model for MED-FF with flash evaporation

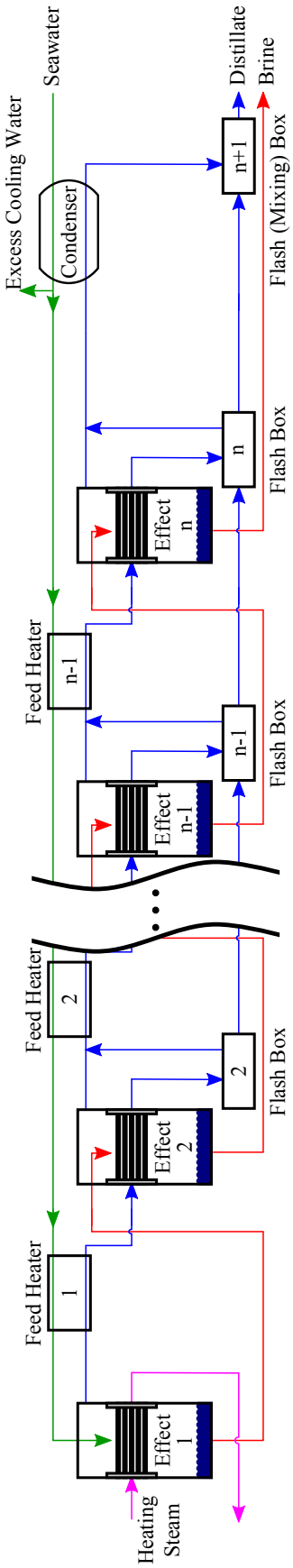

Figure A-1: In a forward feed MED system, the feed water is preheated by condensing distillate vapor from the effects and flash boxes prior to being injected into the first effect to reduce the amount of required heating steam. Water vapor is removed from the feed stream in each effect until the brine is eventually discharged from the final effect.

while assuming that: equal vapor is generated by boiling in each effect other than the first ($D_b = \beta \dot{m}_D$), equal boiling temperature difference between effects (ΔT_e), equal temperature increase of the feed in feed heaters (ΔT_{fh}) and $\Delta T_e = \Delta T_{fh}$, equal specific heat for the brine and feed, equal latent heat (h_{fg}) and BPE. Using these assumptions, Darwish et al. simplified the MED-FF system and approximated the performance ratio for the system:

$$\mathrm{PR} = \frac{\dot{m}_D}{\dot{m}_S} = \frac{n}{1 + n\dfrac{\dot{m}_F c(\mathrm{TTD}_{fh})}{\dot{m}_D \bar{h}_{fg}}} \tag{A.2}$$

where $\dot{m}_F$, $\dot{m}_D$, and $\dot{m}_S$ are the mass flow rates of feed, distillate, and steam respectively, c is the specific heat, h_{fg} is the latent heat, and TTD_{fh} is the temperature difference between the first effect and the feed at the exit of the last feed heater.

A.2.3 El-Dessouky and Ettouney Basic Model

El-Dessouky and Ettouney [13] presented a simplified MED mathematical model where the data generated are related only to brine and distillate flow rates, brine concentration, temperature and heat transfer area. Heat and mass balances for flash boxes and pre-heaters are excluded and it is assumed that the feed enters the first effect at the first effect's saturation temperature (*i.e.*, steam is used only to evaporate distillate in the first effect, not for heating the feed). This model relies on the following assumptions: specific heat is constant at an average temperature, thermodynamic losses are constant across all effects, no vapor flashes in the effects, produced vapor is salt-free, equal thermal loads in all effects, driving temperature difference in the effects is equal to the difference in condensation and evaporation temperatures, and negligible energy losses to the environment. Convergence is achieved while equating the heat transfer area in all effects. Although this greatly simplified model does not address fully practical plants, it provides basic understanding to the process involved in MED desalination.

A.2.4 El-Dessouky and Ettouney Detailed Model

El-Dessouky et al. [161] also presented a detailed MED model that takes into account the pre-heaters and flashing boxes in an MED-FF system (Fig. A-1). The model assumes constant heat transfer areas for both the evaporators and feed pre-heaters in all effects. In addition, the model considers the impact of the vapor leak in the venting system, the variation in thermodynamic losses from one effect to another, the dependence of the physical properties of water on salinity and temperature, and the influence of non-condensable gases on the heat transfer coefficients in the evaporators and the feed pre-heaters. Several correlations are used in this model, particularly to determine the heat transfer coefficients and pressure losses. Two correlations are developed to relate the heat transfer coefficients in the pre-heater and the evaporator to the boiling temperature. Design correlations are also developed to describe variations in the plant thermal performance, the specific heat transfer area, and the specific flow

rate of cooling water in terms of the top brine temperature and the number of effects. Calculations showed that the heat transfer coefficient in the evaporators are greater than those in the pre-heaters and that the effect of TBT on the specific heat transfer area is more pronounced at high number of effects.

A.3 An improved MED model

A thermal model of an MED system is presented that provides a more accurate description of the MED process through relying on fewer assumptions and simplifications. Unlike most of the models in the literature, the present model is solved using a simultaneous equation solver.

A.3.1 Approximations

Several standard engineering approximations are made in this analysis:

- Steady state operation.
- Distillate is pure water (*i.e.*, salinity of product water is 0 g/kg).
- Exchanger area in the effects is just large enough to condense vapor to saturated liquid (i.e., $x = 0$) at the previous effect's pressure.
- Seawater is an incompressible liquid and the properties are only a function of temperature and salinity.
- Heat losses to the environment are negligible.
- Non-equilibrium allowance (NEA) is negligible [13].
- Brine (liquid) and distillate (vapor) streams leave each effect at that effect's temperature. Distillate vapor is slightly superheated.
- The overall heat transfer coefficient is averaged over the length of an exchanger.
- The overall heat transfer coefficient in each effect, feed heater, and condenser is a function of temperature only [13].

A.3.2 Software and solution methodology

While most of the existing models in literature are developed to be solved using an iterative procedure in a sequential numerical package such as MATLAB [83], the present model was developed using a simultaneous equation solver. A fundamental advantage of using an equation solver is that the programmer does not need to develop algorithms for reaching solution convergence. Instead, the governing equations are inputted much as one would write them on paper. The solver then identifies and groups the equations that must be solved and solves for the system iteratively. During the development process, the model was implemented using two different software packages: Engineering Equation Solver (EES) [178] and JACOBIAN [179].

A.3.3 Physical properties

Accurate physical properties for seawater and water vapor are used. Seawater, approximated as an incompressible fluid, properties are evaluated as a function of temperature and salinity [45]. All liquid water states are modeled using this seawater property package: pure water is modeled as seawater with 0 salinity. This property package is used, rather than the electrolyte solution modeling efforts from Chapter 3, due to its computational simplicity and the fact that only standard seawater is considered. Vapor phase water properties are calculated using the fundamental equations of state provided by IAPWS. EES uses the IAPWS 1995 Formulation [101] while the IAPWS 1997 Industrial Formulation [124] was implemented for use in JACOBIAN. Differences between the two formulations are negligible.

A.3.4 Component models

Since MED systems are composed of multiple identical stages, there are several components that are utilized numerous times. In order to simplify the model, each component is modeled individually. The overall system model is then created by instantiating each component the necessary number of times and adding additional equations to connect the various components in the appropriate manner. Component models for the effects, feed heaters, flash boxes, and condenser are presented below. A schematic diagram showing a typical configuration of a forward feed MED system is illustrated in Fig. A-1. A detailed schematic diagram showing the fluid stream connections between components is shown in Fig. A-2.

A.3.4.1 Effects

The effect is the primary component in an MED system. Feed water (F) is sprayed into the effect over a series of tubes. Distillate vapor (D_c) from the previous effect condenses in these tubes. Typically, the effect is maintained at a pressure slightly below the saturation pressure of the feed water which causes a small fraction of the feed to flash evaporate (D_f). As the D_c, it releases the heat of vaporization which is transfered to the feed resulting in the creation of more vapor (D_b). The vapor produced through both flashing and boiling (D) as well as the brine (B) are then extracted from the effect (Fig. A-2). Note: each of the variables should be indexed with an i to indicate that these are array variables; however, for clarity, the index is neglected. A control volume showing the relevant variables that characterize the effect's inlet and outlet streams is presented in Fig. A-3.

Water balance: The feed stream is split into a distillate (vapor) stream and a brine stream. Prior to the evaporation from boiling (internal to the effect), the feed stream can be divided into a brine stream within the effect (B_e) and the distillate formed from flashing. The total distillate produced is the sum of that formed from flashing

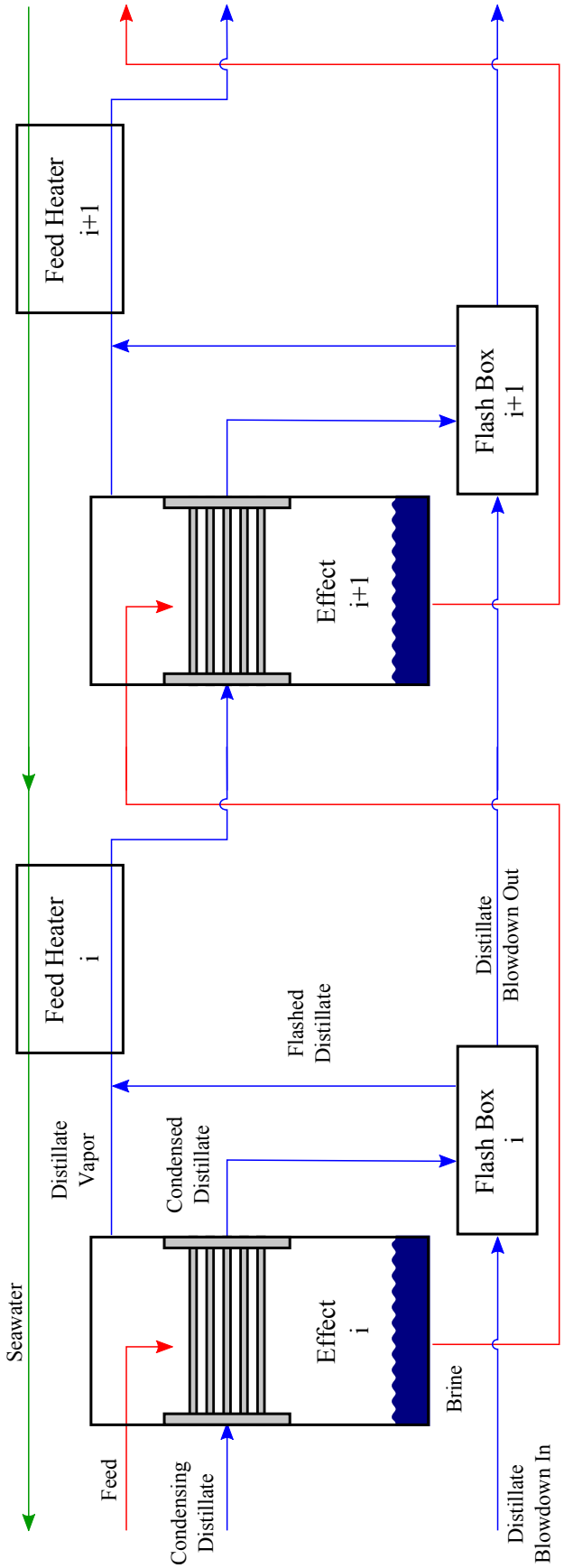

Figure A-2: Detailed view of the stream connections between each of the components in an MED system.

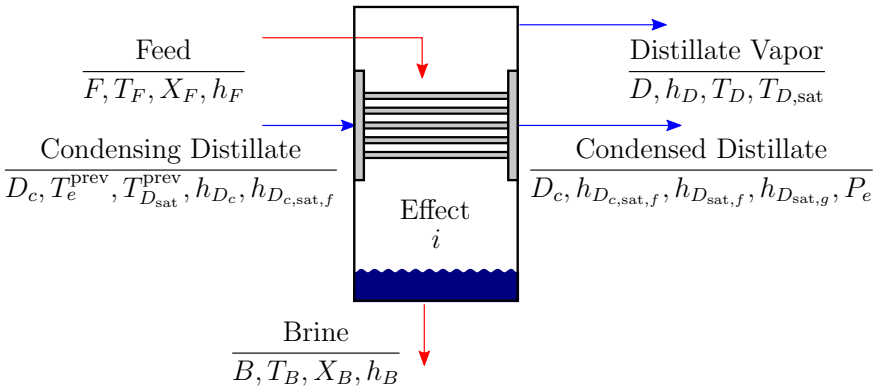

Figure A-3: Variables associated with the inlet and outlet streams of the i^{th} effect.

and boiling.

$$F = B + D \tag{A.3}$$
$$F = B_e + D_f \tag{A.4}$$
$$D = D_b + D_f \tag{A.5}$$

Salt balance: Salinity of the brine stream within the effect (X_{B_e}) and the brine stream leaving the effect (X_B) is found found through a salt balance in which it is assumed that both the distillate formed through flashing and boiling is pure (*i.e.*, $X_{D_f} = X_{D_b} = 0$ g/kg).

$$FX_F = BX_B \tag{A.6}$$
$$FX_F = B_eX_{B_e} \tag{A.7}$$

Energy balance: The change in enthalpy associated with the condensation of the distillate from the previous effect is used to separate the feed stream into new brine and distillate streams.

$$D_c\Delta h_{D_c} = Dh_D + Bh_B - Fh_F \tag{A.8}$$

The value of Δh_{D_c} is discussed below as it is different for the first and the second through n^{th} effects.

Distillate saturation temperature: Salinity causes the boiling point to be elevated. Distillate formed in the effect is superheated by an amount equal to the BPE. The distillate will condense at the saturation temperature in the following feed heater and effect.

$$T_{D_{\text{sat}}} = T_D - \text{BPE}_D \tag{A.9}$$

Heat transfer area: The condensate tube surface area must be large enough to ensure that the distillate vapor from the previous effect condenses completely while heating and evaporating the feed. Since there is phase change on both sides of the tubes, the rate of heat transfer is best modeled by Newton's Law of Cooling, where the

heat transfered is equal to the change in enthalpy associated with the condensation of distillate [*cf.*, Eq. (A.8)].

$$D_c \Delta h_{D_c} = A_e U_e (T^{\text{prev}}_{D_{\text{sat}}} - T_e) \tag{A.10}$$

The temperature at which the distillate from the previous effect condenses is equal to the saturation temperature of the previous effect, $T_c = T^{\text{prev}}_{D_{\text{sat}}}$. The overall heat transfer coefficient in Eq. (A.10) is calculated using a correlation from El-Dessouky and Ettouney [13]:

$$\begin{aligned} U_e = 10^{-3} \times \big[& 1939.1 + 1.40562 (T^{\text{prev}}_{D_{\text{sat}}} - 273.15) \\ & - 0.0207525 (T^{\text{prev}}_{D_{\text{sat}}} - 273.15)^2 \\ & + 0.0023186 (T^{\text{prev}}_{D_{\text{sat}}} - 273.15)^3 \big] \end{aligned} \tag{A.11}$$

where U_e is in kW/m^2-K and $T^{\text{prev}}_{D_{\text{sat}}}$ is in K. The correlations provided by El-Dessouky et al. serve as a good approximation for the overall heat transfer coefficient values. If a model is being developed for an actual physical plant, more accurate U values can be obtained by analyzing the heat transfer processes occurring in the particular geometry.

Fluid properties: The temperature of the brine (T_B) and distillate vapor (T_D) is equal to the effect temperature (T_e). The boiling point elevation (BPE$_D$), effect pressure (P_e), enthalpy of brine after flashing (h_{B_e}), enthalpy of brine (h_B), enthalpy of distillate [from boiling (h_{D_b}), from flashing (h_{D_f}), and total (h_D)], and enthalpies of saturated water ($h_{D_{\text{sat},f}}$) and vapor ($h_{D_{\text{sat},g}}$) are all evaluated as a function of temperature, pressure, and salinity as discussed in Appendix A.3.3.

Some useful temperature differences include the terminal temperature difference in the effect (TTD$_e$), which is the temperature of condensation minus the effect temperature, and the temperature difference between effects (ΔT_e).

$$\text{TTD}_e = T_c - T_e \tag{A.12}$$

$$\Delta T_e = T^{\text{prev}}_e - T_e \tag{A.13}$$

First effect

While the hardware for all effects is identical, there are two slight differences between the first effect and the remaining ones. First, feed enters the first effect below the saturation temperature (subcooled) where as in all subsequent effects, feed enters slightly above the saturation temperature (superheated). Second, steam is used to heat the feed in the first effect while the vapor produced in the previous effect is used to heat the feed in all the subsequent effects. Flashing does not occur in the first effect because the feed stream is subcooled when it enters the first effect.

$$D_f = 0 \tag{A.14}$$

Steam input to the first effect can be accounted for by modifying the effect's energy balance [Eq. (A.8)] to be based on the steam flow rate ($\dot{m}_S$) and latent heat of

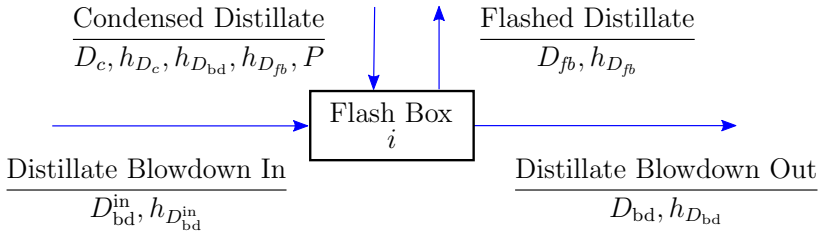

Figure A-4: Variables associated with the inlet and outlet streams of the i^{th} flash box.

vaporization (λ_S):

$$D_c \Delta h_{D_c} \rightarrow \dot{m}_S h_{fg,S} \tag{A.15}$$

Second through n^{th} effect

In all subsequent effects, a portion of the feed stream flashes. An additional energy balance equation [complement to Eq. (A.4)] is needed to fully define the effect.

$$F h_F = B_e h_{B_e} + D_f h_{D_f} \tag{A.16}$$

The enthalpy change of the distillate during condensation may not be equal to the latent heat of vaporization since the distillate from the previous effect may enter the effect as superheated vapor, saturated vapor, or two-phase. It is assumed that complete condensation occurs. Therefore, the change in enthalpy in Eq. (A.8) is defined as:

$$\Delta h_{D_c} = h_{D_c} - h_{D_{c,\text{sat},f}} \tag{A.17}$$

where h_{D_c} is the enthalpy of the distillate at the entrance to the effect's condensing tube.

A.3.4.2 Flash box

The condensed distillate from each effect is collected with all of the condensed distillate from the previous effects. As the distillate is collected in each stage, the distillate pressure is decreased in the flash boxes to correspond with the pressure of the current effect. Part of the distillate blowdown from the previous effect ($D_{\text{bd}}^{\text{in}}$) and the distillate used for condensing in the current effect (D_c) is flashed during the depressurization. The newly produced vapor, D_{fb}, is sent to the feed heater and the remaining liquid distillate, D_{bd} is sent to the next flash box (Fig. A-2). Both D_{fb} and D_{bd} are at p_e. Note: each of the variables should be indexed with an i to indicate that these are array variables; however, for clarity, the index is neglected. A control volume showing the relevant variables that characterize the flash box's inlet and outlet streams is presented in Fig. A-4.

The mixing and flashing process are governed by mass conservation and the First

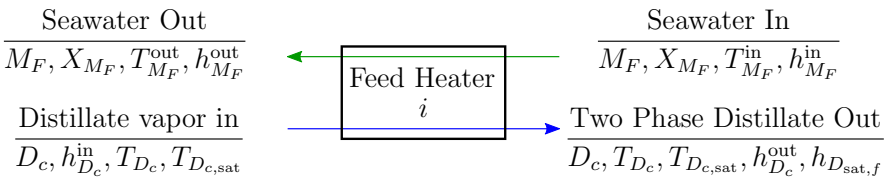

Figure A-5: Variables associated with the inlet and outlet streams of the feed heater.

Law of Thermodynamics:

$$D_{\text{bd}} + D_{fb} = D^{\text{in}}_{\text{bd}} + D_c \tag{A.18}$$

$$D_{\text{bd}} h_{D_{\text{bd}}} + D_{fb} h_{D_{fb}} = D^{\text{in}}_{\text{bd}} h_{D^{\text{in}}_{\text{bd}}} + D_c h_{D_c} \tag{A.19}$$

Distillate blowdown temperature can be evaluated as a function of the blowdown enthalpy and pressure.

A.3.4.3 Mixing box

No flashing occurs in the flash box when all inlet and outlet streams are at the same pressure and the flash box acts as a mixing vessel. The flash box equations can be reduced with the following two equations.

$$D_{fb} = 0 \tag{A.20}$$

$$h_{D_{fb}} = \text{undefined} \tag{A.21}$$

The mixing box is only used to recombine the condensed distillate from the condenser with that from the final flash box (Fig. A-1).

A.3.4.4 Feed heater

Feed heaters are used to recover energy and reduce the amount of steam required for heating the feed in the first effect. In each feed heater, some of the distillate vapor from the effect and the flash box condenses and the heat released is used to heat the seawater (Fig. A-2). Note: each of the variables should be indexed with an i to indicate that these are array variables; however, for clarity, the index is neglected. A control volume showing the relevant variables that characterize the feed heater's inlet and outlet streams is presented in Fig. A-5.

An energy balance and the log mean temperature difference (LMTD) method are

used to calculate the required heat transfer area.

$$D_c\left(h_{D_c}^{\text{in}} - h_{D_c}^{\text{out}}\right) = \dot{m}_F\left(h_{\dot{m}_F}^{\text{out}} - h_{\dot{m}_F}^{\text{in}}\right) \tag{A.22}$$

$$D_c\left(h_{D_c}^{\text{in}} - h_{D_c}^{\text{out}}\right) = A_{fh}U_{fh}\frac{T_{\dot{m}_F}^{\text{in}} - T_{\dot{m}_F}^{\text{out}}}{\ln\dfrac{T_{D_{c,\text{sat}}} - T_{\dot{m}_F}^{\text{out}}}{T_{D_{c,\text{sat}}} - T_{\dot{m}_F}^{\text{in}}}} \tag{A.23}$$

The overall heat transfer coefficient in Eq. (A.23) is calculated using a correlation from El-Dessouky and Ettouney [13]:

$$\begin{aligned} U_{fh} = 10^{-3}\times\big[&1617.5 + 0.1537(T_{D_{c,\text{sat}}} - 273.15) \\ &+0.1825(T_{D_{c,\text{sat}}} - 273.15)^2 \\ &-0.00008026(T_{D_{c,\text{sat}}} - 273.15)^3\big] \end{aligned} \tag{A.24}$$

where U_{fh} is in kW/m^2-K and $T_{D_{c,\text{sat}}}$ is in K. While the log mean temperature difference method is used here, the ε-NTU method yields equivalent results since the feed heaters are essentially single stream heat exchangers.

The minimum temperature difference in the feed heater occurs at the outlet of the seawater.

$$T_{D_c} - T_{\dot{m}_F}^{\text{out}} = \text{TTD}_{fh} \tag{A.25}$$

Enthalpy of the seawater leaving the feed heater is calculated based on the outlet temperature and salinity.

A.3.4.5 Condenser

Distillate from the final effect and flash box is condensed in a condenser, which is essentially a large feed heater. Typically, excess seawater is required in order to meet the required cooling load. Excess seawater is used for cooling purposes alone and is returned to the source after being exhausted from the condenser while the required feed is sent to the first feed heater. Energy balance and heat transfer area calculations for the condenser are similar to those for the feed heaters:

$$D_c\Delta h_{D_c} = \dot{m}_{\text{cond}}\left(h_{\text{sw}}^{\text{out}} - h_{\text{sw}}^{\text{in}}\right) \tag{A.26}$$

$$\dot{m}_{\text{cond}}\left(h_{\text{sw}}^{\text{out}} - h_{\text{sw}}^{\text{in}}\right) = A_cU_c\frac{T_{\text{sw}}^{\text{out}} - T_{\text{sw}}^{\text{in}}}{\ln\left(\dfrac{T_D - T_{\text{sw}}^{\text{in}}}{T_D - T_{\text{sw}}^{\text{out}}}\right)} \tag{A.27}$$

The overall heat transfer coefficient in Eq. (A.27) is calculated using a correlation from El-Dessouky and Ettouney [13]:

$$\begin{aligned} U_c = 10^{-3}\times[&1617.5 + 0.1537(T_D - 273.15) \\ &+0.1825(T_D - 273.15)^2 \\ &-0.00008026(T_D - 273.15)^3\big] \end{aligned} \tag{A.28}$$

where U_c is in kW/m^2-K and T_D is in K. While the log mean temperature difference method is used here, the ε-NTU method yields equivalent results since the condenser is essentially a single stream heat exchanger.

Inlet and outlet seawater enthalpies are calculated as a function of the respective temperatures and the feed salinity.

A.3.5 MED-FF with flash box regeneration system model

Numerous MED system configurations can be created by piecing together the component models presented in Appendix A.3.4. Equations for connecting the relevant components to form the typical MED-FF configuration shown in Fig. A-1 are outlined below. Note that all of the equations are simply matching (or combining) variables from one component to another.

Typical MED systems utilize flash boxes and feed heaters in order to collect the distillate and preheat the seawater prior to injection into the first effect (Fig. A-1) [13, 16, 103, 161]. An advantage of this configuration is that high energy recovery can be achieved while using relatively simple components.

A.3.5.1 Match streams between components

The distillate (D_c) output (in 2 phase state) from the i^{th} feed heater effect is used as the condensing distillate input in the i^{th}+1 effect. The distillate flow rate, temperature, saturation temperature, present enthalpy, and saturated liquid enthalpy must be passed to the i^{th}+1 effect.

For $i \in \{1, \ldots, n-1\}$:

$$\frac{\text{Feed heater, } i}{D_c, T_{D_c}, T_{D_{c,\text{sat}}}, h_{D_c}^{\text{out}}, h_{D_{\text{sat},f}}} \quad \longrightarrow \quad \frac{\text{Effect, } i+1}{D_c, T_e^{\text{prev}}, T_{D_{\text{sat}}}^{\text{prev}}, h_{D_c}, h_{D_{c,\text{sat},f}}}$$

Brine from the i^{th} effect is used as feed for the i^{th}+1 effect. Brine flow rate, temperature, salinity, and enthalpy is passed to the i^{th}+1 effect.

For $i \in \{1, \ldots, n-1\}$:

$$\frac{\text{Effect, } i}{B, T_B, X_B, h_B} \quad \longrightarrow \quad \frac{\text{Effect, } i+1}{F, T_F, X_F, h_F}$$

Distillate boxes

As the distillate condenses in each effect, it is mixed with all of the distillate from the previous effects. The pressure of the distillate is decreased to correspond with the pressure in the effects. As a result, a portion of the distillate flashes and the vapor is then sent to the feed heaters. There is no flash box for the first effect (Fig. A-1). For programming convenience, the flash box index begins with 2, rather than 1.

Distillate from the first effect does not mix with distillate from a (non-existent) previous effect. In order to reuse the flash box code, the blowdown input to the first

flash box ($D_{\text{bd}}^{\text{in}}, h_{D_{\text{bd}}}^{\text{in}}$) is set to zero.

$$\frac{\text{Effect, 2}}{D_c, h_{D_{c,\text{sat},f}}, h_{D_{\text{sat},f}}, h_{D_{\text{sat},g}}, P_e} \longrightarrow \frac{\text{Flash box, 2}}{D_c, h_{D_c}, h_{D_{\text{bd}}}, h_{D_{fb}}, P}$$

For flash boxes 3–n, the inputs are blowdown distillate from the previous distillate box and the newly condensed distillate from the current effect. The output is saturated vapor (to feed heater) and liquid (blowdown to next box).

For $i \in \{2, \ldots, n-1\}$:

$$\frac{\text{flash box, } i}{D_{\text{bd}}, h_{D_{\text{bd}}}} \longrightarrow \frac{\text{flash box, } i+1}{D_{\text{bd}}^{\text{in}}, h_{D_{\text{bd}}}^{\text{in}}}$$

For $i \in \{3, \ldots, n\}$:

$$\frac{\text{Effect, } i}{D_c, h_{D_{c,\text{sat},f}}, h_{D_{\text{sat},f}}, h_{D_{\text{sat},g}}, P_e} \longrightarrow \frac{\text{flash box, } i}{D_c, h_{D_c}, h_{D_{\text{bd}}}, h_{D_{fb}}, P}$$

The final flash box is a mixing vessel to combine the distillate blowdown from the n^{th} distillate box and the distillate that was condensed in the condenser.

$$\frac{\text{flash box, } n}{D_{\text{bd}}, h_{D_{\text{bd}}}} \longrightarrow \frac{\text{flash box, } n+1}{D_{\text{bd}}^{\text{in}}, h_{D_{\text{bd}}^{\text{in}}}}$$

$$\frac{\text{Effect, } n}{h_{D_{\text{sat},f}}} \longrightarrow \frac{\text{flash box, } n+1}{h_{D_c}}$$

Unlike the previous flash boxes, the newly condensed distillate comes from the condenser.

$$\frac{\text{Condenser}}{D_c} \longrightarrow \frac{\text{flash box, } n+1}{D_c}$$

Feed heaters

Seawater is heated in the i^{th} feed heater by distillate vapor from both the i^{th} effect and the i^{th} flash box. The enthalpy of the mixture of distillate vapors is the mass weighted average.

For $i \in \{1, \ldots, n-1\}$:

$$D_c\big|_{\text{Feed heater},i} = D\big|_{\text{Effect},i} + D_{fb}\big|_{\text{Flash box},i}$$
$$(D_c h_{D_c}^{\text{in}})\big|_{\text{Feed heater},i} = (Dh_D)\big|_{\text{Effect},i} + (D_{fb} h_{D,fb})\big|_{\text{Flash box},i}$$

$$\frac{\text{Feed heater, } i}{T_{D_c}, T_{D_{c,\text{sat}}}} \longrightarrow \frac{\text{Effect, } i}{T_D, T_{D_{\text{sat}}}}$$

For feed heaters 1 through $n-2$, the output of one feed heater is the input to the next. Note that the seawater is flowing from higher numbered feed heater to lower numbered feed heater.

For $i \in \{1, \ldots, n-2\}$:

$$\frac{\text{Feed heater, } i+1}{\dot{m}_F, X_{\dot{m}_F}, T^{\text{out}}_{\dot{m}_F}, h^{\text{out}}_{\dot{m}_F}} \quad \longrightarrow \quad \frac{\text{Feed heater, } i}{\dot{m}_F, X_{\dot{m}_F}, T^{\text{in}}_{\dot{m}_F}, h^{\text{in}}_{\dot{m}_F}}$$

The initial feed heater, $n-1$, is fed seawater from the output of the condenser:

$$\frac{\text{Condenser}}{X_{\text{sw}}, T^{\text{out}}_{\text{sw}}, h^{\text{out}}_{\text{sw}}} \quad \longrightarrow \quad \frac{\text{Feed heater, } n-1}{X_{\dot{m}_F}, T^{\text{in}}_{\dot{m}_F}, h^{\text{in}}_{\dot{m}_F}}$$

A condenser is used to condense the distillate vapor from the n^{th} effect and n^{th} flash box. The enthalpy of the mixture of distillate vapors is the mass weighted average.

$$D_c\big|_{\text{Condenser}} = D\big|_{\text{Effect},n} + D_{fb}\big|_{\text{Flash box},n}$$
$$(D_c h^{\text{in}}_{D_c})\big|_{\text{Condenser}} = (Dh_D)\big|_{\text{Effect},n} + (D_{fb} h_{D,fb})\big|_{\text{Flash box},n}$$

The change in enthalpy associated with condensation of the vapor in the condenser is

$$\Delta h_{D_c}|_{\text{Condenser}} = h^{\text{in}}_{D_c}|_{\text{Condenser}} - h_{D_{\text{sat},f}}|_{\text{Effect},n}$$

$$\frac{\text{Effect, } n}{T_D} \quad \longrightarrow \quad \frac{\text{Condenser}}{T_D}$$

The seawater feed into the first effect is the warm seawater output from the last feed heater.

$$\frac{\text{Feed heater, 1}}{T^{\text{out}}_{\dot{m}_F}, X_{\dot{m}_F}, h^{\text{out}}_{\dot{m}_F}} \quad \longrightarrow \quad \frac{\text{Effect, 1}}{T_F, X_F, h_F}$$

The flow rate of feed into the first effect is $F(1) = \dot{m}_F$. Since a portion of the seawater through the condenser is returned to the source, $\dot{m}_{\text{cond}} \geq \dot{m}_F$.

There are two options for constraining the size of the effects. In order to reduce the cost of the system, MED plants are typically built with effects of equal area. If, however, it is desired to have a constant temperature drop across each effect, the temperature difference between effects can be specified instead.

$$A_e(i) = A_e(1) \qquad i \in \{2, \ldots, n\} \tag{A.29}$$

or

$$\Delta T_e(i) = \Delta T_e(1) \qquad i \in \{2, \ldots, n\} \tag{A.30}$$

Similarly, there are two options for constraining the size of the feed heaters. To reduce the cost of the system, all feed heaters should have the same area. However, it

may be desired to have the same TTD in each feed heater.

$$A_{fh}(i) = A_{fh}(1) \qquad i \in \{2, \ldots, n-1\} \tag{A.31}$$

or

$$\mathrm{TTD}_{fh}(i) = \mathrm{TTD}_{fh}(1) \qquad i \in \{2, \ldots, n-1\} \tag{A.32}$$

The amount of water produced is equal to the sum of the distillate produced in each effect. The mass flow rate of steam required is equal to the amount of vapor that must condense in the first effect. The amount of seawater feed required is equal to the feed flow rate in the first effect. The amount of excess cooling is the difference between $\dot{m}_{\mathrm{cond}}$ and $\dot{m}_F$. The final brine flow rate is the difference between the feed and distillate flow rate.

$$\dot{m}_D = \sum_{i=1}^{n} D(i) \tag{A.33}$$

$$\dot{m}_S = D_c(1) \tag{A.34}$$

$$\dot{m}_F = F(1) \tag{A.35}$$

$$\dot{m}_B = B(n) \tag{A.36}$$

A.3.5.2 Required inputs

Feed, steam, operating, and design conditions are required in order to fully specify the flash box based MED-FF model. Number of effects must be specified. Seawater is fully characterized by temperature and salinity ($T_{\mathrm{sw}}^{\mathrm{in}}$, $X_{\mathrm{sw}}^{\mathrm{in}}$). Steam is fully characterized by its saturation temperature since it is assumed that it enters the first effect as saturated vapor and leaves the first effect as saturated liquid. The following variables are set based on the steam temperature:

$$T_e^{\mathrm{prev}} = T_S \tag{A.37}$$

$$T_{D_{\mathrm{sat}}}^{\mathrm{prev}} = T_S \tag{A.38}$$

$$h_{D_c} = h_g(T_S) \tag{A.39}$$

$$h_{D_{c,\mathrm{sat},f}} = h_f(T_S) \tag{A.40}$$

For on-design analysis, the following system characteristics must be specified:

- temperature of the last effect, or a terminal temperature difference between the last effect and the condenser
- mass flow rate of the distillate, feed, or brine
- maximum allowable salinity (or recovery ratio)
- temperature rise in the condenser
- minimum TTD in the feed heaters

Off-design analysis can be performed by inputting area of the effects, feed heaters, and condenser rather than maximum salinity, temperature rise, and TTDs.

A.3.5.3 Performance parameters

Once the above equations have been solved, the productivity ratio (PR), recovery ratio (RR), and specific area (SA) are all calculated.

$$\mathrm{PR} = \frac{\dot{m}_D}{\dot{m}_S} \tag{A.41}$$

$$\mathrm{RR} = \frac{\dot{m}_D}{\dot{m}_F} \tag{A.42}$$

$$\mathrm{SA} = \frac{\sum A_e + \sum A_{fh} + A_c}{\dot{m}_D} \tag{A.43}$$

A.3.5.4 Pressure drops and pumping work

In general, the pressure drop in a condenser is the sum of the pressure drops due to various inlet and exit losses, static head, momentum change, and two-phase friction loss. When considering condensers operating at vacuum conditions, the momentum change results in a pressure regain and the magnitude of the regain may be of the same order of magnitude (might even exceed) as the pressure losses [180]. Since all of the condensers in MED operate at subatmospheric levels, it is a suitable approximation to ignore pressure effects on the condensing side.

A.4 Parametric comparison of MED models

A parametric study is conducted in which the present model is compared to four models from the literature [13, 16, 103, 161]. Performance ratio and specific area are evaluated for each of the models while varying the number of effects, steam temperature, or recovery ratio. In order to ensure that the values of the calculated heat transfer area from one model to the next are comparable, heat transfer coefficients in all models were evaluated using Eqs. (A.11), (A.24), and (A.28), rather than assuming the constant values that were given in the respective papers.

All of the calculations in this section are evaluated under the so-called "on-design" analysis method in which temperature differences, flow rates, and other desired operating conditions are inputs and heat transfer areas and other sizing parameters are evaluated as outputs. This is different from "off-design" analysis in which plant sizing information is used to calculate temperature differences, flow rates, and other operating conditions. A consequence of on-design analysis is that each of the data points presented below represent a different physical plant.

For the following parametric studies, all of the following inputs are held constant except for the parameter that is being investigated: number of effects, 8; steam temperature, 70 °C; last effect temperature, 40 °C; seawater temperature, 25 °C; minimum feed heater TTD, 5 K; temperature rise in condenser, 10 K; BPE/thermodynamic losses, 1 K; feed salinity, 42 g/kg; recovery ratio, 0.4; mass flow rate of distillate produced, 1 kg/s.

The Darwish model uses top brine temperature, rather than steam temperature. For convenience, the same value of T_S is used for TBT. The effect of this is that the Darwish models are being evaluated as if a slightly higher steam temperature is being used (approximately 2-5 K, depending on the number of effects). Using the value of T_S in place of TBT introduces some minor quantitative differences, but the general trends observed are unchanged. Additionally, the Darwish model does not include calculation of the condenser surface area whereas the other models do.

A.4.1 Effect of number of effects

The number of effects is generally considered to be one of the strongest determinants of an MED system's performance. Each additional effect allows for an additional evaporation process in which the heat of vaporization is reused an additional time. In the absence of thermodynamic losses, as the vapor condenses, it would release enough heat to exactly evaporate the same amount of new vapor. Therefore, in the ideal case, each additional effect would increase the performance ratio by one. As a result of losses as well as an increasing heat of vaporization with decreasing saturation temperature, it is observed that each additional effect increases the performance ratio by less than one. Further, the added benefit of each additional effect decreases [16]. The present model, El-Sayed's model, and El-Dessouky's detailed model all show this trend of PR increasing with n, with the effect decreasing as n increases (Fig. A-6). The basic El-Dessouky model and the Darwish model, however, show PR being a nearly linear function of n. Both of these models over-estimate PR at higher number of effects and fail to capture the effect of increasing latent heat with decreasing saturation temperature. Additionally, El-Dessouky basic assumes that the feed enters the first effect at the effect's saturation temperature which implicitly implies that there is perfect energy regeneration (*i.e.*, $\mathrm{TTD}_{fh} = 0$).

Size of an MED plant is also strongly dependent on the number of effects. During the on-design process, adding additional effects results in a smaller driving temperature difference in each effect and lower distillate production in each effect. Therefore, specific heat transfer area increases with number of effects (Fig. A-7). The models by El-Dessouky (Basic), El-Sayed, and Darwish all show SA growing faster with increasing n than does the new model or the detailed El-Dessouky model. All three models assume constant thermodynamic losses (primarily, BPE) in each effect and over-estimate the value of BPE. Equation (A.10) shows that A_e is inversely proportional to the difference between the previous effect's saturation temperature and the current effect's actual temperature, $T_{D,\mathrm{sat}}^{\mathrm{prev}} - T_e$. Using Eq. (A.9), this temperature difference can be written as $T_e^{\mathrm{prev}} - T_e - \mathrm{BPE}_D$. Since these models approximate the temperature difference between effects to be constant and equal to $(T_{\max} - T_{\min})/n$, as n increases while temperature range and BPE remain constant, the driving temperature difference in each effect decreases resulting in a dramatic increase in required heat transfer area in each effect. By properly evaluating BPE for each effect as a function of temperature and salinity, A_e can be more accurately calculated. Additionally, modifying the El-Sayed and Darwish models by calculating BPE at each effect using the correlation provided by Sharqawy et al. [45] results in the two models' prediction of SA to agree

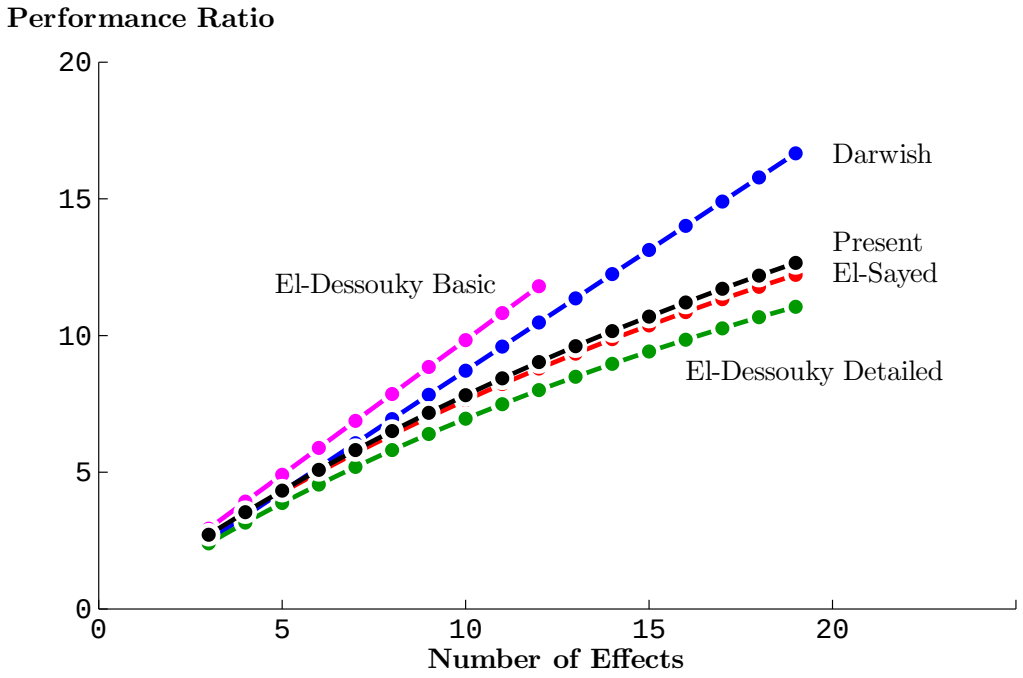

Figure A-6: The added benefit of number of effects on the performance ratio should decrease as n increases as seen by the PR behavior of the El-Sayed, El-Dessouky Detailed, and present models. El-Dessouky Basic and Darwish significantly overestimate PR for large number of effects.

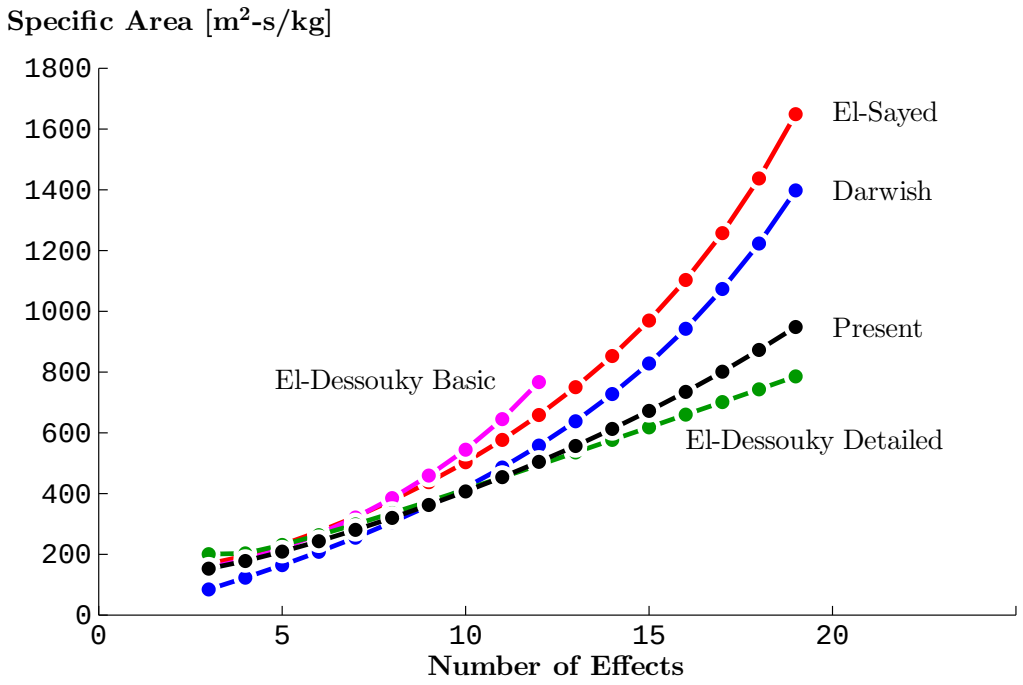

Figure A-7: The required surface area increases nearly exponentially with number of effects. As the number of effects increase, the driving temperature difference decreases, thus requiring additional heat transfer area in order to produce the same amount of distillate.

with the present model within 10% (Fig. A-8). The basic model by El-Dessouky predicts the highest specific area since it assumes no flashing in any of the effects. As a result, all distillate is produced through boiling heat transfer. Correcting the model for BPE and approximating that 10% of the distillate is produced by flashing (typical value based on the other models), the El-Dessouky model calculation of SA also agrees with the present model within 10%.

It is observed that the assumptions of constant overall heat transfer coefficient, latent heat of evaporation, and distillate production in each effect have a minimal effect on the evaluation of overall surface area. The Darwish model predicts a lower specific area for small number of effects than the other models since it does not include the area of the condenser. The size of the condenser is largest for a smaller number of effects since the distillate produced in the last effect increases with decreasing n.

A.4.2 Effect of steam temperature

Increasing top temperature tends to increase the performance of thermodynamic systems. However, in the case of on-design analysis, this is not always the case. The main benefit of increasing the top temperature of an MED system is that it creates a larger temperature range for the desalination process which allows for additional effects. However, when keeping the number of effects fixed and allowing the size of

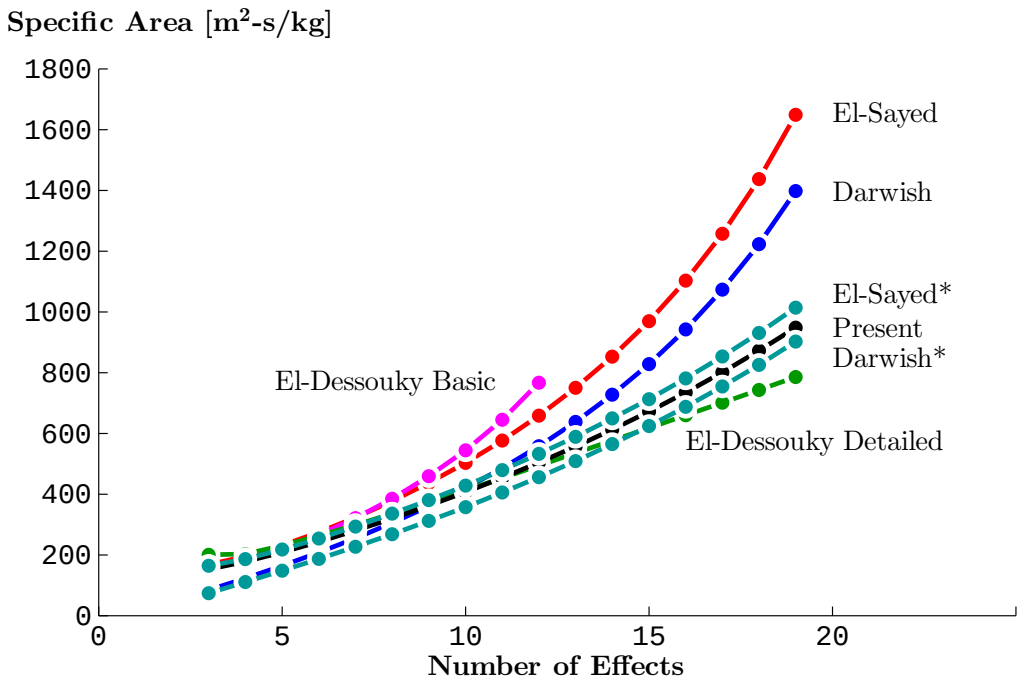

Figure A-8: Modifying the Darwish and El-Sayed models by evaluating boiling point elevation as a function of temperature and salinity in each effect causes both models to predict specific area requirements that are in agreement with El-Dessouky's detailed model and the present model. El-Dessouky's basic model can be modified similarly but is not shown for clarity.

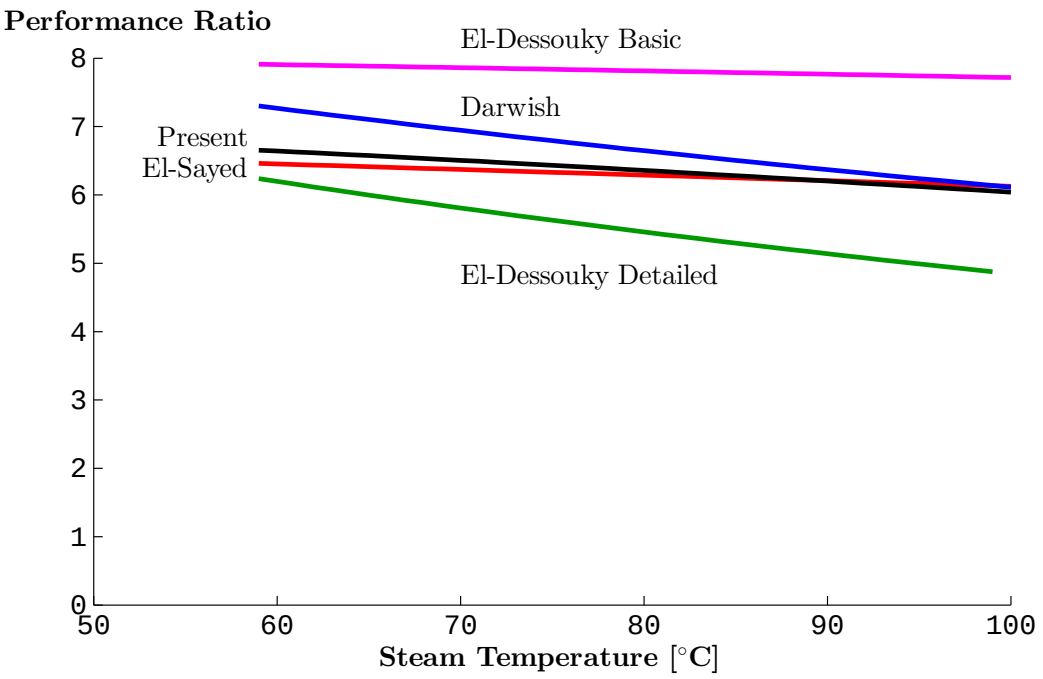

Figure A-9: The performance ratio decreases with increasing steam temperature because the heat of vaporization decreases with increasing temperature. The decrease in heat of vaporization results in additional steam needed to evaporate a given unit of water.

the effects to vary, increasing the top temperature does not have the expected effect on the performance ratio. Since the heat of vaporization decreases with increasing steam temperature, all other things held constant, more steam is needed to evaporate a given quantity of water when the steam is at higher temperature. As a result, PR decreases slightly with increasing steam temperature. All five models illustrate this behavior (Fig. A-9).

While higher temperature steam provides less energy during condensation due to a lessened heat of vaporization, the increased temperature range of the MED system results in a larger temperature difference between each effect. Since the heat transfer within each effect is governed by Newton's Law of Cooling, where the relevant temperature difference is that between the condensing distillate and the evaporating feed, heat transfer increases with increasing ΔT. Since the number of effects and the total distillate flow rate is held constant for this analysis, the amount of heat transfer in each effect remains approximately constant. Therefore, as the driving temperature difference increases, the required heat transfer area decreases. Again, all five models illustrate this trend (Fig. A-10).

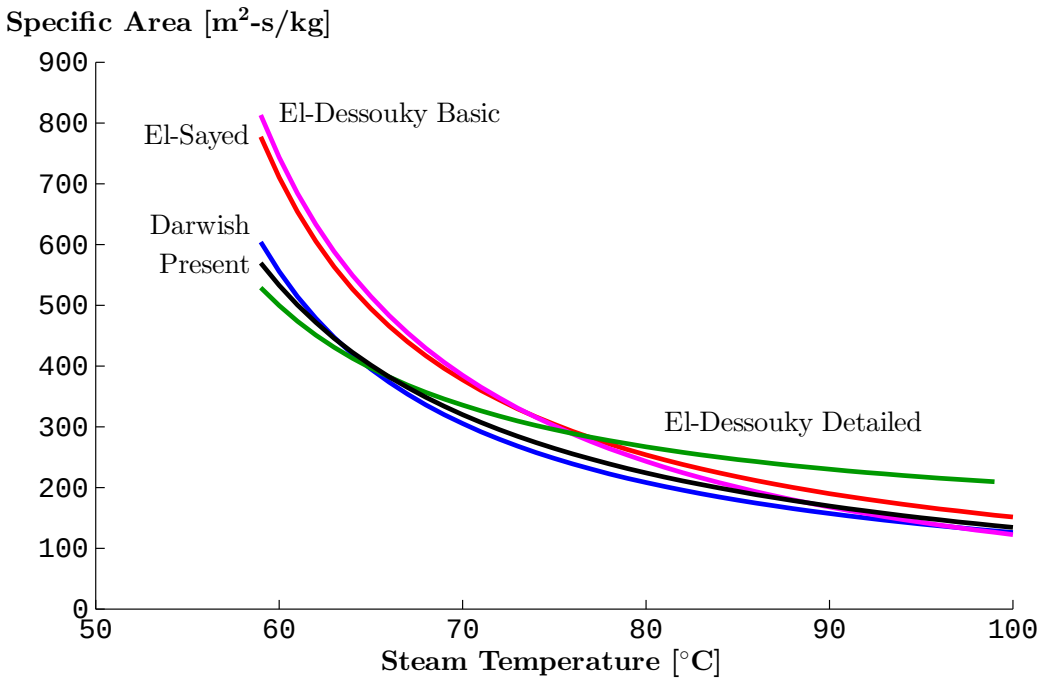

Figure A-10: The driving temperature difference between each effect is increased as the steam temperature increases, thus resulting in smaller heat transfer area requirements.

A.4.3 Effect of recovery ratio

Increasing the recovery ratio, defined as the amount of distillate produced per input feed, has the effect of reducing the amount of feed seawater since the mass flow rate of distillate produced is held constant. Reducing the amount of feed in the system lowers the thermal mass that must be heated by steam. Therefore, for fixed distillate production, an increased recovery ratio decreases the amount of required steam and the performance ratio increases. The models by both Darwish and El-Sayed as well as the present model all follow this trend (Fig. A-11). The El-Dessouky basic model, however, calculates the required steam flow rate based purely on the distillate flow rate, and therefore, is not a function of recovery.

Another consequence of decreasing the feed flow rate is that less feed enters each effect resulting in less distillate vapor produced per effect. Since the amount of total distillate produced needs to remain roughly constant, more distillate must be produced by boiling to make up for the decrease in production from flashing. In order to allow for additional vapor production from boiling, more heat transfer area is required to allow for increased heat transfer. As before, the models by Darwish and El-Sayed, as well as the present model follow this trend while the El-Dessouky basic model is not a function of recovery ratio (Fig. A-12).

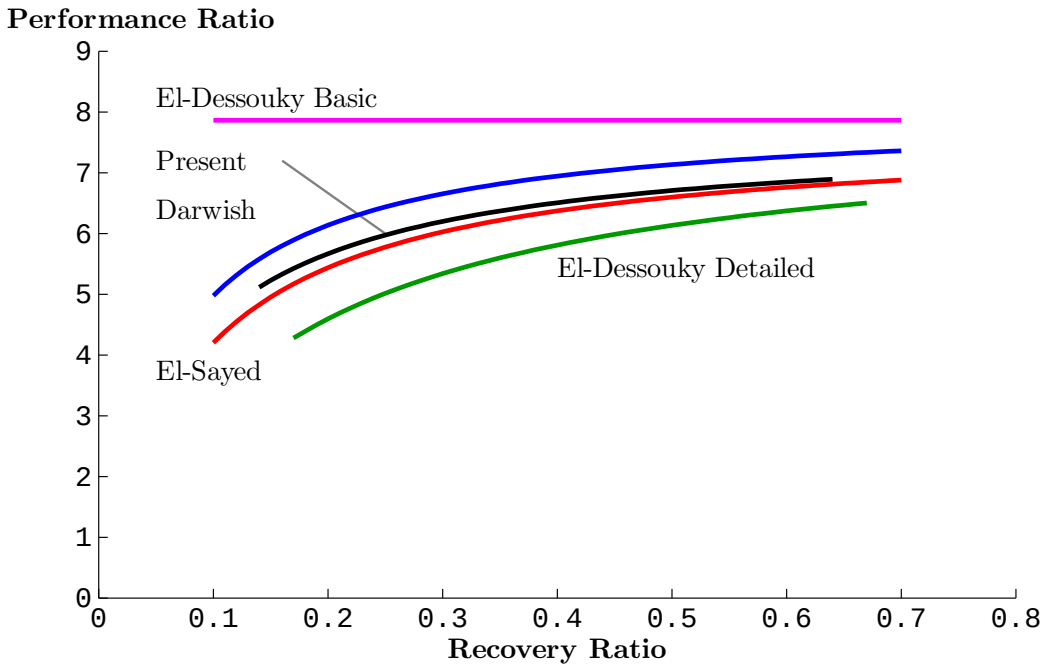

Figure A-11: As the recovery ratio increases for fixed distillate production, the feed flow rate reduces resulting in less heating steam required, and therefore, a higher performance ratio.

A.5 Main findings and key results

Based on a parametric study of the five models, the following conclusions are made:

1. A detailed model is needed in order to properly capture sensitivities of parameters relevant in cogeneration system analysis. The MED model should respond to changes in design conditions (number of effects, terminal temperature differences, *etc*), input conditions (feed temperature, salinity, flow rate, steam temperature, *etc*), and operating conditions (recovery ratio, last effect temperature, *etc*).

2. Use of a simultaneous equation solver allows for the development of more complex numerical models without having to worry about developing solution algorithms. Therefore, fewer major approximations are needed in order to develop an easily solvable model.

3. While the model presented in this chapter provides more detail than the existing models from literature while relying on fewer assumptions, several of the existing models provide consistent results. If only basic information about the system is desired for simple studies (*e.g.*, performance ratio and specific heat transfer area), the simpler models may be sufficient. If, however, detailed information about the area of each component and various temperature profiles are required, the present model is preferable.

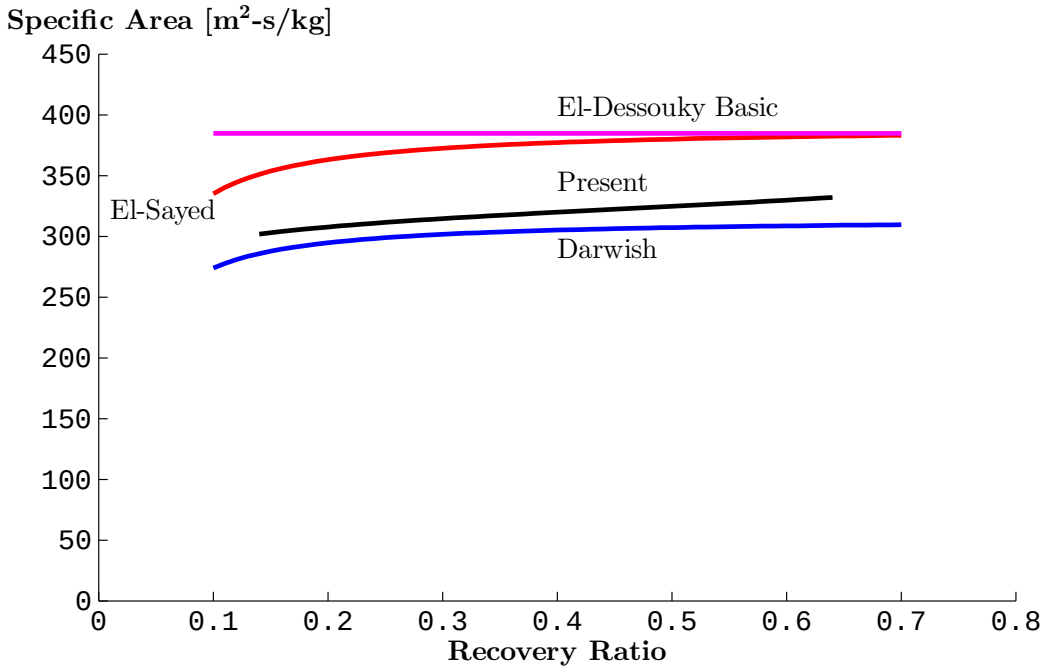

Figure A-12: As the recovery ratio increases for fixed distillate production, the feed flow rate reduces resulting in less vapor produced by flashing in each effect. In order to maintain a constant distillate production rate, more distillate must evaporate through boiling, and therefore, more surface area is required.

4. Approximations such as constant thermodynamic losses, constant properties, and constant distillate production in each effect break down with increasing number of effects. Of these approximations, thermodynamic losses (specifically boiling point elevation) have the greatest effect on the evaluation of specific area.

5. A modular model allows for easily studying various MED configurations such as forward feed and parallel feed without developing new code for each of the subcomponents.

Acknowledgments

The author would like to thank Numerica Technology for providing access to the JACOBIAN software for this research.

Appendix B

Useful conversions

Recovery ratios

$$\frac{r}{\bar{r}} = \frac{1 + \sum_s m_{\mathrm{s},p} M_{\mathrm{s}}}{1 + \sum_s m_{\mathrm{s},f} M_{\mathrm{s}}} \tag{B.1}$$

Mole fraction and molality

To convert from molality of salts to mole fraction of solutes requires a few steps. First, calculate the mole fraction of the cation and anion for each salt.

$$x_{s,+} = \frac{\nu_{s,+} m_s M_{\mathrm{H_2O}}}{1 + M_{\mathrm{H_2O}} \sum_s \nu_s m_s} \tag{B.2}$$

$$x_{s,-} = \frac{\nu_{s,-} m_s M_{\mathrm{H_2O}}}{1 + M_{\mathrm{H_2O}} \sum_s \nu_s m_s} \tag{B.3}$$

Note the sums are over all salt species. The mean mole fraction for the salt is defined analogously to the mean ionic molality [*cf.*, Eq. (3.15)]:

$$x_s = \left(x_{s,+}^{\nu_+} x_{s,-}^{\nu_-}\right)^{1/\nu} \tag{B.4}$$

The mole fraction of the solvent is equal to one minus the sum of all other mole fractions

$$x_{\mathrm{H_2O}} = 1 - \sum_s x_{s,+} - \sum_s x_{s,-} \tag{B.5}$$

Mass fraction and molality

$$w_s = \frac{m_s M_s}{1 + \sum_s m_s M_s} \tag{B.6}$$

Again, the sum is over all salt species.

$$m_s = \frac{w_s}{w_{\mathrm{H_2O}} M_s} \tag{B.7}$$

Salinity is defined as the mass fraction of all solutes in solution. Therefore,

$$y = \sum_s w_s = \frac{\sum_s m_s M_s}{1 + \sum_s m_s M_s} \tag{B.8}$$

Several units are commonly used for salinity:

$$\text{ppm} = 10^3\,\text{ppt} = 10^6 y\,[\text{kg/kg}] \tag{B.9}$$

Conversion from work per mol to work per kg solution

$$\frac{\dot{W}_{\text{least}}}{\dot{m}_p} = \frac{\dot{W}_{\text{least}}}{\dot{n}_{\text{H}_2\text{O},p}} \left(\frac{1}{M_{\text{H}_2\text{O}} + M_{\text{H}_2\text{O}} \sum_s M_{\text{s}} m_{s,p}} \right) \tag{B.10}$$

Appendix C

List of Publications

C.1 Publications

1. **K. H. Mistry**, J. H. Lienhard V, S. M. Zubair, *Effect of entropy generation on the performance of humidification-dehumidification desalination cycles*, International Journal of Thermal Sciences 49 (9) (2010) 1837–1847. doi:10.1016/j.ijthermalsci.2010.05.002.

2. G. P. Narayan, **K. H. Mistry**, M. H. Sharqawy, S. M. Zubair, J. H. Lienhard V, *Energy effectiveness of simultaneous heat and mass exchange devices*, Frontiers in Heat and Mass Transfer, 1 (2) (2010) 1–13 doi:10.5098/hmt.v1.2.3001.

3. **K. H. Mistry**, A. Mitsos, J. H. Lienhard V, *Optimal operating conditions and configurations for humidification-dehumidification desalination cycles*, International Journal of Thermal Sciences 50 (5) (2011) 779–789. doi:10.1016/j.ijthermalsci.2010.12.013.

4. **K. H. Mistry**, R. K. McGovern, G. P. Thiel, E. K. Summers, S. M. Zubair, J. H. Lienhard V, *Entropy generation analysis of desalination technologies*, Entropy, 13 (2011) 1829–1864. doi:10.3390/e13101829.

5. **K. H. Mistry**, M. A. Antar, J. H. Lienhard V, *An improved model for multiple effect distillation*, Desalination and Water Treatment 51 (4–6) (2013) 807–821. doi:10.1080/19443994.2012.703383.

6. **K. H. Mistry**, J. H. Lienhard V, *Effect of composition and nonideal solution behavior on desalination calculations for mixed electrolyte solutions with comparison to seawater*, Desalination 318 (2013) 34–47. doi:10.1016/j.desal.2013.03.015.

7. **K. H. Mistry**, J. H. Lienhard V, *Effect of nonideal solution behavior on desalination of a sodium chloride (NaCl) solution and comparison to seawater*, Journal of Energy Resources Technology (2013). Accepted.

8. **K. H. Mistry**, J. H. Lienhard V, *Generalized least energy of separation for desalination processes*, Entropy, (2013). Accepted.

9. **K. H. Mistry**, J. H. Lienhard V, *An Economics-Based Second Law Efficiency*, Entropy, (2013). Submitted.

C.2 Conferences

1. **K. H. Mistry**, G. P. Naryan, A. Mitsos, J. H. Lienhard V, *Multi-pressure humidification-dehumidification desalination using thermal vapor compression and energy recovery*, Proceedings of the 21st National & 10th ISHMT-ASME Heat and Mass Transfer Conference. ISHMT_USA_015. 1–9. December 27–30, 2011. IIT Madras, India.

2. **K. H. Mistry**, M. A. Antar, J. H. Lienhard V, *An improved model for multiple effect distillation*, European Desalination Society. April 23–26, 2012. Barcelona, Spain. doi:10.1080/19443994.2012.703383.

3. **K. H. Mistry**, J. H. Lienhard V, *Effect of nonideal solution behavior on desalination of a sodium chloride (NaCl) solution and comparison to seawater*, Proceedings of ASME 2012 International Mechanical Engineering Congress and Exposition. IMECE2012-88261. November 9–15, 2012. Houston, Texas, USA.

C.3 Patents

1. G. P. Narayan, **K. H. Mistry**, J. H. Lienhard V, and S. M. Zubair. High-Efficiency Thermal-Energy-Driven Water Purification System. Assigned to MIT, Patent Pending. #USSN 13/028,170. Feb 15, 2011.

Bibliography

[1] T. Oki, S. Kanae, Global hydrological cycles and world water resources, Science 313 (2006) 1068–1072.

[2] V. Smakhtin, C. Revenga, P. Döll, Taking into account environmental water requirements in global-scale water resources assessments, in: Comprehensive Assessment Research Report 2, Comprehensive Assessment Secretariat, International Water Management Institute, Colombo, 2004.

[3] Water for People, Water for Life, Executive Summary, Technical Report, The United Nations World Water Development Report, 2003.

[4] UNICEF, Children and water: global statistics, Online: `http://www.unicef.org/wash/index_31600.html`, 2006.

[5] F. C. Lopez, Jr., Camp pendleton seawater desalination project feasibility study, in: Desalination: An Energy Solution, IDA_HB2010-Lopez, International Desalination Association, Huntington Beach, CA, USA.

[6] J. Yardley, Beneath booming cities, China's future is drying up, The New York Times, 2007.

[7] K. S. Spiegler, Y. M. El-Sayed, A Desalination Primer: Introductory book for students and newcomers to desalination, Balaban Desalination Publications, Santa Maria Imbaro, Italy, 1994.

[8] A. Steffen, Worldchanging: A User's Guide for the 21st Century, Abrams, New York, NY, 2008.

[9] M. A. Shannon, P. W. Bohn, M. Elimelech, J. G. Georgiadis, B. J. Marinas, A. M. Mayes, Science and technology for water purification in the coming decades, Nature 452 (2008) 301–310.

[10] R. Semiat, Energy issues in desalination processes, Environmental Science & Technology 42 (2008) 8193–8201.

[11] T. Pankratz, IDA Desalination Yearbook 2012–2013, Media Analytics Ltc, Oxford, UK, 2013. International Desalination Association, Global Water Intelligence, and DesalData.

[12] C. Sommariva, Desalination and Advanced Water Treatment: Economics and Financing, Balaban Desalination Publications, Hopkinton, MA 01748, 2010.

[13] H. T. El-Dessouky, H. M. Ettouney, Fundamentals of Salt Water Desalination, Elsevier, Amsterdamn, The Netherlands, 2002.

[14] R. L. Stover, Development of a fourth generation energy recovery device. a 'CTO's notebook', Desalination 165 (2004) 313–321. Desalination Strategies in South Mediterranean Countries.

[15] R. L. Stover, Isobaric energy recovery technology — history and future opportunities, in: Desalination: An Energy Solution, IDA_HB2010-Stover, International Desalination Association, Huntington Beach, CA, USA.

[16] Y. M. El-Sayed, R. S. Silver, Principles of Desalination, volume A, Academic Press, New York, NY, 2nd edition, pp. 55–109. 1980.

[17] A. Cipollina, G. Micale, L. Rizzuti (Eds.), Seawater Desalination: Conventional and Renewable Energy Processes, Green Energy and Technology, Springer-Verlag, Berlin Heidelberg, 2009.

[18] M. Al-Ahmad, F. A. Aleem, Scale formation and fouling problems effect on the performance of msf and ro desalination plants in saudi arabia, Desalination 93 (1993) 287–310. Proceedings of Desal '92 Arabian Gulf Regional Water Desalination Symposium.

[19] J. C. Cowan, D. J. Weintritt, Water-Formed Scale Deposits, Gulf Publishing Company, Houston, TX, 1976.

[20] L. Awerbuch, Water desalination process using ion selective membranes, 2006.

[21] K. H. Mistry, R. K. McGovern, G. P. Thiel, E. K. Summers, S. M. Zubair, J. H. Lienhard V, Entropy generation analysis of desalination technologies, Entropy 13 (2011) 1829–1864.

[22] K. H. Mistry, J. H. Lienhard V, Generalized least energy of separation for desalination processes, Submitted to Entropy (2013).

[23] K. H. Mistry, J. H. Lienhard V, Effect of nonideal solution behavior on desalination of a sodium choloride (NaCl) solution and comparison to seawater, in: Proceedings of ASME 2012 International Mechanical Engineering Congress and Exposition, IMECE2012-88261, American Society of Mechanical Engineers, Houston, TX.

[24] K. H. Mistry, J. H. Lienhard V, Effect of nonideal solution behavior on desalination of a sodium choloride (NaCl) solution and comparison to seawater, Journal of Energy Resources Technology (2013). Accepted.

[25] K. H. Mistry, H. A. Hunter, J. H. Lienhard V, Effect of composition and nonideal solution behavior on desalination calculations for mixed electrolyte solutions with comparison to seawater, Desalination 318 (2013) 34–47.

[26] K. H. Mistry, J. H. Lienhard V, An economics-based second law efficiency, Entropy (2013). Submitted.

[27] K. H. Mistry, J. H. Lienhard V, S. M. Zubair, Effect of entropy generation on the performance of humidification-dehumidification desalination cycles, International Journal of Thermal Sciences 49 (2010) 1837–1847.

[28] H. C. Simpson, R. S. Silver, Technology of sea water desalination, in: Desalination Research Conference Proceedings, volume 942, National Academy of Sciences, National Research Council Publication, Washington, D. C., 1963, pp. 387–413.

[29] J. W. Tester, M. Modell, Thermodynamics and Its Applications, Prentice Hall PTR, Upper Saddle River, New Jersey, 3rd edition, 1997.

[30] M. H. Sharqawy, J. H. Lienhard V, S. M. Zubair, On exergy calculations of seawater with applications in desalination systems, International Journal of Thermal Sciences 50 (2011) 187–196.

[31] A. Bejan, Advanced Engineering Thermodynamics, John Wiley & Sons, Inc., Hoboken, New Jersey, 3rd edition, 2006.

[32] J. R. McCutcheon, R. L. McGinnis, M. Elimelech, Desalination by ammonia — carbon dioxide forward osmosis: Influence of draw and feed solution concentrations on process performance, Journal of Membrane Science 278 (2006) 114–123.

[33] R. L. McGinnis, M. Elimelech, Energy requirements of ammoniacarbon dioxide forward osmosis desalination, Desalination 207 (2007) 370–382.

[34] O. Bamaga, A. Yokochi, B. Zabara, A. Babaqi, Hybrid fo/ro desalination system: Preliminary assessment of osmotic energy recovery and designs of new fo membrane module configurations, Desalination 268 (2011) 163–169.

[35] R. L. McGinnis, N. T. Hancock, M. S. Nowosielski-Slepowron, G. D. McGurgan, Pilot demonstration of the nh3/co2 forward osmosis desalination process on high salinity brines, Desalination 312 (2013) 67–74. ¡ce:title¿Recent Advances in Forward Osmosis¡/ce:title¿.

[36] K. H. Mistry, A. Mitsos, J. H. Lienhard V, Optimal operating conditions and configurations for humidification-dehumidification desalination cycles, International Journal of Thermal Sciences 50 (2011) 779–789.

[37] K. H. Mistry, G. P. Narayan, A. Mitsos, J. H. Lienhard V, Optimization of multi-pressure humidification-dehumidification desalination using thermal vapor compression and hybridization, in: Proceedings of the 21st National & 10th ISHMT-ASME Heat and Mass Transfer Conference, ISHMT_USA_015, Indian Society for Heat and Mass Transfer and American Society for Mechanical Engineers, IIT Madras, India, pp. 1–9.

[38] G. P. Narayan, M. H. Sharqawy, E. K. Summers, J. H. Lienhard V, S. M. Zubair, M. Antar, The potential of solar-driven humidification-dehumidification desalination for small-scale decentralized water production, Renewable and Sustainable Energy Reviews 14 (2010) 1187–1201.

[39] G. P. Narayan, M. H. Sharqawy, J. H. Lienhard V, S. M. Zubair, Thermodynamic analysis of humidification dehumidification desalination cycles, Desalination and Water Treatment 16 (2010) 339–353.

[40] G. P. Narayan, M. G. S. John, S. M. Zubair, J. H. Lienhard V, Thermal design of the humidification dehumidification desalination system: An experimental investigation, International Journal of Heat and Mass Transfer 58 (2013) 740–748.

[41] A. Bajpayee, T. Luo, A. Muto, G. Chen, Very low temperature membrane-free desalination by directional solvent extraction, Energy Environ. Sci. 4 (2011) 1672–1675.

[42] T. Luo, A. Bajpayee, G. Chen, Directional solvent for membrane-free water desalination—a molecular level study, Journal of Applied Physics 110 (2011) 054905.

[43] J. R. Cooper, Release on the IAPWS formulation 2008 for the thermodynamic properties of seawater, The International Association for the Properties of Water and Steam (2008) 1–19.

[44] R. Feistel, A Gibbs function for seawater thermodynamics for −6 to 80 °C and salinity up to 120 g kg^{-1}, Deep Sea Research Part I: Oceanographic Research Papers 55 (2008) 1639–1671.

[45] M. H. Sharqawy, J. H. Lienhard V, S. M. Zubair, Thermophysical properties of seawater: A review of existing correlations and data, Desalination and Water Treatment 16 (2010) 354–380.

[46] M. H. Sharqawy, J. H. Lienhard V, S. M. Zubair, Thermophysical properties of seawater, Online `http://web.mit.edu/seawater`, 2012.

[47] M. J. Moran, Availability Analysis: A guide to efficient energy use, ASME Press, New York, NY, corrected edition, 1989.

[48] R. Singh, Sustainable fuel cell integrated membrane desalination systems, Desalination 227 (2008) 14–33. First Oxford and Nottingham Water and Membranes Research Event 24 July 2006, Oxford, UK.

[49] S. Al-Hallaj, F. Alasfour, S. Parekh, S. Amiruddin, J. Selman, H. Ghezel-Ayagh, Conceptual design of a novel hybrid fuel cell/desalination system, Desalination 164 (2004) 19–31.

[50] B. Liberman, Present and future: Energy efficient seawater desalination, in: Desalination: An Energy Solution, IDA_HB2010-Liberman, International Desalination Association, Huntington Beach, CA, USA.

[51] L. D. Banchik, J. H. Lienhard V, Thermodynamic analysis of a reverse osmosis desalination system using forward osmosis for energy recovery, in: Proceedings of ASME 2012 International Mechanical Engineering Congress and Exposition, IMECE2012-86987, American Society of Mechanical Engineers, Houston, TX.

[52] M. H. Sharqawy, S. M. Zubair, J. H. Lienhard V, Second law analysis of reverse osmosis desalination plants: An alternative design using pressure retarded osmosis, Energy 36 (2011) 6617–6626.

[53] J. W. Post, J. Veerman, H. V. Hamelers, G. J. Euverink, S. J. Metz, K. Nymeijer, C. J. Buisman, Salinity-gradient power: Evaluation of pressure-retarded osmosis and reverse electrodialysis, Journal of Membrane Science 288 (2007) 218–230.

[54] E. Lewis, R. Perkin, The practical salinity scale 1978: conversion of existing data, Deep Sea Research Part A. Oceanographic Research Papers 28 (1981) 307–328.

[55] ASTM International, Standard practice for the preparation of substitute ocean water, 1998.

[56] Public Health and the Environment, Desalination for Safe Water Supply — Guidance for the Health and Environmental Aspects Applicable to Desalination, Technical Report WHO/SDE/WSH/07/0?, World Health Oranization, Geneva, 2007.

[57] P. Biesheuvel, Thermodynamic cycle analysis for capacitive deionization, Journal of Colloid and Interface Science 332 (2009) 258–264.

[58] F. La Mantia, M. Pasta, H. D. Deshazer, B. E. Logan, Y. Cui, Batteries for efficient energy extraction from a water salinity difference, Nano Letters 11 (2011) 1810–1813.

[59] A. Nafey, H. Fath, A. Mabrouk, Thermoeconomic design of a multi-effect evaporation mechanical vapor compression (MEE-MVC) desalination process, Desalination 230 (2008) 1–15.

[60] F. Banat, N. Jwaied, Exergy analysis of desalination by solar-powered membrane distillation units, Desalination 230 (2008) 27–40.

[61] M. Thomson, M. S. Miranda, D. Infield, A small-scale seawater reverse-osmosis system with excellent energy efficiency over a wide operating range, Desalination 153 (2003) 229–236.

[62] M. Liu, S. Yu, J. Tao, C. Gao, Preparation, structure characteristics and separation properties of thin-film composite polyamide-urethane seawater reverse osmosis membrane, Journal of Membrane Science 325 (2008) 947–956.

[63] K. Klinko, W. Light, C. Cummings, Factors influencing optimum seawater reverse osmosis system designs, Desalination 54 (1985) 3–18.

[64] A. Achilli, T. Y. Cath, A. E. Childress, Power generation with pressure retarded osmosis: An experimental and theoretical investigation, Journal of Membrane Science 343 (2009) 42–52.

[65] Koch Membrane Systems, Fluid systems TFC-FR 4" element — high rejection, fouling resistant low pressure ro element for brackish water, Technical Data Sheet, Wilmington, MA, 2011.

[66] J. F. Zemaitis, Jr., D. M. Clark, M. Rafal, N. C. Scrivner, Handbook of Aqueous Electrolyte Thermodynamics: Theory & Application, Design Institute for Physical Property Data (DIPPR) and American Institute of Chemical Engineers (AIChE), New York, NY, 1986.

[67] K. S. Pitzer, Thermodynamics, McGraw-Hill, Inc., New York, 3rd edition, 1995.

[68] R. A. Robinson, R. H. Stokes, Electrolyte Solutions, Dover Publications, Inc., Mineola, New York, second revised edition, 2002.

[69] W. Stumm, J. J. Morgan, Aquatic Chemistry: Chemical Equilibria and Rates in Natural Waters, John Wiley & Sons, Inc., New York, 3rd edition, 1996.

[70] L. A. Bromley, D. Singh, P. Ray, S. Sridhar, S. M. Read, Thermodynamic properties of sea salt solutions, AIChE Journal 20 (1974) 326–335.

[71] M. H. Sharqawy, J. H. Lienhard V, S. M. Zubair, Thermophysical properties of seawater, Online `http://web.mit.edu/seawater/`, 2012.

[72] P. Debye, E. Hückel, Zur theorie der elektrolyte. I. gefrierpunktserniedrigung und verwandte erscheinungen, Physikalische Zeitschrift 24 (1923) 185–206. "On the Theory of Electrolytes I. Freezing Point Depression and Related Phenomena".

[73] P. Debye, E. Hückel, Zur theorie der elektrolyte. II. das grenzgesetz für die elektrische leitfähigkeit, Physikalische Zeitschrift 24 (1923) 305–325. "On the Theory of Electrolytes II. Limiting Law for Electric Conductivity".

[74] P. Debye, Over ionen en hun activiteit, Chemisch Weekblad 20 (1923) 562–568. "On Ions and Their Activity".

[75] J. S. Newman, Electrochemical Systems, Prentice-Hall, Inc., Englewood Cliffs, N.J., 1973.

[76] K. S. Pitzer, Thermodynamics of electrolytes. I. Theoretical basis and general equations, The Journal of Physical Chemistry 77 (1973) 268–277.

[77] K. S. Pitzer, G. Mayorga, Thermodynamics of electrolytes. II. Activity and osmotic coefficients for strong electrolytes with one or both ions univalent, The Journal of Physical Chemistry 77 (1973) 2300–2308.

[78] K. S. Pitzer, G. Mayorga, Thermodynamics of electrolytes. III. Activity and osmotic coefficients for 2-2 electrolytes, Journal of Solution Chemistry 3 (1974) 539–546. 10.1007/BF00648138.

[79] K. S. Pitzer, J. J. Kim, Thermodynamics of electrolytes. IV. Activity and osmotic coefficients for mixed electrolytes, Journal of the American Chemical Society 96 (1974) 5701–5707.

[80] K. S. Pitzer, Thermodynamics of electrolytes. V. Effects of higher-order electrostatic terms, Journal of Solution Chemistry 4 (1975) 249–265.

[81] P. Debye, Osmotische zustandsgleinchung und activität verdünnter starker elektrolyte, Physikalische Zeitschrift 25 (1924) 97–107. "Osmotic Equation of State and Activity of Diluted Strong Electrolytes".

[82] K. S. Pitzer, J. C. Peiper, R. H. Busey, Thermodynamic properties of aqueous sodium chloride solutions, Journal of Physical and Chemical Reference Data 13 (1984) 1–102.

[83] The MathWorks, MATLAB R2011a, Software, 2011.

[84] M. Wilf, The Guidebook to Membrane Desalination Technology, Balaban Desalination Publications, L'Aquila, Italy, 2007.

[85] K. L. Benko, J. E. Drewes, Produced water in the western united states: Geographical distribution, occurrence, and composition, Environmental Engineering Science 25 (2008) 239–246.

[86] G. P. Thiel, S. M. Zubair, J. H. Lienhard V, An analysis of likely scalants in the treatment of produced water from Nova Scotia, in: Heat Exchanger Fouling and Cleaning X, Budapest. Submitted.

[87] K. S. Spiegler, Y. M. El-Sayed, The energetics of desalination processes, Desalination 134 (2001) 109–128.

[88] F. Alasfour, M. Darwish, A. B. Amer, Thermal analysis of ME-TVC+MEE desalination systems, Desalination 174 (2005) 39–61.

[89] N. Kahraman, Y. A. Çengel, Exergy analysis of a MSF distillation plant, Energy Conversion and Management 46 (2005) 2625–2636.

[90] J. M. Veza, Mechanical vapour compression desalination plants — a case study, Desalination 101 (1995) 1–10.

[91] Y. Cerci, Exergy analysis of a reverse osmosis desalination plant in california, Desalination 142 (2002) 257–266.

[92] R. L. McGinnis, Personal communication, 2013.

[93] M. J. Moran, H. N. Shapiro, Fundamentals of Engineering Thermodynamics, John Wiley & Sons, Inc., New Jersey, 6th edition, 2007.

[94] Global Water Intelligence, Desaldata.com, Online `http://desaldata.com`, 2013.

[95] J. E. Miller, Review of Water Resources and Desalination Technologies, Technical Report SAND 2003-0800, Sandia National Laboratories, Livermore, CA, 2003.

[96] G. J. Crisp, Actual energy consumption and water cost for the swro systems at perth, in: Desalination: An Energy Solution, IDA_HB2010-Crisp, International Desalination Association, Huntington Beach, CA, USA.

[97] R. L. Stover, Seawater reverse osmosis with isobaric energy recovery devices, Desalination 203 (2007) 168–175. EuroMed 2006: Conference on Desalination Strategies in South Mediterranean Countries.

[98] C. Fritzmann, J. Lwenberg, T. Wintgens, T. Melin, State-of-the-art of reverse osmosis desalination, Desalination 216 (2007) 1–76.

[99] K. H. Mistry, M. A. Antar, J. H. Lienhard V, An improved model for multiple effect distillation, in: Desalination for the Environment: Clean Water and Energy, European Desalination Society, Barcelona, Spain.

[100] K. H. Mistry, M. A. Antar, J. H. Lienhard V, An improved model for multiple effect distillation, Desalination and Water Treatment 51 (2013) 807–821.

[101] W. Wagner, A. Pruss, The IAPWS formulation 1995 for the thermodynamic properties of ordinary water substance for general and scientific use, Journal of Physical and Chemical Reference Data 31 (2002) 387–535.

[102] A. Bejan, General criterion for rating heat-exchanger performance, International Journal of Heat and Mass Transfer 21 (1978) 655–658.

[103] M. Darwish, F. Al-Juwayhel, H. K. Abdulraheim, Multi-effect boiling systems from an energy viewpoint, Desalination 194 (2006) 22–39.

[104] K. W. Lawson, D. R. Lloyd, Membrane distillation, Journal of Membrane Science 124 (1997) 1–25.

[105] R. B. Saffarini, E. K. Summers, H. A. Arafat, J. H. Lienhard V, Economic evaluation of stand-alone solar powered membrane distillation systems, Desalination 299 (2012) 55–62.

[106] J. Rodriguez-Maroto, L. Martinez, Bulk and measured temperatures in direct contact membrane distillation, Journal of Membrane Science 250 (2005) 141–149.

[107] L. Martinez-Diez, F. Florido-Diaz, Desalination of brines by membrane distillation, Desalination 137 (2001) 267–273.

[108] L. Song, B. Li, K. K. Sirkar, J. L. Gilron, Direct contact membrane distillation-based desalination: Novel membranes, devices, larger-scale studies, and a model, Industrial & Engineering Chemistry Research 46 (2007) 2307–2323.

[109] H. Lee, F. He, L. Song, J. Gilron, K. K. Sirkar, Desalination with a cascade of cross-flow hollow fiber membrane distillation devices integrated with a heat exchanger, AIChE Journal 57 (2011) 1780–1795.

[110] V. Bui, L. Vu, M. Nguyen, Modelling the simultaneous heat and mass transfer of direct contact membrane distillation in hollow fibre modules, Journal of Membrane Science 353 (2010) 85–93.

[111] J. H. Lienhard IV, J. H. Lienhard V, A Heat Transfer Textbook, Dover Publications, Mineola, NY, 4th edition, 2011. `http://ahtt.mit.edu`.

[112] H. E. Fath, S. M. Elsherbiny, A. A. Hassan, M. Rommel, M. Wieghaus, J. Koschikowski, M. Vatansever, PV and thermally driven small-scale, stand-alone solar desalination systems with very low maintenance needs, Desalination 225 (2008) 58–69.

[113] F. Banat, N. Jwaied, M. Rommel, J. Koschikowski, M. Wieghaus, Desalination by a "compact SMADES" autonomous solar-powered membrane distillation unit, Desalination 217 (2007) 29–37.

[114] S. E. Aly, Gas turbine total energy vapour compression desalination system, Energy Conversion and Management 40 (1999) 729–741.

[115] J. Lara, G. Noyes, M. Holtzapple, An investigation of high operating temperatures in mechanical vapor-compression desalination, Desalination 227 (2008) 217–232. Issue 1 First Oxford and Nottingham Water and Membranes Research Event 2-4 July 2006, Oxford, UK.

[116] N. Lukic, L. Diezel, A. Frba, A. Leipertz, Economical aspects of the improvement of a mechanical vapour compression desalination plant by dropwise condensation, Desalination 264 (2010) 173–178.

[117] Energy Recovery Inc, Eri power model, Online `http://www.energyrecovery.com/index.cfm/0/0/56-Power-Model.html`, 2010. San Leandro, CA.

[118] Energy Recovery Inc, Technology overview, Online `http://www.energyrecovery.com/index.cfm/0/0/33-Overview.html`, 2011. San Leandro, CA.

[119] M. Elimelech, W. A. Phillip, The future of seawater desalination: Energy, technology, and the environment, Science 333 (2011) 712–717.

[120] Desalitech Ltd, Doing away with ro energy-recovery devices, Desalination & Water Reuse 20 (2010) 26–28.

[121] K. H. Mistry, Second Law Analysis and Optimization of Humidification-Dehumidification Desalination Cycles, Master's thesis, Massachusetts Institute of Technology, Cambridge, MA, 2010.

[122] G. P. Narayan, K. H. Mistry, M. H. Sharqawy, S. M. Zubair, J. H. Lienhard V, Energy effectiveness of simultaneous heat and mass exchange devices, Frontiers in Heat and Mass Transfer 1 (2010) 1–13.

[123] R. W. Hyland, A. Wexler, Formulations for the thermodynamic properties of dry air from 173.15 K to 473.15 K, and of saturated moist air from 173.15 K to 372.15 K, at pressures to 5 MPa, ASHRAE Transactions Part 2A (RP-216) (1983b) 520–535.

[124] J. R. Cooper, Revised release on the IAPWS industrial formulation 1997 for the thermodynamic properties of water and steam, The International Association for the Properties of Water and Steam (2007) 1–48.

[125] M. Tribus, J. P. Pezier, Concerning the economic value of experimentation in the design of desalting plants, Desalination 8 (1970) 311–349.

[126] R. B. Evans, G. L. Crellin, M. Tribus, Chapter 1 - thermoeconomic considerations of sea water demineralization, in: K. Speigler (Ed.), Principles of Desalination, Academic Press, 1980, pp. 1–54.

[127] R. B. Evans, G. L. Crellin, M. Tribus, Chapter 2 - thermoeconomic considerations of sea water demineralization, in: K. Spiegler (Ed.), Principles of Desalination, Academic Press, 1966, pp. 21–76.

[128] K. Spiegler, Thermodynamic analysis, Desalination 44 (1983) 3–16.

[129] A. London, Economics and the second law: An engineering view and methodology, International Journal of Heat and Mass Transfer 25 (1982) 743–751.

[130] Y. M. El-Sayed, Advances in the methodologies of optimal thermal design, Desalination 92 (1993) 79–101. ¡ce:title¿Proceedings of {DESAL} '92 Arabian Gulf Regional Water Desalination Symposium¡/ce:title¿.

[131] A. Bejan, G. Tsatsaronis, M. Moran, Themal Design & Optimization, John Wiley & Sons, Inc., New York, 1996.

[132] H. Sayyaadi, A. Saffari, A. Mahmoodian, Various approaches in optimization of multi effects distillation desalination systems using a hybrid meta-heuristic optimization tool, Desalination 254 (2010) 138–148.

[133] A. K. Plappally, J. H. Lienhard V, Costs for water supply, treatment, end-use and reclamation, Desalination and Water Treatment 51 (2013) 200–232.

[134] A. K. Plappally, J. H. Lienhard V, Energy requirements for water production, treatment, end use, reclamation, and disposal, Renewable and Sustainable Energy Reviews 16 (2012) 4818–4848.

[135] V. G. Gude, N. Nirmalakhandan, S. Deng, Renewable and sustainable approaches for desalination, Renewable and Sustainable Energy Reviews 14 (2010) 2641–2654.

[136] T. Mezher, H. Fath, Z. Abbas, A. Khaled, Techno-economic assessment and environmental impacts of desalination technologies, Desalination 266 (2011) 263–273.

[137] Committee on Advancing Desalination Technology, National Research Council, Desalination: A National Perspective, The National Academies Press, Washington, DC, 2008.

[138] A. M. Bilton, R. Wiesman, A. Arif, S. M. Zubair, S. Dubowsky, On the feasibility of community-scale photovoltaic-powered reverse osmosis desalination systems for remote locations, Renewable Energy 36 (2011) 3246–3256.

[139] A. M. Bilton, A Modular Design Architecture for Application to Community-Scale Photovoltaic-Powered Reverse Osmosis Systems, Ph.D. thesis, Massachusetts Institute of Technology, Cambridge, MA, 2013.

[140] M. S. Peters, K. D. Timmerhaus, R. E. West, Plant Design and Economics for Chemical Engineers, McGraw Hill, 2003.

[141] R. L. Stover, Personal communication, 2013.

[142] The Dow Chemical Company, DOW FILMTEC Membranes: SW30XHR-440i Seawater Reverse Osmosis Element with iLEC Interlocking Endcaps, Online: `http://www.dowwaterandprocess.com/products/membranes/sw30xhr_440i.htm`, 2013.

[143] R. Huehmer, S. Alt, J. Lozier, A. Kupp, T. Nading, K. Egrican, B. Emerson, Evaluation and Optimization of Emerging and Existing Energy Recovery Devices for Desalination and Wastewater Membrane Treatment Plants, Technical Report, CH2M HILL, WateReuse Research Foundation, Alexandria, VA, 2013.

[144] Pentair Codeline, 8" Side Entry: 80S Series Membrane Housings, Online: `http://www.codeline.com/products/80S_side_entry.html`, 2013. Codeline 80S120-6.

[145] AtlanticRO, Reverse osmosis membranes and pressure vessels, Online: `http://www.atlanticro.com/Code.pdf`, 2013.

[146] Big Brand Water Filter, Inc, Danfoss APP30, Online: `http://www.bigbrandwater.com/danfoss25.html`, 2013.

[147] Danfoss, RO Solutions Brochure, Online: `http://www.danfoss.com/NR/rdonlyres/A2F103E1-CC9E-4BCD-BB4B-8E47F204B49C/0/521B1191_ROImagebrochure_USSize_web.pdf`, 2012. APP 30.

[148] Baldor: A Member of the ABB Group, 501 Stock Product Catalog: IEC Frame Motors, Online: `http://www.baldor.com/support/501catalog.asp`, 2012.

[149] Energy Recovery Inc, PX Pressure Exchanger Devices, Online: `http://www.energyrecovery.com/px-pressure-exchanger-devices`, 2013. PX-300.

[150] A. Hafez, S. El-Manharawy, Economics of seawater RO desalination in the red sea region, egypt. part 1. a case study, Desalination 153 (2003) 335–347.

[151] H. M. Ettouney, H. T. El-Dessouky, R. S. Faibish, P. J. Gowin, Evaluating the economics of desalination, Chemical Engineering Progress 12 (2002) 32–38.

[152] A. Helal, S. Al-Malek, E. Al-Katheeri, Economic feasibility of alternative designs of a pv-ro desalination unit for remote areas in the united arab emirates, Desalination 221 (2008) 1–16. European Desalination Society and Center for Research and Technology Hellas (CERTH), Sani Resort, Halkidiki, Greece.

[153] U.S. Energy Information Administration, Electric Power Monthly with Data for February 2013, Technical Report, U.S. Energy Information Administration, U.S. Department of Energy, Washington, DC, 2013.

[154] A. Efraty, R. N. Barak, Z. Gal, Closed circuit desalination—a new low energy high recovery technology without energy recovery, Desalination and Water Treatment 31 (2011) 95–101.

[155] Y. Dreizin, Ashkelon seawater desalination project—off-taker's self costs, supplied water costs, total costs and benefits, Desalination 190 (2006) 104–116.

[156] E. K. Summers, H. A. Arafat, J. H. Lienhard V, Energy efficiency comparison of single-stage membrane distillation (MD) desalination cycles in different configurations, Desalination 290 (2012) 54–66.

[157] European Desalination Society, Desalination with solar energy, intensive course, course, 2011.

[158] F. Banat, N. Jwaied, Economic evaluation of desalination by small-scale autonomous solar-powered membrane distillation units, Desalination 220 (2008) 566–573. European Desalination Society and Center for Research and Technology Hellas (CERTH), Sani Resort, Halkidiki, Greece.

[159] A. Ophir, F. Lokiec, Advanced med process for most economical sea water desalination, Desalination 182 (2005) 187–198. Desalination and the Environment.

[160] M. Darwish, A. Alsairafi, Technical comparison between tvc/meb and msf, Desalination 170 (2004) 223–239.

[161] H. El-Dessouky, I. Alatiqi, S. Bingulac, H. Ettouney, Steady-state analysis of the multiple effect evaporation desalination process, Chemical Engineering & Technology 21 (1998) 437–451.

[162] H. T. El-Dessouky, H. Ettouney, Multiple-effect evaporation desalination systems. thermal analysis, Desalination 125 (1999) 259–276. European Conference on Desalination and the Environment.

[163] H. T. El-Dessouky, H. M. Ettouney, F. Mandani, Performance of parallel feed multiple effect evaporation system for seawater desalination, Applied Thermal Engineering 20 (2000) 1679–1706.

[164] M. Darwish, H. K. Abdulrahim, Feed water arrangements in a multi-effect desalting system, Desalination 228 (2008) 30–54.

[165] M. El-Allawy, Predictive simulation of the performance of med/tvc desalination distiller, in: IDA Conference, International Desalination Association, Bahams.

[166] N. H. Aly, A. K. El-Figi, Thermal performance of seawater desalination systems, Desalination 158 (2003) 127–142. Desalination and the Environment: Fresh Water for All.

[167] M. Al-Sahali, H. Ettouney, Developments in thermal desalination processes: Design, energy, and costing aspects, Desalination 214 (2007) 227–240.

[168] M. Ameri, S. S. Mohammadi, M. Hosseini, M. Seifi, Effect of design parameters on multi-effect desalinationsystem specifications, Desalination 245 (2009) 266–283. Engineering with Membranes 2008 - Membrane Processes: Development, Monitoring and Modelling From the Nano to the Macro Scale, Engineering with Membranes 2008.

[169] R. Kamali, S. Mohebinia, Experience of design and optimization of multi-effects desalination systems in iran, Desalination 222 (2008) 639–645. European Desalination Society and Center for Research and Technology Hellas (CERTH), Sani Resort, Halkidiki, Greece.

[170] R. Kamali, A. Abbassi, S. S. Vanini, M. S. Avval, Thermodynamic design and parametric study of med-tvc, Desalination 222 (2008) 596–604. European Desalination Society and Center for Research and Technology Hellas (CERTH), Sani Resort, Halkidiki, Greece,.

[171] K. Minnich, J. Tonner, D. Neu, A comparison for heat transfer requirement and evaporator cost for med/tvc and msf, in: IDA Conference, International Desalination Association, Abu Dhabi, UAE.

[172] H.-S. Choi, T.-J. Lee, Y.-G. Kim, S.-L. Song, Performance improvement of multiple-effect distiller with thermal vapor compression system by exergy analysis, Desalination 182 (2005) 239–249. Desalination and the Environment Desalination and the Environment.

[173] M. Darwish, N. Al-Najem, Energy consumptions and costs of different desalting systems, Desalination 64 (1987) 83–96.

[174] N. M. Al-Najem, M. Darwish, F. Youssef, Thermovapor compression desalters: energy and availability — analysis of single- and multi-effect systems, Desalination 110 (1997) 223–238.

[175] O. Hamed, Thermal assessment of a multiple effect boiling (meb) desalination system, Desalination 86 (1992) 325–339.

[176] O. Hamed, A. Zamamiri, S. Aly, N. Lior, Thermal performance and exergy analysis of a thermal vapor compression desalination system, Energy Conversion and Management 37 (1996) 379–387.

[177] A. Greogorzewski, K. Genthner, Multieffect distillation: A study and comparison of different process configuration, in: IDA Conference, International Desalination Association, Abu Dhabi, UAE.

[178] S. A. Klein, Engineering Equation Solver, Academic Professional, Version 8, Software, 2010.

[179] Numerica Technology, JACOBIAN Modeling and Optimization Software, `http://www.numericatech.com`, 2009. Accessed March 2010.

[180] A. C. Mueller, Heat Exchanger Design Handbook, volume 3: Thermal and hydraulic design of heat exchangers, Hemisphere Publishing Corporation, Washington, pp. 3.4.7–1–3.4.7–2.